Indian and Northern Affairs Canada
Affaires indiennes et du Nord Canada

YUKON GEOLOGY

Volume 2

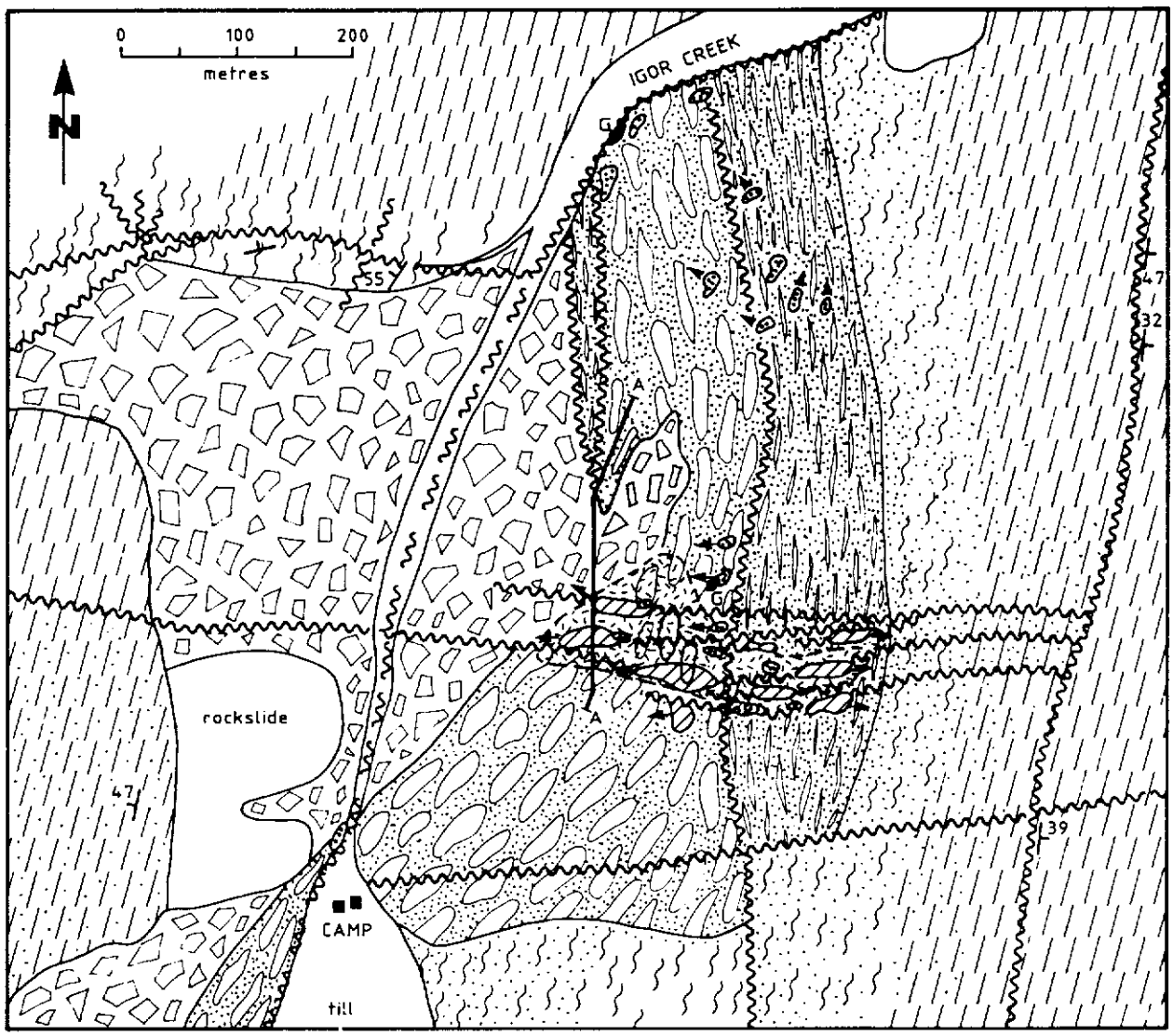

Canada

COVER: The Wernecke Breccias, in the mid-Proterozic Wernecke Supergroup, are engimatic hosts for iron, copper, uranium, cobalt and gold. This map, which shows the complex field relations displayed by the breccias is shown as Figure 2 in "Wernecke breccias and Re, Cu, U mineralization: Quartet Mountain-Igor area (NTS 106 E)" by Petter Laznicka and David Gaboury.

Exploration and Geological Services Division of Northern Affairs Program invites readers to write and inform us of their language preferences for Yukon Exploration and Geology Reports and other geological reports prepared by the division.

Please write to:

Exploration and Geological Services Division
Northern Affairs Program
200 Range Road
Whitehorse, Yukon
Y1A 3V1

La Division de l'exploration et des services géologiques du Programme des Affaires du Nord, dans la région du Yukon, invite ses lecteurs à lui écrire et à lui communiquer dans quelle langue ils préfèreraient recevoir les rapports sur l'exploration et la géologie du Yukon, et les autres rapports géotechniques préparés par la Division. Veuillez vous adresser à:

la Division de l'exploration et des services géotechniques
Programme des Affaires du Nord
Ministère des Affaires Indiennes et du développement du Nord
200 Range Road
Whitehorse, Yukon
Y1A 3V1

YUKON GEOLOGY

Volume 2

Exploration and Geological Services Division
Mineral Resources Directorate
Northern Affairs Program, Yukon
Indian and Northern Affairs Canada

Edited by Grant Abbott

Published under the authority of the
Hon. Bill McKnight, P.C., M.P.,
Minister of Indian Affairs and
Northern Development,
Whitehorse, 1988

QS-Y044-000-EE-A1

Available in Canada through
Associated Bookstores
and other booksellers

or by mail from
Canadian Government Publishing Centre
Supply and Services Canada
Ottawa, Canada K1A 0S9

Primarily available from
Exploration and Geological Services
Indian and Northern Affairs Canada
200 Range Road, Whitehorse
Yukon, Canada, Y1A 3V1

Catalogue No. R71-40/2E
ISBN 0-662-15713-3

It is recommended that reference to this report be made in the following form:

INAC, (1988). Yukon Geology Volume 2, 1987; Exploration and Geological Services Division, Yukon, Indian and Northern Affairs Canada.

PREFACE

This second volume of Yukon Geology contains reports by government and university geologists who are undertaking fieldwork in the Yukon. There are mainly preliminary and are intended to provide timely information about ongoing field activities. Although most reports are written by geologists with Exploration and Geological Service Division or by graduate students sponsored by the Division, we welcome papers from all geologists working in the Yukon.

Grant Abbott
Minerals Geologist
EGSD

LOCATION OF PAPERS

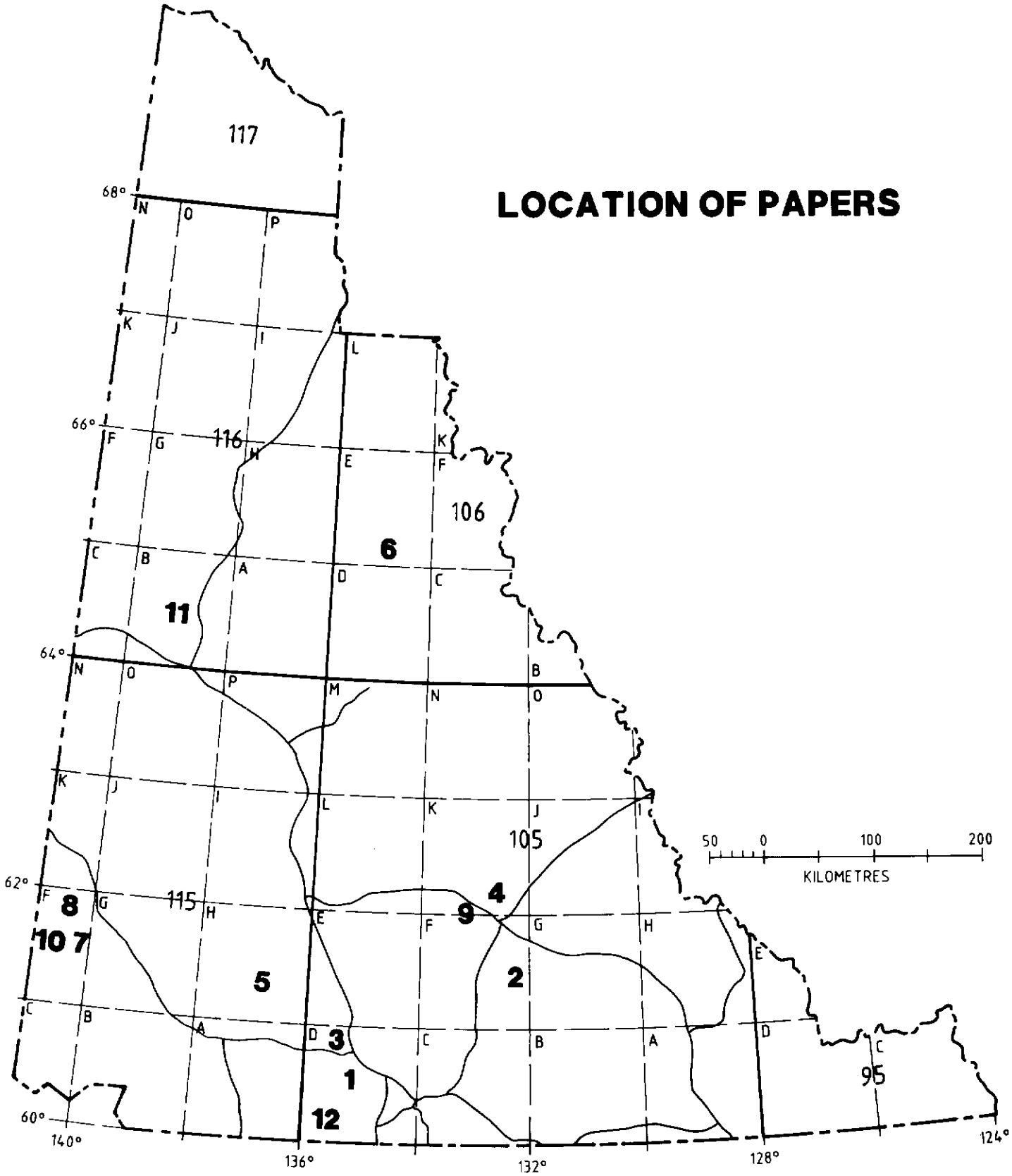

TABLE OF CONTENTS

GEOLOGY OF THE WHITEHORSE COAL DEPOSIT

Trevor Bremner
Exploration and Geological Services Division
Indian and Northern Affairs Canada
Whitehorse, Yukon

BREMNER, T., 1988. Geology of the Whitehorse Coal Deposit; in Yukon Geology, Vol. 2; Exploration and Geological Services Division, Yukon, Indian and Northern Affairs Canada, p. 1 -7.

ABSTRACT

Anthracite in floodplain deposits of the Cretaceous Tantalus Formation is preserved in a west-trending graben on the south side of Mt. Granger, 24 km southwest of Whitehorse. The graben extends from Fish Lake to Double Mountain, a distance of 20 km. Two main seams are exposed by bulldozer trenches across the central part of the Mt Granger property. The upper seam is about 1.8 m thick at surface and has been traced almost continuously over a strike length of 2 km. The lower seam is at least 3.3 m thick at surface and can be traced for more than 1 km. The seams dip at about 30°-50° to the north. Rotary drilling in 1985 on the central showing penetrated up to 22.25 m of coal. The best continuous coal intersection was 13.1 m in WC-85-6. Open pittable reserves were calculated at 180,033 tonnes over a 335 m strike length.

Six days of mapping in 1987 confirmed the continuity of the two main coal seams which are deformed by open north-plunging folds. A north-trending fault along Fisher Creek cuts off massive conglomerate channel deposits interbedded with the coal in the main showing area against recessive floodplain deposits to the west, where up to five coal-bearing horizons occur in a thick shale sequence. Additional reserves may lie beneath the low-lying overburden-covered area west of the Fisher Creek fault.

RÉSUMÉ

L'anthracite présent dans des dépôts de plaine inondable dans la formation crétacée de Tantalus est conservé dans un graben d'orientation générale ouest sur le versant sud du mont Granger, à 24 km au sud-ouest de Whitehorse. Le graben s'étend du lac Fish au mont Double, c'est-à-dire sur une distance de 20 km. Deux grands filons sont exposés dans des tranchées creusées au bulldozer, à travers la partie centrale de la propriété de Mt Granger. Le filon supérieur a environ 1,8 m d'épaisseur en surface, et a été suivi de façon presque continue sur une longueur de 2 km en direction. Le filon inférieur a au moins 3,3 m d'épaisseur en surface, et a pu être suivi sur plus de 1 km. Les filons ont un pendage d'environ 30-50° vers le nord. En 1985, un forage rotatif effectué dans la venue centrale a traversé jusqu'à 22,25 m de charbon. La meilleure intersection avec un filon continu de charbon se trouvait à 13,1 m dans WC-85-6. On a calculé que les réserves exploitables à ciel ouvert s'élevaient à 180 033 tonnes sur une longueur de 335 m en direction.

En 1987, en six jours de travaux cartographiques, on a pu confirmer la continuité des deux principaux filons houillers qui sont déformés par des plis légers de plongement nord. Une faille d'orientation générale nord qui borne le ruisseau Fisher (Fisher Creek) recoupe des gîtes linéaires, en forme de traînées, de conglomérat massif interstratifié avec le charbon dans la principale zone de venues, en bordure de dépôts récessifs de plaine inondable à l'ouest, où jusqu'à cinq horizons carbonifères sont présents dans une succession d'argile litée. Il est possible qu'il existe des réserves supplémentaires au-dessous de la région basse, recouverte de morts-terrains, à l'ouest de la faille de Fisher Creek.

HISTORY

Coal was first discovered on Mt. Granger in 1899 and reported by McConnell in 1901. By 1906 coal occurrences had been traced over a 20 km strike length and between 1906 and 1908 several trenches and an 18 metre adit were excavated into the uppermost of three coal seams exposed in Fisher Creek on the southwest side of Mt. Granger. In 1908, Cairnes reported the results of four analyses, one from the face of the adit and three from outcrop. The results indicated semi-anthracite coal with an average 36% ash content.

In 1942, the U.S. Army Corps of Engineers briefly examined the coal deposit and shipped a small tonnage for use in Whitehorse that winter.

Luscar Ltd acquired three coal exploration licences in the area in 1969. Consultants R.S. Taylor and Associates Ltd. undertook reconnaissance geological mapping, hand trenching and sampling on Luscar's behalf. One to three seams up to 1.83 m thick were described within a coal-bearing section which was traceable over a strike length of 10 km. More than 2,386,125 tonnes of recoverable coal were estimated to lie above the level of the valley floor.

In 1975, B. Savage acquired two coal exploration licences and prospected the area. J. Hughes reviewed available data.

P. Poggenburg et al. staked a coal mining lease in 1981 and acquired a coal exploration licence on an area to the southeast. Two additional mining leases were added in 1982 and Whitehorse Coal Corporation was formed. Construction began on an access road from Wolf Creek. Three trenches were excavated in the Fisher Creek and West Hill areas and a geological reconnaissance was made by R. Hill. Combustion tests on three samples taken by Mr. Hill indicated the samples were meta-anthracites with an average 3.5% moisture, 38.2% ash and 19,765 kj/kg heating value.

A further six trenches were excavated in 1983, the access road was completed and J. Perry undertook three days of geological reconnaissance. Perry estimated in situ coal reserves of 85 million tonnes assuming a thickness of 3.05 metres, a strike length of 10 km and a downdip extent of 500 metres.

In 1985 two short bulldozer trenches were excavated and six vertical rotary holes totalling 275 m were drilled along the slope above the main showing along a 335 m strike length. Gamma-neutron, density, resistivity and caliper logs were run. The logs showed good correlation between five of the six drillholes. Drill cuttings were logged by L. Carlyle. Coal intersections up to 13.1 m were encountered. In WC-85-4 a total of 22.25 m coal was penetrated in 8 layers interbedded with conglomerated and shale. The best single intersection in this drillhole was 8.5 m. Some of the cleaner coal bands contained as little as 15% ash. Carlyle calculated drill-indicated reserves of 180,033 tonnes within the drilled area.

In 1986 the main pit was surveyed and enlarged, with a head-

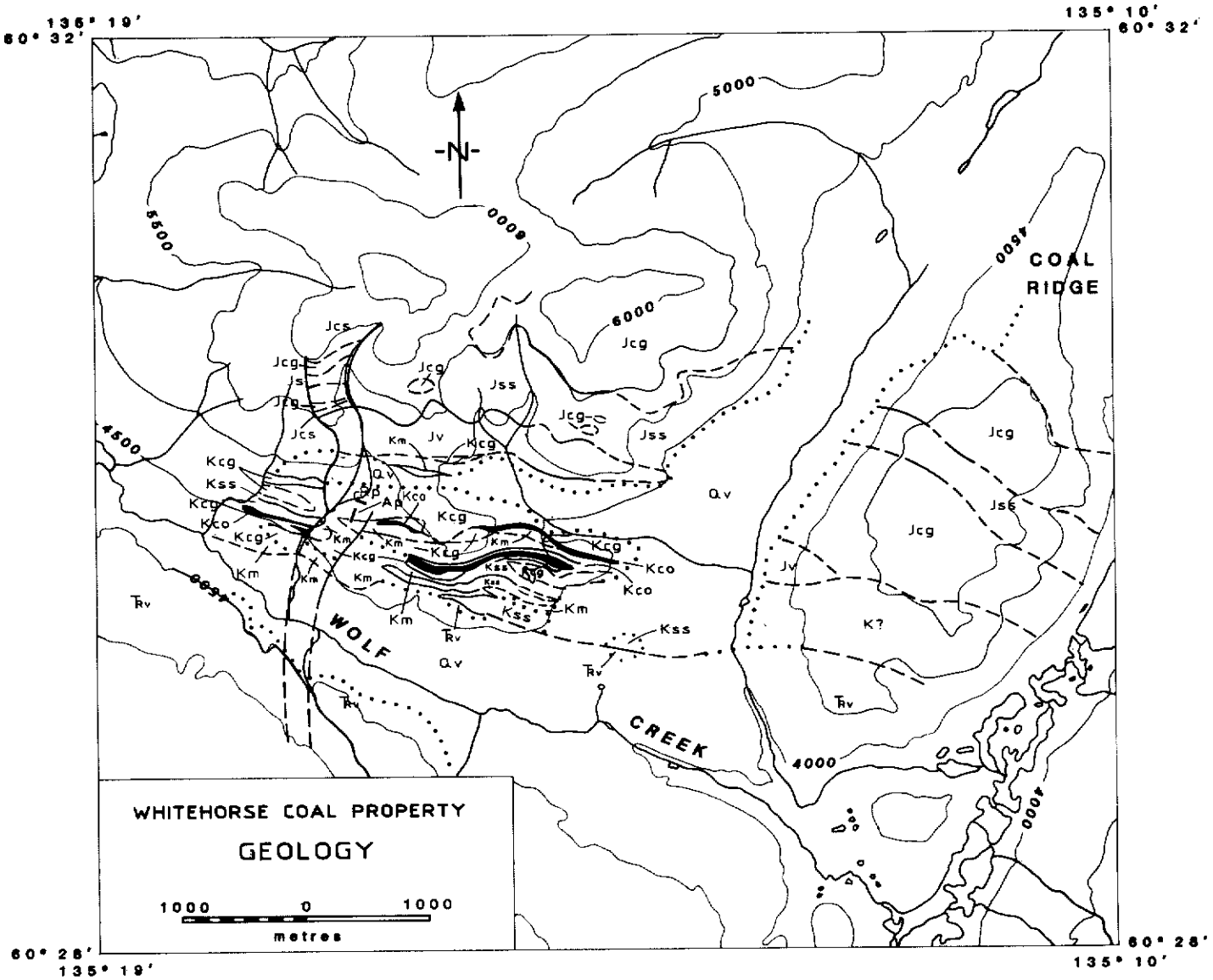

Figure 1 Geological map of the Whitehorse Coal property.

wall slope of 60°. The volume of the main pit was estimated at 15,297 cubic metres.

STRATIGRAPHY

The Whitehorse coal deposits lie within non-marine strata of the Early Cretaceous Tantalus Formation which occupy a graben 1.7 km long extending from Double Mountain which lies 10 km east of Mt Granger to Fish Lake 10 km northwest of Mt Granger. Figure 1 shows the central part of the graben which is bounded on the north side by coarse submarine fan conglomerates and deep basinal shale and greywacke of the Jurassic Laberge Group (J. Dickie, personal communication), and on the south side by pyroclastic rocks and siltstone of the Triassic Lewes River Group.

LEGEND

QUATERNARY

QV alluvium, glacial deposits.

EOCENE?

Rp rhyolite-porphyry dykes.

EARLY CRETACEOUS

Tantalus Formation (non-marine floodplain deposits).

Kcg conglomerate: generally clast-supported. Well-rounded chert pebbles in sandstone matrix.

Kss sandstone, commonly coarse-grained, pebbly to gritty, displays trough cross bedding.

Km mudstone, commonly carbonaceous grading to coal. Associated fine dark silty sandstone and siltstone.

Kco coal, with variable shale partings and thin mudstone bands.

JURASSIC

Laberge Group (submarine fan and basinal deposits).

Jcg conglomerate, massive, weathers pinkish: matrix-supported with well rounded cobbles 15-20 cm dia. of augite porphyry, green and white speckled crystal tuff and lesser granodiorite in a dark muddy matrix.

Jss sandstone, feldspathic, weathers pinkish. Grades to greenish crystal tuff.

Js argillite: dark grey with minor very fine silt and sand laminations.

Jcs chert, banded, and siliceous hornfels.

TRIASSIC

Lewes River Group (island arc volcanics).

Trv tuff, green and white speckled lithic tuff with feldspar crystals.

Tra argillite, dark grey, weathers brown.

The Tantalus Formation in the Mt. Granger area is approximately 670 m thick and consists of braided river or alluvial fan conglomerate and sandstone interlayered with fine-grained siltstone, mudstone and coal. More than nine major channels can be mapped near the Mt. Granger area. Individual channels up to 2 km wide are flat-bottomed and lenticular in cross-section and appear to have a width to depth ratio of more than 16:1. Paleocurrent indicators show the main flow was from a northwest to northeast direction. Floodplain deposits are laterally extensive and well preserved due to the lack of downcutting by the aggrading channels above.

Channel-fill deposits range from clast-supported pebble conglomerate to matirx-suported conglomerate, coarse grit and pebbly sand. The coarser channel fill (Figure 2) consists of rounded 1-4 cm pebbles of dark grey chert and minor white quartz in a matrix of fine well-sorted scoured sand. Lag deposits may contain pebbles up to 8 cm. The channels show scoured bases, with flute casts commonly preserved on the underside (Figure 3). The finer channel deposits are commonly cross-stratified with beds 5-30 cm thick. Both coarsening and fining-upward trends are seen and some depositional units show reversals.

Floodplain deposits consist of crossbedded silty sandstone, siltstone, mudstone, carbonaceous shale and coal (Figure 4). Mudstone bands up to 15 cm thick and shale partings in the coal seams caused by frequent overbank flooding are reflected in the high ash contents of some samples.

Two main coal seams have been reported in the area (Figures 5 and 6). The lower seam, exposed in trenches at the base of West and East Hills ("Coal Zone B" of Perry, 1984) is a minimum of 3.3 m thick and is overlain by up to 6 metres of siltstone, mudstone and fine-grained crevasse-splay sands. Mapping strongly suggests the lower seam is continuous over a strike length of at least 1 km with no decrease in thickness. In the main pit at the base of West Hill a 15 cm thick rhyolite sill intrudes the coal seam. For 8 cm either side of the dyke the coal has been baked to a porous coke-like material showing columnar jointing (Figure 7). Coal sampled in the main pit may be of higher rank than coal elsewhere on the property due to the local heating.

The upper seam (Perry's "Coal Zone A") is 1.8 m thick and is exposed almost continuously in trenches and pits between Fisher Creek and East Hill, a strike length of 2 km. The coal layer is overlain directly by massive channel-fill conglomerate, or separated from it by less than 1 metre of mudstone. Coal seams of similar thickness and stratigraphic position are reported to outcrop on Coal Ridge and Double Mountain, up to 8.4 km along strike to the east.

The upper coal seam is also exposed on the west side of Fisher Creek where it was penetrated by an adit prior to 1906. However, it appears to have been displaced across a north-trending fault which follows the lower part of the creek. On the west bank of the creek the fine-grained floodplain deposits underlying the upper coal seam are at least 69 metres thick and contain at least four other coal seams including the middle and lower seams reported by Cairnes (1906), Taylor (1969) and Hill (1982). A greater thickness of recessive floodplain sediments on the west side would explain the lack of outcrop west of the fault.

STRUCTURE

Figure 8 shows discordant bedding attitudes across the bounding faults of the graben. Within the graben the Tantalus Formation is deformed by large open upright folds which plunge northward. Pervasive north-south cleavage is probably axial planar to these folds (Figure 9).

Figure 10 shows channel-fill conglomerate at the east end of the main pit on West Hill folded into an open anticline. The coal intersected in drillholes above the main pit appears to be thickened in the axis of this anticline. Several small faults with about 2 metres displacment have offset the underlying coal and mudstone layers only, suggesting soft-sediment deformation.

Fisher Creek appears to follow the trace of a sinuous strike-slip fault. Slickensides along the creek plunge consistently northward at low angles. Approximately 100 metres of sinistral movement would account for the displacement of Coal Zone across the creek.

Figure 2 Channel-filled deposit: massive chert-pebble conglomerate.

Figure 3 Flute casts at the base of the channel which overlies the lower coat seam.

DISCUSSION

Fine-grained floodplain sediments in the Mt Granger area tend to be recesive-weathering while the channel deposits outcrop as resistant ridges. The association of the coal with the floodplain facies suggests that these low-lying areas should be the focus of further exploration

Figure 4 Conglomerate channel scoured into silty and fine sandy floodplain deposits exposed in main pit. A 3.4 m coal seam (coal zone 'B') is exposed at the base of the section.

Figure 5 East Hill from the summit of West Hill. Upper and lower coal seams dip 30-50 degrees N between layers of channel-filled conglomerate.

The Tantalus Formation sediments observed in the Mt Granger area are friable and unmetamorphosed. Even the conglomerate can be broken by a bulldozer blade (P. Poggenburg, personal communication). Consequently, coal seams exposed at the surface should be readlily mineable along strike by open-pit methods, but coal-bearing strata generally dip at a 30-50° angle, and substantial reserves would only be accessible by underground mining. Variations in the thickness of the seams may be found due to the open north-plunging folds.

Variations in coal rank may be expected due to local thermal alteration by intrusive rocks which intrude the coal-bearing sediments. A rhyolite and an andesite dyke outcrop on the ridge east of Fisher Creek, and rhyolite sills intrude coal at the West Hill showing. The extent of these volcanic rocks is still unknown.

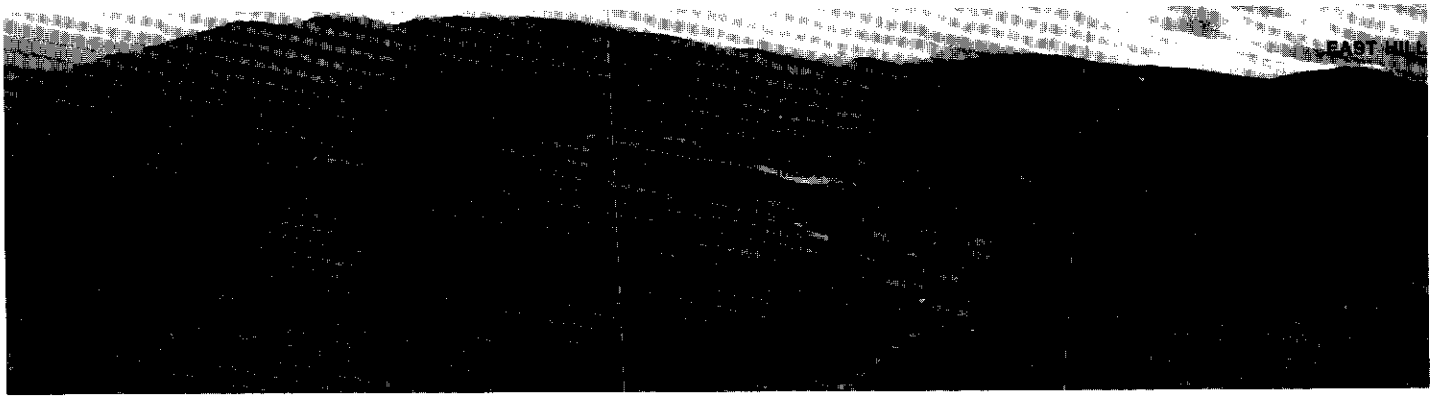

Figure 6 Whitehorse Coal Property looking south, showing location of upper and lower coal seams.

Figure 7 Baked margins of lower coal seam which has been cut by a thin rhyolite sill. Coal shows columnar jointing for about 8 cm on either side of the sill.

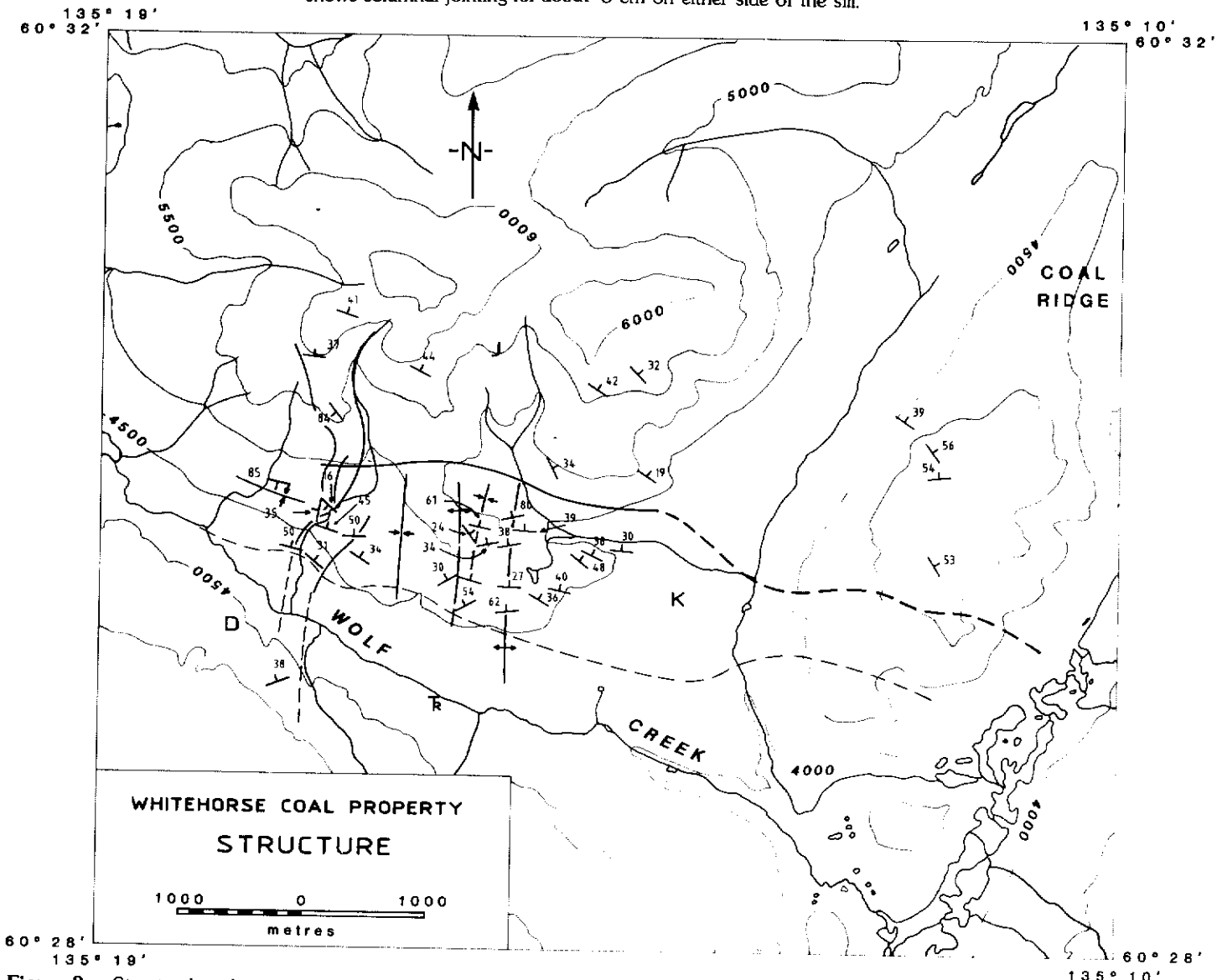

Figure 8 Structural geology of the Whitehorse Coal Property.

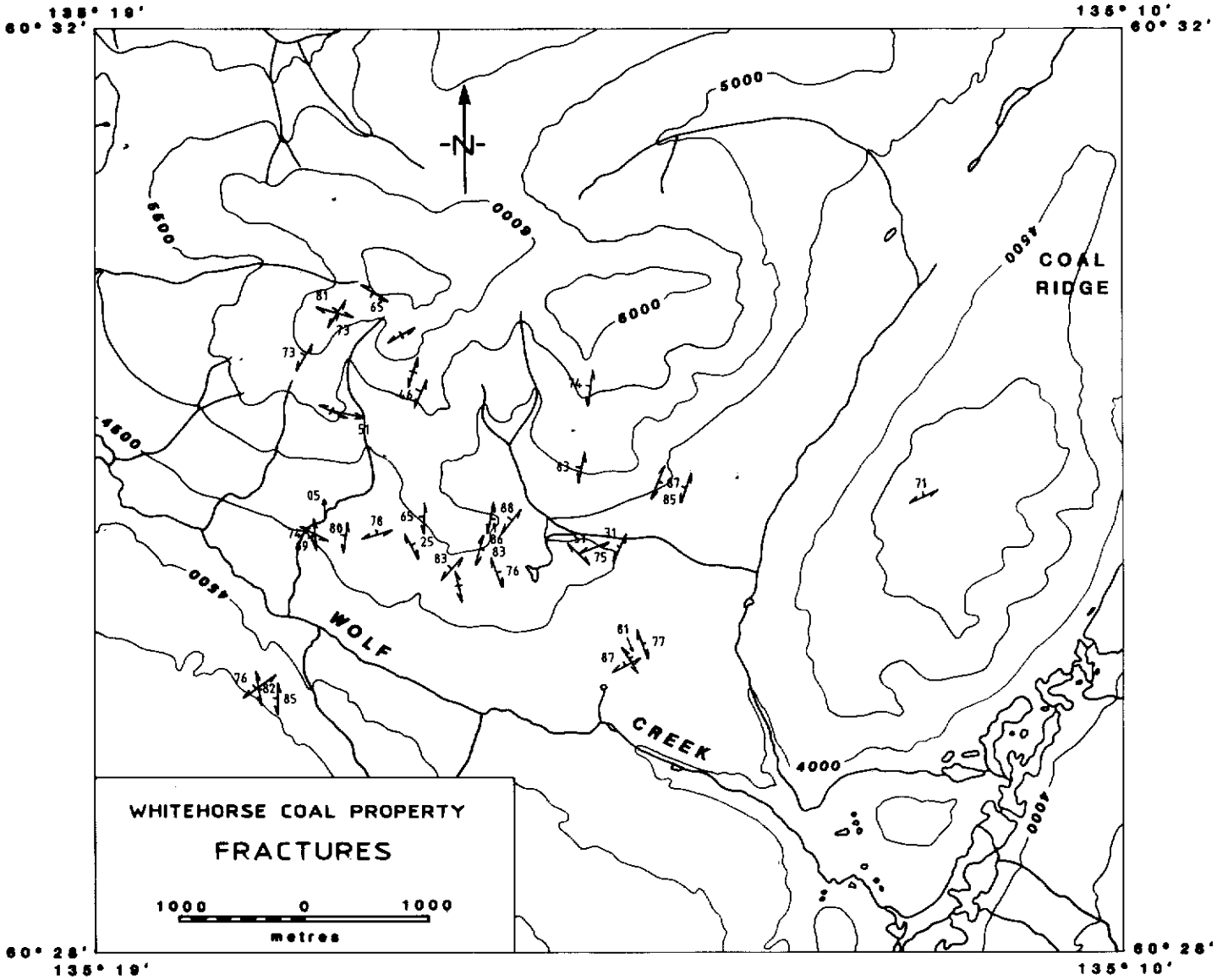

Figure 9 Fractures on the Whitehorse Coal Property.

WEST EAST

Figure 10 Synsedimentary faulting of coal and mudstone layers at east end of main pit.

REFERENCES

CARLYLE, L.W., 1985. Report on the 1985 Drill program, Whitehorse Coal Property, Whitehorse Mining District, Yukon; Unpublished Assessment Report #092012.

CLARK,D., 1986. Whitehorse Coal Coporation: Construction Summary for Excavation of Pit #1; Unpublished Assessment Report #092045.

DOWNING, D.A., 1986. Whitehorse Coal: a summary by D.A. Downing of assessment report 061248 by J.H. Perry; in Yukon Exploration, 1984, Indian and Northern Affairs Canada p.72.

GALLOWAY, W.E. and HOBDAY, D.K., 1983. Terrigenous Clastic Depositional Systems: Applications to Petroleum, Coal and Uranium Exploration; Springer-Verlag.

HILL, R.P., 1983. Whitehorse Coal Corporation; Unpublished Assessment Report #062148.

HUGHES, J.E., 1975. Watson Coal Prospects, Yukon. Unpublished Assessment Report #061735.

PERRY, J.H., 1984, 1986. Report on the Whitehorse Coal Property, Yukon Territory for Whitehorse Coal Corporation; Unpublished Assessment Reports #062171 and #092024.

SAVAGE, A.T., 1986. Prospecting and Examination Report; Unpublished Assessment Report #061734.

TAYLOR, R.S., 1969. Unpublished Consultant Report for Luscar Limited.

GOLD AND SILVER, LEAD DEPOSITS OF THE KETZA RIVER DISTRICT, YUKON: PRELIMINARY RESULTS OF FIELD WORK

Michael S. Cathro
Department of Geology and Geological Engineering
Colorado Schools of Mines
Golden, Colorado 80401

CATHRO, M.S., 1988. Gold and silver, lead deposits of the Ketza River District, Yukon: Preliminary results of field work; in Yukon Geology, Vol. 2; Exploration and Geological Services Division, Yukon, Indian and Northern Affairs Canada, p. 8 - 25.

ABSTRACT

The Ketza River gold deposits, in central Yukon, are gold-bearing, massive sulphide mantos and chimneys in Lower Cambrian limestone. Mining is presently confined to oxidized portions of the deposits. The deposits are bounded on three sides by silver-rich veins. Metal zoning corresponds to a pronounced domal uplift that is thought to be related to a buried Cretaceous intrusion. The zoning may partly reflect stratigraphic control, but distance from the buried intrusion is considered the prime control.

RÉSUMÉ

Les gîtes aurifères de Ketza River, dans le centre du Yukon, sont des mantos et cheminées de minerai sulfuré massif aurifère, à l'intérieur de calcaires du Cambrien inférieur. Actuellement, l'exploitation minière se limite aux portions oxydées des gîtes. Ces gîtes sont limités sur trois faces par des filons argentifères. La zonation des métaux correspond à un soulèvement prononcé en forme de dôme, qui à notre avis est lié à la présence d'une intrusion crétacée située en profondeur. Il est possible que la zonation reflète partiellement le contrôle stratigraphique, mais on considère la distance de l'intrusion enfouie comme le principal élément de contrôle stratigraphique.

INTRODUCTION

The Ketza River gold deposit, jointly owned by Canamax Resources Inc. and Pacific Trans-Ocean Resources Ltd. is the largest lode gold deposit discovered in Yukon to date, and is the Yukon's next gold mine. The Ketza River deposit is bounded on three sides by numerous silver-lead veins informally known as the "Iona Silver Property". Together, these deposits comprise the Ketza River District.

Two aspects of the geology are of particular interest. Firstly, the style of gold mineralization is new to Yukon. Auriferous epigenetic massive iron, arsenic and copper sulphides or supergene, iron oxides occur mainly as stratabound "mantos" (or blankets) in thickly bedded Lower Cambrian limestone. Lead and zinc minerals are rare and silver values low. The mantos comprise a previously unrecognized type of gold deposit in the northern Cordillera, and perhaps present a gold-rich analogue of the silver-rich replacement deposits at Midway, British Columbia; Leadville, Colorado; Bingham and Tintic, Utah; and Santa Eulalia, Mexico.

Secondly, the district exhibits an obvious concentric zoning pattern of metals and style of mineralization, with gold occurring near the centre of a conspicuous, domal uplift, and silver-lead mineralization occurring more distally. The zoning may be partly the result of stratigraphic control of mineralization. The uplift is probably underlain by a middle Cretaceous stock although no intrusive rocks have been located. Mineralization in the Ketza River District is thought to be genetically related to this stock.

This report presents the preliminary results of field work which will form the basis of a Master of Science thesis at the Colorado School of Mines. It is based on outcrop, drill-core and underground examinations of the Ketza River gold deposits during the 1984 and 1986 field seasons. Study of the surrounding silver-lead occurrences during 1986 was confined to examination of surface exposure and dump material because most of the workings are inaccessible and drill-core is not available.

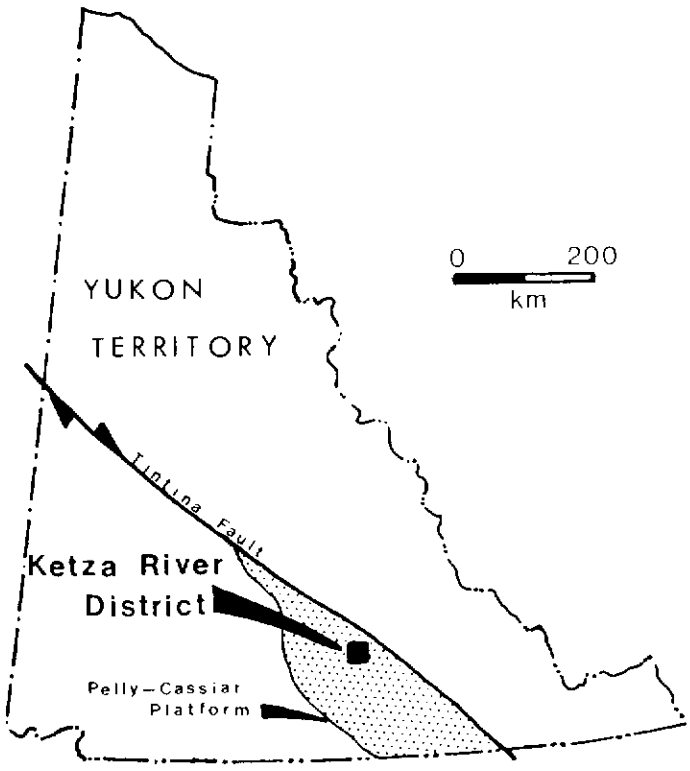

Figure 1. Location map of the Ketza River District, Yukon.

LOCATION AND HISTORY

The Ketza River District (Fig. 1) covers an area roughly 10 km by 10 km. It is centered 50 km south of the town of Ross River in

the rugged St. Cyr Range of the Pelly Mountains (N.T.S. 105 F 09, 61°32'N, 132°15'W). A 45 km gravel road connects the Canamax camp with the Robert Campbell Highway at a point 23 km southeast of Ross River.

The first discovery in the district was a silver-lead vein found in 1947 by Hudson Bay Mining and Smelting Co. Ltd. The Ketza River gold deposit (formerly known as the BOOM or WOODCOCK showing) and many of the larger silver-lead occurrences, were discovered by Conwest Exploration Co. Ltd. and others in 1954 and 1955. The silver-lead veins have been intermittently explored with trenching, drilling, and underground work (12 short adits) by various interests until the present with only limited success. Only very minor production of hand cobbed ore has taken place. The STUMP (or 1) vein, discovered in 1966, is the best explored and by far the largest of the veins with probable reserves of 49,800 tonnes grading 20.0% Pb and 719.9g/t Ag (Orssich et al., 1985).

Conwest explored the Ketza River gold deposit with trenching and 59 drill holes from 1955 until 1960, and outlined sulphide reserves of 68,000 tonnes grading 12 g/t Au (Rotherham, 1958). The property then lay dormant until 1984 when Pacific Trans-Ocean Resources Ltd optioned the property from Conwest and entered into a joint venture agreement with Canamax Resources Ltd. Aggressive drilling and underground development to the end of 1986 had delineated reserves of 1.0 million tonnes averaging 13.7 g/t Au (Northern Miner, February 9, 1987).

Two factors have been primarily responsible for the greatly increased tonnage and economic viability of the Ketza River gold deposit: 1) appreciation by Canamax geologists of the geometry and ore controls of similar deposits in the U.S. and 2) recognition of the potential for large tonnages of metallurgically superior oxide mineralization in structurally prepared zones.

REGIONAL GEOLOGY

This summary of the regional geology is based on published descriptions of the geology of the Pelly Mountains and Ketza River District, including Wheeler et al. (1960), Tempelman-Kluit (1977a, 1977b, 1979, in prep.), Tempelman-Kluit et al. (1975, 1976), Read (1980), and Abbott (1986). The Ketza River district is underlain by moderately folded and faulted Paleozoic miogeoclinal strata of the Pelly-Cassiar Platform (Fig. 1), which are interpreted as autochthonous and parautochthonous to the North American craton by Tempelman-Kluit (1977a).

Four significant thrust faults, the McConnell, Porcupine-Seagull, Cloutier, and St. Cyr Thrusts, run parallel to the Tintina Fault and dip generally southwest (Abbott, 1986). Most rocks in the Ketza River District are part of the Cloutier Thrust Sheet although two small klippen belong to the overlying Porcupine-Seagull Thrust Sheet. Thrusting probably occured during the Late jurassic and Early Cretaceous (Tempelman-Kluit, 1979). The northwest-trending Tintina Fault located 15 km northeast of the District, (Fig. 1), has experienced at least 450 km of dextral, transcurrent offset since the middle Cretaceous (Gabrielse, 1985).

The most prominant structural feature in the Pelly Mountains is the Ketza-Seagull Arch (Abbott, 1986), an elongate, northwest-trending window through the Porcupine-Seagull Thrust that is probably underlain by, and related to buried Cretaceous intrusions. Abbott considered the Arch to be made up of two smaller domal structures, the Seagull Upleft and Ketza Uplift. Structure in the window is characterized by steeply dipping normal faults.

The Ketza Uplift, situated in the center of the Ketza River District (Fig. 3, was first postualted to be underlain by an intrusion by Parry et al. (1984). This theory is supported by the presence of a magnetic anomaly, hornfelsing, and hydrothermal alteration immediately north of the Ketza River gold deposit. The hornfels has been dated by whole-rock K-Ar as Middle Cretaceous (101 ±4 Ma; K.M. Dawson, .S.C., 1986, pers. comm. to S.E. Parry).

LOCAL GEOLOGY

The Ketza River District is underlian by five main units that range in age from Lower Cambrian to Missisippian. These are shown in

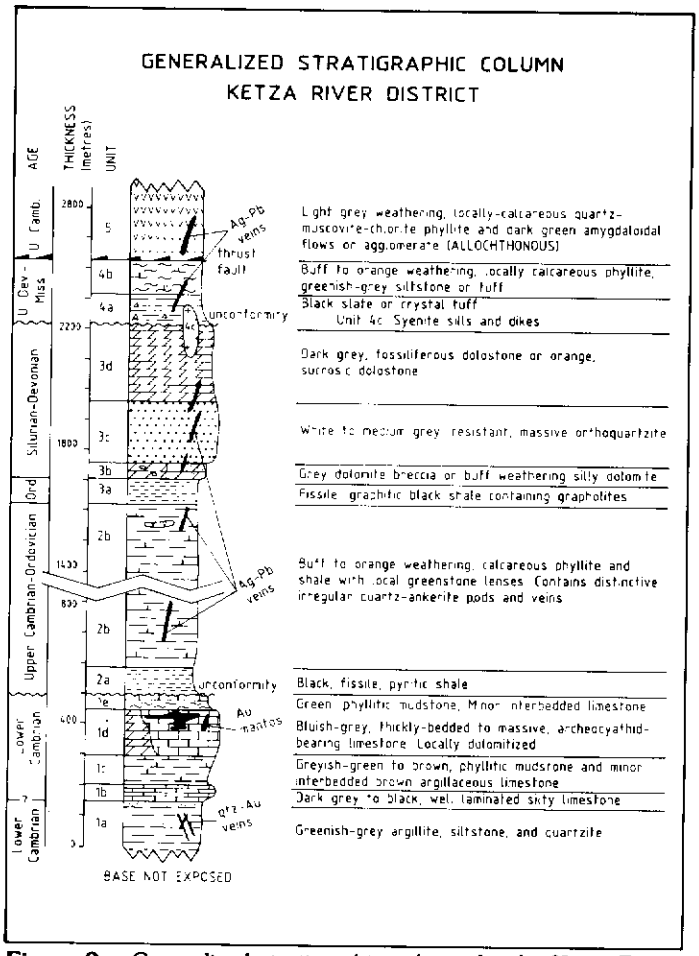

Figure 2. Generalized stratigraphic column for the Ketza River District including the relative positions of important mineral deposit types (modified after Tempelman-Kluit, 1977a; Read, 1980; and unpublished Canamax Resources reports).

Figures 2 (generalized stratigraphic column) and 3 (simplified geology map). Cambrian through Mississippian strata of units 1 to 4 belong to the Clouteir Thrust Sheet and strata of unit 5 belong to the structurally overlying Porcupine-Seagull Thrust Sheet.

An excellent description of the Lower Cambrian sedimentary rocks (Unit 1) near the Ketza River gold deposit has been presented by Read (1980). His terminology of subunits within Unit 1 is adopted here with minor modifications. The other units are mainly modified after Templeman-Kluit (1977a) and unpublished company maps.

Unit 1: Lower Cambrian

The Lower Cambrian succession has been split into five lithostratigraphic subunits (1a through 1e) with an aggregate thickness greater thatn 500 m. The lower contact is not exposed and the upper contact is an uncomformity of probable Upper Cambrian age.

Unit 1a contains the oldest rock exposed and comprises green argillite, siltstone, and quartzite. The unit contains a strong hornfels on the north side of the ridge that hosts the Ketza River gold deposits.

Unit 1b, a narrow bed (25 to 60 m thick) of resistant, dark grey to black, well laminated, silty limestone conformably overlies Unit 1a. Contacts are sharp and the unit is an excellent marker.

Unit 1c consists Early Cambrian fossils and is composed of greyish green to brown, recesive-weathering, calcareous, phyllitic mudstone with minor interbedded argillaceous limestone. Large pyrite cubes may be present. This unit may be as much as 100 m thick. The upper contact with Unit 1d is gradational and arbitrary since it is defined as the point where carbonate makes up to more than half of the rock (Read, 1980).

Unit 1d, the main host for gold mineralization, is distinctive grey-blue, thickly bedded to massive, archeocyathid-bearing, cliff-forming limestone (Fig. 4). The unit is 120 to 180 m thick and made up

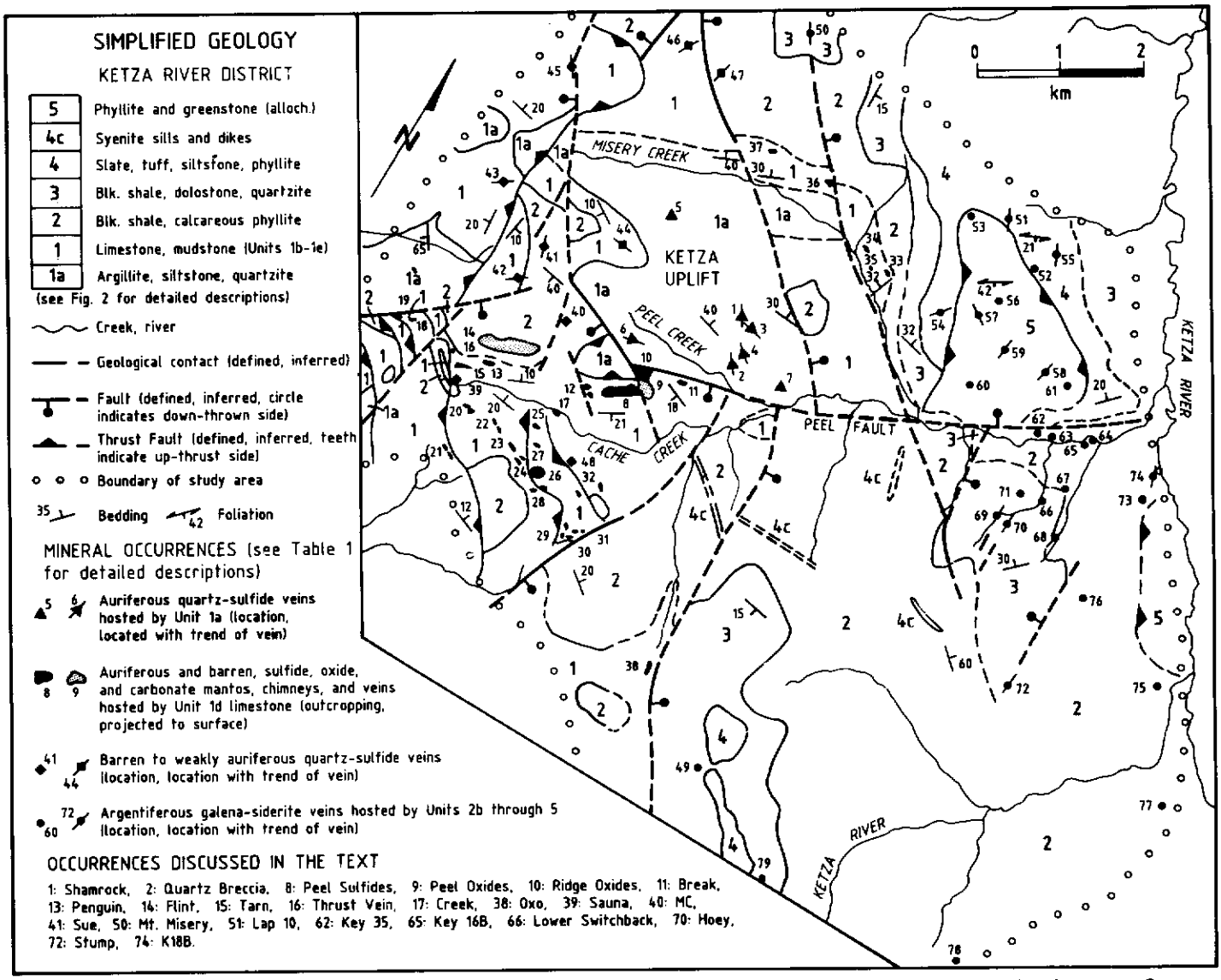

Figure 3. Simplified geology map of the Ketza River District including the locations of mineral occurrences discussed in this paper. Summary descriptions of all occurrences are given in Table 1. (Geology modified after Tempelman-Kluit, 1977a; 1980; and unpublished Canamax Resources maps).

predominantly lime mudstones with argillaceous interbeds near its base. Large archeocyathid buildups (archeocyathid bindstone and skeletal sand) are reported near the bottom of Unit 1d along the southern edge of the district (Read, 1980). Bedding attitudes are generally difficult to determine because the rocks are strongly bioturbated. To the west and north of the main Ketza River gold deposit, the limestones are strongly dolomitized and are blocky and orange weathering.

Unit 1e, a narrow (0 to 50 m thick) marker bed of non-calcareous, phyllitic green mudstone is interbedded with limestone within 10 m of the top of Unit 1d. In places, the upper limestone and green mudstone are completely missing, suggesting that the upper contact is an unconformity.

Unit 2: Upper Cambrian-Ordovician

Cambro-Ordovician rocks in the Ketza River District comprise a lower unit of black shale (Unit 2a) and a thick, upper unit of buff weathering, calcareous phyllite or shale (Unit 2b). Both weather recessively, making thicknesses and contact relations difficult to determine.

Drilling has shown Unit 2a to be at least 30 to 100 m thick. Unit 2b is at least 1000 m thick. A major unconformity probably exists beneath the black shale (Unit 2a). This unit was not described by Tempelman-Kluit (1977a), or Read (1980). It's age, though uncertain, is probably Upper Cambrian. In this study, it is grouped with Unit 2b. Unit 2b is strongly deformed and contains small, distinctive, irregular quartz-ankerite veins. Near large quartz veins, the calcareous phyllite is altered to blocky weathering, sucrosic dolomite. Large galena-siderite veins are hosted by Unit 2b.

Unit 3: Ordovician-Silurian-Devonian

Unit 3 includes four distinctive subunits that range in age from Ordovician to Devonian. Most host galena-siderite veins.

Unit 3a, the lowermost member, is recessive, fissile, graphitic, black graptolitic shale with minor interbedded calcareous, silty, and muddy beds. It is 50 to 100 m thick and Ordovician to Silurian in age.

Unit 3b, overlying the black shale, is a thin discontinuous interval of buff weathering, grey, silty dolomite and well indurated dolomite breccia with a dark grey dolomite matrix. Large coral fragments have been found at one location. This unit hosts weakly disseminated and vein-type Ag-Pb mineralization at the LOWER SWITCHBACK showing.

Unit 3c is distinctive white to medium grey, massive, resistant orthoquartzite. In many places it lies directly on Unit 3a black shale.

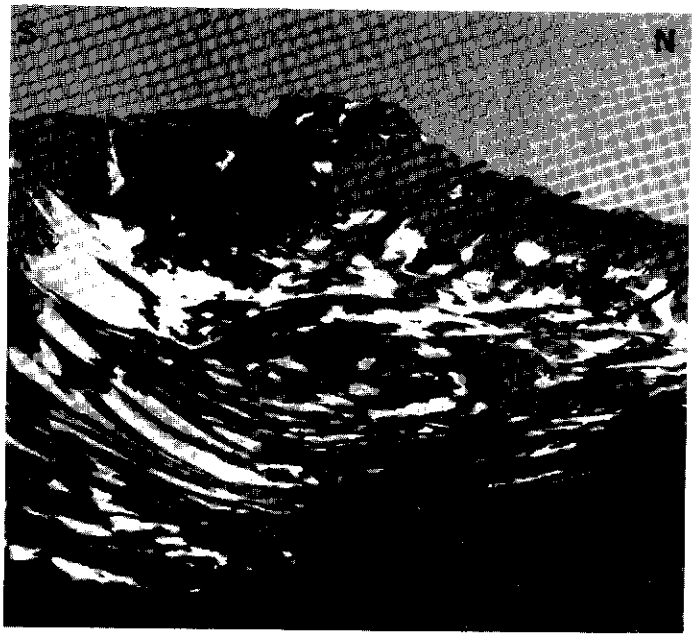

Figure 4. Thrust imbrication of Unit 1d limestone at the head of Cache Creek (looking west). Unit 1d hosts gold-rich sulfide/oxide mantos and chimneys in the district.

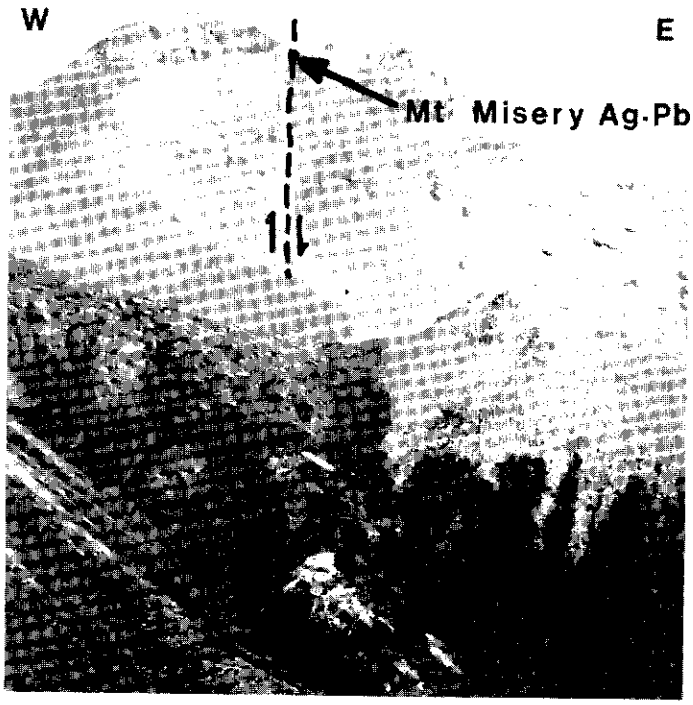

Figure 5. North-trending, steeply dipping fault in saddle on Mt. Misery. The east side of the fault has moved down approximately 100 m. Galena-siderite vein mineralization occurs in the fault (Occurrence #50).

It is at least 150 m thick and is Silurian. It hosts galena-siderite and quartz-pyrite-gold mineralization at the MT MISERY and HOEY showings.

Unit 3d is predominantly well-bedded, dark grey fossiliferous dolostone of Devonian age. On Mt. Misery, fine to medium-grained sucrosic, orange weathering dolomite overlying the quartzite (Unit 3c) is probably equivalent to Unit 3d.

Unit 4: Devonian-Mississippian

These rocks are equivalent to the Earn Group of Gordey et al. (1985) and consist of a lower member (Unit 4a) of black slate and dark grey to black, cherty siltstone or crystal tuff with minor interbedded chert, sandstone, chert pebble conglomerate and green tuff. The lower contact with carbonate is usually unconformable (Gordey et al., 1985).

Unit 4b overlies the black slate and includes buff-orange weathering, locally calcareous phyllite, and greenish-grey siltstone or tuff of unknown thickness.

Mississippian intrusive rocks (Unit 4c), consist of rare syenitic sills and dykes. A small diorite plug near the KEY 3 showing is surrounded by a pyrite aurole and alteration in overlying Mississippian volcanic rocks.

Unit 5: Upper Cambrian and Ordovician

Two klippen of volcanic rocks belonging to the Porcupine-Seagull Thrust Sheet occur near the junction of Cache Creek and The Ketza River. They are predominantly recessive, light grey weathering, locally calcareous, quartz-muscovite-chlorite phyllite, and green, moderately foliated, amygdaloidal volcanic flows and agglomerate, Minor chert and dark green diorite has also been reported (Orssich et al., 1985). The larger of the two lkoppen occurs north of Cache Creek, dips gently to the south, and is in contact with all rocks types from the Upper Cambrian phyllite to Mississippian volcanic rocks. The unit exceeds 200 m in thickness.

STRUCTURE

As stated above, the Ketza Uplift dominates the Ketza River District. The most obvious structures are southwest-dipping thrust faults with relatively small displacements, and steeply dipping, east, north and northwest trending normal faults. Most strata are gently folded and moderately dipping except near thrust, where drag folding has occurred.

Northeast-directed thrusts other than the Porcupine-Seagull Thrust are only documented in the well studied Lower Cambrian rocks (Fig.4). The highly contorted nature of the Cambro-Ordovician calcareous phyllite (Unit 2b) suggests that this unit may also have been inbricated by thrusting. Thrust-related folds have gently dipping axial planes and upright to overturned forelimbs (Fig. 4).

At least three sets of steeply dipping faults cut the thrust faults. These faults form the eastern, western and southern margins of the Ketza Uplift and are thought to reflect intrusion-related doming.

The Peel Fault is an east-trending, steeply north-dipping reverse fault located immediately north of the Ketza River gold deposit. The fault extends down Cache Creek and responsible for the 200 to 300 m of offset of strata on either side of the Cache Creek valley.

Northwest-trending faults are nearly vertical. The fault east of the SHAMROCK zone with at least 400 m offset is one of the largest and may be the offset extension of the fault east of the OXO showing. Most of the silver-lead occurrences occur near vertical north-trending faults of relatively small displacement (Fig. 5).

Faults near the Ketza River gold deposit are complex and are an important control on mineralization. The strong northwest-trending fault set crosscuts the east-trending Peel Fault and thrust faults.

MINERALIZATION

Over a hundred mineral showings occur in the Ketza River District. These can be broadly classified into four main types as follows:

1. auriferous quartz-arsenopyrite + pyrite veins cutting Lower Cambrian argillite/quartzite (Unit 1a),

2. auriferous and barren sulphide, carbonate and oxide mantos, chimneys and veins hosted in Lower Cambrian limestone (Unit 1D),

3. barren to weakly auriferous quartz + arsenopyrite veins and stockworks cutting Lower Cambrian limestone (Unit 1d) and Cambrian-Ordovician calcareous phyllite (Unit 2b),

4. argentiferous galena-siderite veins cutting Upper Cambrian through Mississippian strata (Unit 2b to Unit 5).

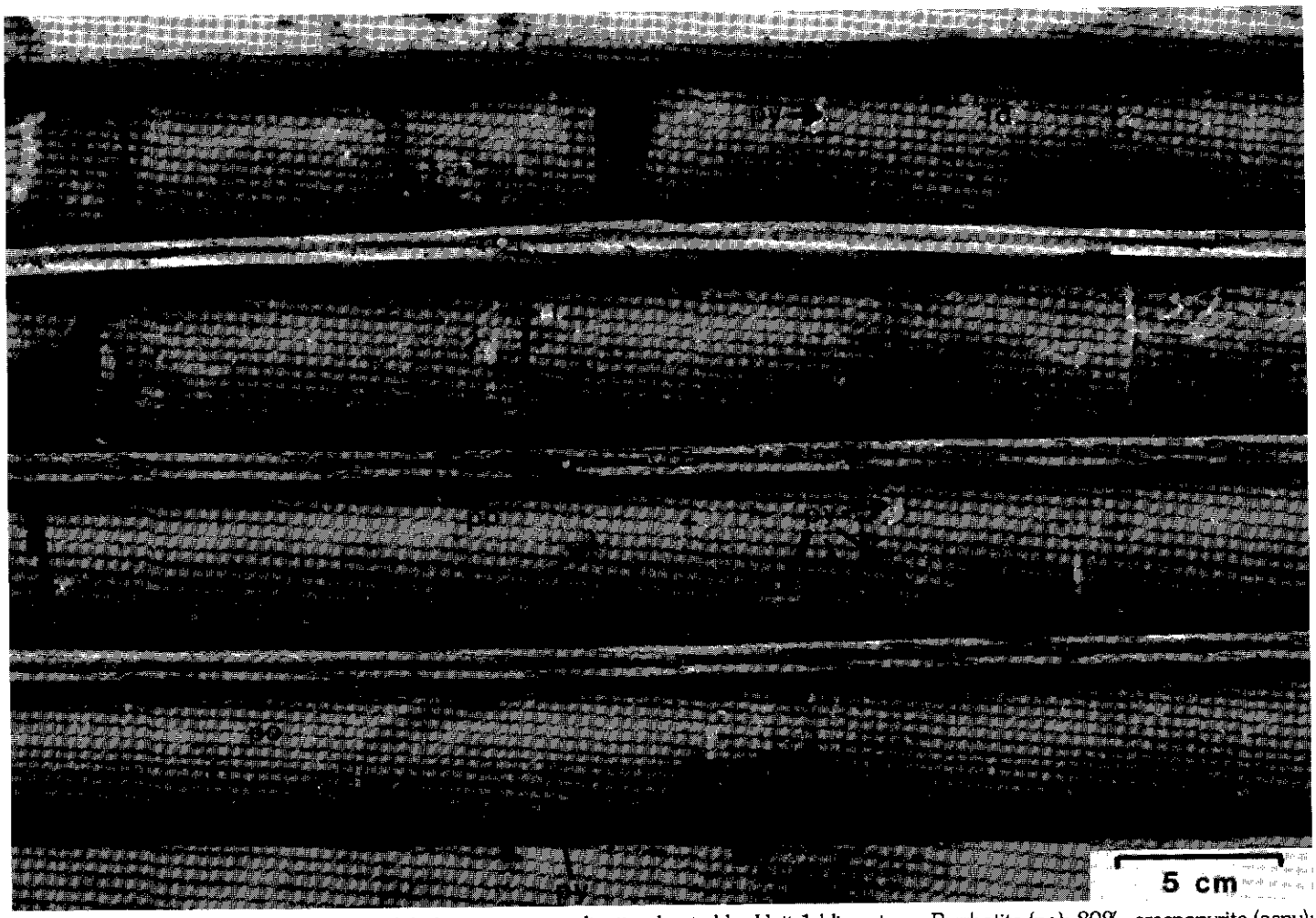

Figure 6. Typical, gold-rich massive sulphide manto mineralization hosted by Unit 1d limestone. Pyrrhotite (po): 80%, arsenopyrite (aspy): 10%, pyrite (py): 2%, chalcopyrite (not visible): 0.5%, remnant Unit 1d limestone fragments (1d): 7-8%. (Peel Zone, DDH KR-84-09).

These deposit types are zoned and coincide with the distribution of rock types about the Ketza Uplift. Type 1 fold-rich quartz veins are surrounded by Type 2 gold-rich mantos which are in turn surrounded by Type 4 silver-lead veins. Type 3 veins show an erratic distribution. For simplicity, the types are described in this order.

Locations of the showings are shown on Figure 3 and some of the important features (mineralogy, attitude, host rock, etc.) are given Table 1.

(1) Gold in Proterozoic argillite

Important gold-bearing quartz-arsenopyrite veins at the SHAMROCK and QUARTZ BRECCIA zones (Fig. 3) occur in argillically altered argillite and quartzite of Unit 1a near the approximate centre of the Ketza Uplift. The QUARTZ BRECCIA zone is a vein zone 200 m long by 24 m wide that strikes 300° and dips moderately east just north of Peel Creek. At surface, veins are composed of coarse, granular quartz, scorodite, and minor arsenopyrite. In the SHAMROCK zone 700 m farther north, similar veins also trend northwesterly. Surface samples containing mostly scorodite have returned assays up to 1000 g/t au (Northern Miner Magazine, March, 1987, p. 35).

FRED'S VEIN occurs approximately 500 m north of the Ketza River gold deposit in hornfelsed argillite of Unit 1a. It trends east-northeast, dips steeply and has a higher sulphide content than the Shamrock-type veins. Locally, this vein contains massive pyrrhotite-arsenopyrite not unlike the sulphide mantos and veins in Lower Cambrian limestone.

(2) Gold in Lower Cambrian limestone

Lower Cambrian limestones of Unit 1d host the Ketza River gold deposit and similar but smaller, lower grade occurrences over an area of 6 km by 4 km (Fig. 3). The deposits consist of massive sulphide, carbonate, or oxide mantos, chimneys, and veins. The largest deposits (the TARN, PENGUIN, FLINT, BREAK and PEEL zones (occurrences 8 to 15) fall along a 2 km lineament trending 080° (Fig. 3) suggesting structural control. All deposits occur in the upper 100 m of the Lower Cambrian limestone, indicating that stratigraphy is also an important ore control.

The deposits are either sulphide-rich or oxide-rich. The latter appear to be in situ supergene replacements of the sulphides. Their superior metallurgical properties and grade (average 18 g/t versus 9 g/t for sulphides), make the oxides the most economically important. The sulphides are more common and better exposed.

Sulphide mineralogy

The mineralogy of the sulphide bodies is simple, consisting mainly of semi-massive to massive pyrrhotite, with variable quantities of arsenopyrite, pyrite and minor chalcopyrite (Fig. 6). Some deposits south of Cache Creek contain significant siderite.

Arsenopyrite averages 5 to 10% by volume and forms large (2 to 5 mm) euhedral grains disseminated throughout the pyrrhotite. Arsenopyrite also locally forms narrow (5 mm) bands around remnant limestone clasts enclosed in pyrrhotite (Fig. 6). In some places massive pyrrhotite contains small (3 m by 20 m) discrete lenses of massive (90%) arsenopyrite.

Figure 7. Underground exposure of oxide mineralization consisting of earthy limonite (near hammer) and dark brown "hisingerite" (h). Gold values are often associated with "hisingerite". (1450 level, Peel Zone oxides).

Pyrite is common as large (to 5 cm) subhedral masses but rarely makes up more than 50% of the total sulphides. Chalcopyrite is common as a fine network between other sulphide grains and makes up 0.5 to 1% of the sulphides by volume.

Gold is irregularly distributed but correlates best with arsenopyrite and total sulphide content. Only in the PEEL zone are sulphides consistently auriferous. Only erratic high values have been encountered in showings distal from the PEEL zone. Tooney (1985) determined that gold generally occurs as 0.5 to 25 micron grains associated with native bismuth and chalcopyrite which fill fractures in other sulphides. Spheroidal gold inclusions in pyrrhotite and pyrite were also noted.

Galena and sphalerite are extremely rare in most sulphide deposits, with small amounts noted in the PEEL zone and the CREEK showing and significant quantities in the OXO showing (Fig. 9).

Oxide mineralogy

Gold-bearing oxide material is composed of limonite, hematite, other unidentified hydrous iron oxide minerals and quartz. Gold grades are often highest where an unusual yellow, orange, red or brownish black, conchoidally-fracturing amorphous mineral is present (Fig. 7). Conwest geologists referred to this as "hisingerite" which is actually a mineraloid. This material resembles yukonite in appearance.

Shape and size of ore bodies

The auriferous bodies vary in shape and size. All crosscut the enclosing limestone and are clearly epigenetic. The largest and most continuous of the sulphide bodies are conformable, nearly flat-lying blankets or "mantos". The deposits occur near the top of the massive Lower Cambrian limestone (Fig. 8), from 0 to 100 m beneath the green mudstone (Unit 1e). The thickness of the mantos varies greatly, from less than 10 cm to greater than 30 m. Vertical stacking of parallel lenses (Fig. 8) is common. The maximum drilled dimensions of the PEEL zone (sulphides plus oxides) are approximately 500 m by 300 m. The FLINT zone may be larger, with a drilled thickness of over 30 m (Fig. 9) and a possible strike length of over 1500 m based on geophysical data.

Mantos are extremely irregular in detail despite their strong overall stratigraphic control. Massive sulphides pinch and swell and interfinger with barren limestone (Fig. 10) or weakly sulphide-veined limestone. Locally, mantos become calcite and quartz-rich at their margins.

Sulphides consistently crosscut earlier-formed irregular calcite veins (5 - 20% of host limestone) proving that the deposits are epigenetic (Fig. 11).

Contacts between sulphides and limestone are invariably sharp (Fig. 12); only faint bleaching of limestone is occasionally visible. In some places, irregular sulphide veins form a strong crackle breccia. As sulphide content approaches 30 to 40%, incipient brecciation is evident, with no appreciable rotation of limestone clasts (Fig. 13). The clasts have irregular, rounded outlines (Fig. 14). These textures suggest gradual replacement of limestone by sulphides.

Crosscutting chimneys and irregular sulphide veins (Fig. 15) are common and have a variety of orientations. The THRUST vein and a number of unnamed crosscutting bodies south of Cache Creek are the best exposed. The BLUFF zone may be a vein occurrence.

The THRUST VEIN (Fig. 16) is a 2 m wide vein of pyrrhotite-pyrite-quartz- calcite striking northwest and dipping moderately south. It is in a thrust fault which juxtaposes Unit 1d (limestone) against Unit 2a (black shale) and has a strike length of over 100 m. At its west end, the THRUST VEIN changes to quartz and calcite with no sulphides. Similar veins occupy thrust faults in the cliffs south of Cache Creek, roughly 1 km south of the PEEL zone.

Auriferous iron oxide deposits (RIDGE, BREAK and PEEL OXIDE zones) can have the same general shape as sulphide bodies although they show a greater affinity for structurally disrupted sites.

The PEEL OXIDE zone is a flat-lying manto contiguous with the PEEL SULPHIDE zone but generally lies east of the major NW Fault. In some places, unoxidized sulphides are above the oxides suggesting that groundwater flow patterns the position of oxide mineralization.

The RIDGE zone (Fig. 3) is an irregular, northwest-plunging, pipe-shaped oxide body up to 30 m by 100 m across and at least 100 m below surface. It appears to occupy the junction between the PEEL Fault and the NW Fault. The RIDGE zone is mainly in limestone (Unit 1d) and merges with the PEEL OXIDES.

The BREAK zone, discovered in 1986, is 500 m east of the RIDGE zone in a similar structure and appears to be oriented in an easterly direction. The mineralogy and grade are similar to the RIDGE zone.

In summary, pyrrhotite, arsenopyrite, siderite and iron oxide mantos, veins and chimneys are in Lower Cambrian limestone (Unit 1d) beneath a layer of green mudstone (Unit 1e). The deposits are gold-rich only near the junction between the PEEL fault and the NW fault. Oxide deposits are developed in zones of structural complexity which apparantly controlled groundwater flow and in situ oxidation of sulphides. The sulphide deposits, although stratabound, are clearly epigenetic.

(3) Quartz-sulphide veins

Barren to weakly auriferous quartz-sulfide veins and stockworks (Fig. 17) are common. They are economically unimportant, and have not received much attention but may indicate a large intrusion-centered hydrothermal system. The SAUNA, MC and SUE show-

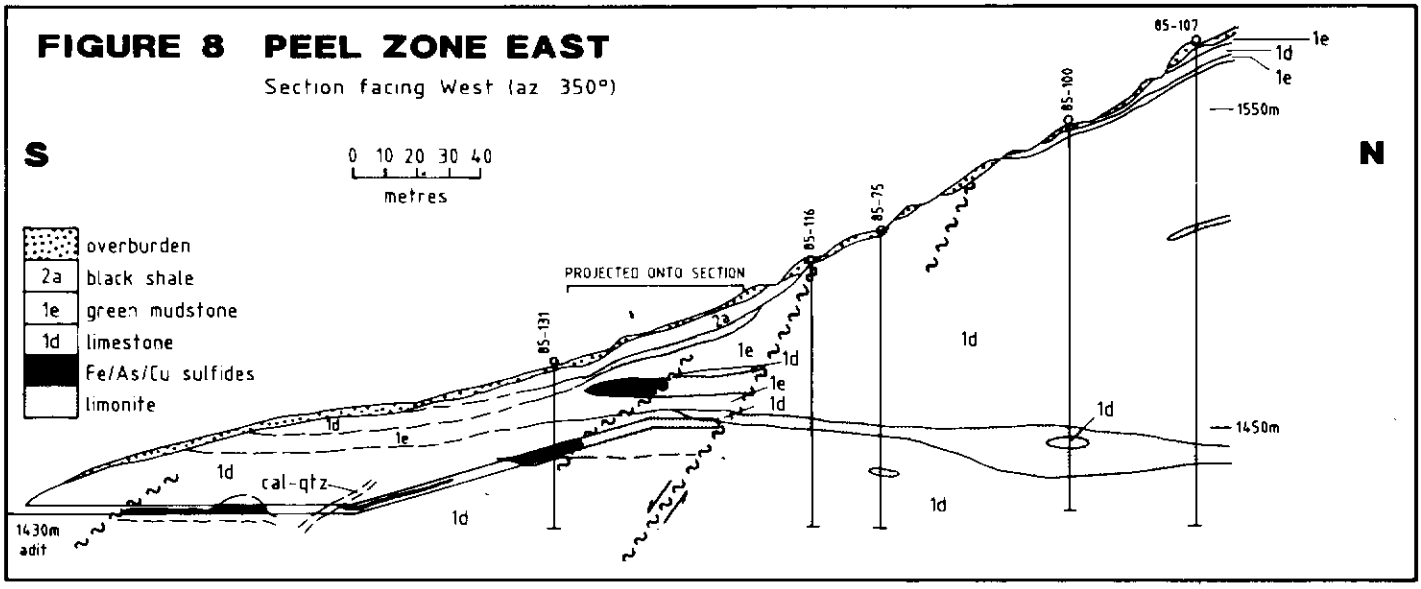

Figure 8. Cross section facing west through the Peel gold zone.

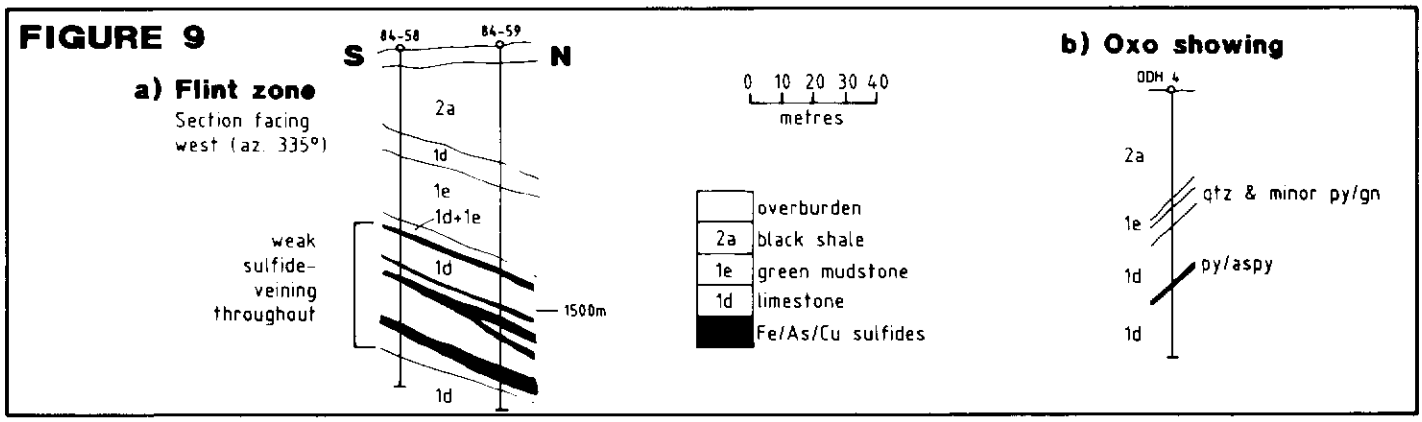

Figure 9. (a) Cross section facing west through the Flint zone. (b) DDH #4, OXO showing.

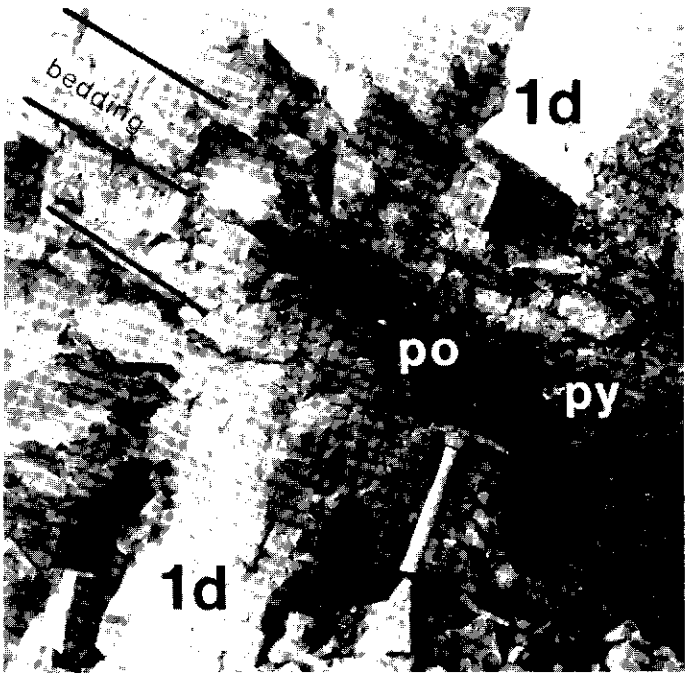

Figure 10. Bedding and fracture controlled replacement of Unit 1d limestone (1d) by massive pyrrhotite (po) and minor pyrite (py). (Occurrence #23).

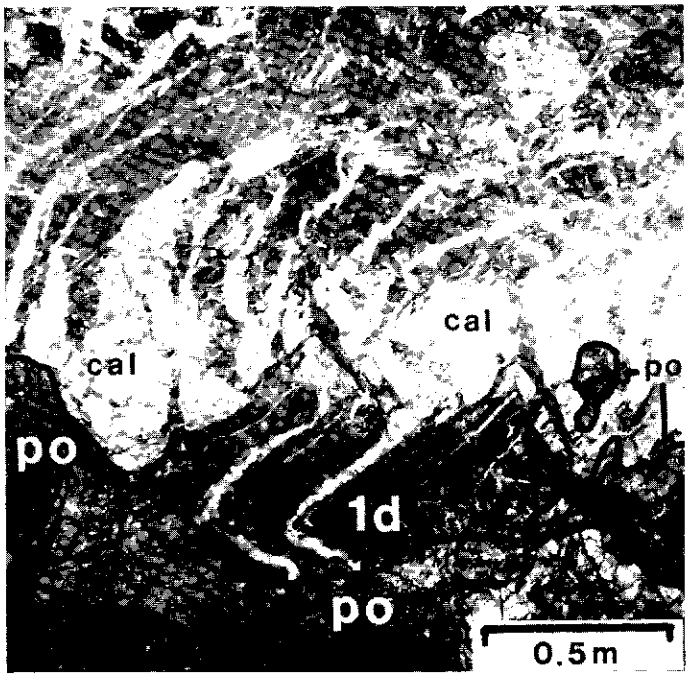

Figure 11. Underground photograph showing definitive epigenetic relation- ship between sulphides and host rock. Massive pyrrhotite (po) crosscuts calcite-veined (cal) Unit 1d limestone (1d). (1430 level, Peel Zone).

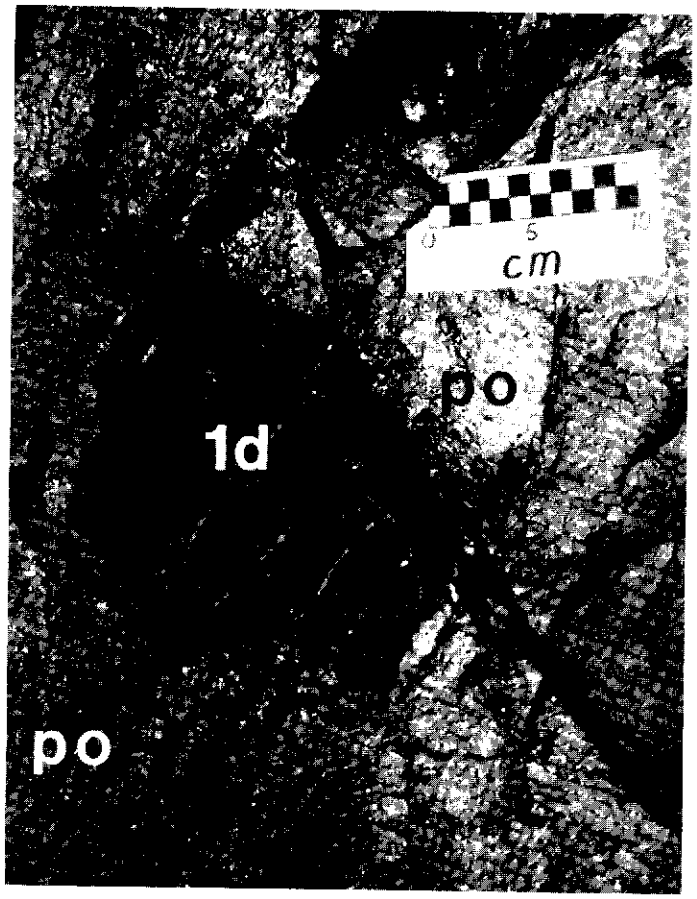

Figure 12. Close-up of a typical razor-sharp contact between an unaltered fragment of Unit 1d limestone (1d) and massive, engulfing pyrrhotite (po). (1430 level, Peel Zone).

ings are the best example. Similar but unnamed showings occur south and west of the MT MISERY showing and north and west of the OXO showing (Fig. 3).

The veins are randomly oriented and are predominantly quartz with subordinate (less than 2%), chalcopyrite or arsenopyrite, accessory pyrrhotite, pyrite, galena or tetrahedrite. Strong dolomitization of host carbonate rocks is ubiquitous near the veins. At the MC zone where a stockwork of small quartz veins is developed in Lower Cambrian limestone, chalcopyrite is the predominant sulphide. The SUE showing is a large (up to 3 m wide) quartz vein, with very minor disseminated chalcopyrite, in Upper Cambrian calcareous phyllite.

The relationship of the veins to pyrrhotite-arsenopyrite mantos and the auriferous quartz sulphide veins is not well understood. They may simply represent quartz-rich examples of the former, or gold-poor examples of the latter.

(4) Silver-lead veins in Upper Cambrian and younger rocks

At least thirty silver-lead-bearing veins have been discovered in the Ketza River District. Most are shown on Figure 3. All occur in Upper Cambrian to Mississippian strata. Fissure vein fillngs predominate although wall rock adjacent to the veins contains weak disseminations and stringers. The gangue is mainly siderite (some may be ankerite) with lesser, but locally abundant quartz, calcite and fragments of wallrock. Coarsely disseminated galena and pyrite form shoots in the siderite veins or massive veins up to 50 cm wide. Chalcopyrite, tetrahedrite, arsenopyrite, sphalerite and pyrrhotite are accessory. Silver grades up to 17,000 g/t have been reported from tetrahedrite-rich material (Woodcock, 1955) but hand-picked, massive galena typically assays between 1000 to 4000 g/t Ag. When sampled over the entire width, siderite-galena veins generally grade 10 to 25% Pb, 300 to 800 g/t Ag, and trace to 2 g/t Au (Green, 1966; Findlay, 1967, 1968, 1969; Orssich et al., 1985).

Several veins contain significant gold. The HOEY showing (Fig. 18) consists of galena and siderite on surface but drilling and underground development have intersected a gold-bearing quartz-pyrite vein (21.6 g/t Au over 0.70 m for a length of 9.15 m) (Findlay, 1969; Orssich et al., 1985). Silurian quartzite encloses the vein at depth. Moderate gold values in a lens of pyrite and arsenopyrite have also been reported from the K16B zone (Orssich et al., 1985).

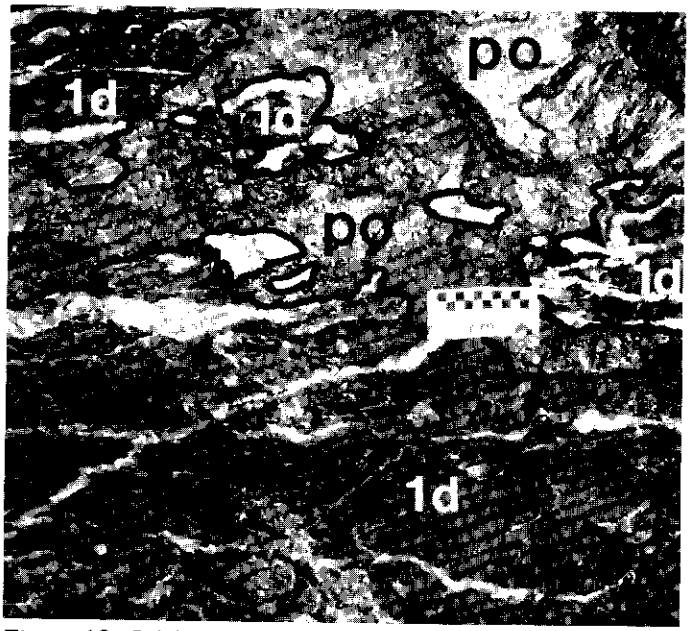

Figure 13. Sulphide breccia with clasts of Unit 1d limestone (1d). Note that a calcite vein can be traced between adjacent 1d clasts in the extreme upper left corner - showing that there has been no appreciable rotation of breccia clasts.

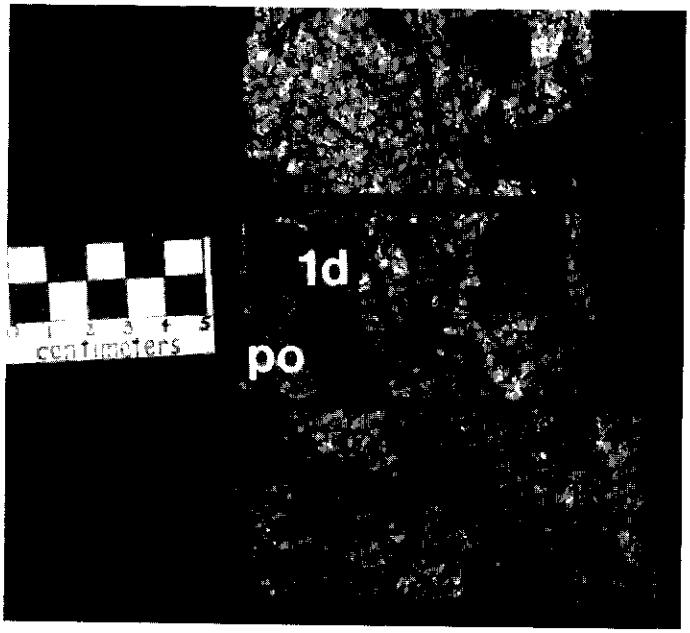

Figure 14. Remnant clasts of Unit 1d limestone (1d) engulfed by massive pyrrhotite (po). Note the irregular, rounded outlines of the clasts. (Flint Zone, DDH KR-84-58), 73.0 m).

Vein-faults generally strike within 20° of north and dip steeply, either east or west. The orientations of most veins are given in Table 1. A few veins have slightly different attitudes. At the KEY 3 showing, a siderite- quartz-galena-tetrahedrite vein has an attitude of 010/30W, the LAP 10 vein is oriented between 030/15W and 010/45W, and a pyritic fault zone at the KEY 35 showing is oriented at 057/68N (Orssich et al., 1985). Dolomite breccia (Unit 3a) nearby contains narrow galena veins trending 350°.

The amount and direction of movement on the vein-faults is dif-

Figure 15. Irregular, vertically oriented vein-type pyrrhotite body (po). Bedding of host Unit 1d limestone (1d) is roughly horizontal. (Occurrence #23).

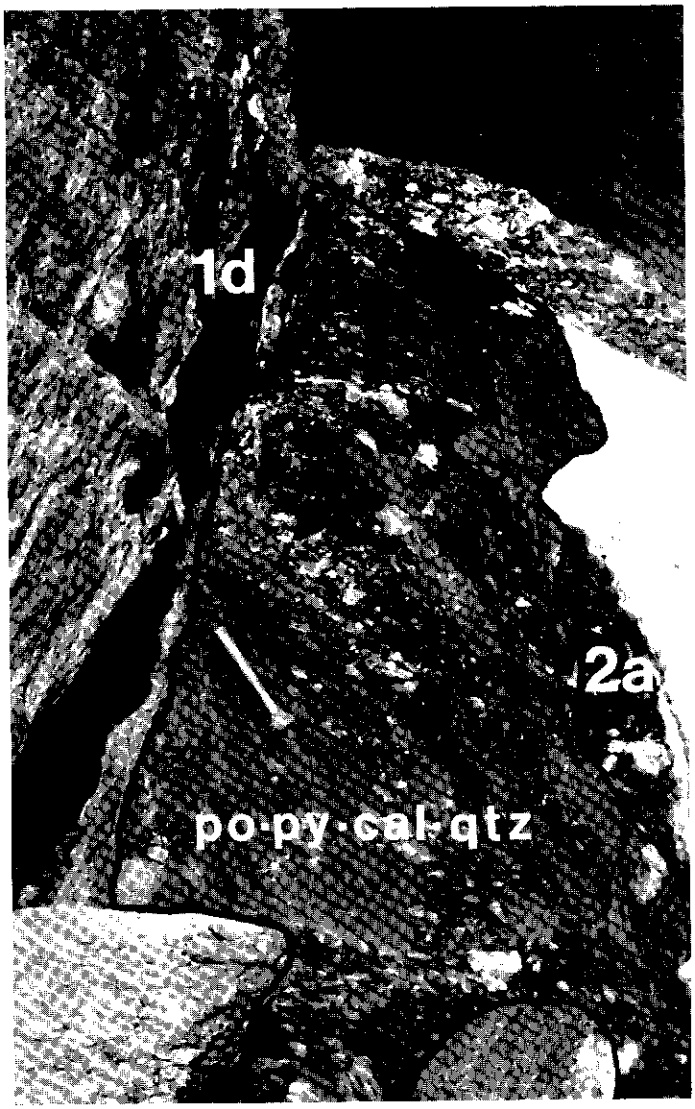

Figure 16. Thrust vein (Occurrence #16). Pyrrhotite-pyrite-calcite-quartz (low Au) are localized in a fault bringing Unit 1d limestone (1d) over Unit 2a black shale (2a). Both bedding and the fault dip to the southwest (left side of photo).

ficult to estimate but most displacement is probably vertical. The fault at the MT MISERY vein moved east side down by as much as 100 m. The HOEY vein is in a steep, east-dipping, reverse fault with an offset of at least 20 m. Offset on many of the other vein-faults is probably minimal. Some veins show good continuity. The STUMP vein can be traced on surface for 250 m while the HOEY and LAP 10 veins have been traced for 275 m and 140 m respectively. The MT. MISERY vein can be traced for 60 m and is covered by scree at both ends.

The veins vary in width from a few cm to more than 5 m but average 2 m, of which 15 to 60 cm may be galena. The galena tends to split into parallel bands, 10 to 20 cm wide. The only veins with defined tonnages are the STUMP vein (49 800 tonnes grading 20% Pb and 719 g/t Ag) and the KIBB vein (8065 tonnes grading 14.4% Pb and 873 g/t) (Orssich et al., 1985).

Galena-siderite veins cut nearly all rock types from Unit 2b (Upper Cambrian-Ordovician) to Unit 4 (Mississippian) as well as Unit 5 Upper Cambrian. Clearly the veins were emplaced after thrusting (Mesozoic) since they show no change in orientation or mineralogy across the thrust fault. Mineralization must also postdate formation of the north-trending fault set. It is not known whether these north-trending faults are related to the formation of the Ketza Uplift.

DISCUSSION AND CONCLUSIONS

Ore controls and mode of formation

Stratigraphy, thrust faults and steep faults control the pyrrhotite-arsenopyrite + siderite manto and vein showings. Gold-rich deposits of this class are confined to the area adjacent to the PEEL fault, particularly where this structure intersects northwest-trending cross-faults. Detailed mapping has shown that the sulphide deposits are clearly discordant and therefore epigenetic. Sulphide textures include vein stockworks, incipient breccia, and massive sulphide lenses suggesting variable replacement of limestone along bedding and fractures. Open-space textures, such as colloform banding are poorly developed and rubble breccias and laminated silt are absent. For these reasons, karst solution channels are not thought to have played an important role in controlling ore deposition. The author believes that pyrrhotite- arsenopyrite + siderite were deposited from hydrothermal solutions that gained access to the Lower Cambrian limestone along steep faults (i.e. the PEEL fault and cross-faults). These structures are thought to have formed in response to Middle Cretaceous intrusion and doming which has resulted in the Ketza Uplift. The hydrothermal solutions were confined beneath a thick sequence of impermeable shales (Units 1e, 2a, 2b) and therefore travelled laterally away from the faults. The gold-poor and siderite-rich mantos located far from the PEEL Fault may reflect the expected drop in temperature

Figure 17. Quartz-sulphide vein stockwork in dolomitized Unit 1d limestone. Sulphides make up 5 to 20% of veins and are predominantly pyrite and chalcopyrite in this case (Occurrence #39).

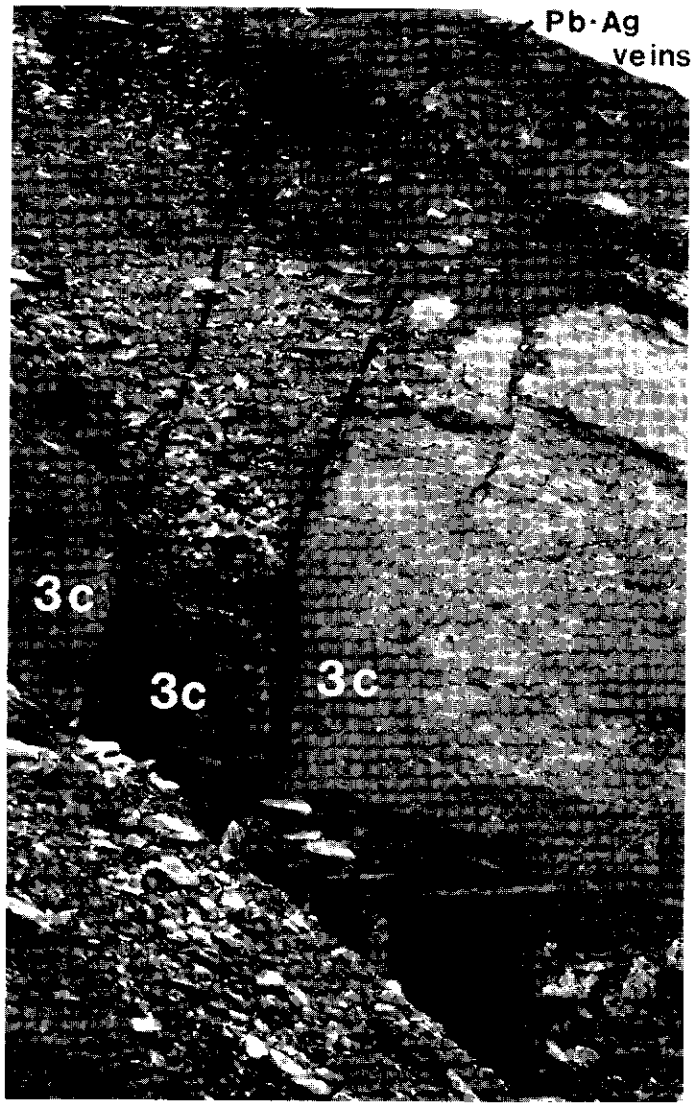

Figure 18. Hoey (F2) vein (looking south) (Occurrence #70). Two parallel, north-trending faults cut Unit 3c quartzite (3c) and are mineralized near the top of the photo. Drifting on the faults encountered a quartz vein with 5% disseminated pyrite which graded 21.6 g/t Au over 0.70 m for a length of 9.14 m.

and pressure of fluids moving away from the intrusion.

The important gold-rich, iron oxide deposits of the RIDGE, BREAK, and PEEL OXIDE zones occur in strong fault zones. These deposits are believed to have formed by the in situ, supergene oxidation of primary sulphide mantos and veins in zones of high groundwater flow.

Silver-bearing galena-siderite veins follow north-trending, steeply dipping faults in Upper Cambrian (Unit 2b) and younger rocks. The faults may also be middle Cretaceous in age. No regional zoning of galena-siderite vein mineralogy has been recognized.

Quartz-sulfide mineralization occurs in Proterozoic to Upper Cambrian strata but is only gold-rich in the Proterozoic rocks. These auriferous veins generally strike northwest and dip moderately east. Barren and weakly auriferous quartz-sulfide veins and stockworks in Cambrian limestone and calcareous phyllite (Units 1d and 2b) are randomly oriented.

Metal zoning and relative timing

Metals and occurrence types are zoned about the center of the Ketza Uplift from: quartz-arsenopyrite-gold veins; to auriferous pyrrhotite-arsenopyrite mantos and veins; to barren pyrrhotite-siderite mantos and veins; and finally, to galena-siderite veins on the perimeter. The zonation can be partly explained by strong stratigraphic control. This control can be summarized as follows:

1. quartz-arsenopyrite gold veins, mainly in Proterozoic argillite-quartzite (Unit 1a)

2. gold-rich pyrrhotite-arsenopyrite mantos and veins (or their oxidized equivalents), mainly in Lower Cambrian limestone (Unit 1d)

3. barren pyrrhotite-pyrite-siderite mantos and veins in Lower Cambrian limestone (Unit 1d)

4. silver-rich galena-siderite veins, mainly in Upper Cambrian and younger strata (Unit 2b through Unit 5).

An alternate exploration for the observed concentric zonation proposes that the different types of mineralization may all be part of a large, district-scale hydrothermal system. The change from gold and arsenic-rich, to silver and lead-rich deposits may be a direct result of a decrease in fluid temperature and pressure of the hydrothermal fluids as they migrated away from the heat source. In this case the heat source is a Middle Cretaceous stock, postulated to underlie the Ketza Uplift. The relative ages of the deposit types are unclear because they occur in different rock units and no cross- cutting rela-

tionships are seen. Isotopic studies and geothermomentry may help sort out these problems.

Implications for exploration

The suggestion that the various deposit types in the Ketza River District are related to a common source has important implications for exploration in the district and elsewhere. If silver-lead veins can be proven to be distal to a large intrusion-centred hydrothermal system with gold mineralization near the centre, then silver veins are a useful exploration guide for quartz-sulfide vein or sulphide manto deposits. Other silver camps in the Cordillera such as Keno Hill, Plata, Tintina, Quartz Lake and Midway should be re-evaluated with the Ketza zoning model in mind, especially if carbonate rocks are present.

ACKNOWLEDGEMENTS

Financial support for this study has been provided by the Exploration and Geological Services Division of Indian and Northern Affairs Canada. I am grateful to Grant Abbott and Jim Morin of INAC for advice and encouragement. Thanks are also extended to the management of Canamax Resources Inc. for accommodation in field, access to drill core, underground workings, and confidential exploration data, and for permission to publish. Special thanks must go to Canamax geologists Steve Parry, Jeff Toohey, Fred Harris, and Cyrril Orssich for inspiring and critical discussion. Kate Rodd and Karen Smith helped with proof-reading, typing and drafting and their assistance is greatly appreciated.

REFERENCES

ABBOTT, J.G., 1986. Epigenetic mineral deposits of the Ketza-Seagull district, Yukon; in Yukon Geology, Vol. 1, Exploration and Geological Services Division, Yukon, Indian and Northern Affairs Canada, p. 56-66.

FINDLAY, D.C., 1967. The mineral industry of Yukon Territory and southwestern District of Mackenzie, 1966; Geological Survey of Canada, Paper 67-40, p. 56-58.

FINDLAY, D.C., 1968. The mineral industry of Yukon Territory and southwestern District of Mackenzie, 1967; Geological Survey of Canada, Paper 68-68, p. 75-77.

FINDLAY, D.C., 1969. The mineral industry of Yukon Territory and southwestern District of Mackenzie, 1968; Geological Survey of Canada, Paper 69-55, p. 44-46.

GABRIELSE, H., 1985. Major dextral transcurrent displacements along the Northern Rocky Mountain Trench and related lineaments in north-central British Columbia; Geological Society of America Bulletin, Vol. 96, p. 1-14.

GORDEY, S.P., ABBOTT, J.G., TEMPELMAN-KLUIT, D.J. and GABRIELSE, H., 1987. "Antler" clastics in the Canadian Cordillera in Geology; Vol. 15, p. 103-107.

GREEN, L.H., 1966. The mineral industry of Yukon Territory and southwestern District of Mackenzie, 1965; Geological Survey of Canada, Paper 66-31, p. 64-68.

MORIN, J.A., 1981. Element distribution in Yukon gold-silver deposits; in Yukon Geology and Exploration, 1979-80, Exploration and Geological Services Division, Yukon, Indian and Northern Affairs Canada, p. 68-84.

ORSSICH, C.N., HARRIS, F.R. and WATTS, A.C., 1985. Iona Silver Property: 1985 property report; Unpublished company report, Canamax Resources Inc., 59 p.

PARRY, S.E., HARRIS, F.R., CATHRO, M.S. and WYTRWAL, Z.J., 1984. Ketza River Property: 1984 summary report; Unpublished company report, Canamax Resources Inc., 41 p.

READ, B.C., 1980. Lower Cambrian archeocyathid buildups, Pelly Mountains, Yukon; Geological Survey of Canada, Paper 78-18, 54 p.

ROTHERHAM, D.C., 1958. Ketza River, 1958; Unpublished company report, Conwest Exploration Co. Ltd.

ROTHERHAM, D.C., 1959. Report on the Ketza River Property; Unpublished company report, Conwest Exploration Co. Ltd.

TEMPELMAN-KLUIT, D.J., 1977a. Geology of Quiet Lake and Finlayson Lake map areas, Yukon Territory (105 F and G); Geological Survey of Canada, Open File 486.

TEMPELMAN-KLUIT, D.J., 1977b. Stratigraphic and structural relations between the Selwyn Basin, Pelly-Cassiar Platform and Yukon crystalline terrane in the Pelly Mountains, Yukon; in Report of Activities, Part A: Geological Survey of Canada, Paper 77-1A, p. 223-227.

TEMPELMAN-KLUIT, D.J., 1979. Transported cataclasite, and granodiorite in Yukon: Evidence of arc-continent collision; Geological Survey of Canada, Paper 79-14, 27 p.

TEMPELMAN-KLUIT, D.J., ABBOTT, G., GORDEY, S. and READ, B.C., 1975. Stratigraphic and structural studies in the Pelly Mountains, Yukon Territory; in Report of Activities, Part A: Geological Survey of Canada, Paper 75-1A, p. 45-48.

TEMPELMAN-KLUIT, D.J., GORDEY, S.P. and READ, B.C., 1976. Stratigraphic and structural studies in the Pelly Mountains, Yukon Territory; in Report of Activities, Part A: Geological Survey of Canada, Paper 76-1A, p. 97-106.

TOOHEY, J., 1986. Geology and ore controls of the Ketza River gold deposits, Yukon; Unpublished term project report, Queen's University, Kingston, Ontario, 111 p.

WHEELER, J.O., GREEN, L.H. and RODDICK, J.A., 1960. Quiet Lake, Yukon Territory; Geological Survey of Canada, Map 8-1960.

WOODCOCK, J.R., 1955. Ketza River Area, Yukon Territory: 1955 Field Season; Unpublished company report, Conwest Exploration Co. Ltd., 60 p.

TABLE 1: Summary of mineral occurrences in the Ketza River District

Occurrence Number	Name of Occurrence	Mineralogy (see key)	Host Unit (see Fig. 2)	Attitude	Dimensions	Type of Occurrence	Comments/Reference
Gold-bearing quartz-arsenopyrite veins and other occurrences hosted by Unit 1a (Proterozoic quartzite, argillite, siltstone).							
1*	Shamrock (MMM)	qtz, aspy, scor	1a	trends 330	est. 50 cm wide	vein	Up to 1000 g/t Au reported from surface samples (Northern Miner Magazine, March, 1987, p. 35).
2*	Quartz Breccia (QB)	qtz, aspy, scor	1a	averages 320/50E	3 parallel veins to 20 m wide	vein	
3*	-	qtz, aspy, scor	1a	290/80N	15-30 cm wide	vein	
4*	-	qtz, aspy, scor	1a	trends 330	1 m wide	vein	
5	Quill	po, aspy, py	1a	? (float only)	?	vein ?	Up to 2.8 g/t Au, 2.3 g/t Ag and 32.83% As. Sulphide boulders are associated a stockwork of narrow, qtz veins containing py aspy (Abbott, 1986).
6*	Fred's Vein (Peel 4, Peel 6)	qtz, po, py, aspy, cpy	1a	trends 070	1-2 m wide over 500 m	vein fault	Channel samples up to 7.2 g/t Au over 1.5 M (Northern Miner Magazine, March, 1987, p. 35).
7*	Peg-Fury Limonite (Fury 26, Peg 13)	limonite-cemented soil and scree	1a	-	500 x 200 m	gossan	Appears to be a transported (exogenous) gossan
Auriferous and barren, sulfide, oxide and carbonate mantos, chimneys and veins hosted by Unit 1d (Lower Cambrian Limestone).							
8*	Peel Sulfides (Boom, Woodcock, Peel 3a, 3b, 5a, Fury 30b)	po, aspy, py, cpy, qtz	1d	flat	400 x 300 x 5 m	manto	499,000 tonnes of 8.9 g/t Au (Northern Miner, Feb. 9, 1987
9*	Peel Oxides	lim, his, qtz	1d	flat	250 x 100 x 5 m	oxidized manto	499,000 tonnes of 18.2 g/t Au (Northern Miner, Feb. 1987).
10*	Ridge Oxides (Peel 3c)	lim, his, qtz	1d/1a	NW plunging pipe	100 x 30 m to at least 100 m depth	pipe/ chimney	
11*	Break Oxides	lime, his, qtz	1d	120/45S	30 x 60 x 5 m	pipe or vein	41,730 tonnes of 16.8 g/t Au to 60 m drill depth (Northern Miner March, 1987).
12*	Bluff (Fury 30a)	qtz, po, py, aspy, cpy	1d	?	100 x 2 m	manto or vein	Occurs on north-trending fault structure
13*	Penguin (Penguin 6)	po, py, aspy, cpy, qtz	1d	flat	100 x 30 x 5 m	manto	Generally low Au
14*	Flint	po, py, aspy, cpy, qtz	1d	dips 15 N	30 m thick	manto	Estimated strike length of 1500 m based on geophysics, width not known. Does not outcrop. Intersected in drill holes. Low Au.
15*	Tarn	po, py, aspy, cpy, qtz	1d	flat	125 x 75 x 5 m	manto	Generally low Au

16*	Thrust Vein	po, py, qtz, cal, minor aspy, cpy	1d/2a	300/45 S	125 x 2 m	vein	Low Au. Vein occurs in a fault bring Unit 1d over Unit 2a.
17*	Creek (Penguin 4)	po, py, aspy, cpy	1d (dol)	flat	50 x 25 m	manto ?	Galena reported in Conwest drill hole from 1950's.
18*	-	aspy, po, py	1d	flat	small	manto/ vein	Low Au
19*	-	aspy, po, py	1d	flat	small	manto/ vein	Low Au
20*	-	po, py, aspy	1d	flat	100 x 10 x 1 m	manto	Low Au
21*	- (2 showings)	1) po, cpy and 2) mag, aspy	1d	flat	5 x 2 m	manto	Low Au
22*	-	qtz, cal and po, aspy	1d	flat	100 x 2 m	manto	Low Au
23*	- (2 showings)	po, aspy, py	1d	1) 140/30 S 2) steep dip	40 x 0.5 m 1 x 5 m	manto pipe/ vein	High Au in grab sample. Manto changes to cal/qtz along strike.
24*	- (2 showings)	1) po, py, cal 2) po, py	1d	1) vertical 2) 080/60 S	20 x 10 x 20 m 30 x 4 m	pipe/ vein vein/manto?	Low Au
25*	-	po, py, cpy	1d	flat	2 x 5 m	manto	
26*	- (8 showings)	py, po, aspy	1d	flat	30 x 30 x 2 m (maximum)	mantos	Low Au
27*	-	sid, py, po	1d	flat	2 x 10 m	manto	Low Au
28*	- (3 showings)	sid, po, py	1d (dol)	flat	50 x 30 m (maximum)	mantos	Low Au. Adjacent to thrust fault
29*	- (4 showings)	sid, po, py	1d (dol)	flat	100 x 40 m (maximum)	mantos	Low Au. Adjacent to thrust fault
30*	- (2 showings)	py, sid	1d (dol)	trends 060 steep dip	30 x 5 m	manto/ vein	Low Au. On thrust fault.
31*	-	po	1d (dol)	340/80 W	very small	vein	Low Au.
32*	- (3 showings)	sid, py, po	1d (dol)	flat	50 x 10 x 1 m (maximum)	manto	Low Au. Adjacent to thrust fault.
33*	-	py, po, aspy	1d	float only	small	manto/ vein?	
34*	-	po, aspy, py	1d	float only	50 x 50 m area	?	
35*	-	py, po	1d	flat	30 cm pods	manto	
36*	-	po, py	1d	float only	20 x 20 m	?	
37*	-	po, py	1d	float only	20 x 20 m	?	

Table 1: Summary of mineral occurences in the Ketza River District Continued

Occurrence Number	Name of Occurrence	Mineralogy (see key)	Host Unit (see Fig. 2)	Attitude	Dimensions	Type of Occurrence	Comments/Reference
38*	Oxo	py, gn, sph, po, qtz, cpy	1d/2a/3a	flat	5 x 5 x 30 m	manto	Changes to qtz/cpy vein (trending 320) along strike to S. Drilled 1524 m in 21 holes in 1969 with disappointing results (Green, 1969).
Barren to weakly auriferous quartz-sulphide veins							
39*	Sauna	qtz, aspy, po	1d (dol)	-	300 x 150 m zone	vein of 2-5 cm veins	Low Au. stockwork
40*	MC	qtz, cpy	1d	-	10 x 20 m area	vein stockwork	Low Au.
41*	Sue	qtz, cpy, mal	2b (dol)	340/70	1 to 2 m wide	vein	
42*	-	qtz, mal	1d	trends 045	to 1 m wide	vein	
43*	-	qtz, cal, cpy	1d (dol)	trends 045	to 1 m wide	vein	
44*	-	qtz, cal, cpy	1d (dol)	trends 280	to 1 m wide	vein swarm	
45*	Fury	qtz, cpy, tet	1d	trends NW?	15 cm to 1.4 m wide	veins for 100 m	Abbott, 1986
46*	-	qtz, cpy, aspy	1d	020/70 E	narrow	veins	
47*	-	qtz, aspy, scor	1d (dol)/ 2a	010/70E	to 0.5 m wide	veins	Veins occur at faulted contact between Unit 1d and Unit 2a.
48*	-	qtz, cal, py	1d/1c	trends 300	?	vein ?	In thrust fault.
Argentiferous galena-siderite veins in Upper Cambrian through Mississippian rocks.							
49*	Carl 2	gn, sph	1d/3b or 3d?	float only	?	vein ?	Abbott, 1986.
50*	Mt. Misery (Tom 3a)	gn, py, sid, qtz	3c/3d	trends N, steep dip	est. 1 to 2 m wide by 70 m long	vein fault	A single boulder of py/aspy/ sid/qtz was found on the dump in front of the adit. Estimated 100 m displacment on fault (east side down).

51*	Key 3 (Ketzakey)	gn, tet, py, sid, qtz, cal	4a/4b	360/20 W	discontinuous 1 to 5 m wide vein at least 100 m long	vein fault	Sulfides occur as clots and veinlets within the siderite-quartz gangue. Grades up to 17,000 g/t Ag were reported by Woodcock (1955). Three short adits and an open cut were driven in the 1950's although all are now caved. Woodcock reported that adit #2 encountered a 1 x 8 m 30 W dipping vein fault with buff weathering slate and argillite in the hanging wall and cherty quartzite in the footwall. This vein is apparently a splay off a larger fault oriented at 155/48 W. The vein in adit #1 was poorly exposed but apparently had a similar orientation to the vein in adit #2.
52	Zinc	sph	?	float only	?	vein ?	Approx. location from old Iona Silver Mines report.
53	Key 1a	gn	4b?	?	?	vein	Description and location from Woodcock, 1955.
54*	Lap 10 (Laprarie, Strike 8a)	gn, sid	4b	variable 035/15 W to 010/45 W	1 x 140 m	vein	Steely or coarse grained galena forms a massive vein 20 to 45 cm wide within siderite gangue. An adit and raise driven beneath the vein failed to intersect mineralization.
55*	Key 6a	gn, sid, mal	4b	340/80W	5 cm x 5 m	vein	25 cm x 1.3 lens of galena located by Woodcock (1955).
56	Key 7a (Trench, Smitheringale 2)	aspy, sid, py, sph	5	float only	4.5 m wide zone	?	Aspy boulders occur on W side of a dike-like body of greenstone cutting phyllite (Woodcock, 1955; Orssich et al., 1985).
57*	Key 9a (Knoll)	sid, gn, aspy (phyllite)	5	320/40 W	10 cm wide fault	vein	
58*	Key 11a (Blazed Tree)	gn, sid, lim, cal (grnstone)	5	350/70 W by 10 m long	10 - 20 cm wide	vein	Float fragments to 20 x 40 cm of steely and coarse-grained galena.
59	-	sid, gn	5	360/80 W	1 x 15 m	vein	Orssich et al., 1985.
60	Strike 4a (OK)	?	5 (grnstone)	310/10 SW	10 cm wide	vein fault	Woodcock, 1955.
61	Dip	sid, gn	5	?	?	vein	Orssich et al., 1985.
62*	Key 35 (Cache Creek 1) (2 types of mineralization)	1) qtz, py, gn, dol, lim 2) lim, gn, sid	3a 3b	57/68 N 170/90	7 m wide by 8 m long to 3 cm wide	veins diss. veinlets	Pyrite occurs disseminated and along foliation planes in black shale while gn/sid veinlets occur in a nearby, small block of dolomite breccia (Unit 3b). (Orssich et al., 1985).

63*	Key 13a (Cache Creek 2, Smitheringale 4)	sid, py, gn, qtz, cpy	2b	trends N, steep dip	1.5 m wide by 40 m long	vein fault	1985 drill hole intersected 1.6 m of massive py/aspy (Orssich et al., 1985). Woodcock (1955) reported that a short adit encountered two diverging faults (oriented at 128/80 NE and 155/90) and the sedimentary rock between them is completely replaced by pyrite and ankerite. Near the intersection of the faults is a small lens containing galena and sphalerite.
64*	Key 16a (Smitheringale 5)	sid, qtz, aspy py, gn	2b	010/90	30 to 60 cm wide	vein fault	
65*	Key 16b	aspy, py, qtz, sid	2b	irregular, partly conformable	10 x 5 m	irr. vein or manto	Adjacent to fault trending N, dipping 68 W.
66*	Lower Switchback (F 1?)	sid, gn, py	3b (dol bxa)	015/90	1 to 2 cm wide veinlets over 10 x 20 m area	veinlets	Narrow siderite veinlets with minor galena.
67*	Upper Switchback	gn	3b	float only	5 x 15 m area	disseminated or vein ?	Orssich et al., 1985
68*	F3 (Hoey "J")	lim, sid, gn, qtz	3a/3b/3c	350/65W	1 to 2 m wide intermittently over 100 m	vein	Vein mainly occurs in Unit 3b dolomite breccia at contact with Unit 3a black shale.
69*	Canyon (F7, Gopher Copter)	gn, py, sid, qtz	3b/3c	015/70 W	1 x 60 m	vein fault	
70*	Hoey (F2, Hoey "H", Galena vein)	sid, gn, py, qtz	3c	010/70E	1 to 5 m wide intermittently over 300 m. Locally to 10 m wide	vein fault	Parallel bands of gn/py up to 30 cm wide occur on surface 30 m S of the adit portal. A quartz vein with minor pyrite (no siderite or galena) is present between two parallel faults in the adit. 32 m S of the portal this vein assays 21.6 g/t Au over a width of 0.7 m for 9.14 m of the drift (Orssich et al., 1985).
71	Gem	gn	3c	360/62 W	2 to 10 cm wide by 3 m long	vein	Discovered in 1977; description from Iona Silver report. Location not precisely known.
72*	Stump (A1 and A2)	sid, gn, py, cpy, qtz	2b	350/60 W	up to 1.2 m wide over 315 m long	vein fault	Discovered by soil geochmistry in 1966. Mineralized structure exposed on surface for over 315 m. Drifting on two levels has defined probable reserves of 49,000 tonnes grading 20% Pb and 719 g/t Ag (Orssich et al., 1985).
73	K18A	gn, sid	2b?	?	float over 70 m	vein ?	Findlay, 1969 length

Table 1: Summary of mineral occurences in the Ketza River District Continued

Occurrence Number	Name of Occurrence	Mineralogy (see key)	Host Unit (see Fig. 2)	Attitude	Dimensions	Type of Occurrence	Comments/Reference
74*	K188 (Key 188, Ketzakey)	gn, py, sid, qtz, cal, tet	2b	010/70 W	1.7 x 32 m	vein fault	Discovered by soil geochemistry in 1968. Development on two levels has defined probable reserves of 8065 tonnes grading 14.4% Pb and 873 g/t Ag (Orssich et al., 1985).
75	F4 (South Fault)	gn, sph, tet	3a/3b/2b	?	very small pods	vein ?	Green, 1966; Orssich et al., 1985.
76	F5	gn, sid	?	?	?	vein ?	Location from Silver Key Mines, information for shareholders, March, 1967.
77*	F6 (Regehr, South showing)	gn, py, sph, lim (minor 2b, 5)	3b	float only	?	?	
78*	Sharon	gn, py, cpy, sid, cal, qtz	2b	005/70 E & 110/70 N	max. 1.8 m wide by 21 m long	vein fault	Two mineralized veins approx. 400 m apart.
79	Carl 1	qtz, gn, sph	3d?	?	30 m wide zone of narrow qtz veins	veins	Selected sample assayed 16.0% Pb, 7.73% Zn, 0.1% Cu, 506.4 g/t Ag (Abbott, 1986).

* Occurrence visited by author

KEY TO ABBREVIATIONS:

po: pyrrhotite / aspy: arsenopyrite / py: pyrite/ cpy: chalcopyrite / gn: galena / sph: sphalerite / tet: tetrahedrite / lim: limonite / his: hisingerite / mal: malachite / scor: scorodite / sid: siderite / qtz: quartz / cal: calcite / bxa: breccia / diss: disseminated / dol: dolomitized / dolo: dolomite or dolostone.

FACIES AND DEPOSITIONAL SETTING OF LABERGE CONGLOMERATES (JURASSIC), WHITEHORSE TROUGH

John R. Dickie and
Frances J. Hein
Department of Geology,
Dalhousie University,
Halifax, Nova Scotia,
B3H 1J5

DICKIE, J.R. and HEIN, F.J., 1988. Facies and depositional setting of Laberge conglomerates (Jurassic), Whitehorse Trough, Yukon; in Yukon Geology, Vol. 2; Exploration and Geological Services Division, Yukon, Indian and Northern Affairs Canada, p. 26 - 32.

ABSTRACT

The Whitehorse Trough, south-central Yukon, originated as a Mesozoic fore-arc basin separating the allochthonous Stikine Terrane to the west from the North American craton. Late Triassic erosion of a volcanic arc supplied detritus to the basin. Subsequent cessation of volcanism, unroofing and deep erosion of the arc into the Middle Jurassic resulted in a progressive increase in granodioritic sediment.

Late Triassic-Jurassic Laberge conglomerate within the Whitehorse Trough are coarse, polymictic and typically massive. Inverse or normal grading, planar stratification and cross-bedding are less common. Conglomerates are debris flow, sheet-flood and bar deposits of braided alluvial fan-deltas. These conglomerates usually overlie and grade basinward into feldspathic graywacke or arkosic sandstone. Crystal tuffs grade laterally into sandstone and occur as interbeds as well. Sandstones commonly display trough cross-bedding or planar stratification. Hummocky cross-stratification rarely occurs in sandstones interbedded with bioturbated silty mudstone. Other facies include graded sandstone-mudstone with Bouma BC(E) sequences; float-stone/micritic limestone; and rare calcarenite/rudite. Sandstone-conglomerate facies transitions indicate a vertical progression from shallow marine and shoreface sedimentary strata of Late Triassic age to coarse alluvial fan conglomerates of Jurassic age, reflecting progradation of fan-delta systems with progressive infilling of the basin. The Stikine Terrane accreted to North America in the Late Jurassic with basin shallowing and closure reflected by changes in the sedimentary sequences.

RÉSUMÉ

Dans la partie sud-centrale du Yukon, la fosse de Whitehorse était initialement, au Mésozoïque, un bassin d'avant-arc qui à l'ouest séparait le terrane allochtone de Stikine du craton nord-américain. Durant le Trias supérieur, l'érosion d'un arc volcanique a fourni des débris au bassin. Ensuite, l'interruption du volcanisme, la découverture et l'érosion profonde de l'arc durant le Jurassique moyen ont eu pour effet une augmentation progressive de l'épaisseur des sédiments granodioritiques.

Le conglomérat de Laberge, d'âge triasique supérieur à jurassique, situé à l'intérieur de la fosse de Whitehorse, est grossier, polymictique et typiquement massif. Le granoclassement inverse ou normal, la stratification horizontale et la stratification oblique sont moins courants. Les conglomérats se composent de coulées boueuses, de dépôts d'inondation en nappe et de dépôts de bancs fluviatiles dans des cônes de déjection anastomosés. Généralement, ces conglomérats recouvrent des grauwackes ou des grès arkosiques, et passent progressivement à ce type de sédiments vers l'intérieur du bassin. Des tufs cristallins passent latéralement à des grès et se présentent également sous forme d'interstratifications. Généralement, les grès montrent une stratification croisée en auge ou une stratification plane. On rencontre rarement une stratification en bosses et creux dans les grès interstratifiés avec des pélites limoneuses bioturbées. Un autre faciès comprend des grès ou pelites granoclassés avec les séquences de Bouma BC(E); une roche de type float-stone/calcaire micritique; et très rarement des calcarénites/rudites. Des transitions de faciès du grès au conglomérat indiquent une progression verticale de strates marines peu profondes et de strates sédimentaires de zone infratidale, d'âge triasique supérieur, à des conglomérats grossiers de cônes alluviaux d'âge jurassique, ce qui indique une progradation des systèmes de cônes de déjection à mesure que s'est effectué le comblement du bassin. Le terrane de Stikine s'est joint par accrétion à l'Amérique du Nord pendant le Jurassique supérieur, et la diminution de profondeur et la fermeture du bassin se sont traduits par des modifications des séquences sédimentaires.

INTRODUCTION

The Whitehorse Trough, a northwest-trending synclinorium in the Cordilleran Intermontaine Belt (Fig. 1), contains a thick succession (6700 m +) of Late Triassic to Early Cretaceous calc-alkaline volcanic and volcaniclastic rock, reef limestone, greywacke, argillite, and conglomerate (Wheeler, 1961).

The Whitehorse Trough originated as a Triassic fore-arc basin (Templeman- Kluit, 1979). A volcanoplutonic arc, situated on the leading edge of the allochthonous Stikine Terrane, supplied volcanic flows and detritus to the basin. Tethyan-type framework and patch reefs, with bedded inter-reef deposits, flanked the arc in Carnian to Norian time (Reid et al., 1987). Arc-derived sediments were transported from the west to the basin by braided fan-deltas.

Jurassic sedimentary strata overlying upper Triassic limestone are the Laberge Group; whereas the limestone, interbedded clastics, and volcanics of Triassic age constitute the Lewes River Group. These units are separated by a discontinuous erosional unconformity along the basin margin, being conformable at the basin axis (Wheeler, 1961), Laberge/Lewes River beds were deposited by a single, continuously-operating depositional system, and have been (informally) considered as a single stratigraphic unit (Tempelman-Kluit, 1978; Hills et al., 1981). Jurassic basin-fill is predominantly coarse, polymictic conglomerate. In this study, Triassic-Jurassic conglomerates of the Whitehorse Trough are referred to as "Laberge conglomerates".

Nine stratigraphic sections of Laberge conglomerates were measured in detail on a bed-by-bed basis in the Whitehorse area.

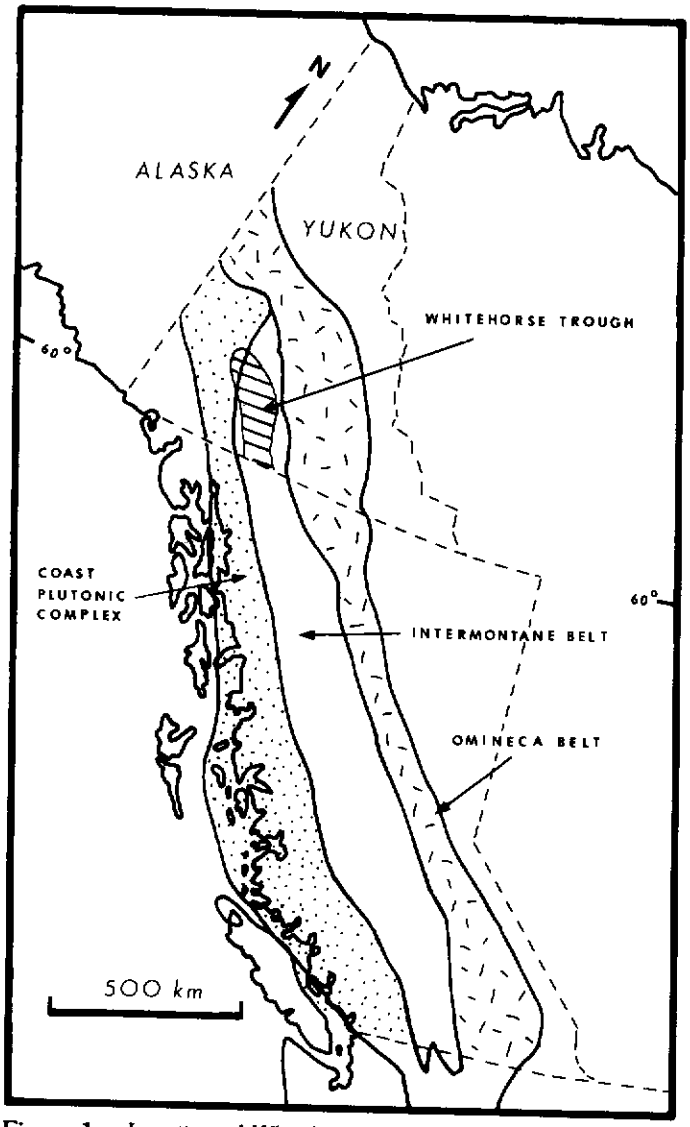

Figure 1. Location of Whitehorse Trough, northern cordillera.

Only three sections (Braeburn, Takhini Hotsprings and Fish Lake) provided continuous exposure and reliable fossil dates. Braeburn and Takhini Hotsprings (Fig. 2) conformably overlie the uppermost limestone of the Lewes River Group, which has a correlatable Carnian-Norian chronohorizon (Spondylospira lewesensis fauna; Tozer, 1958). The Fish Lake section (Fig. 2), ranges in age from Toarcian to (late) early Bajocian (Harpoceras to Stephanoceras ammonite zones; Wheeler, 1961). Braeburn and Takhini Hotsprings sections show marine to alluvial transition, whereas Fish Lake strata are entirely marine.

METHODS OF STUDY

Facies were delineated on the basis of lithology, sedimentary structures, and biogenic features. Facies sequences were used to interpret depositional environments. Fining- or coarsening-up sequences and bed-thinning or thickening trends were determined by plotting maximum particle size (MPS) (ave. of 10 largest clasts) and bed thickness against stratigraphic position. Moving average plots, using point-sets of 3, were used to smooth the data, thus eliminating bed-scale perturbations.

Clast lithology was plotted against stratigraphic position. Granodiorite (arc pluton) and volcanic clasts (tuff, basalt, dacite, andesite) are arc-derived, relating directly to erosion of the source terrane. Limestone clasts, eroded from Norian arc-flanking reefs and back-reef areas, were dated on the basis of conodont fauna. Trend recognition, coupled with facies interpretation, was used to separate autocyclic and allocyclic processes in these sections, thus putting constraints on depositional processes and controlling mechanisms.

FACIES

Facies for Laberge conglomerates were defined as follows:

1) Floatstone/Micritic Limestone Facies

Thick-bedded, grey, micritic limestone contains dispersed pelecypod, gastropod, calcareous sponge, and coral fragments. Rare sedimentary structures occur as parallel-laminated siliciclastic sand. This facies represents deposition in a carbonate lagoon/back-reef setting.

2) Calcarenite/Rudite Facies

Calcarenite/rudite is interbedded with facies (1) or grades from arkosic to greywacke sandstone beds. Fossil fragments (as in facies 1; ave. 4 cm) occur in clast-support with a sandy micrite matrix. Calcarenite/ rudite resulted from sandy turbulent flows eroding exposed (or shallow water) reef crests.

3) Red Mudstone

Red mudstone occurs as thick-bedded, typically massive beds (rare desiccation cracks with sand in-filling) (subfacies 3a), or as thin bedded, heavily bioturbated mudstone interbedded with grey arkosic sandstone (subfacies 3b). The former represents suspension deposition in abandoned alluvial fan stream channels, whereas the latter is indicative of a shallow marine (near shore) setting.

4) Interbedded Sandstone/Mudstone

Very fine sandstone/mudstone couplets display fining-up partial (BCE) Bouma sequences. Presence of ammonites indicates marine deposition, probably as delta-front turbidites. Similar beds, displaying coarsening-up sequences expressed as a vertically-increasing sand/shale ratio, represent prodelta deposits.

5) Stratified Sandstone

Fine to medium-grained sandstone occurs as planar-stratified beds (subfacies 5a), deposited by bar-top sheet-floods in a distal fan setting; or as low-angle stratified sandstone (subfacies 5b), which is defined by heavy mineral accumulations and represents shoreface bars created through fluvial/marine interaction.

6) Massive/Normally-graded Sandstone (Fig. 3)

Massive (also normally-graded) sandstone occurs in several environments, primarily representing deposition through subaquenous turbulent flows in a distal fan-delta setting (fluvial and shallow marine).

7) Cross-Stratified Sandstone

Trough cross-stratified sandstone (subfacies 7a) occurs in close association with hummocky cross-stratified sandstone (subfacies 7b), both of which occur in a shallow marine setting. The former occurs where reef influence prevented storm waves from breaking on the shoreline; whereas the latter represents storm-reworking along a non-barred coast.

8) Pebbly Sandstone

Pebbly sandstone occurs as normally-graded granule/pebble size (broken) euhedral plagioclase grains and lithic fragments set in a medium sand matrix (subfacies 8a). Trough cross-bedded pebbly sandstones (sets to 2.4 m) display pebble-

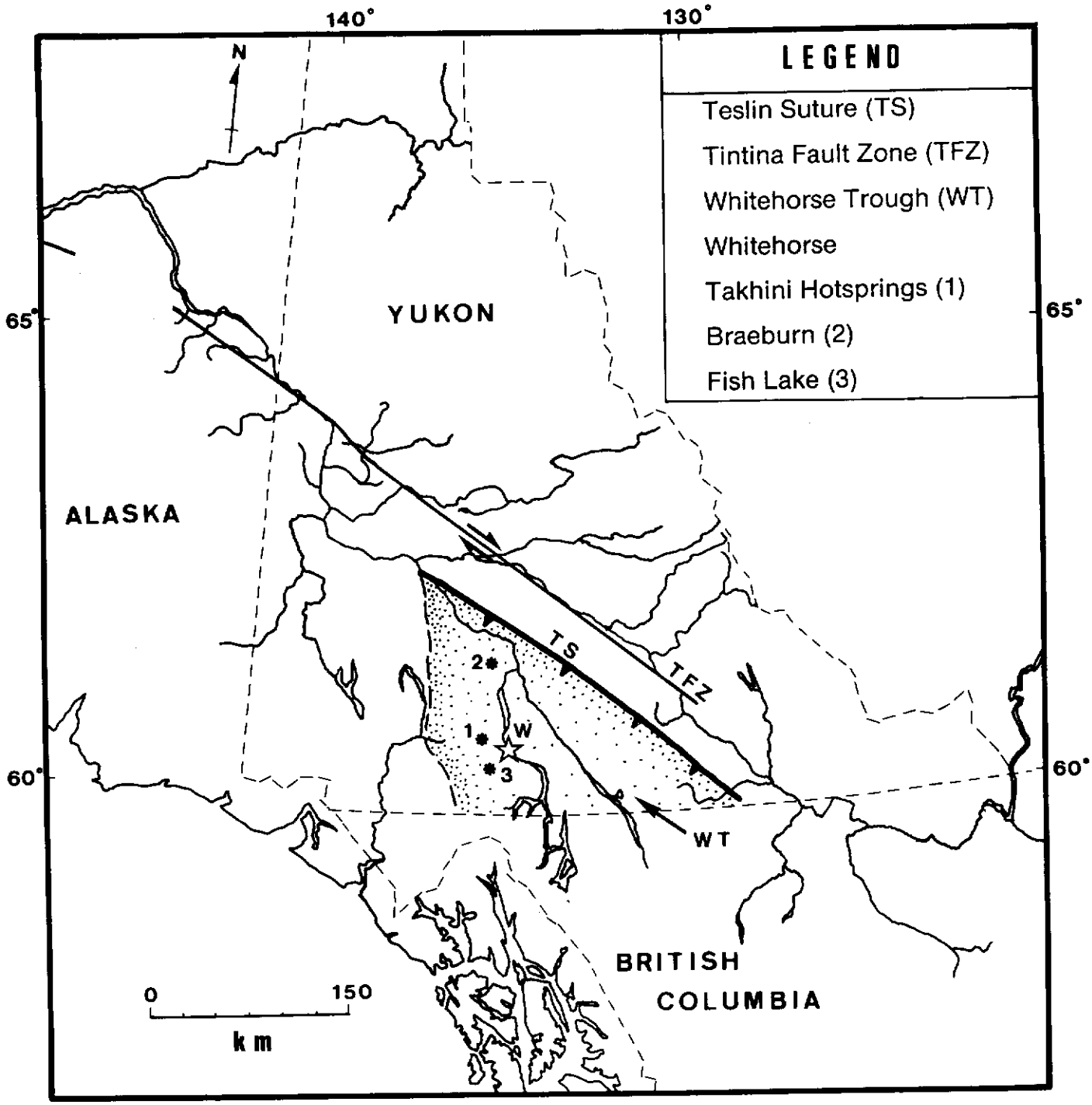

Figure 2. Location Map for studied sections and major tectonic features.

defined cross-beds (subfacies 8b). Low-angle cross-bedded pebbly sandstones line shallow scours, and grade into sheets (subfacies 8c). These represent subaqueous grain-flows, fluvial channel megaripples, and fan sheet-flood deposits, respectively.

9) Planar-Tabular Cross-Bedded Conglomerate

Matrix-supported polymictic conglomerate, displaying low-angle planar-tabular cross-beds (sets 50-80 cm), formed as foresets on transverse bars in the braided reach of a fan-delta.

10) Clast-Supported Conglomerate

Polymictic, chaotic, massive framework conglomerate (subfacies 10a) (Fig. 3) rarely displays a fabric with a-b planes of discoidal clasts parallel to bedding. Openwork (rarely) matrix-filled conglomerate (subfacies 10b) is typically massive, but rarely displays crude low-angle planar-tabular cross-beds. These reflect deposition by mass-flow gravel dispersions and braid-bar foresets, respectively.

11) Matrix-Supported Conglomerate

Normally-graded polymictic conglomerate (subfacies 11a) suggests deposition by hyperconcentrated flows, whereas reverse-graded conglomerate, typically displaying a sheared sandy mudstone base (subfacies 11b) is indicative of debris flow deposition.

12) Boulder Conglomerate (Fig. 4)

Boulder conglomerate is massive, containing clasts up to 2.5 m in diameter. Incised channel features, defining the base of many of these beds, suggest these conglomerates are proximal fan trench-fill deposits.

Figure 3. Laberge conglomerates, Annie Lake. Note that pebble conglomerate (Facies 10a) overlies scour-based coarse massive sandstone (Facies 6).

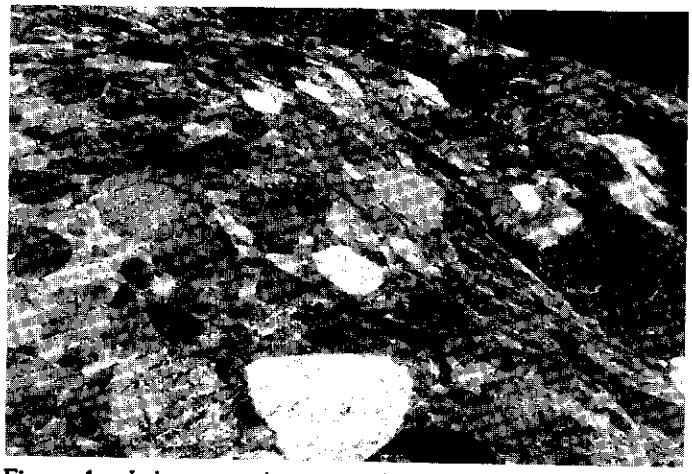

Figure 4. Laberge conglomerate, Alaska Highway Boulder conglomerate (Facies 12) displays chaotic fabric and clast-support. Hammer for scale.

FACIES TRENDS

Conglomerate beds at Takhini Hotsprings were observed to display an apparent cyclic nature, recognized as fining-up sequences (to mudstone) 5-15 m thick. In order to test for cyclicity, an embedded Markov Chain Analysis was performed (Miall, 1973). An identical test was performed on the correlative section at Braeburn. Braeburn trends were much less ordered, with the only strong trend exhibited as coarsening-up sequences.

The preferred facies trend at Takhini Hotsprings is shown in Figure 5. This sequence represents deposition within the braided reaches of possible fan-delta complexes. The lower coarsening-up sequence, from cross-bedded pebbly sandstone to sheet-like gravel lined scours and parallel laminated sandstone, is interpreted as a transition from a normal channel sedimentation to flood-flow deposition. The overlying chaotic conglomerates (debris flows) were perhaps triggered by similar flood events which deposited the underlying facies. Braided-reach conglomerate and debris flow facies tend to be overlain by fining-up siltstone-silty mudstone. Desiccation cracks suggest that these beds were deposited in spill-over channels which became exposed and inactive during low-flood conditions.

Fish Lake and Braeburn sections show few facies trends. Facies are very coarse and typically randomly stacked. At Braeburn there is some coarse-tail normal grading of angular volcanic clasts in pebbly sandstone beds. Fish Lake beds are mainly massive pebble/cobble conglomerates. Turbidite occurs at the base of the section; whereas minor bioturbated silty mudstone occurs toward the top. Fish Lake strata are interpreted as distal submarine fan-delta deposits with shallow marine facies at the top (upper 150 m).

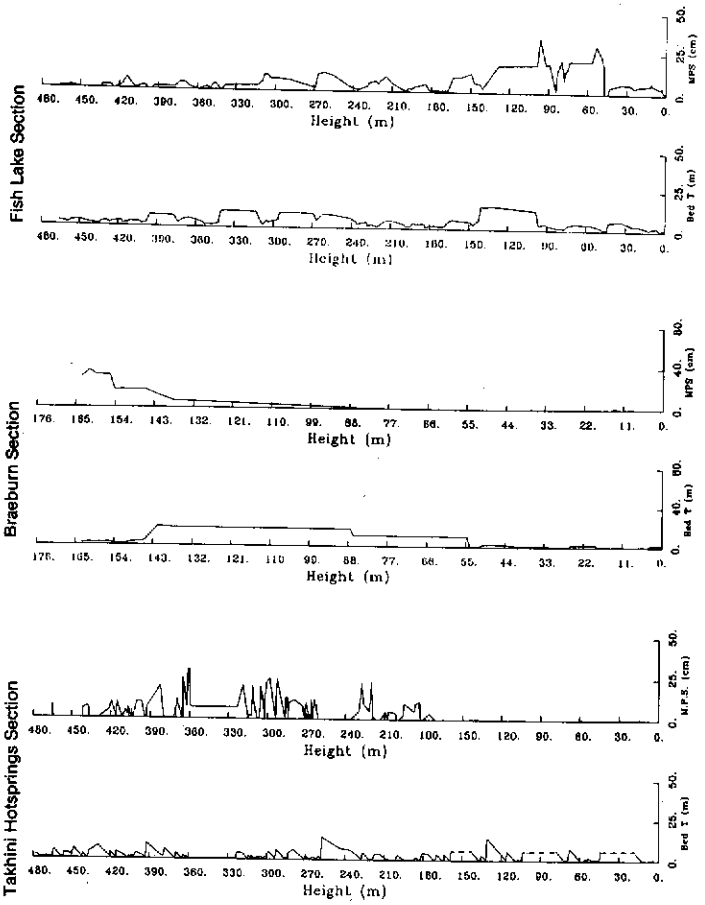

Figure 5. Maximum particle size (MPS) and bed thickness (Bed +) plots for measured sections. Takhini Hotspring data is non-smoothed, whereas the Braeburn and Fish Lake plots have been subjected to moving average techniques.

Broad-scale trends show that the three sections display coarsening-up sequences (120 m thick), with fining-up sequences at the top. Fish Lake strata are indicative of channel switching (or abandonment), followed by reactivation and progressive coarsening until shallow marine facies appear (top 150 m). Influx of arc-derived clasts follows grain-size trends (Fig. 6), suggesting tectonic activity controlled structural unroofing of arc plutons and fault talus generated in the source terrane. Bed-thickening trends are vague, but reflect channel abandonment cycles where conglomerates are capped by thick mudstone facies (Takhini Hotsprings section). This points to erosion-dominated, moderate-gradient fan surfaces, where short-lived depositional events were followed by long periods of non-deposition or erosion (Fig. 7) (abundant intraclasts; thick mudstone plugs). Bed-thinning trends at Braeburn are indicative of a steep-gradient erosion-dominated fan. Fining-up sequences probably represent re-equilibration of fan sediments to faulting, or back-stepping of source terrane faults which is unlikely to be extensive in a collisional (compressive) tectonic setting.

CONCLUSIONS

The Whitehorse Trough developed through oblique collision of the Stikine arc terrane with the North American craton. Arc deformation, resulting from vectoral separation of oblique subduction into normal and transcurrent stress fields (Beck, 1986), supplied detritus to the basin through exhumation and erosion of plutonic and volcanic arc material. Minor facies cycles represent ephemeral channel switching/abandonment on a distal fan (Takhini Hotsprings); whereas progressive overlap of proximal over medial fan debris flow facies (Braeburn) indicates fan progradation. Large-scale trends represent fan progradation and retreat, indicative of tectonic events in the source terrane. The overall effect is one of increasing "alluvial influence" on

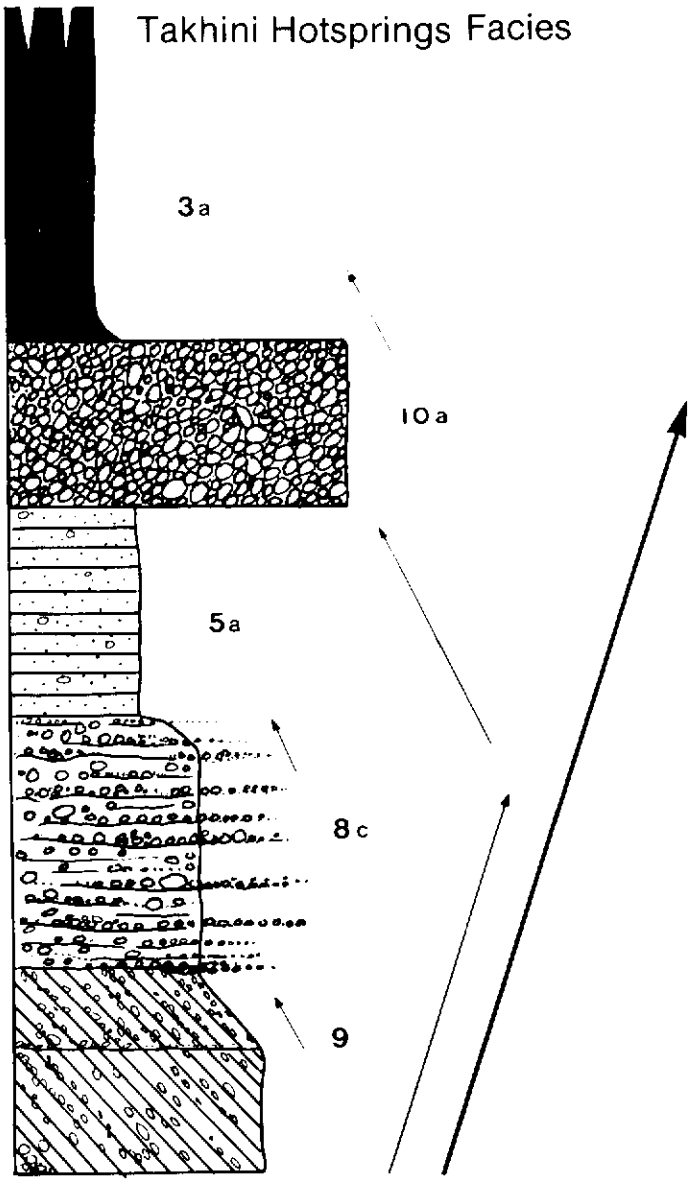

Figure 6. Preferred facies sequence; Takhini Hotsprings. Arrows depict bed-scale fining/coarsening trends and sequence-scale coarsening up trends.

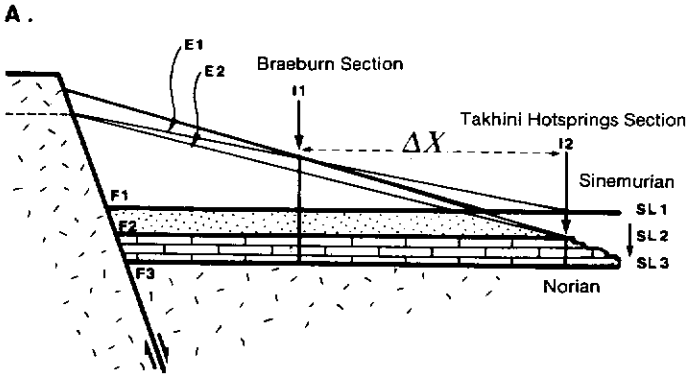

Figure 7a. Tectonic subsidence creates progradation and basinward migration of intersection point (I1 to I2) and erosion surface (E1 to E2). Braeburn section (proximal fan) and Takhini Hotsprings sections shown.

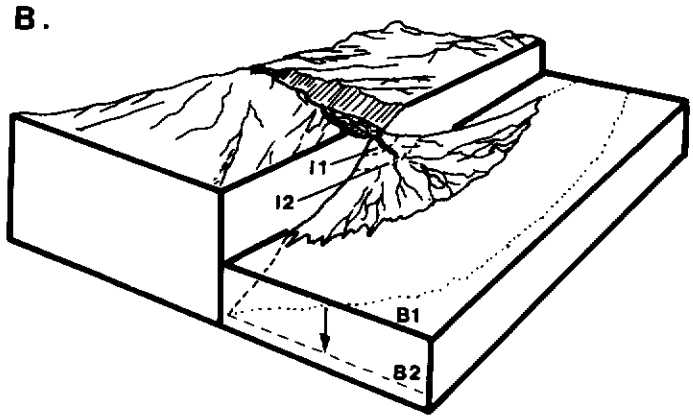

Figure 7b Block diagram of fan progradations. Drop in base level (B1 to B2) creates progradation of intersection point (I1 - I2).

sedimentation. Shallowing-up trends at Fish Lake occurred when the Stikine terrane accreted to the craton. Obduction of the arc terrane over the miogeocline (tectonic ramp) (C. Beaumont, 1988, pers. comm.) in Early Jurassic time (Tempelman- Kluit, 1979) created lithospheric depression of the ancient rifted margin, and induced tectonic subsidence, reflected by prograding (coarsening-up, erosion-dominated fans. By the Middle Jurassic, obduction caused the tectonic-subsidence regime to change to an orogenic regime. The transition is expressed in the sedimentary record as shoaling-up facies sequence.

ACKNOWLEDGEMENTS

We would like to express our thanks to E. Kreft, J. Brown, and B. Petherick at Takhini Hotsprings; and to S. Morison, G. Abbott, and T. Bremner, Geological Services Division, D.I.A.N.D. Funding was through an NSERC grant to F.J. Hein.

Summary Facies Table

Facies	Lithology	Grading	Structures	Average Thickness
1	Floatstone/ Micrite	None	Planar Lamination (rare)	1.00 m
2	Calcarenite/ Rudite	None	None	1.40 m
3a	Red Mudstone	Normal	Desiccation cracks	3.30 m
3b	Red Mudstone	None	Bioturbation	0.40 m
4	Sandstone/Mudstone Couplets	Normal	BC (E) sequences	—
5a	Planar Stratified Sandstone	None	Planar stratification	0.50 m
5b	Low-angle Stratified Sandstone	None	Low-Angle stratification	0.15 m
6	Massive Sandstone	Normal	None	0.70 m
7a	Cross-Stratified Sandstone	None	Trough Cross-stratification	0.83 m
7b	Hummocky Cross-Stratified Sandstone	None (Normal)	HCS	0.40 m
8a	Granule/Pebble Sandstone	Normal; Reverse-to-Normal	None	1.00 m
8b	Trough Cross-Bedded Pebbly Sandstone	Normal	Trough Cross beds	1.00 m
8c	Low-Angle Stratified Pebbly Sandstone	None	Inclined stratification	0.40 m
9	Planar-Tabular Cross-Bedded Pebbly Sandstone	None	Planar-tabular Cross-beds	0.65 m
10a	Conglomerate (Clast-Support)	None (normal)	Massive; Imbrication	2.00 m
10b	Conglomerate (Openwork/Matrix-Filled)	None (Normal)	Massive (Inclined stratification)	0.90 m
11a	Conglomerate (Matrix-Support)	Normal (Coarse-Tail)	Massive	2.00 m
11b	Conglomerate (Matrix-Support)	Reverse; Reverse-to-Normal	Massive (Imbrication)	2.00 m
12	Conglomerate (Boulder/Clast-Support)	None (Reverse) (Normal)	Massive (a-b Axis Alignment)	2.50 m

REFERENCES

BECK, Jr., M.E. 1986. On the mechanism of tectonic transport in zones of oblique subduction; Tectonophysics, Vol. 93, p. 1-11.

HILLS, L.V., SANGSTER, E.V., and SUNEBY, L.B. (eds.) 1981. Lexicon of Canadian Stratigraphy (Vol. 2); Yukon Territory and District of Mackenzie; Canadian Society of Petroleum Geologists, p. 105-106.

MIALL, A.D., 1973. Markov chain analysis applied to an ancient alluvial plain succession; Sedimentology, Vol. 20, p. 347-364.

REID, R.P., and TEMPELMAN-KLUIT, D.J. 1987. Upper Triassic Tethyan-type reefs in the Yukon; Bulletin of Canadian Petroleum Geology, Vol. 35, No. 3, p. 316-332.

TEMPELMAN-KLUIT, D.J., 1979. Transported cataclasite, ophiolite and granodiorite in Yukon: Evidence of arc-continent collision; Geological Survey of Canada, Paper 79-14, 27 p.

TOZER, E.T., 1958. Stratigraphy of the Lewes River Group (Triassic), central Laberge area, Yukon Territory. Geological Survey of Canada, Bulletin 43, 28 p.

WHEELER, J.O., 1961. Whitehorse map-area, Yukon Territory (105 D); Geological Survey of Canada Memoir 312, 156 p.

PERMO-TRIASSIC ISOTOPIC DATES FOR BLUESCHIST, ROSS RIVER AREA, YUKON

P. Erdmer
Department of Geology,
University of Alberta,
Edmonton, Alberta, T6G OW3

and

R.L. Armstrong
Department of Geological Science,
University of British Columbia,
Vancouver, B.C., V6T 2B4

ERDMER, P., and ARMSTRONG, R.L., 1988. Permo-Triassic dates for blueschist, Ross River area, Yukon; in Yukon Geology, Vol. 2; Exploration and Geological Services Division, Yukon, Indian and Northern Affairs Canada, p. 33 - 36.

ABSTRACT

Rb-Sr and K-Ar age determinations for muscovite-bearing blueschist in the Yukon-Tanana terrane near Ross River indicate a minimum metamorphic age of approximately 250 Ma, and a mid-Paleozoic protolith age. The blueschist is associated with eclogite in a tectonized assemblage of phyllite, quartzite, micaschist, and serpentinite. Neither mid-Jurassic metamorphism nor mid- Cretaceous regional plutonism have affected these high-pressure rocks to the point of resetting the isotopic systems. Parts of the Yukon-Tanana terrane thus record a Late Paleozoic metamorphism. If the blueschist and eclogite were part of the trench melange of the Lewes River Arc, their age implies that the arc was active in Late Paleozoic time.

RÉSUMÉ

Les datations par les méthodes Rb-Sr et K-Ar d'un schiste bleuté à glaucophane contenant de la muscovite, provenant du terrane de Yukon-Tanana près de Ross River, indiquent que le métamorphisme date au minimum d'environ 250 Ma, et que la roche originelle date du Paléozoïque moyen. Le schiste bleuté à glaucophane est associé à de l'éclogite dans un assemblage tectonisé de phyllite, quartzite, micaschiste et serpentinite. Ni le métamorphisme du Jurassique moyen ni le plutonisme régional du Crétacé moyen n'ont modifié ces roches formées dans des conditions de pression élevée au point de remettre à zéro les systèmes isotopiques. Ainsi, des portions du terrane de Yukon-Tanana ont enregistré un métamorphisme d'âge paléozoïque supérieur. Au cas où le schiste bleuté à glaucophane et l'éclogite feraient partie du mélange présent dans la fosse de l'arc de Lewes River, leur âge signifierait que l'arc était actif durant le Paléozoïque supérieur.

INTRODUCTION

This note presents the results of Rb-Sr and K-Ar age determinations of blueschist near Ross River, along the tectonic contact between high-pressure metamorphic rocks of the accreted Yukon-Tanana terrane, and lower-grade rocks, dominantly of North American affinity, to the east. The petrology and regional significance of the blueschist and of associated eclogite have been documented previously (Erdmer, 1987); the isotopic data presented here support the published structural and petrologic interpretation. The high-pressure rocks are part of a high-pressure tectonic melange, formed in an Upper Paleozoic arc before being accreted to North America in mid-Mesozoic time. These rocks were not affected by early to mid-Jurassic and mid-Cretaceous regional metamorphism which are pervasive elsewhere in the Yukon-Tanana terrane.

SETTING

The newly dated rocks are located east of Tintina Fault, in the hanging wall of Vangorda Fault (Tempelman-Kluit, 1972), a northwest-striking, steeply southwest-dipping structure which juxtaposes serpentinite, and mylonitic rocks of Nisutlin Allochthon (Tempelman-Kluit, 1979a), against lower-grade basalt of the Anvil Range Group (Gordey, 1983), and against underlying rocks of North American miogeoclinal affinity to the east. Vangorda Fault is part of the Finlayson Lake fault zone (Mortensen and Jilson, 1985). Other northwest-striking, steeply-dipping faults that occur in the vicinity are related to the Finlayson Lake system or to the Tintina system, and have a complex displacement history that includes early reverse, strike-slip, and late normal periods of movement (Pigage and Jilson, 1985). The tectonic slice of high-pressure rocks is thus internally disrupted, and highly exotic with respect to adjacent rocks to the east.

The blueschist locality is easily accessible from the Pelly River, or by a helicopter flight of a few minutes from either Ross River or Faro. The best exposure is on a small knoll at locality PE85-25 (Fig. 1; UTM coordinates E617025, N6884225; Grid Zone 8V, 1:100 000 Square: PD). Blueschist occurs on several hills a few hundred metres long, as quartz-muscovite-glaucophane- garnet schist and as glaucophane-muscovite quartzite. Other associated rock types, more abundant than the glaucophane-bearing rocks, are muscovite phyllite, graphitic quartzite, and biotite micaschist. Compositional layering and schistosity dip moderately to steeply to the southwest.

RESULTS

A sample of micaceous quartzite (sample 1) and of micaschist (sample 2) were analyzed. Isotopic data are given in Table 1.

Rb-Sr determinations on whole rock and muscovite yield concordant muscovite dates at approximately 246 Ma. The indicated whole rock age is approximately 344 Ma, which suggests a protolith of Mississippian or somewhat older age for the metasedimentary sequence. The protolith age of the accompanying eclogite is unknown. It is assumed to be Mississippian or younger as the eclogite is probably derived from basic dykes or sills intruded into the metasedimentary sequence.

The K-Ar dates are slightly older (256 and 267 Ma), but their two sigma errors overlap the Rb-Sr results, and the age difference is not considered geologically significant.

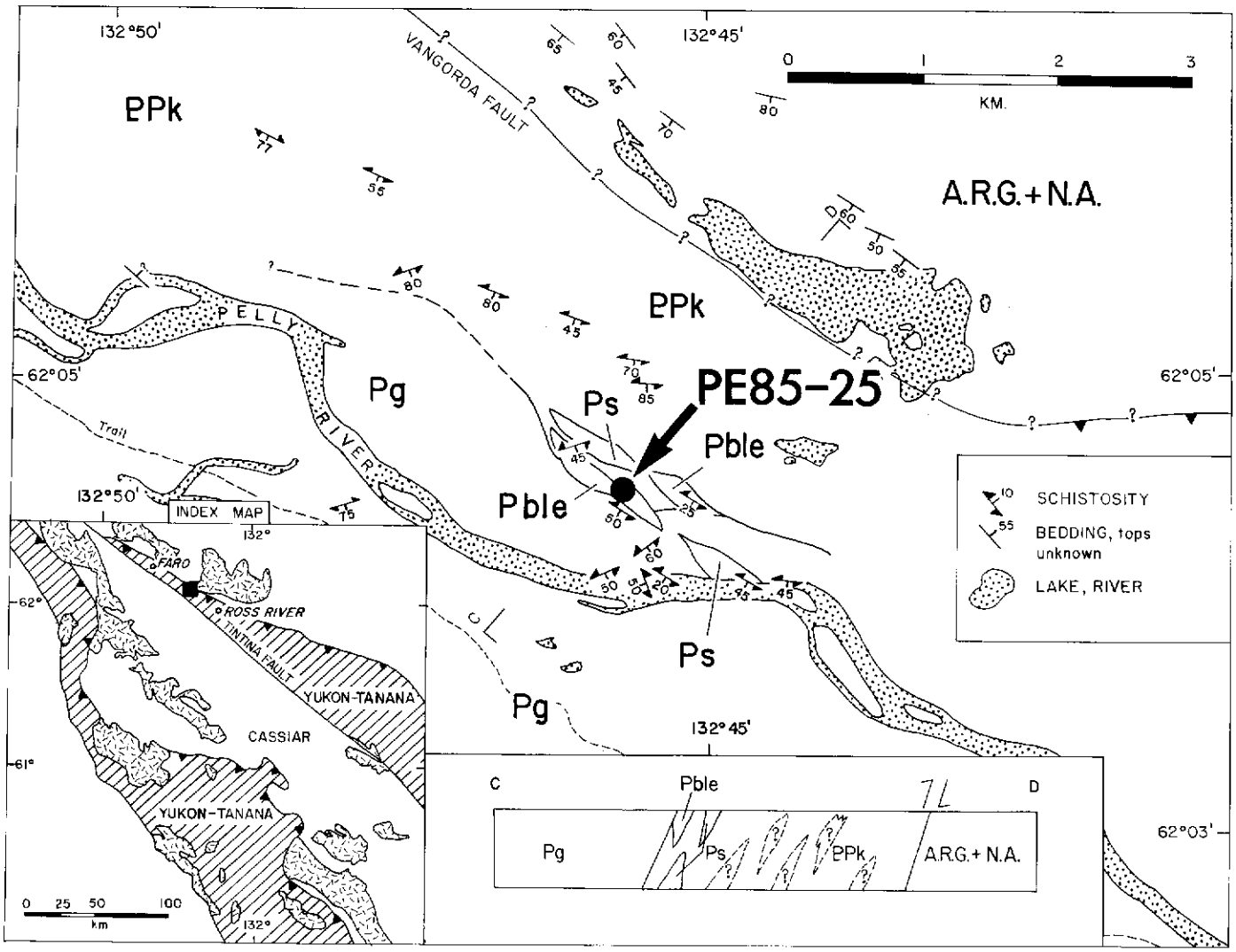

Figure 1. Geological setting and location of the blueschist locality near Ross River. Abbreviations: PPk: mylonitic phyllite, graphitic quartzite, and micaschist; Pble: blueschist and eclogite; Pg: actinolite and hornblende greenstone; Ps: serpentinite; A.R.G.+ N.A.: rocks of the Anvil Range Group and of North American affinity (see text). Symbols: teeth on thrust fault are in hanging-wall. Index map symbols: hachures: Yukon-Tanana terrane; dash pattern: mid-Cretaceous quartz-monzonite plutons; Cassiar terrane includes rocks equivalent to N.A. strata. Geology after Tempelman-Kluit 1972, from personal communication by G.A. Jilson, and from field work in 1985 and 1986.

DISCUSSION

The Late Permian/Early Triassic minimum age (250 Ma) of metamorphic muscovite in the blueschist is comparable to a mid-Permian age of 258 Ma (recalculated using modern constants from an age of 255 Ma) obtained by Wanless et al. (1978) for muscovite in eclogite at Faro, 30 km along strike in the same tectonic slice.

Two main conclusions can be drawn. The first is that neither regional mid-Cretaceous plutonism (exemplified by the Anvil Batholith near Faro, emplaced approximately 100 Ma ago (Pigage and Anderson, 1985) nor early to mid-Jurassic metamorphism in the Yukon-Tanana terrane (160-180 Ma isotopic dates, Tempelman-Kluit and Wanless, 1975; 185-213 Ma dates, Hansen, 1987) have affected the blueschist and eclogite. Parts of the Yukon-Tanana terrane thus preserve a record of Late Paleozoic metamorphism.

The second conclusion is that although cataclasis is Late Triassic or younger as recorded in rocks of Nisutlin Allochthon (Upper Triassic conodonts in deformed parts of Nisutlin Allochthon, Templeman-Kluit, 1979b; and Rb-Sr data for the Klondike Schist which suggest an age of cataclasis of 202 Ma, Metcalfe and Clark, 1983), the 250 Ma minimum age of peak metamorphism and ductile deformation in the high-pressure rocks is distinctly older. If the blueschist and eclogite were part of trench melange of the Lewes River Arc (Tempelman-Kluit, 1979a), the arc must have been active in Late Paleozoic time (see discussion in Erdmer, 1987). The isotopic age also implies that high- grade fabrics in other parts of Nisutlin Allochthon may have developed during the late Paleozoic, rather than during the Mesozoic. Early Triassic to Late Paleozoic K-Ar dates for muscovite (245 Ma) and amphibole (278 Ma) of the Clinton Creek area (Htoon, 1979) are another example where Paleozoic isotopic dates are preserved in the Yukon-Tanana terrane. It is worth noting that all known localities for older dates are located in the northernmost part of the terrane in Canada.

The work was financed by NSERC operating grants (PE and RLA) and by a grant from the Boreal Institute for Northern Studies (PE).

Table 1. Analytical results

A. Rubidium-strontium data from whole rock analysis and muscovite

Sample No.	Type	ppm Sr ± 5%	ppm Rb ± 5%	Rb/Sr ± 2%	$^{87}Rb/^{86}Sr$	± 0.01% $^{87}Sr/^{86}Sr$	Age (Ma) ± 10	Initial $^{87}Sr/^{86}Sr$	Comments
PE85-25 (1) WR	micaceous quartzite whole rock	44.6	54.9	1.232	3.57	0.72457	344 ± 10	0.7071 ± 2	Whole rock age is mid-Paleozoic
MS	muscovite	60.2	269.5	4.47	13.01	0.75762	246 ± 7	0.7121 ± 5	
PE85-25 (2) WR	micaschist (whole rock)	223	63.6	0.286	0.827	0.71114	249 ± 6	0.7082 ± 1	
– MS	weakly magnetic muscovite	111	182	1.643	4.76	0.72507	246 ± 4	0.7083 ± 1	Concordant muscovite dates at ≈246 Ma
– MS-NM	nonmagnetic muscovite	109	209	1.914	5.55	0.72749	243 ± 6	0.7083 ± 1	

B. Potassium-argon data for muscovite

Samples No.	Type	%K	$^{40}Ar^*$ x $10^{-6}cm^3/g$	$^{40}Ar^*/^{40}Ar$ total	Age (Ma) ± 10
PE85-25 (1)	muscovite	8.51 ± 0.06	90.769	0.891	256 ± 8
PE85-25 (2)	muscovite	7.60 ± 0.10	84.885	0.904	267 ± 8

Ar^* indicates radiogenic argon.

All analyses were done at the Geochronometry Laboratory, Department of Geology, University of British Columbia, by D. Runkle, R.L. Armstrong, and J. Harakal.

Rb and Sr concentrations were determined by replicate analysis of pressed powder pellets using x-ray fluorescence. U.S. Geological Survey rock standards were used for calibration; mass absorption coefficients were obtained from Mo Ka Compton scattering measurements. Rb/Sr ratios have a precision of 2% (1). Sr isotopic composition was measured on unspiked samples prepared using standard ion exchange techniques. The mass spectrometer, V.-G. Isomass 54R, has data aquisition digitized and automated using a H.P. 85 computer. Experimental data have been normalized to a $^{86}Sr/^{88}Sr$ ratio of 0.1194 and adjusted so that the NBS standard $SrCO_3$ (SRM987) gives a $^{87}Sr/^{86}Sr$ ratio of 0.71020 ± 2 and the Eimer and Amend Sr a ratio of 0.70800 ± 2. The precision of a single $^{87}Sr/^{86}Sr$ ratio is -×-0.00010 (1). Rb-Sr dates are based on a Rb decay constant of $1.42 \times 10^{-11}a^{-1}$. Regressions are calculated according to the technique of York (1967).

K is determined in duplicate by atomic absorption using a Techtron AA4 spectrophotometer and Ar by isotope dilution using an AEI MS-10 mass spectrometer and high purity ^{38}Ar spike. The constants used are:

$$K_e = 0.581 \times 10^{-10}s^{-1},\ K_B = 4.962 \times 10^{-10}a^{-1},\ ^{40}K/K = 0.01167 \text{ atom percent.}$$

Decay constants are those recommended by the IUGS Subcommission on geochronology (Steiger and Jager 1977). Errors reported are for one standard deviation or the standard error on the mean, unless otherwise noted.

REFERENCES

ERDMER, P., 1987. Blueschist and eclogite in mylonitic allochthons, Ross River and Watson Lake areas, southeastern Yukon; Canadian Journal of Earth Sciences, Vol. 24, p. 1439-1449.

GORDEY, S.P., 1983. Thrust faults in the Anvil Range and a new look at the Anvil Range Group, south-central Yukon Territory; in Current Research, Part A, Geological Survey of Canada, Paper 83-1A, p. 225-227.

HANSEN, V.L., 1987. Tectonic correlations of the Yukon-Tanana (YTT) and Slide Mountain terranes; Geological Society of America, Cordilleran Section Annual Meeting, Program w. abstracts, p. 386.

HTOON, M., 1979. Geology of the Clinton Creek asbestos deposit, Yukon Territory; M.Sc. thesis, University of British Columbia, 194 p.

METCALFE, P., and CLARK, G.S. 1983. Rb-Sr whole-rock age of the Klondike Schist, Yukon Territory; Canadian Journal of Earth Sciences, Vol. 20, p. 886-891.

MORTENSEN, J.K., and JILSON, G.A. 1985. Evolution of the Yukon-Tanana terrane: evidence from southeastern Yukon Territory; Geology, Vol. 13, p. 806-810.

PIGAGE, L.C., and ANDERSON, R.G. 1985. The Anvil Plutonic Suite, Faro, Yukon Territory; Canadian Journal of Earth Sciences, Vol. 22, p. 1204-1216.

PIGAGE, L.C., and JILSON, G.A. 1985. Major extensional faults, Anvil Pb-Zn district, Yukon; Geological Society of America, Cordilleran Section Annual Meeting, Program with abstracts, p. 400.

STEIGER, R.H., and JAGER, E. 1977. Subcommission on Geochronology: Convention on the use of decay constants in geo- and cosmochronology; Earth and Planetary Science Letters, Vol. 36, p. 359-362.

TEMPELMAN-KLUIT, D.J., 1972. Geology and origin of the Faro, Vangorda, and Swim concordant zinc-lead deposits, central Yukon Territory; Geological Survey of Canada, Bulletin 208, p. 73.

TEMPELMAN-KLUIT, D.J., 1979a. Transported cataclasite, ophiolite, and granodiorite in Yukon: evidence of arc-continent collision; Geological Survey of Canada, Paper 79-14, p. 27.

TEMPELMAN-KLUIT, D.J., 1979b. Five occurrences of transported synorogenic clastic rocks in Yukon Territory; in Current Research, Part A, Geological Survey of Canada, Paper 79-1A, p. 1-12.

TEMPELMAN-KLUIT, D.J., and WANLESS, R.K. 1975. Potassium-argon age determinations of metamorphic and plutonic rocks in the Yukon Crystalline Terrane; Canadian Journal of Earth Sciences, Vol. 17, p. 1895-1909.

WANLESS, R.K., STEVENS, R.D., LACHANCE, G.R., and DELABIO, R.N. 1978. Age determinations and geological studies: K-Ar isotopic ages, report 13; Geological Survey of Canada, Paper 77-2, p. 60.

THE TECTONIC SETTING OF THE AISHIHIK BATHOLITH, SW YUKON

Stephen T. Johnston
Department of Geology
University of Alberta
Edmonton, Alberta
T6G 0P9

JOHNSTON, S.T., 1988. The tectonic setting of the Aishihik Batholith, SW Yukon; in Yukon Geology, Vol. 2; Exploration and Geological Services Division, Yukon, Indian and Northern Affairs Canada, p. 37 - 41.

ABSTRACT

The Aishihik Batholith is comprised of foliated and lineated, equigranular hornblnde granodiorite and crystallized at about 216 Ma. The batholith is in contact to the west with a metamorphic terrane of continental affinity. However, this contact lacks intrusive features common to the margins of most granitic bahtoliths. In addition, rocks adjacent to the contact are mylonitized and ductiley deformed. These relationships suggest that the Aishihik Batholith does not intrude the adjacent metamorphic terrane, but is allochthonous above it. Kinematic indicators are consistent with the Middle Jurassic quartz monzonite plutons cut the detachment implying that tectonism occurred during, or prior to the Early Jurassic.

The significance and regional extent of this detachment remains a matter of conjecture. The batholith, part of the Stikine volcanic arc, may have originally intruded the metamorphic terrane. Tectonic modification of this relationship could have occured during collision of Stikinia with North America. Alternatively, Stikinia may be far travelled with respect to the batholith.

RÉSUMÉ

Le batholite d'Aishihik est composé de granodiorite isogranulaire à hornblende, feuilletée et portant des linéations, dont la cristallisation a eu lieu il y a environ 216 Ma. A l'ouest, le batholite se trouve au contact d'un terrane métamorphique d'affinités continentales. Toutefois, ce contact ne montre pas les caractères d'intrusion courants sur les marges de la plupart des batholites granitiques. En outre, les roches jouxtant le contact sont mylonitisées et ont subi une déformation ductile. Ces relations suggèrent que le batholite d'Aishihik n'est pas intrusif dans le terrane métamorphique adjacent, mais est allochtone au-dessus de celui-ci. Les indicateurs cinématiques indiqueraient que le batholite a été tectoniquement mis en place le long d'un décollement d'orientation approximative ouest. Les plutons de monzonite quartzique d'âge jurassique moyen ont été mis en place et le tectonisme s'est produit durant ou avant le Jurassique inférieur.

L'importance et l'extension régionale de ce décollement sont encore un sujet de spéculation. Le batholite, qui fait partie de l'arc volcanique de Stikine, a peut-être été initialement intrusif dans le terrane métamorphique. La modification tectonique de cet ensemble a peut-être eu lieu durant la collision du secteur de Stikinia avec l'Amérique du Nord. Autrement, ce secteur de Stikinia s'est peut-être déplacé fortement par rapport au batholite.

INTRODUCTION

The Aishihik Batholith is one of a series of Late Traissic granodiorite batholiths which underlie the west margin of the Northern Intermontane Belt, or Whitehorse Trough. To the east the Aishihik Batholith is overlain by or intrudes Triassic and younger volcanic, volcaniclastic and sedimentary rocks of the Lewes River and Laberge Groups. A metamorphic terrane of continental affinity, comprised of amphibolite grade rock of Paleozoic(?) age, underlies the are immediatley west of the batholith (Fig. 1). This assemblage played a key role in the evolution of the Northern Cordillera. The batholith and volcanic rocks are thought to have developed within a volcanic arc active in the Triassic and Early Jurassic. The arc, known as Stikinia, may have developed on continental crust, represented by the metamorphic sequence. Accretion of Stikinia to North America, beginning in the Early Jurassic, is though to be responsible for deformation and overthrusting of North American miogenosynclinal strata to the east (Tempelman-Kluit, 1979).

This model is based on the regional distribution of exotic terranes with respect to North American rocks. There remains, however, little detailed documentation of individual tectonic units and their relationships to one another (e.g. Erdmer, 1986, Hanson, 1987). This study, part of an ongoing Ph. D program being undertaken at the University of Alberta under the supervision of Dr. P. Erdmer, aims to test part of this model by documenting the nature and origin of the Aishihik Batholith. In this paper a petrographic description of the batholith is presented and the structure of the west margin of the batholith described.

The batholith is allochthonous above the adjacent metamorphic terrane and was tectonically emplaced during the Late Triassic along a west-verging detachment. Some of the tectonic implications of these observations are briefly discussed.

THE AISHIHIK BATHOLITH

The Aishihik Batholith consists largely of foliated and lineated, coarsely crystalline, equigranular, hornblende granodiorite (Fig. 2). In the unglaciated parts of central Aishihik Lake Map Area highly weathered granodiorite forms large isolated 'castles'. Along Aishihik Lake relatively fresh granodiorite is exposed in smooth, glaciated outcrops. Preliminary U-Pb results from zircons separated from four samples of the batholith indicate a crystallization age of about 216 Ma.

Petrography

The batholith exhibits a narrow compositional range. Granodiorite and quartz-monzodiorite are the most common phases; quartz-diorite and quartz-monzonite occur infrequently. Andesine plagioclase comprises 40% to 50% of the rock and ocurs as mildly zoned, euhedral laths. It appears chalky white in hand specimen and exhibits sericite ±epidote ±calcite alteration. Potassium feldspar constitutes up to 20% of the rock and occurs both as euhedral grains interstitial to plagioclase and locallly as large poikilitic megacrysts containing small hornblende grains. Myrmekitic intergrowths of feldspar and quartz frequently mantle the megacrysts. Potassium

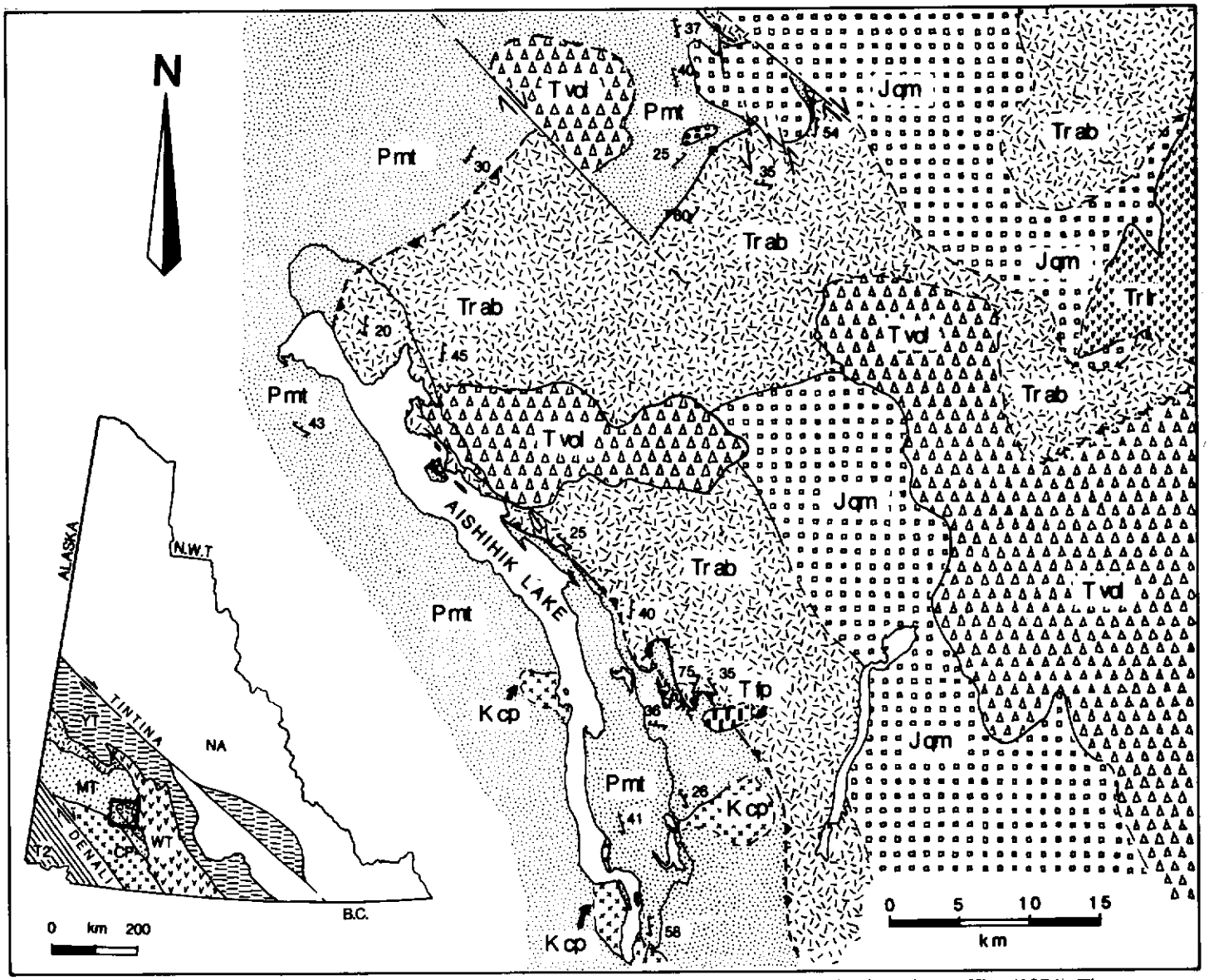

Figure 1. Map of the bedrock geology of part of the Aishihik Lake Map Area. Geology is in part after Templeman-Kluit (1974). The map area is outlined on the index map.

LEGEND (FIGURE 1)

TERTIARY

- Tvol — undifferentiated, felsic and intermediate volcanics, including rocks of the Carmacks Group.
- Tfp — Andesitic, feldspar porphyry dykes and plugs. Dykes are not indicated on map.

CRETACEOUS

- Kcp — Coarsely crystalline, hornblende granodiorite and diorite of the Ruby Range, part of the Coast Plutonic Complex.

JURASSIC

- Jqm — Feldspar porphyritic, leucocratic, pink quartz-monzonite.

TRIASSIC

- Trlr — Green, andesitic volcanics and volcaniclastics, thought to be correlative with rocks of the Lewes River Group.
- Trab — Coarsely crystalline, foliated and lineated, hornblende granodiorite of the Aishihik Batholith.

PALEOZOIC(?)

- Pmt — undifferentiated, regionally metamorphosed, amphibolite grade, quartzite, metapelite, marble and amphibolite.

INDEX MAP

- CP — Intrusions of the Coast Plutonic Complex, including rocks of the Ruby Range (Kcp).
- MT — Metamorphic terrane of continental affinity.
- NA — North American miogeosynclinal strata and younger intrusions and molasse deposits.
- T2 — Paleozoic and younger, sedimentary, volcanic, and plutonic rocks of Terrane 2.
- WT — Mesozoic andesitic and basaltic volcanics, volcaniclastics, and sediments of the Whitehorse Trough.
- YT — Paleozoic and younger, metamorphosed and deformed, ophiolite, paragneiss, and orthogneiss of the Yukon-Tanana, or Yukon Cataclastic terrane.
- Late Triassic, hornblende granodiorite batholiths (including the Aishihik Batholith) which are thought to have developed within the Stikine volcanic arc.

Aishihik Lake Road .....

Geological contact; defined, assumed .....

Foliation .....

Strike slip fault; defined, assumed .....

Normal fault; defined, assumed .....

Detachment (bounding west margin of Trab); defined, assumed ..

feldspar usually appears grey in hand specimen but weathers to a light pink. Quartz occurs interstitially to other grains and constitutes up to 25% of the rock, averaging 15% to 20%.

Mafic minerals account for less than 15% of the rock, with hornblend dominant over biotite which comprises less than 3% of the rock. The hornblende forming euhedral black to dark green prisms that show spotty to chlorite ±epiodote ± calcite. Accessory minerals include sphene, apatite and zircon.

The batholith is penetratively foliated and lineated. The lineation (L_{gd}) is defined by the alignmennt of elongate hornblende prisms. The foliation (gd) is defined by the parallel alignment of plagioclase laths and varies from weakly developed to well developed gneissic banding (Fig. 2). The development of S_{gd} was accommodated by recrystallization and cataclasis. Plagioclase grains are folded and fractured. Dissolution is often apparent along grain boundaries and fractures. Quartz grains are often recrystallized, have experienced grain-size reduction and exhibit suture boundaries and undulose extinction. Mosaic quartz has developed in strain shadows near feldspar grains.

Figure 2. Foliated, coarsely crystalline hornblende granodiorite of the Aishihik Batholith. Foliation is defined by the subparallel alignment of plagioclase lathes.

Two types of inclusions are recognized within the Aishihik Batholith. Mafic inclusions are the most extensive and consist largely of hornblende and locally of hornblende-biotite (Fig. 3). These inclusions are frequent along the west margin of the batholith and most common along the east shore of Aishihik Lake. They are well foliated, often form tabular rafts aligned with granodiorite. Several inclusions exhibit complex internal deformation not evident in the surrounding grandiorite, including ptygmatic folding of pegmatite horizons. The inclusions are often closely associated with local migmatization.

The migmatites exhibit both sharp and gradational contacts with the surrounding granodiorite. Often the migmatites are evident only as thin concordant veins of leucosome. With increased migmatization the leucosome begins to form discontinuous pods mantled by thin mafic selvages (Fig. 4).

The origin of the mafic inclusions and the migmatities remains unclear. They may represent relict fragments of the source rock which melted to produce the batholith. If true, this may indicate that a very deep portion of the batholith outcrops along its west margin. No inherited zircons from an older source rock have been found in either the migmatities or inclusions. Alternatively, they may represent an early cumulate phase of the batholith which was subsequently reworked and fragmented.

Tabular inclusions of the micaschist were seen in three localities in batholith (Fig. 5). These inclusions are muscovite-biotite schist like that of the adjacent metamorphic terrane. However, no micaschist inclusions were observed along the contact and none were directly attributable to the adjacent terrane. The origin of the inclusions remains unclear.

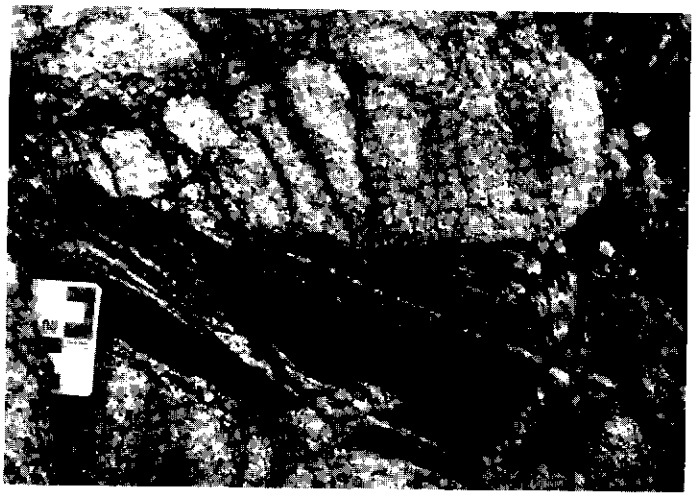

Figure 3. Mafic inclusion comprised of hornblende schist. The inclusion is cut by this pegmatite veins not continuous into the surrounding granodiorite.

Figure 4. Migmatite comprised of discontinuous pods of leucosome mantled by thin mafic selvages. These migmatites are closely associated with mafic inclusions.

Figure 5. Well foliated inclusion of gametiferous, muscovite-biotite schist. Schistosity is truncated and disrupted by granodiorite at center.

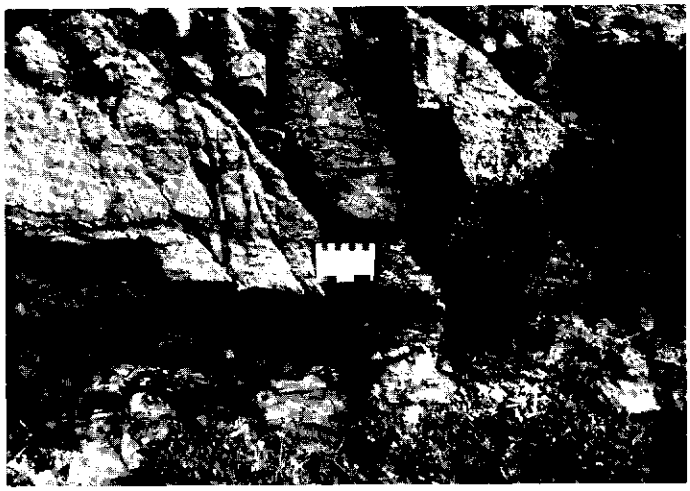

Figure 6. Contact bounding the west margin of the Aishihik Batholith. The contact is a sharp plane which dips into the photograph and separates more resistant granodiorite of the batholith (above), from more recessive schist of the metamorpic terrane (below). A thin lense of tectonized marble is evident just beneath the contact.

Figure 7. Anastomosing band of mylonite which truncates schistosity. The photograph is taken approximately 5 m beneath the detachment within the metamorphic terrane.

Figure 8. Regularly spaced extensional Riedel shears displacing a feldspathic band within the metamorphic terrane. The photograph is taken looking north, approximately 10 m beneath the detachment. The sense of asymmetry (west-dipping extensional shears) is consistent with a top to the west sense of shear.

Nature of the west margin of the batholith

The contact bounding the west margin of the Aishihik Batholith parallels foliation both in the batholith and in the adjacent metamorphic terrane. The contact dips regionally to the east, but is disrupted by younger folds, faults, and plutons (Fig. 1).

Along Aishihik Lake the contact is deformed along shallow plunging, north-trending, asymmetric, west-verging folds and locally dips to the west. In part of north-central Aishihik Lake Map Area the contact dips to the northwest beneath the metamorphic terrane. This area is thought to lie along the overturned limb of a large, asymmetric fold which is recumbent to the east. Further study is necessary to determine the relationship of this fold with the west-verging structures described above.

Middle-Jurassic pink quartz-monzonite plutons and Tertiary feldspar porphyry dykes and plugs intrude the contact and Tertiary andesitic volcanic rocks of the Carmacks Group unconformably overlie it.

Both strike-slip and normal faults of limited displacement disrupt the contact. In north-central Aishihik Lake Map Area northwest-trending right-lateral strike-slip faults and conjugate north-trending left-lateral faults are apparent. Northwest-trending normal faults cut the contact along Aishihik Lake and exhibit both east and west side down displacement.

The contact is a sharp plane that lacks features common to most intrusive contacts (Fig. 6). No dykes of the granodiorite cut the contact and intrude the metamorphic rocks. No inclusions of schist found in the batholith are directly attributable to the adjoint metamorphic terrane. No chilled margin is developed in the batholith and no contact metamorphic aureole overprints the metamorphic rocks.

While the contact lacks common igneous relationships, it is characterized by an abundance of structures indicative of tectonism. Thin and discontinuous lenses of tectonized marble are present (Fig. 6). Foliation in the granodiorite is folded and disrupted by rare, thin, anastomosing, poorly developed mylonite zones up to 3 cm thick. The metamorphic rocks are much more deformed within 150 m of the contact. Large bands of anastamosing, recrystallized mylonite truncate schistosity (Fig 7). Isoclinal, overthickened, rootless folds and refolded folds are present. In addition, intimate tectonic intermixing of amphibolites, quartzites, meta-pelites and marble, not seen elsewhere, is apparent.

In summary, the western contact of the Aishihik Batholith lacks igneous features of the margins of large granitic intrusions (s.l.). Tectonic structures include intimate tectonic intermixing of several rock-type, mylonitization, and ductile deformation are, however, present along the contact. These features suggest that the contact is a tectonic detachment and that the batholith does not intrude the adjacent metamorphic terrane but is allochthonous above it.

Kinematic indicators present along the detachment, including microstructures, Riedel shears and asymmetric boudins, are consistent with the batholith having been emplaced westward over the metamorphic terrane (Fig. 8). Tectonism occurred during, or prior to, the Early Jurassic, as constained by Middle Jurassic quartz-monzonite plutons which cut the detachment (Fig.1). Blocks of foliated granodiorite similar to that of the Aishihik batholith are incorporated into the overlying Lewes River Group. This suggest that tectonic emplacement of the batholith occurred in the Late Triassic and resulted in its uplift and subsequent exposure.

DISCUSSION

The Aishihik Batholith and the overlying volcanics of the Whitehorse Trough developed the Stikine volcanic arc, which was active in the Triassic and Jurassic. The metamorphic terrane along the west margin of the Aishihik Batholith has been considered part of an exotic continental block into which the batholith was emplaced (Tempelman-Kluit, 19879). The batholith does not, however, intrude the metamorphic terrane but is allochthonous above it and was

tectonically emplaced during the Late Triassic along a west-verging detachment. The significance and regional extent of this detachment remains a matter of conjecture.

The batholith does contain micaschist inclusions which resemble and may have been derived from, part of the metamorphic terrane. This would imply that Stikinia did develop upon the metamorphic terrane and that subsequent tectonism resulted in modification of this relationship.

Alternatively, the inclusions may have been derived from simmilar metamorphic rocks present northeast of the Stikine arc within the Yukon Cataclastic, or Yukon-Tanana terrane (Fig. 1). The Stikine are could be far travelled with respect to the metamorphic terrane and the two were possible juxtaposed in the Late Triassic during as as yet unrecognized tectonic event.

ACKNOWLEDGEMENTS

This study was funded by two Northern Science Training Grants from the Boreal Institute of Canada. Funding was also provided by the Department of Indian Affairs and Northern Development and by an NSERC grant to Dr. P. Erdmer.

This paper benefited from discussions with Dr. P. Erdmer and Grant Abbott, and was critically read by M.J.M. Duke. Able field assistance was provided by Paul Baxter and Siegfried Joiner. Brian Turner provided technical assistance.

REFERENCES

ERDMER, P., 1985. An examination of the cataclastic and structures of parts of Nisutlin, Anvil and Simpson allochthons, central Yukon: test of the arc-continent collision model; Jour. Structural Geol., Vol. 7, p. 57-72.

HANSEN, V.L., 1986. Petrotectonic study of the Teslin Suture Zone, Yukon: a progress report; in Yukon Geology, Vol. 1; Exploration and Geological Services Division, Yukon, Indian and Northern Affairs Canada, p. 125-130.

TEMPELMAN-KLUIT, D.J., 1974. Reconnaissance geology of Aishihik Lake, Snag and part of Stewart River map-areas, west central Yukon; Geological Survey of Canada, Paper 73-71, p. 97.

TEMPELMAN-KLUIT, D.J., 1979. Transported cataclasite, ophiolite and granodiorite in Yukon: evidence of arc-continent collision; Geological Survey of Canada, Paper 79-14, p.27.

WERNECKE BRECCIAS AND Fe, Cu, U MINERALIZATION: QUARTET MOUNTAIN-IGOR AREA (NTS 106 E)

Peter Laznicka,
University of Manitoba,
Winnipeg, Manitoba

and

David Gaboury,
Granges Explorations,
Flin Flon, Manitoba

LAZNICKA, P. and GABOURY, D., 1988. Wernecke breccias and Fe, Cu, U mineralization: Quartet Mountain-Igor area (NTS 106E); in Yukon Geology, Vol. 2; Exploration and Geological Services Division, Yukon, Indian and Northern Affairs Canada, p. 42 - 50.

ABSTRACT

The "Wernecke Breccias" are enigmatic, but significant features of the Middle Proterozoic Wernecke Supergroup in the Wernecke and Ogilvie Mountains. This report describes the breccias near Quartet Mountain and the Igor prospect in the Wernecke Mountains. Widespread, pervasive metasomatism and greenschist facies metamorphism of both the breccias and wall rocks is demonstrated by the development of chlorite, calcite, dolomite, calcite, siderite, albite, hematite, sericite, biotite, and quartz. Altered fragments are multicoloured and give the appearance that they are transported, and exotic, but all are locally derived. Structures in relatively unaltered breccias suggest that brecciation was accompanied by mylonitization and faulting. Repeated brecciation, metasomatism, and faulting characterize development of the breccias. Small gabbro and diabase dykes and sills are associated with the breccias. The breccias contain numerous, small occurences of copper, iron, barium, molybdenum, uranium, cobalt, gold, and silver. Crustal extension and detachment faulting, and large buried intrusions beneath the breccias are suggested as possible genetic mechanisms.

RÉSUMÉ

Les "brèches de Wernecke" sont énigmatiques, mais représentent des éléments significatifs du supergroupe de Wernecke, d'âge protérozoïque moyen, dans les monts Wernecke et Ogilvie. Dans ce rapport, on décrit les brèches situées à proximité du mont Quartet et le gîte possible d'Igor présent dans les monts Wernecke. Le métasomatisme et le métamorphisme du faciès des schistes verts, étendus et omniprésents, qui ont touché à la fois les brèches et les roches encaissantes, se sont traduits par l'apparition de chlorite, de calcite, de dolomite, de sidérite, d'albite, d'hématite, de séricite, de biotite et de quartz. Les fragments altérés sont multicolores et semblent avoir été transportés, et ont une apparence exotique, mais tous ont une provenance locale. Dans les brèches relativement non altérées, les structures observées suggèrent que la bréchification a été accompagnée de processus de mylonitisation et de la formation de failles. La bréchification répétée, le métasomatisme et l'apparition de failles caractérisent le développement des brèches. De petits dykes et filons-couches de gabbro et de diabase sont associés aux brèches. Ces dernières contiennent de nombreuses et petites venues de cuivre, fer, baryum, molybdène, uranium, cobalt, or et argent. On a suggéré comme mécanisme possible de génèse l'expansion de la croûte et les failles formées par décollement, et la présence de vastes intrusions enfouies au-dessous des brèches.

INTRODUCTION

"Wernecke Breccias" (an informal term) are conspicuous rocks; in their most spectacular form composed of pink or maroon albitite fragments resting in an identically coloured or green "rock flour" matrix. These and similar breccias have a regional although spotty distribution in the Proterozoic (meta)sediments of the Wernecke and Ogilvie Mountains. They appear to be an important component of the local geology and a key to interpretation of the regional geotectonics, magmatism and metallogeny.

The breccias were almost simultaneously introduced into the literature in the late 1970s by Morin (1976), Bell and Delaney (1977) and Laznicka (1976, 1977a). Subsequent studies of the "Wernecke Breccias" emphasized their regional distribution, setting and stratigraphy (Bell 1978, 1982, 1986; Delaney 1981); exploration significance (Archer and Schmidt, 1978); and detailed geology and petrology of local alteration-mineralization centres (Laznicka 1977b, Laznicka and Edwards, 1979). All the above contributions included observations on the Cu, Fe, U, Co, Au and Ag occurrences, widespread within and in the immediate vicinity of the breccias.

In the summer of 1985, Laznicka and Gaboury assisted by Brian Carlson studied breccia localities in a 15 x 5 km strip between the Quartet Mountain and Igor prospects (S.E. corner of Wind River 1:250,000 map sheet; Fig. 1). The study was supported by contracts from the Department of Indian and Northern Affairs.

ACKNOWLEDGEMENTS

Thanks are due to Jim Morin who suggested the project and provided the logistic support. R.T. (Dick) Bell shared his considerable experience with us. A.R. Archer kindly gave us the permission to study the mining properties owned or managed by Archer, Cathro and Associates (1981) Ltd and supplied many valuable pieces of non-proprietary information. ESSO Minerals kindly donated one day of their helicopter time, to fly us into the Igor camp.

REGIONAL SETTING

The core of the Wernecke Mountains is underlain by the Middle to Late Proterozoic Wernecke Supergroup (Delaney, 1981). The lower and middle portions of the Supergroup comprise monotonous thin to medium-bedded, recrystallized to greenschist-metamorphosed siltstone, argillite and quartzite of the Fairchild Lake and Quartet Groups (estimated by Delaney to be at least 9,000 m thick). The upper portion, conformably overlying the lower, is a dolomite-rich sequence assigned to the Gillispie Lake Group. The Wernecke Supergroup, at least its lower division, resembles the Belt-Purcell Supergroup as developed along both sides of the U.S. - Canada

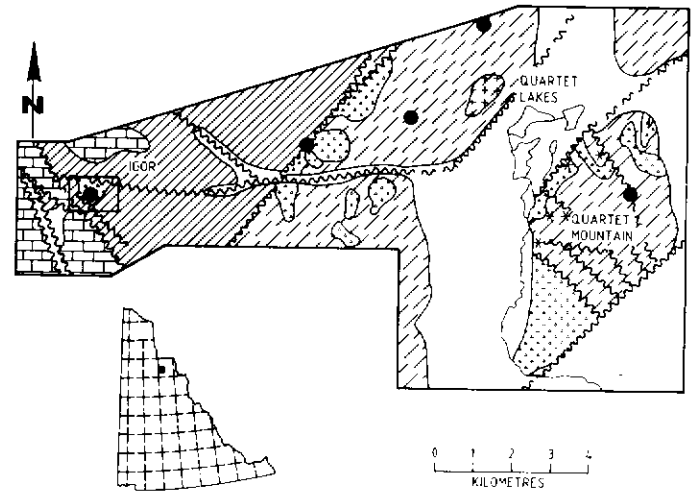

EXPLANATIONS:

QUATERNARY

Sediments

PALEOZOIC

Sediments

PROTEROZOIC

Gabbro (outcrop)

Gabbro and lamprophyre dikes (out of scale)

WERNECKE SUPERGROUP

Low-grade load metamorphosed but generally unaltered dark gray alternating slate, siltite, quartzite ("Quartet Group")

Thermally metamorphosed biotite and calc-silicates containing fine detrital metasediments

Metasediments containing introduced or deposited chlorite, albite, carbonate, indurated, or wholly alteration converted into a bleached phyllite, chlorite or sericite schist, albitite, carbonate metasomatite ("Fairchild Lake Group")

Wernecke Breccia bodies

Recorded mineralized (Cu,U) occurrences

Fig. 1 Quartet Lakes-Igor area: location and reconnaissance geology

border and both supergroups probably originated in a similar, although not necessarily synchronous, setting. The base of the Wernecke Supergroup is not seen. Delaney (1981) provided substantial paleocurrent data, indicating an east-west trending depositional axis and northerly derivation of the terrigenous detritus.

The Wernecke Supergroup is locally unconformably overlain by varicoloured sediments of the "Pinguicula" and Rapitan Groups, and is in fault contact with Proterozoic sediments of the Knorr Range Succession east of the Knorr Fault (Norris, 1979). Cambrian to Cretaceous terrigenous sedimentary rocks, having a transgressive or tectonic contact, envelope the Proterozoic outcrop area on all sides. The entire region is devoid of magmatic intrusions. Minor gabbro and diabase sheets and small masses representing less than 0.1% of the outcrop area intrude the Wernecke Supergroup. Even rarer are lamprophyre and ultramafic dykes.

The earlier Proterozoic core is a broad uplift ramified and intersected by the northwest-trending Richardson Fault Array and broken by northeast-trending faults. Bell (1986) recorded isolated northerly and south-westerly dipping thrusts in the Wernecke Supergroup, but open folding and shallow to moderate dips predominate except near breccias. There, segments of tight isoclinal folding complicated by cleavage grade into "broken formations" and into breccias that are of several probably related and unrelated varieties. Bell (1986) introduced the term megabreccia to account for "breccia bodies (that) contain clasts in the kilometre-size range" which, although "laterally connected and following an arcuate pattern", are interpreted as derived from the lower levels and compared with the South Australian "diapirs".

LOCAL GEOLOGY

Figure 1 is a compilation map of the study area. The local geology includes three divisions: the Proterozoic core; the Paleozoic sedimentary rocks west of Igor; and the Quaternary cover. Our efforts were devoted to the study and interpretation of Division 1 and the alteration and mineralization superimposed on it.

The Proterozoic strata have been correlated with the Fairchild Lake Group and the overlying Quartet Group, (Bell, 1986; unpublished mineral occurrences and compilation geological map provided by A.R. Archer), or their earlier correlatives (Hcs and Hs; Blusson, 1974).

Our work, however, failed to confirm any substantial lithologic difference between rocks mapped as Fairchild Lake and those mapped as Quartet Groups and we suggest that, at least in the present study area, the more "massive" Fairchild is a metamorphically and metasomatically modified equivalent of the Quartet, exposed in structurally positive areas that are at least in part thermal domes. Because the intensity and style of alteration are to a considerable degree influenced by the original lithology, an impression of stratigraphic contacts and superimposition is strong.

The often considerable petrographic (and geochemical) variety of rock types encountered at hand specimen to outcrop scales primarily reflect the style and intensity of deformation, and the composition, intensity and style of alteration. Both are superimposed on a small number of very simple and persistent original rock types. Breccias and cataclasites are part of the entire package, transitional and fully gradational into the undisturbed (meta) sediments and cannot be considered separately as has often been the case in the past.

Lithologic variation in the lower Wernecke Supergroup here, as in the Dolores Creek area (Laznicka, 1976) reflect variation of grain size and ratios of three common minerals: (1) quartz; (2) light micro to macro-mica (sericite to muscovite), derived from original clay minerals; (3) detrital or authigenic K and Na-Ca feldspar. The rock-forming minerals have been partially to fully recrystallized under conditions of at least zeolite but more commonly greenschist facies, so the rocks are technically metamorphic. The simplest rock is a (meta)quartzite composed of an equigranular crystalline mosaic of 0.1 - 0.3 mm diameter quartz grains, in which scattered grains of sodic plagioclase and/or muscovite are the main accessory. Our evidence indicates that the pure quartzites are the result of tectono-metamorphic refinement of originally finer-grained and impure arenites, and that the discontinuous bodies are structurally controlled. Sericite (muscovite) quartzite is a much more widespread and truly (meta)sedimentary rock, forming persistent beds and horizons. This rock was probably a well-sorted terrigenous quartz-rich sublitharenite.

With decreasing quartz grain size (below 0.1 mm) and increasing mica/ quartz ratio, sericite quartzite grades into a fine (meta)sediment intermediate between "quartzite" and "argillite", termed "siltite" in the Belt Supergroup (Harrison and Jobin, 1963).

In addition to the three major component minerals listed above, the (meta) sediments also contain chlorite, carbonate (calcite or dolomite in the "rocks", grading to siderite in the "ore zones"), biotite, albite and hematite pigment. Additional (introduced) quartz and sericite (muscovite) also occur. All these minerals are characteristic for rocks of the "Fairchild Lake Group" which form units distributed over distances of several kilometres. In the "Quartet Group" the minerals have a spotty distribution, usually clearly related to disturbance. Even in the Fairchild Lake Group, individual rock types (e.g. carbonate, chloritic phyllite) are impersistent in the sense that they do not form a single bed or a bedset traceable for distances of several hundred metres away from a disturbance/alteration centre, without changing their mineralogical facies. We interpret the above minerals to result from post-depositional alteration.

Carbonate-rich rocks

Delaney (1981) made a wide use of markers, particularly carbonate horizons which he considered sedimentary, to establish the Fairchild Lake Group and its subdivision. We can now state with a high degree of confidence that all the "rock" (as well as "ore") carbonate occurrences in the Quartet Lakes are post- depositional metasomatites. They formed in several stages by preferential replacement of certain beds or by almost total replacement of an entire rock body. Replacement carbonate can be easily recognized in thin sections by (1) its corrosion of quartz or sericite-rich bands; (2) by widespread trains

of impurities discordant to the trend of the carbonate body; (3) by gradation of high grade carbonate into tongues of partial replacement; (4) by the presence of poikilitic or internally homogeneous metacryst rhombs.

It is uncertain whether sedimentary carbonates are missing in the Quartet Lakes area only, or whether they are absent in the entire lower Wernecke Supergroup. All the carbonates I have newly examined or re-examined (e.g. those associated with the Gremlin chalcopyrite orebody, Kiwi Lake; those at Dolores Creek and vicinity; Laznicka and Edwards, 1979) are metasomatites. Even the rhythmically banded "ribbed-weathering limestone-siltstone member" in Cobalt Cirque is "secondary", although it could have formed by metamorphic recrystallization of a sedimentary carbonate causing partial corrosion of the adjacent quartz or silicate bands.

Biotite-rich rocks

Biotite substitutes for sericite (muscovite quartzites and less commonly, "siltites". Such biotite is fine-grained and is visible only as brownish shades on the rocks. The biotite-containing (meta)sediments tend to be hard and massive. At this stage, we interpret them as products of the highest-grade prograde thermal metamorphism achieved in the region. Biotite is relatively rare, and in less than 5% of the rocks.

Chlorite-rich rocks

Chlorite is substantially more widespread and more abundant than biotite in the metasediments. (1) Flaky chlorite substitutes for sericite in certain "slate" and is both a product of prograde or even-grade sericite replacement, and retrograded from earlier biotite. The former chlorite is more widespread, particularly in association with a concurrent albitization; (2) flaky chlorite substituting for interstitial mica in quartzite; (3) hydrothermal or hydrothermal-metamorphic intersitital structureless, metacolloform, radiating, fibrous, etc. chlorite replaces matrix and partly replaces large grains in quartzites, metasomatic carbonates and other rocks. It also fills a variety of dilational openings and is widespread in breccia matrix.

The most conspicuous chloritic rocks (chloritic phyllite or schist) occur in alteration-mineralization centres marked by breccias and mafic intrusions. In the talus derived from a poorly accessible cirque about 6 km southwest of Quartet Lakes, dark-green well-foliated chloritic schists and spotted-chlorite rocks grade into breccia on both sides of a "slate" and quartzite/gabbro (diabase) contact. Less advanced chloritized rocks occur on the N.W. slope of Quartet Mountain, where chlorite substitutes for sericite in the originally dark-gray mixtites.

Some of the chlorite-rich rocks"(greenschists, greenstone)"are probably mylonitized and sheared, hydrated gabbros/diabases, but most are clearly metasomatically modified metasediments. Chloritization is the result of magnesian metasomatism of which at least some is attibutable to postemplacement destruction of mafic intrusions followed by outward-progressing Mg fronts. Much (but not all) chloritization is concurrent with albitization.

Albite-rich rocks

Albite is the most conspicuous of altered breccias and of mafic intrusions, and it also overprints adjacent metasediments producing a variety of metasomatites and dilation fillings. The "overprinting albite", however, did not travel far from the centres of sodic metasomatism and is a good proximity indicator to such centres.

The most common result of albitization is a pseudomorphic replacement of quartz-rich metasedimentary bands, leaving adjacent sericite bands intact. The quartz-replacing granoblastic albite mosaic usually maintains the grain of size of earlier quartz mosaic or is 10-20% larger. The albite may be slightly clouded by the impurities inherited from its precursor. Unless fracture-controlled, albitized bands grade into the quartz mosaic, showing a diminishing proportion of wholly albitized quartz grains.

In folded and fractured zones, replacement albite alternates with fracture, fold and bedding dilation-filling albite. This variety shows

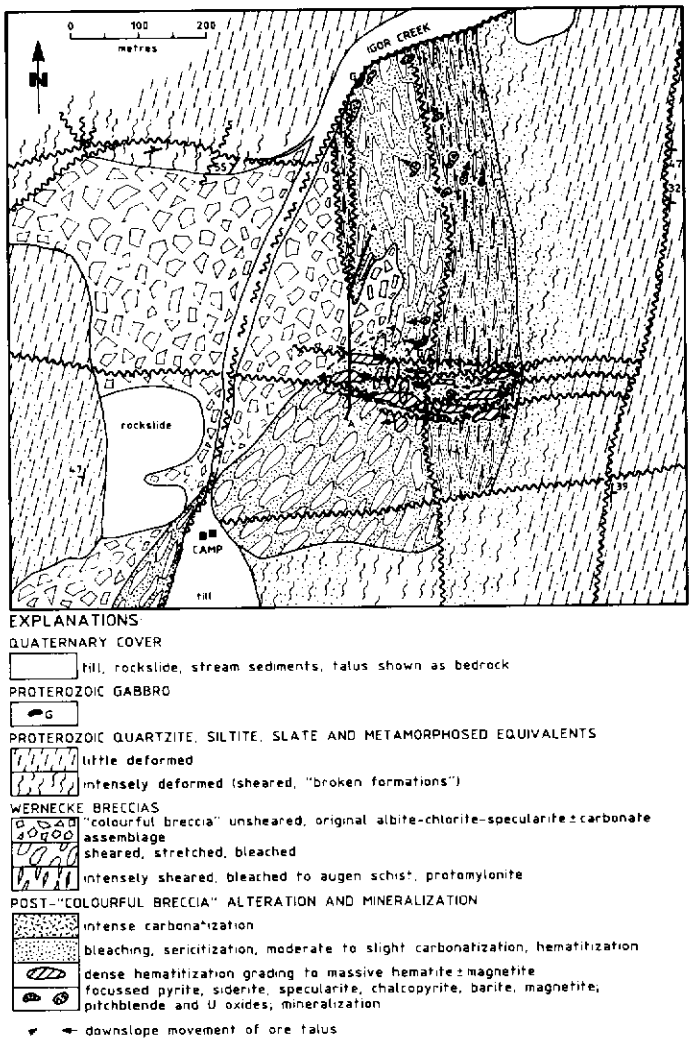

Fig. 2 Igor Prospect, geology, alteration, mineralization map

rapid variations in crystal size (0.01 to 3 mm) reaching exceptional lengths of 12 mm. Such albite is free of impurities, is usually twinned and its mosaic has a high proportion of idioblastic grains. Replacement and open space filling albites are contemporaneous, or they may belong to two or more different generations indicated by cross-cutting relationships.

Bleached rocks ("phyllites")

These are light-green, lustrous banded rocks composed of sericite and chlorite laminae enclosing usually discontinuous thin lenses of granoblastic albite, white quartz or ankeritic carbonate. Kinks, crenulations as well as a variety of dilations filled by mobilisates are common. Much of these rocks are tectonites and are either the result of pigment bleaching from previously unaltered "siltites" and "slates", or they form by retrogressive sericitization of an earlier albitite, mylonite or cataclasite. A variety of gradations into other rock types exits. Alteration-mineralization centres contain most of the "bleached rocks" and fault zones contain minor occurrences.

Silicified rocks

Silica is displaced from quartzite and "siltite" during albitization and is responsible for silicification and veining of some densely fractured rocks (e.g. the "spires" at the southwest side of the Quartet Mountain).

Intrusive rocks

Altered gabbro to diabase form small bodies in the breccia-

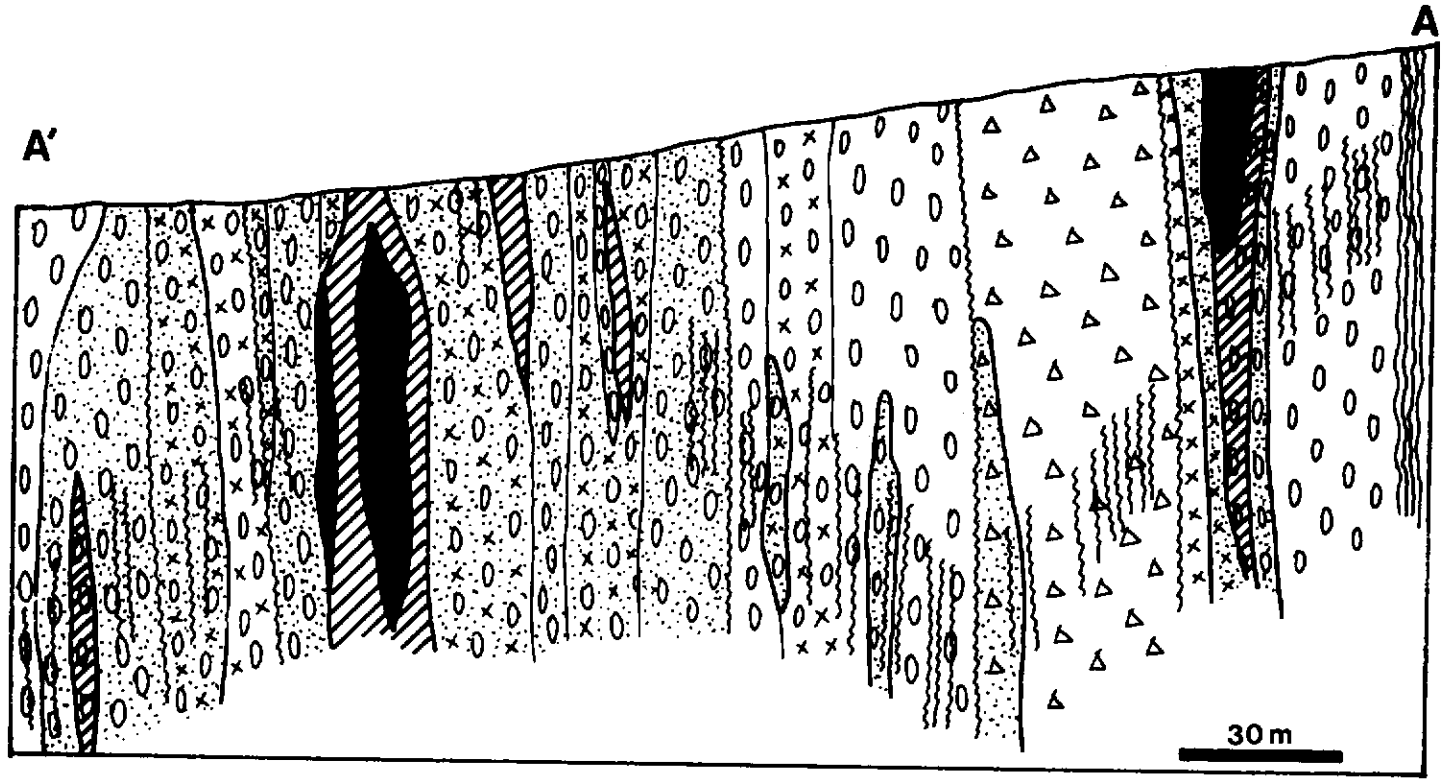

EXPLANATIONS

"Colourful breccia", massive, pink and green spotted (albite-chlorite association), minimal re-brecciation

Strained, bleached, partly stretched breccia, relic fabric still preserved and recognizable

Shears, marked by sericite schist with occasional relics of augen, original breccia fabrics are completely obliterated

chloritized microbreccia

chloritized partly stretched breccia

MINERALIZATION: estimated percentage of magnetite, hematite, barite, pyrite, chalcopyrite and uranium oxides

80-100%

10-80%

0-10%

0%

slip surfaces, gouge filled/coated fractures

Fig. 3 Igor Prospect, north-south cross-section between drill holes 80100 and 801012.

crushed aggregates of albite grains 0.1 - 1 mm in size enveloped by dominant fine sericite or paragonite schist. Most of the fine micas formed at the expense of the original breccia constituents (mainly albite and chlorite) so the shearing had to be concurrent with hydration, potash metasomatism and Mg removal. Outside of the limit of the early breccia, however, much of the "sericite" was probably derived by retexturing of the metasedimentary "slate" or "siltite".

The sericitic mylonitic schists differ from TB's by their pastel shades and an almost uniform beige colour and are gradational into TB's via an intermediate member mapped as "pastel-coloured breccias". The "pastel breccias" tend to have a high content of sideritic to ankeritic carbonate of both pre-shearing and post-shearing generation. The former appear as stretched augen, while the latter replaces the relics of albitite, siderite and fills dilations.

"Re-breccias" are most common along late crosscutting fault zones previously unaffected by shearing and fine mica generation. The original TB's were milled partly along the earlier fragment boundaries, partly across them and the rock is now a hard, cohesive cataclasite without fluxion structure in which a wide range of 2 - 20 mm large porphyroclasts is embedded in a compositionally equivalent finer matrix. Higgins' (1971) term "microbreccia" is probably the most fitting.

Preferential orientation of constituents is rarely apparent. Introduced chlorite and specularite fill the pores produced by dilation

dominated alteration centres (Quartet Mountain, 6 km southwest of Quartet Lakes, Igor). Intensive cataclasis and alteration of both the mafic rocks and surrounding breccias and metasediments make the intrusion indistinct and almost impossible to outline.

The least altered variety obtained from float is a coarse olivine-pyroxene gabbro rich in accessory sphene. Deuteric alteration probably caused uralitization of pyroxenes and around 30% of phases postdate cataclasis and part of the overall areal alteration. Epidote, chlorite and albite are the dominant alteration minerals. Epidote is the most proximal and is confined exclusively to the intrusive rocks, whereas albite and chlorite display no such preference. With increasing proportions of late alteration minerals, the original ophitic texture is reduced to relics before disappearing altogether. A coarse crystalline (3-4 mm) albite-chlorite "syenite" found in float is a metasomatite resulting from replacement of the original gabbro by albite and chlorite.

Olivine-biotite lamprophyre dykes ("kimberlite")

Olivine-biotite lamprophyre have been recorded on the western and northern slopes of the Quartet Mountain. They form dykes 10-30 cm thick, and postdate the main alteration phase (they enclose xenoliths of the intruded albitized and hematitized metasediments), but are offset by late faults. These rocks are fine grained, gray, grayish-green to bluish-gray weathering tan to light-brown (white when talc-altered). They contain scattered inclusions of cellular serpentinized olivine, isolated sheets of biotite or phlogopite, up to 2 cm wide crystals of Ti-magnetite, and minor perowskite grains up to 1 cm wide. The contacts are unaltered, or there is a recrystallization band 3-10 cm thick.

BRECCIA

A large petrographic variety of breccias occur in float, particularly in stream beds (Fig. 3). Bedrock occurrences, however, are less satisfactory for study because most are covered by talus and virtually no breccia body is exposed in three dimensions and an unequivocal understanding as to its shape, contacts and origin is not possible.

"Typical"(or "Wernecke", "Colourful") breccia (TB)

The most "typical" or spectacular breccia is composed of light angular to subrounded pink or maroon fragments surrounded by chlorite and/or specularite- rich "rock flour" matrix. "Typical breccias" are widely distributed through the Wernecke and the Ogilvie Mountains.

"Typical breccias" are a heterolithologic to pseudoheterolithologic rud- rock (Laznicka, 1987), composed of multicoloured angular to rounded fragments set in a recrystallized or metasomatic groundmass. All fragments are locally derived and their great visual variety is to a considerable degree a consequence of alteration, rather than the original lithology. The pink and maroon fragments are composed of albite granoblastite: a chert-like, dense and hard, massive or faintly laminated rock that is textural equivalent of (meta) quartzite and is composed of a mosaic of hypautomorphic albite crystals having an average dimension of 0.1 - 0.2 mm. The only difference between the pink and maroon variety is the state of the pigmenting hematite, which is red, fine powdery in the first case and specularitic in the second. Tiny flakes of specularite are almost uniformly distributed throughout the rock.

Fragments range in size from rock flour through an average 1-3 cm to blocks over 1 m long. The small fragments are usually equidimensional, structureless to faintly laminated. Most large blocks are slabs of banded albitized (meta)quartzite or "siltite". Superimposed carbonatization causes brown weathering colours and still greater visual diversity of breccia fragments. The honey-yellow to light brown-weathering siderite rhomb meta- crysts scattered on the aphanitic pink or maroon albitite background make the fragments resemble felsic porphyries, with which they were originally confused.

The breccia matrix is a "microbreccia" (recrystallized and cemented rock flour), the grain size of which ranges from about 3 mm to about 0.01 mm. Typically a mixture of albite fragments, albite crystalloclasts, chloritite and sericitite fragments are recrystallized and cemented by a new generation of albite and chlorite with specularite and carbonate.

The whole transitional sequence between two end-members: the fractured protolith (sericite quartzite to "siltite") and the roundstone transported breccia (fractured quartzite - crackle breccia - mosaic breccia - breccia with rotated angular fragments - roundstone transported breccia) is represented, although the intermediate members are most "typical" preferred orientation of fragments and the matrix is rare.

Transition of the "typical breccia" into a less evolved protolith ("pre-breccia")

The transition of TB into an albitized quartzite or "siltite" petrographically identical with the breccia fragments has already been outlined above. Another series of transitions can be observed in a gully opposite (northwest of) the Igor property. There, a TB is partly transitional into, partly fault-separated from, a well-bedded outcrop of thick, planar, pink and maroon albitite beds with thin chlorite schist partings. These altered rocks are separated by a 115° trending fault from a hill to the north- east which is underlain by "tortured" quartzite-"slate" metasedimentary mixtite. Original sedimentary bedding is generally discernible and dips 35° NW, but the cataclastic quartzite is broken by a dense network of tectonically polished mylonitic slip surfaces into a black silvery mylonite in place of the former "slate" partings. Melange-like sections of attrition-rounded quartzite blocks in a slivery mylonite matrix and transitional arrangements, also occur.

This rock is not substantially hydrothermally altered and the transition from partly and fully altered equivalents is recorded in blocks in talus and in the creek under the Igor property. Hydrothermal metasomatism resulted in pseudomorphic conversion of the brittle quartzite component into albitite fragments and the ductile slivery and slickensided mylonite into a crystalline chlorite matrix.

Several tens of metres under this outcrop, alternating quartzite and "slate" are interrupted by numerous unaltered cataclastic zones, peneconcordant with bedding, in which rafts of dismembered cataclastic quartzite are embedded in a slivery matrix of sericitic blastomylonite or mylonitic schist. Both in turn are interrupted by tongues and lenses of a "slurry breccia". The breccia is of local derivation, but was clearly transported for a short distance into its present site. Its contacts with the immediately overlying and underlying mylonitic "slate" are sharp, but this is largely due to the ductility contrast. Lacking alteration, this rock is unspectacular and inconspicuous, spotty, greenish-gray and of low cohesion, so it is an insignificant component of talus and float that easily escapes attention. A variety of breccia bodies also fill superimposed crosscutting faults and fractures.

In another gully 1 km to the west, equivalent peneconcordant "slurry breccia" has been block-faulted and hydrothermally converted into the typical maroon, pink and green-spotted variety.

Transition of TB into repeatedly fragmented, sheared and hydrothermally altered breccias (re-breccias and ploy breccias).

At the Igor property and at several other places, the TB's formed early and were overprinted by several phases of deformation and alteration. These modifications were not confined to and controlled by the original breccia and they extend beyond it, but it was within the breccia where the products are most complex.

At Igor, the structural framework for the post-breccia modifications appears to be a wide north-trending shear zone and several parallel, discontinuous shears. These are cut by numerous east, northeast and northwest-trending faults. Along the highest strain zones within the shear, TB's have been converted into a sericitic mylonitic schist and augen schist (using Higgins' 1971 terminology) by concurrent cataclasis and neomineralization-recrystallization. Such a rock has a distinct fluxion texture (cataclastic foliation) and consists of subordinate augen or groups of grains of albite porphyroblasts, or

(expansion) in the time of origin, and replace earlier constituents. Another re-breccia variety is high in ankeritic to sideritic carbonate. At Igor, re-breccias are the most consistently mineralized hosts. Examination of several tens of thin sections indicated up to ten pulses of re-brecciation and a variety of fluxion-textured schists or microbreccia-schist hybrids superimposed on earlier microbreccias.

Other breccia varieties

Combinations of the "key varieties" of the Wernecke Breccias described above with the various types of hydrothermal alteration, can produce hundreds of varieties of "custom-made" breccias to be enjoyed by a breccia connoiseur, best of all in boulders in the stream draining the Igor valley. The most consistent feature of Wernecke Breccias thus appears to be their variability. Other, less spectacular breccias are also locally present:

- Concordant sharpstone to roundstone breccias or conglomerates within the unaltered and unsheared Wernecke Supergroup (meta)sediments. Several blocks found in the float consist of quartzite clasts supported by siltite matrix. These are probably intraformational debris flows. In tectonized and altered sections such as N.W. of Igor, similar rocks are indistinguishable from the syntectonic breccias.

- Mosaic breccias resulting from expansion along fracture cleavage and/or foliation surfaces and a variety of fold and fault breccias, some of them carbonatized, are on the fringe of alteration-mineralization centres.

- Crackle to rubble breccias superimposed on earlier metasomatic or dilation-filling carbonates.

- A variety of fault breccias cemented by carbonate or quartz.

- Sharpstone conglomerate zones in the Paleozoic sediments, widespread in float and drift.

- Cemented recent talus breccias.

ALTERATION AND MINERALIZATION

Five named copper, iron and/or uranium showings, all discovered by Archer, Cathro and Associates, and several tens of minor occurrences of the same metals, are known in the area covered by Figure 2. Only the Igor property has been explored by drilling and trenching. Over 2454 m (8171 ft) of diamond drilling was completed between 1976 and 1982.

Igor showings

Igor is on a low ridge on the south-eastern slope of a valley about 14 km southwest of Quartet Lakes. Concentrated mineralization underlies an area about 700 x 300 m alligned north-south. A broad north-trending shear zone and numerous east-west and other faults and fractures discussed in connection with the re-breccias and polybreccias control mineralization. Most of the Igor property is talus-covered and accurate mapping is next to impossible. Only several "key faults" are shown on our map; drill core reveals thousands of microbreccia, mylonite and gouge-coated and filled slip and fracture surfaces with a wide range of coherence. Semi-coherent and incoherent cataclasites are the youngest and probably at least partly reflect repeated reactivation of older surfaces over a long period of time. The wide spread of radiometric ages obtained for U occurrences affiliated to breccias in the Wernecke Mountains (Archer et al., 1986) suggests late faulting and therefore a depth range of several kilometres and greenschist-stable to near-surface conditions.

Mineralization is in a "typical" albitite-chlorite breccia body measuring 700 x 700 m adjacent sericite quartzite, "siltite", and "slate" of the Wernecke Supergroup. Two small mylonitized and altered mafic intrusions have been recorded in the original TB. Repeated faulting, shearing, fracturing and brecciation were synchronous with or overlapped hydrothermal alteration and mineralization. The hydrothermal fluids apparently issued simultaneously from many "emanation centres", rather than a single discrete point conduit such as a vent or a diatreme. Most were probably faults and their intersections. As a consequence parageneses and mineralization-alteration zonings are local and interfere with one another, although it is possible to put together a composite local paragenetic diagram based on statistical maxima.

Alteration contemporary with metallic mineralization (albitization, sericitization and paragonitization, chloritization, spotty growth of hydrothermal biotite and/or muscovite metacrysts, hematitization) is identical with the breccia-forming alterations, already discussed above. The ore minerals association: siderite and ankerite, magnetite, hematite, pyrite, barite, chalcopyrite and uraninite is simple and corresponds to the "standard" regional association. The deposits range from haphazardly scattered grains and blebs of chalcopyrite in virtually all the cataclasites (including the pre-shearing TB's), to a more localized and densely accumulated chalcopyrite associated with abundant magnetite, specularite, pyrite and/or siderite (ankerite).

Iron minerals form scattered metacrysts (magnetite octahedra, specularite tablets and plates, siderite rhombs, pyrite cubes) that, with increasing density, produce interconnected grain aggregates. Massive magnetite, siderite or martite (hematite replacing magnetite) bodies, however, need not be richer in copper than low-iron hosts.

Barite seems to be widespread but inconspicuous, replacing albite and carbonate in breccia and mixing with the ore minerals mentioned above. Blocks of white or pink crystalline barite enclosing scattered magnetite crystals can be seen in transported breccias in the creek. Several small pods of white to pink fine crystalline barite crop out on the property.

Uranium in the form of pitchblende and several bright yellow, orange and green secondary minerals, occurs as (a) veinlets and coatings on hairline fractures in the pink barite pod near the top of the ridge; (b) as blebs in white to gray barite; (c) as disseminations, scattered grains and blebs in the complex massive siderite, magnetite, pyrite, chalcopyrite ore; (d) as disseminations and veinlets in the martitized hematite bodies.

Fe, Cu, U, Au and Ag grades and ore tonnages calculated from the drill core assays have not been made available to us, so we are not in the position to provide an economic assessment of the property. No single, sharply outlined medium to high-grade deposit of any element but, perhaps, iron is apparent. Five or six small lenses of almost massive hematite and martite in the southern portion of the mineralized zone would hardly make a mine under the present economic conditions. The low grade "bulk" potential of the entire zone for Cu, U, Au and Ag, if any, has not been released.

Alteration zoning at Igor is imperfectly developed, mostly because it resulted from several superimposed events by fluids moving from numerous centres. Briefly, the early stage breccia-associated albite-chlorite (hematite) alteration appears to either terminate abruptly against virtually unaltered rocks, or it fades away into alteration ankerite having the form of scattered rhomb metacrysts, fracture veinlets or slight impregnations in quartzite. The subsequent strong shearing was accompanied by an albite- destructive sericite and/or paragonite alteration. Only small patches of TB, and microbreccia marked by strong chloritization are unaltered. Siltites outside the breccia body are bleached. Siderite and ankerite (carbonatization) coincide with the fine mica alteration mentioned above; intensity and iron content decrease away from the deposits.

Hematitization is widespread and has many forms. Fine (pigment) specularite produced the maroon albite granofels and its formation was prominent in the early stages of TB formation. Subsequently, widespread specularite accompanied chloritization in microbreccias and caused the martitization of magnetite. Martitization of magnetite bodies at or near the ridge top may have been related to near paleosurface oxidation.

Silicification, quartz veining, quartz metacryst and mosaic formation in breccias was (a) early and contemporaneous with albitization, and (b) fairly late replacing albite, carbonate and barite in microbreccias and orebodies.

Quartet Mountain

In contrast to Igor, Quartet Mountain contains only small scattered occurrences of chalcopyrite, siderite, brannerite and probably pitchblende, none of which has been drilled or trenched. Most copper is in chalcopyrite, forming scattered blebs along fractures in carbonatized (meta)sediments and blebs to small masses in albite, chlorite, carbonate and quartz dilation fillings. Most showings are in the impressive scree covering the mountain slopes.

The most interesting radioactive Quartet occurrence prospected by Archer, Cathro and Associates, is on the north-eastern slope of the mountain near the crest. There, thin fracture veinlets contain pitchblende and a metamict Ti-Fe-Si-U mineral that gives the brannerite x-ray pattern after heating. A similar occurrence is in talus on the northern slope of the mountain, where the mineralization corresponds to types 1 and 2 on Figure 2 in Delaney et al (1982). There, the host rock is a partly altered (albitized and chloritized) laminated "siltite", situated between two bodies of TB breccia. A zone of intense parallel shearing is healed by lit-par-lit fillings of alternating coarse ("pegmatitic") albite and fine crystalline mosaic quartz. Brannerite crystals up to 2 cm in size are scattered in albite.

DISCUSSION AND CONCLUSIONS

The origin of the "Wernecke Breccias" has been keenly debated for about ten years because these rocks are, rightly, considered an important clue for interpretation of the geological history of this part of Canada, and because they seem to have an economic potential. Many small pieces of factual data have accumulated so far and several genetic hypotheses and intercontinental comparisons have been proposed but, so far, there is not yet a credible overall synthesis. More research is, clearly, needed.

The present study is based on a single field season and was constrained to a small area by the high cost of logistics. Several observations, however, have been made that constrain some of the recent comparisons made between the Wernecke Breccias and the

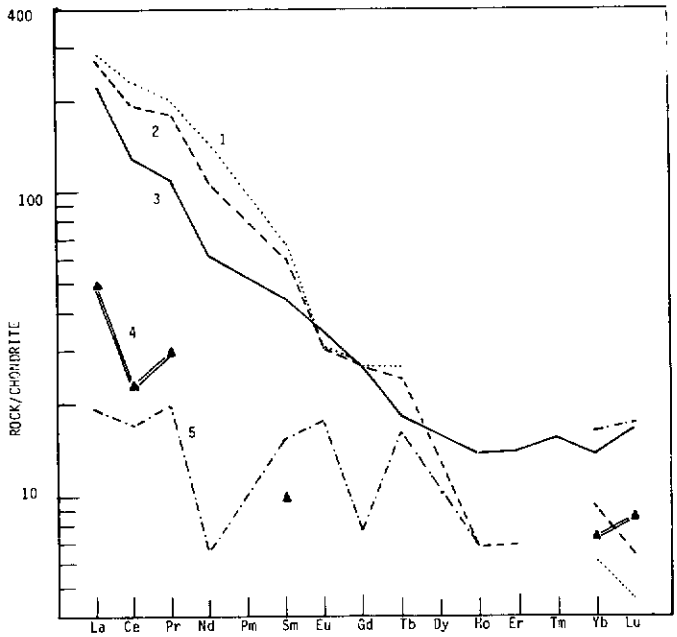

Fig. 4 Chondrite-normalized plot of rare earths elements in Proterozic intrusives (1-3) and deformed/metasomatized metasediments (4, 5) including breccia (4) and a completely metasomatic carbonate (5). The plot shows a lack of correlation between both sets, militating against the subcrustal derivation of the latter. Analyses were performed by the X-ray Assay Laboratories.

Adelaiden diapiric breccias, Mt. Painter and Olympic Dam breccias in South Australia (Bell, 1982, 1986) and contribute to exploration planning

We emphasize the dynamism and polyphase origin of the Wernecke Breccias. Apparently, their initial control is structural. Localized tight folding accompanied by fracture cleavage gradational into cataclastic folding as well as major fault zones provided the framework and produced several broken and mechanically weakened foci partly filled by "pre-breccias". The breccias form low-angle sheets (and their remnants), high-angle (subvertical) sheets and irregular bodies, suggesting contemporaneous low and high angle faulting, and brecciation. Detachment faulting triggered by basement extension documented in the southern Cordillera (e.g. Davis, 1983) could be the answer.

The early and main phases of breccia development in the Wernecke Mountains took place under greenschist facies metamorphism, close to the elastico-frictional and quasi-plastic regimes of Sibson (1977; see also discussion in Laznicka, 1987, p. 640-644). This is indicated by the absence of uncemented or infiltration-cemented fault gouges and breccias and presence of partially pressure-dissolved fragmentites, protoclasites, microbreccias and mylonites, in which cementation, replacement and/or blastic recrystallization were contemporaneous with deformation. Deformation was both brittle and ductile, and occurred in a fairly "wet" environment necessary for neomineralization. Fluids could have been the result of (a) metamorphic dehydration at depth; (b) expulsion or convection triggered by the heat of igneous intrusion; (c) both.

The spatial and temporal association of diabase or gabbro dikes and sills; albite, chlorite, carbonate and hematite metasomatism; breccias; and small Fe, Cu, Co, Ag, U, Au, etc. occurrences is a worldwide phenomena (Laznicka, 1985a, 1987) and it is particularly well represented in the Wernecke (Laznicka, 1976; Laznicka and Edwards, 1979). At Dolores Creek, some breccia dykes were clear forerunners of diabase dykes filling the same fractures, as breccia dykes are forerunners of granitic dykes in the roofs of some porphyry copper systems (e.g. at Silver Bell, Arizona). All major occurrences of the Wernecke Breccias near Quartet Lakes contain small altered mafic bodies.

The "typical breccia" clearly originated from a "pre-breccia" by fabric loosening (with or without fragment rotation), albitization and chloritization. The breccias formed at depth and are hardly high-level diatremes, but could have formed in the roof of a buried intrusion. The breccias are all local and autochthonous; fragments only travelled a few metres. This observation has been repeatedly clouded by the conspicuous apparent petrographic variety of the breccia fragments (pink, maroon, white, brown, green, even bluish spotted "heterolithologic breccias"), which is due to alteration of interbedded quartzite, "siltite", "slate", by a variety of hydrothermal fluids. Truly exotic fragments have not been credibly documented. Thus the "homolithologic breccias" of Bell (1986) and other authors are our monochrome "pre-breccias", and "heterolithologic breccias" are the "typical" altered Wernecke Breccias. The lack of truly heterolithologic breccias makes the comparison with the South Australian "diapirs" questionable. Fragment heterogeneity is a strong feature of the breccias at Arkaroola, Oraparinna, Burra, Blinman and Beltana (Laznicka, 1985b and 1981 field visit).

One of the outstanding problems in the Wernecke is the existence, if any, of large buried intrusions. The scattered alteration-mineralization centra that are also foci of anomalous deformation superimposed on the background of an overall "gentle tectonics", would support this interpretation. Unfortunately, there are no geophysical data to support or refute this hypothesis. If there are major intrusions are they; mafic as suggested by the known gabbro/diabase occurrences, "granitic" as suggested by some structural analogies with the southern Cordillera and the high trace Mo contents in some ores recorded by Archer and Schmidt (1978), or peralkaline, alkaline or syenitic like the Cretaceous intrusions in the Tombstone Range as also suggested by the high Mo content? Although an alkaline affiliation of the Wernecke mineral occurrences has been suggested several times, based on the presence of olivine-rich lamprophyres ("kimberlites") in the area and several probably genuine kimberlite-carbonatite diatremes further away (Godwin,

1976), the role of widespread alkaline metasomatism in the Wernecke alteration-mineralization centres is not yet clear. Chondrite-normalized plots of rare earths elements in two samples of clearly epigenetic and replacement carbonates, potential carbonatites, do not correlate with REE plots of the lamprophyres and gabbros (Fig. 5). Even if the "kimberlites" are real, they tend to be isolated or form separate provinces so they are not necessary indicators of the full development alkaline ultramafic, agpaitic, miaskitic, etc. (compare Laznicka, 1985a, Chapter 33).

Not a single marginally economic ore zone is so far known from the 100 or 50 scattered Cu, Fe, Co, U occurrences. The metal content is everywhere "unfocussed": a bleb of chalcopyrite here, a veinlet there, few scattered grains of brannerite or tetrahedrite, minor pitchblende infiltrations along fault zones and numerous small hematite bodies. Most of the ore metals can be locally accounted for, and their quantities are proportional to the trace metal amounts displaced from rocks and set in motion through destruction of their original carrier minerals. The estimated amounts of Cu and Co at Dolores Creek balance closely with the interpreted volumes of albitized and chloritized gabbros and their trace Cu and Co losses. Enough iron to form the known orebodies was released during albitization of the mafic intrusions as well as the ordinary (meta) sediments. The source of U is more difficult to pinpoint, although the miniscule amounts found so far could have been easily derived from the "black slate" horizon at the base of the "Quartet Group" (Bell, 1986); its chloritic alteration must have caused the uranium displacement.

Unless there was a major focussing mechanism to collect, channel and locally confine the metal "flow" originating from many scattered centra into a single major structure in which it could accumulate, another Olympic Dam can hardly be expected unless, of course, one invokes the "bowels of the Earth" as Descartes did two centuries ago and Gabelman (1977) did recently, in the case of uranium. This, however, is a different story, difficult to tackle in the wilds of the Quartet country.

REFERENCES

ARCHER, A., BELL, R.T. and THORPE, R.I., 1986. Age relationships from U-Th-Pb isotope studies of uranium mineralization in Wernecke Breccias, Yukon Territory; Geological Survey of Canada Paper 86-1A, p. 385-391.

ARCHER, A. and SCHMIDT, U., 1978. Mineralized breccias of early Proterozoic age, Bonnet Plume River district, Yukon Territory; C.I.M. Bull. Vol. 71, p. 53-58.

BELL, R.T., 1978. Breccias and uranium mineralization in the Wernecke Mountains, Yukon - a progress report; Geological Survey of Canada Paper 78-1A, p. 317-322.

BELL, R.T., 1982. Comments on the geology and uraniferous mineral occurrences of the Wernecke Mountains, Yukon and District of Mackenzie; Geological Survey of Canada Paper 82-1B, p. 279-284.

BELL, R.T. and DELANEY, G.D., 1977. Geology of some uranium occurrences in Yukon Territory; Geological Survey of Canada Paper 77-1A, p. 33-37.

BLUSSON, S.L., 1974. Nadaleen River map-area of Operation Stewart; Geological Survey of Canada Open File Report No. 205.

DAVIS, G.H., 1983. Shear-zone model for the origin of metamorphic core complexes; Geology, 11, p. 342-347.

DELANEY, G.D., 1981. The mid-Proterozoic Wernecke Supergroup, Wernecke Mountains, Yukon Territory; Geological Survey of Canada Paper 81-10, p. 1-23.

DELANEY, G.D., JEFFERSON, C.W., YEO, G.M., MCLENNAN, S.M., AITKEN, J.D. and BELL, R.T., 1982. Some Proterozoic sediment-hosted metal occurrences of the northeastern Canadian Cordillera; Idaho Bur. Miner. Geol. Bull. 24, p. 97-116.

GABELMAN, J.W., 1977. Migration of uranium and thorium-exploration significance; Amer. Assoc. Petrol. Geol., Studies in Geology 3, p. 168.

GODWIN, C.I., 1976. Kimberlitic diatremes and dykes in the Mackenzie Fold Belt, Yukon and adjacent Northwest Territories; Paper presented at 4th Geoscience Forum, Whitehorse, Dec. 6-7, 1976.

HIGGINS, M.W., 1971. Cataclastic rocks; U.S. Geol. Surv., Prof. Paper 687.

LAZNICKA, P., 1976. Dolores Creek area provides one example of copper, cobalt and radioactivity in Yukon's Ogilvie and Wernecke Mountains; Northern Miner, Nov. 25, 1976, B8-B10.

LAZNICKA, P., 1977a. Geology and mineralization in the Dolores Creek area, Bonnet Plume Range, Yukon; Geological Survey of Canada Paper 77-1A, p. 435-439.

LAZNICKA, P., 1979. Geology and mineralization in the Dolores Creek area, Yukon; Indian and Northern Affairs Canada, Open File, May 1977, pp. 87.

LAZNICKA, P., 1985a. Empirical Metallogeny, Vol. 1; Devel. in Econ. Geology, Elsevier, Amsterdam, 1, 754 p.

LAZNICKA, P., 1985b. Concordant versus discordant ore deposits and ore trans- formations; in Wolf, K.H., ed., Handbook of Stratiform and Stratabound Ore Deposits, Vol. 11, Elsevier, Amsterdam, p. 119-316.

LAZNICKA, P., 1987. Breccias and Coarse Fragmentites: Petrology, Environments, Associations, Ores; Devel. in Econ. Geol., Elsevier, Amsterdam, 832 p.

LAZNICKA, P. and EDWARDS, R.J., 1979. Dolores Creek, Yukon-a disseminated copper mineralization in sodic metasomatites; Econ. Geol. 74, p. 1352-1370.

MORIN, J.A., 1977. Uranium-copper mineralization and associated breccia bodies in the Wind-Bonnet Plume River area; in Yukon Mineral Industry Report for Yukon Territory 1976, Indian and Northern Affairs Canada, p. 101-107.

NORRIS, D.K., 1982. Wind River, Yukon; Geological Survey of Canada Map 1528A.

SIBSON, R.H., 1977. Fault rocks and fault mechanisms; Geological Society of London, Journal, Vol. 133, p. 191-213.

LANDSLIDING AT CEMENT CREEK, KLUANE RANGES, SOUTHWESTERN YUKON

M. A. Power
Department of Physics
University of Alberta
Edmonton, Alberta

POWER, M.A., 1988. Landsliding at Cement Creek, Kluane Ranges, southwestern Yukon; in Yukon Geology, Vol. 2; Exploration and Geological Services Division, Yukon, Indian and Northern Affairs Canada, p. 51 - 60.

ABSTRACT

A large block slide affecting an area of approximately 1.0 square km was reported to have occurred on Cement Creek Y.T. (115 G 5) between February 15 and March 15, 1983. Landsliding is confined to basaltic andesites in the lower unit of the Wrangell Lavas. Hydrothermal alteration of flow-top breccias and the tilting of strata towards an open face bordering Cement Creek predispose rock to slip along bedding planes. Surveys conducted during June to August 1986 detected displacements of 10-12 cm during an 8 week period. Seismic refraction and electrical resistivity surveys conducted on the slide mass suggest that most ground failure was caused by strong ground motion during an initial episode of rapid displacement and that the rupture surface lies beneath the lower limit of permafrost. Groundwater accumulation on and above the rupture surface followed by landslide initiation during a burst of low magnitude seismicity is suggested as a slide mechanism.

RÉSUMÉ

Un vaste éboulement touchant une superficie d'environ 1,0 km² a été signalé à Cement Creek, dans le territoire du Yukon (115 G 5); il aurait eu lieu entre le 15 février et le 15 mars 1983. Ce glissement de terrain est confiné aux andésites basaltiques de l'unité inférieure des laves de Wrangell. L'altération hydrothermale des brèches supérieures d'épanchement et l'inclinaison des strates en direction d'une face exposée bordant le ruisseau Cement favorisent les glissements de la roche selon les plans de stratification. Des levés réalisés de juin à août 1986 ont permis de déceler des déplacements de 10 à 12 cm sur une période de 8 semaines. Les levés de sismique-réfraction et de résistivité électrique dont a fait l'objet la masse en mouvement suggèrent qu'en majeure partie, les glissements de terrain ont été causés par de forts mouvements du sol durant un épisode initial de déplacement rapide, et que la surface de rupture se trouve au-dessous de la limite inférieure du pergélisol. On propose, comme mécanisme de glissement, l'accumulation des eaux souterraines à la surface et au-dessus de la surface de rupture, puis le déclenchement du glissement de terrain durant un épisode de sismicité de faible magnitude.

INTRODUCTION

During the winter of 1983 a large landslide was reported at Cement Creek in the St. Elias Mountains, southwestern Yukon (115 G 5, Fig. 1). D. Makkonen, a pilot with Trans North Air Ltd. in Haines Junction reported that the landslide occurred between February 15 and March 15, 1983 and affected an area approximately 1 km in diameter. Some later observers felt that uplift might be occurring since the feature was centred on a domal hill and accompanied by radial ground cracks.

Investigations were conducted during June-August, 1986 to determine the rate and sense of deformation and its cause. A microgeodetic survey grid and a series of trilateration stations were constructed to measure the rate of displacement of individual parts of the landslide. Geological mapping, and logging and sampling of exposed sections were conducted to delineate the factors controlling the landslide. Seismic refraction and electrical resistivity surveys were conducted to delineate the geological controls on the landslide and to gain information on the geotechnical properties of the material in the slide mass. A topographic survey was undertaken to permit subsequent slope stability analysis.

GEOLOGY

Cement Creek is located in the northwest St. Elias Mountains. The area is underlain by Permo-Pennsylvanian through Pliocene volcanic and sedimentary rocks assigned to the Wrangellia Suspect Terrane (Campbell and Dodds, 1979). The area has been mapped by Muller (1967), Dodds (1979), and Skulski and Francis (1986). The general geology of the area near the Cement Creek landslide is shown in Figure 2. Pleistocene and Holocene surficial deposits cover four stratigraphic rock units.

The Permo-Pennsylvanian Station Creek Formation is exposed at the northern edge of the map area, in the core of a plunging anticline as a series of rusty-weathering, slightly vesicular basalt flows 3-6 m thick.

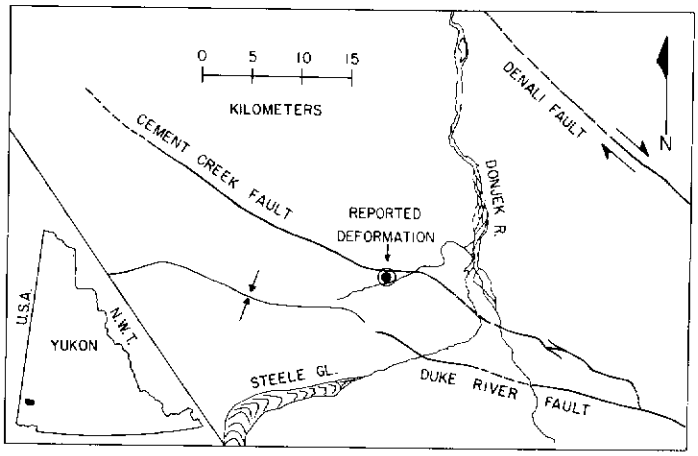

Figure 1. Location of ground failure reported in 1983.

The overlying Paleocene to Miocene Amphitheatre Formation is an assemblage of continental clastic rocks (Eisbacher, 1975). The succession exposed at Cement Creek includes polymictic conglomerate with intermittent cross-stratified sandstone and coal-rich siltstone. These rocks are well indurated and resistant to weathering except where altered near the Cement Creek fault.

The Miocene to Pliocene Wrangell Lavas cover most of the map area and from an engineering standpoint are the most hazardous rocks in this portion of the St. Elias Mountains. The petrology and tectonic setting of these rocks has been described by Muller (1967), Souther and Stanciu (1975), and Skulski and Francis (1986). The

Cement Creek landslide is underlain by the lower Wrangell Lavas (Dodds, 1979). A 150 m section immediately east of the main slide consists of basaltic andesite flows, 5-15 m thick, with rusty weathering flow-top breccias. Two 3-5 m thick syntectonic felsite dykes cut bedding at a slight angle at the base and middle of the section.

The breccias capping the flows consist of altered purple to red brown clasts 5-30 cm long in an altered matrix of montmorillonite, kaolinite, muscovite and local chlorite. Rare voids in these horizons are filled by quartz and actinolite. The intense hydrothermal alteration in the flow top breccias presumably reflects their great initial permeability. They form ideal landslide rupture surfaces since the flow tops are smooth and the alteration products in the breccias render them mechanically weaker.

Hydrothermal alteration has also proceded along joint sets perpendicular to a fold axis affecting rocks in the slide mass and may have weakened them at depth. The major medial fissure bisecting the slide mass in Figures 3(c), 3(d) and Figure 4, has walls which are intensely altered and is faintly visible as an a-c joint in Figure 3(b). Other major cracks near the toe of the slide are controlled by jointing. Hydrothermal alteration is also localized along the Cement Creek fault and in a discordant nearly vertical band of kaolinite which parallels the northwest-trending creek in the west of the map area.

The Wrangell Lavas have been intruded by syntectonic dacites, rhyolites and trachytes (Souther and Stanciu, 1975; Skulski and Francis, 1986). A plug of light grey rhyolite or dacite, dated by Muller (1967) as Pliocene to Recent, outcrops north of the Cement Creek fault (Fig. 2). No Amphitheatre strata were found between this unit and the Cement Creek Fault, thus it may be fault bounded to the south. The intrusion could be as old as Miocene (Dodds, 1979) although Muller speculates that these rocks are petrogenetically and perhaps temporally related to younger rocks such as the White River Ash (1400 years B.P.).

Glacial till and periglacial deposits of clay and silt overlie bedrock throughout the map area. Thicknesses on up-valley facing slopes are 0.5-2 m thick, but reach 5 m in the headwall scarp on the lee side of the slide mass.

STRUCTURE

Structure in the map area of Figure 2 is dominated by two elements: the Cement Creek fault and a pericline immediately south of it.

The Cement Creek fault is an extension of the Wade Mountain fault zone of Read and Monger (1975), originally mapped by Souther and Stanciu (1975). Skulski and Francis (1986) refer to it as the "Cement Creek Fault" and this nomenclature is retained. Including the Wade Mountain extension, this fault runs from the Burwash Uplands to the outwash plain of the Klutlan Glacier where it disappears beneath Holocene deposits. It is vertical, and shows no topographic expression. This, and the fact it splays from the Duke River Fault suggest that right lateral strike slip displacement has occurred along it. Where it outcrops in the eastern part of Figure 3, it is a steeply-dipping, 20 m wide zone of sheared and bleached rock. In places bedding has been folded about nearly horizontal axes, suggesting some local dip slip displacement. No obvious indications of recent movement were observed at Cement Creek. Souther and Stanciu (1975) documented the tilting of both bedrock and overlying Plio-Pleistocene surficial deposits near the fault at Bull Creek and therefore it may still be active.

An east-striking synclinal pericline is located south of the Cement Creek fault (Fig. 2). At its east and west ends, the fold axis plunges at 15° towards a depression located north of Cement Creek. The influence of this structure on landslide kinematics is discussed in the context of the slide morphology (see below).

The Cement Creek landslide occurred in a region of high historical seismicity coincident with the Duke River, Shakwak and Totschunda faults (Horner, 1983). Earthquakes up to M = 6.0 have occurred near the Duke River Fault and microseismicity is high. The regional seismograph network is capable of detecting events down to M = 2.0, and locating them to within 20 km (Horner, 1983; Clague, 1979). Seismicity during the period in which the landslide is bracketed is summarized in Table 1. An earthquake of M = 5.0 was recorded within 20 km of the slide on March 30, 1983. The region of after-

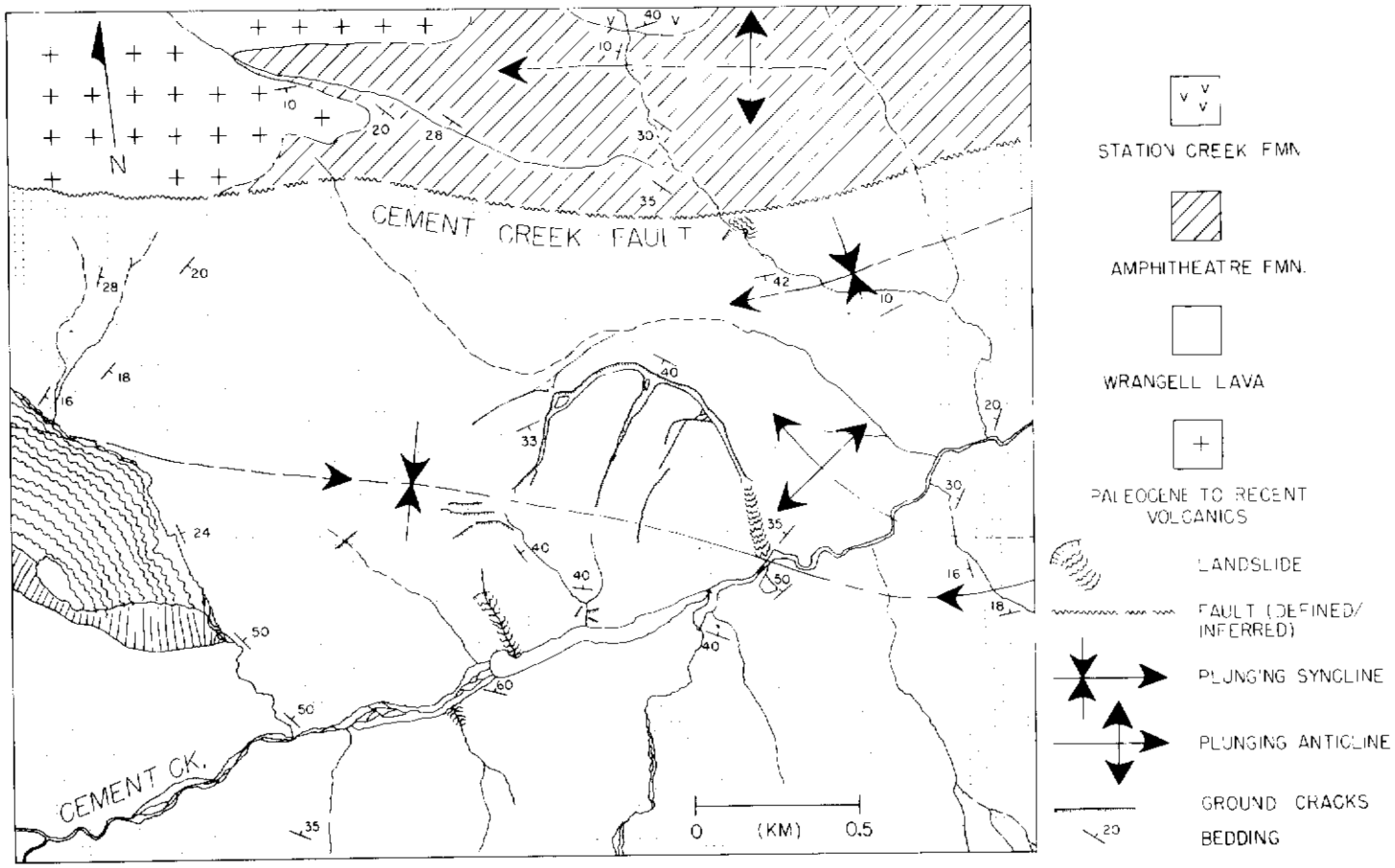

Figure 2. Geology and geomorphology of the Cement Creek area.

TABLE I

Recorded Seismic Events within 160 Km of Cement Creek Slide Between 14 February 1983 and 15 March 1983.

DATE/TIME (U.T)	MAGNITUDE (M_S)	DISTANCE (KM)
7 MAR 83/16:18:25	2.7	90
8 MAR 83/12:12:42	3.8	150
9 MAR 83/12:28:58	3.1	75
1 MAR 83/22:43:26	2.7	110
13 MAR 83/02:45:49	2.3	110

(Sources: Earth Physics Branch/NEIS)

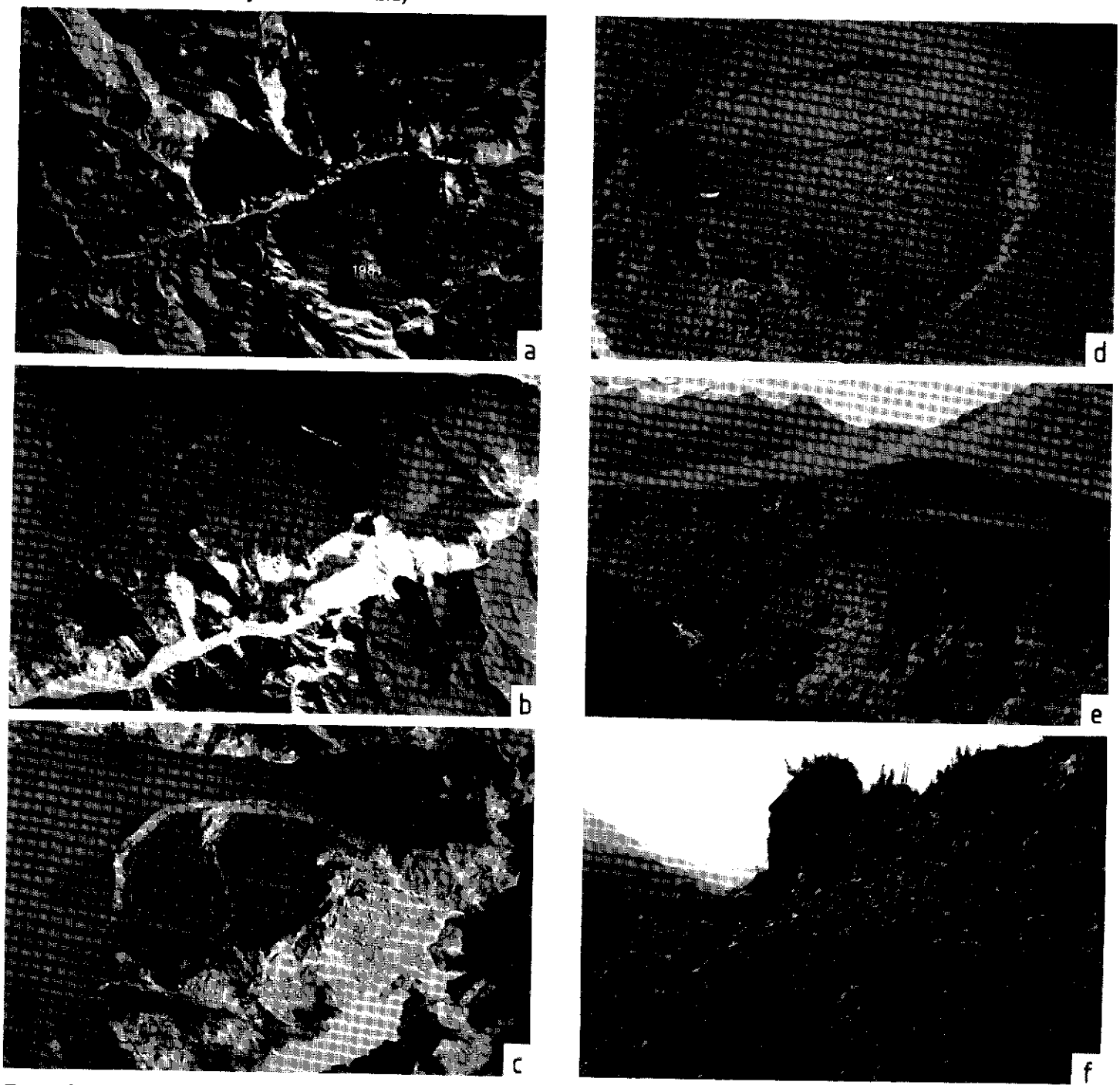

Figure 3. (a) Airphotograph of Cement Creek area (1981). Cement Creek runs west-southwest to east-southeast across the photgraph; and the plateau on which landsliding occurred is in the centre, bordering Cement Creek to the north. (b) Enlargment of the same airphotograph showing the incipient landslide. (c) - (d) Main slide and accessory damage viewed from the southwest and east respectively. (e) View of the main slide from the south. Wrangell strata, visible in foreground, dip towards Cement Creek in the slide area. (f) View of the toe of the slide. Slip surface outcrops as a ledge overlain by debris and intact spires of rock.

shocks included the Cement Creek site and low magnitude foreshocks (i.e., M 2.0) possibly triggered the landslide.

GEOMORPHOLOGY

Landsliding and related ground failure at Cement Creek is confined to the south margin of the triangular plateau in the centre of Figure 3(a). The landslide is 850 m wide, centred on a domal hill protruding 110 m above the plateau. Holocene down-cutting by Cement Creek has incised a 90 m deep canyon which forms the south boundary of the plateau. Landsliding occurs where bedding dips out of this open face. The landslide is a block slide with breakup of the slide mass occurring only at the toe. There, large spires of rock up to 60 m high have separated from the slide mass. The slide mass is perched on a bedrock ledge outcropping half way up the exposed face. It is evidently intact since large blocks of slide debris are supported by it (Fig. 3(f)). Maximum landslide displacements appear to be 30 or 40 m.

This landslide is unusual in that displacements have a rotational component and the headwall scarp has developed midway up the hill comprising the slide mass. Both of these effects can be ascribed to bedding control.

The morphology of the headwall scarp and the distribution of ground cracks indicate that both slight clockwise rotation and downslope translation occurred. The headwall scarp varies in width along strike, narrowing from 70 m wide in the east to 20 cm wide on the west flank where it eventually disappears. This effect is produced by clockwise rotation of the slide mass away from the scarp. The distribution of major cracks on and adjacent to the landslide is shown in Figure 4. The trend of these cracks varies progressively from east to west with cracks nearest the toe being parallel to the exposed face and those higher up, oblique to it. This suggests that as blocks move down the rupture surface, they are progressively rotated in a clockwise sense.

For reasons discussed previously, bedding is thought to be a significant factor controlling landsliding of these rocks. The displacement suggested by the crack pattern is consistent with oblique slip down bedding in the north limb of the synclinal pericline dominating the local structure. Dip slip would be inhibited by the inflection of bedding at the fold axis, and the flexure of bedding at the depression of the pericline could account for the rotational component of motion as shown in Figure 5. This would occur as the gradient in the direction of the fold axis was progressively reduced in approaching the depression of the pericline. The component of motion directed

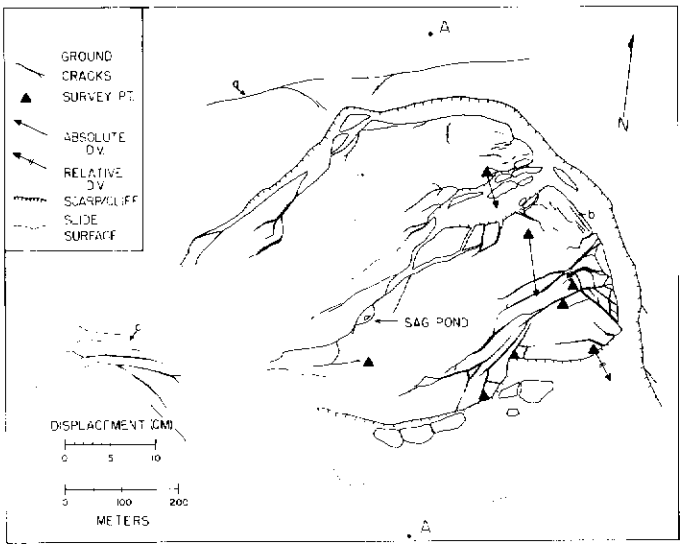

Figure 4. Map of principal ground cracks and displacement vectors. Three types of cracks are indicated: (a) Ground cracks formed prior to 1983; (b) Cracks developed on north face of the slide mass as a consequence of block rotation; (c) Cracks unaccompanied by landsliding.

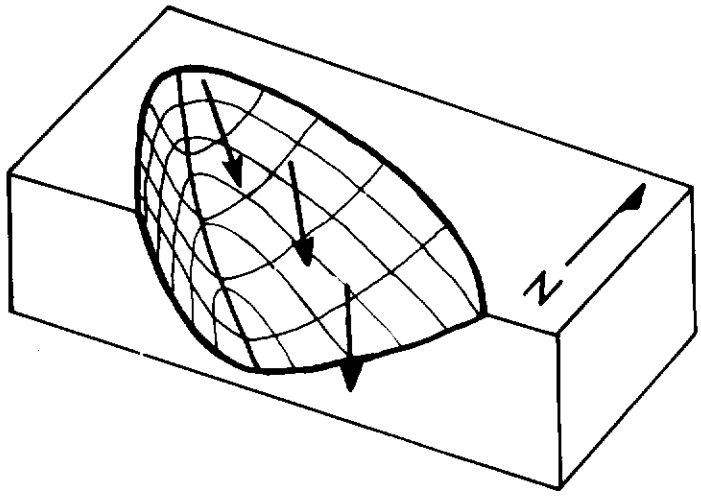

Figure 5. Schematic diagram of slide surface. Displacement vectors are rotated because of changes in gradient, primarily along the fold axis.

along the axis would decrease while that perpendicular to it would be relatively unaffected. A net rotation results.

The peak velocity of the landslide could not have been great; no evidence of splash is visible on the slopes of the south wall of the canyon. The debris fan dammed Cement Creek, impounding a lake 1 km long behind it, but the dam is permeable; during a dry spell in June, 1986, the creek's discharge percolated through the barrier with no surface flow. Levees approximately 10 m high border the creek where it cuts through the toe of the slide and the stream is clearly not competent to remove this debris.

The slip surface of the landslide is a prominent ledge, visible in Figure 3(b) as a tree covered ramp on the front face of the slide and as it appeared in 1986 in Figure 3(f). Debris in the toe of the slide has obliterated all evidence of any prior tree cover, but the ledge is still intact and able to support large spires of rock which have ridden out on it. It consists of relatively unaltered lower Wrangell lava flows and is oriented consistently with nearby bedding. That portion of the slip surface visible in the headwall scarp dips at approximately 50° towards the toe of the slide. Rock exposed here is highly altered with bedding largely obliterated. The dip of the slip surface is greater than that of bedding, indicating that the rupture surface departs from bedding at depth, cutting up to the headwall scarp.

The upper part of the rupture surface appears to be concave as some evidence exists that the north slope of the slide mass has been rotated to vertical. This is afforded by a series of ground cracks cutting across the steep north face of the hill involved in the landslide (b in Fig. 4). These cracks are at most 40 cm deep and involve only sod and the upper layer of the soil horizon. They have not developed on the stationary portion of the hill below the headwall scarp and appear to result from solifluction of the top layer of permafrost during seasonal thawing. The fact that these features are present only on the back face of the slide mass and not on the hill below the headwall scarp suggests that the north face of the slide has rotated through an angle sufficient to to destabilize the overlying vegetation. A composite cross section incorporating the results of both topographic and geophysical surveys is displayed in Figure 6.

In addition to the solifluction cracks, three other broad classes of cracks are visible on, and near the landslide. These include cracks predating the 1983 landslide, surficial and deep cracks formed during the 1983 slide, and others dating from 1983 west of the landslide.

A series of cracks, clearly older than those developed during 1983, are found north of the landslide at the break in slope between the hill and plateau (a in Fig. 4). These, individually up to 100 m long, form a linear en echelon array 570 m long. They strike across the northwest side of the landslide, deviating only near a kink in the headwall scarp. They do not wrap around the back of the slide as would be expected if they reflected headward migration of the slip surface; instead they continue northeast and disappear in a stream bed at

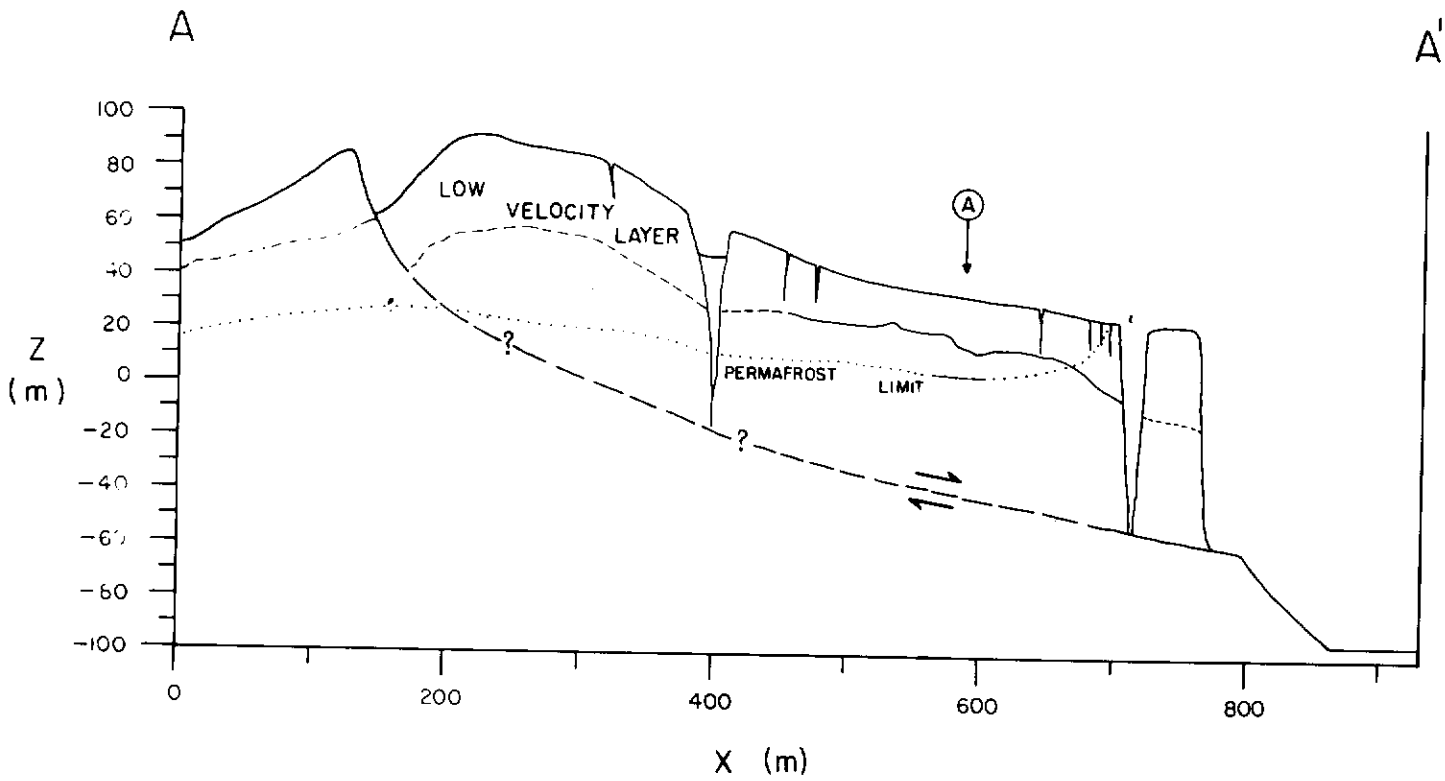

Figure 6. Composite cross section integrating the results of geophysical and topographic surveys. Low velocity layer of weathered rock and surficial deposits mapped from seismic surveys. Permafrost limit mapped from electrical resistivity soundings. Location of slip surface determined from topographic surveys. Line of section indicated in Figure 4. Inferred boundaries are dashed.

the foot of the hill on which the slide is located. The cracks expose bare earth and are up to 40 cm deep with weathered and partially overgrown sides. The linearity of these cracks, irrespective of local topography, coupled with their length and depth argue against their being some unusual frost effect. They are faintly visible on enlargements of airphotographs shot in 1943, 1972 and 1981. They appear to parallel some anisotropy in bedrock and may have developed during a landslide prior to 1943.

The second class of ground cracks are those formed by the 1983 landslide. These can be subdivided into two categories on the basis of apparent depth. Most are rooted at depths no greater than 10 - 20 m and are most abundant near the toe of the landslide. Geophysical evidence, discussed below, suggests that they do not extend to the slip surface. The second class includes larger, longer cracks at least 40 m deep extending down to the slip surface. These cracks separate major blocks in the landslide which to some degree move independently of each other. This effect was detected in measurements of absolute displacement of points on either side of the medial crack which bisects the slide (Fig. 3(b), 3(c), 4).

The third class of cracks is a series which formed in 1983 immediately west of the landslide. These are 5-8 m deep and are clustered on the edge of a small spur immediately west of the main slide (bottom right quadrant of Figure 3(b)). They do not appear to be structurally connected to those on the main slide; the headwall scarp crack ends about 100 m north of this site and these cracks strike perpendicular to it. No evidence of deep seated bedrock displacement was observed.

The area involved in the 1983 landslide appears to have undergone mass movement prior to 1943. The incipient trace of the headwall scarp and medial crack is faintly visible in airphotography shot prior in 1943, 1972 and 1981. The ledge which forms the slip surface and underlies the toe of the slide is tree covered in enlargements of 1981 airphotographs, suggesting that the landslide has been inactive for at least a century (Fig. 3(b)). Displacement prior to 1983 appears to have been minimal since the slide mass remained essentially intact and the incipient headwall scarp was approximately 10 m wide.

DEFORMATION RATES

In order to ascertain whether motion of all or part of the landslide was still occurring, a series of survey stations were installed to measure absolute and relative deformation rates. Motion relative to the presumably stationary plateau was monitored by means of a microgeodetic survey network (Fig.7). Relative displacement across apparently active cracks was measured using the method of trilateral signs outlined by Ter Stepanian (1980). Lastly, an attempt was made to measure the rate of crack propagation by means of pegs offset perpendicularly from the tips of individual cracks. Significant displacement was detected only in the first two of these studies.

The microgeodetic survey grid consisted of three stations sited around the perimeter of the landslide. At each station, motion of one or two sites on the slide was measured with respect to two fixed points on the plateau. Survey sites consisted of a tripod positioned over a hub and anchored into the permafrost. During each survey, the distance along three sides of the triangle formed by the two points off the slide and the one on it were measured using a Sokkisha Red-1A electronic distance measuring device (EDM). The vertical angles between points 1, 2 and 3, their respective reference points and the sites on the slide were measured using a Kern DKM-II triangulation theodolite. EDM measurements were corrected for air temperature and pressure; no corrections for refraction were made to angular measurements. The position of each station on the slide was then calculated relative to a rectangular coordinate system centred at each of points 1, 2 and 3, with the positive X-axes being the horizontal projections of the vectors 1-1A, 2-2A and 3-3A and the Y-axes pointing towards the landslide in the horizontal plane. The apparent motion of points on the landslide was projected into the horizontal plane and plotted in Figure 8.

The sources and magnitude of error in these surveys strongly influenced the significance of the results. EDM standard error was less than 1 cm over the distances used in the network. Systematic distance measurement error was overcome by normalizing the measurements against the repeated measurements of the distance between the fixed reference points. Refraction error was negligible

since angles never exceeded 10°. Levelling error was significant; tripods were prone to shifting between shots and 30"s of arc was assigned as the angular measurement error. EDM and angular measurement error translated into a maximum combined error of +/- 3.0 cm in the position of any point in the plane of projection.

The criteria used to establish true displacement were: (1) initial and final points be separated by at least 6.0 cm; and (2) the overall trend of the apparent motion be smooth. The apparent random motion of points 1B and 3B are therefore attributed to frost heave or some other site specific effect not related to landsliding. Motion was detected at sites 2B and 2C where displacement vectors were 10 ± 6 and 12 ± 6 cm, respectively.

Relative displacement across major and/or apparently active cracks was measured using the method of trilateral signs outlined by Ter Stepanian (1980). Measurement error was calculated using extreme values rather than the geometrical construction he developed. Relative displacements were detected across cracks at sites T-1 and T-4 (Fig. 7) and are plotted in Figure 8.

Absolute displacement at sites 2B and 2C is consistent with the overall pattern of ground cracks in the slide mass (Fig 7.) and with observations on the activity of the landslide made by the field party. The clockwise sense of rotation of the displacement vectors matches that suggested by the ground cracks. No indications of significant motion were apparent in 1986. If the slide was active, unstable debris in the toe of the slide should have been displaced. Particular attention was paid to a large block perched near the front edge of the ledge forming the slide surface (Fig. 3(f)) which leaned towards the creek at about 15°. No motion of this, or any other debris was noted. The small amount of detected displacement was in rocks resting on the steepest portions of the rupture surface. This may be a seasonal feature caused by the infiltration of groundwater from summer run-off. Relative displacement at T-1 is due to the separation of an island of trees and frozen surficial deposits from the slide mass in the toe. Its displacement vector reflects the local orientation of the slip surface in the immediate area and not its overall morphology. Deep seated creep appears to still be occurring in the slide mass, but this process cannot account for the observed ground failure.

GEOPHYSICAL SURVEYS

Refraction seismic and electrical resistivity surveys were conducted to map the rupture surface at depth and to obtain data on the geotechnical properties of the slide material. The philosophy behind such investigations is outlined by Muller (1977). Fracturing of rock in a slide mass lowers P-wave velocity and allows ground water to percolate to the slip surface. Often an impermeable gouge layer

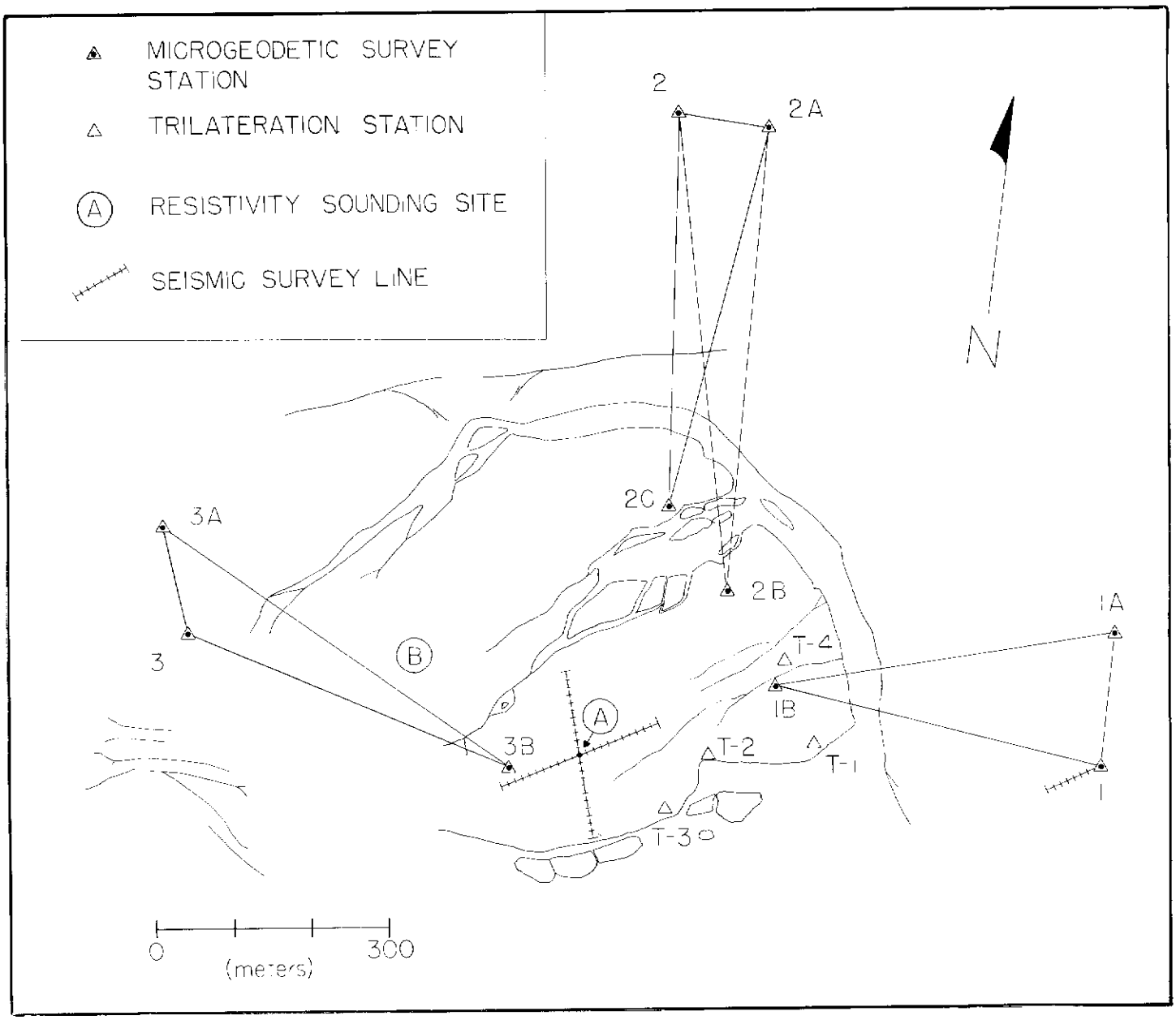

Figure 7. Location of microgeodetic survey grid and geophysical survey sites.

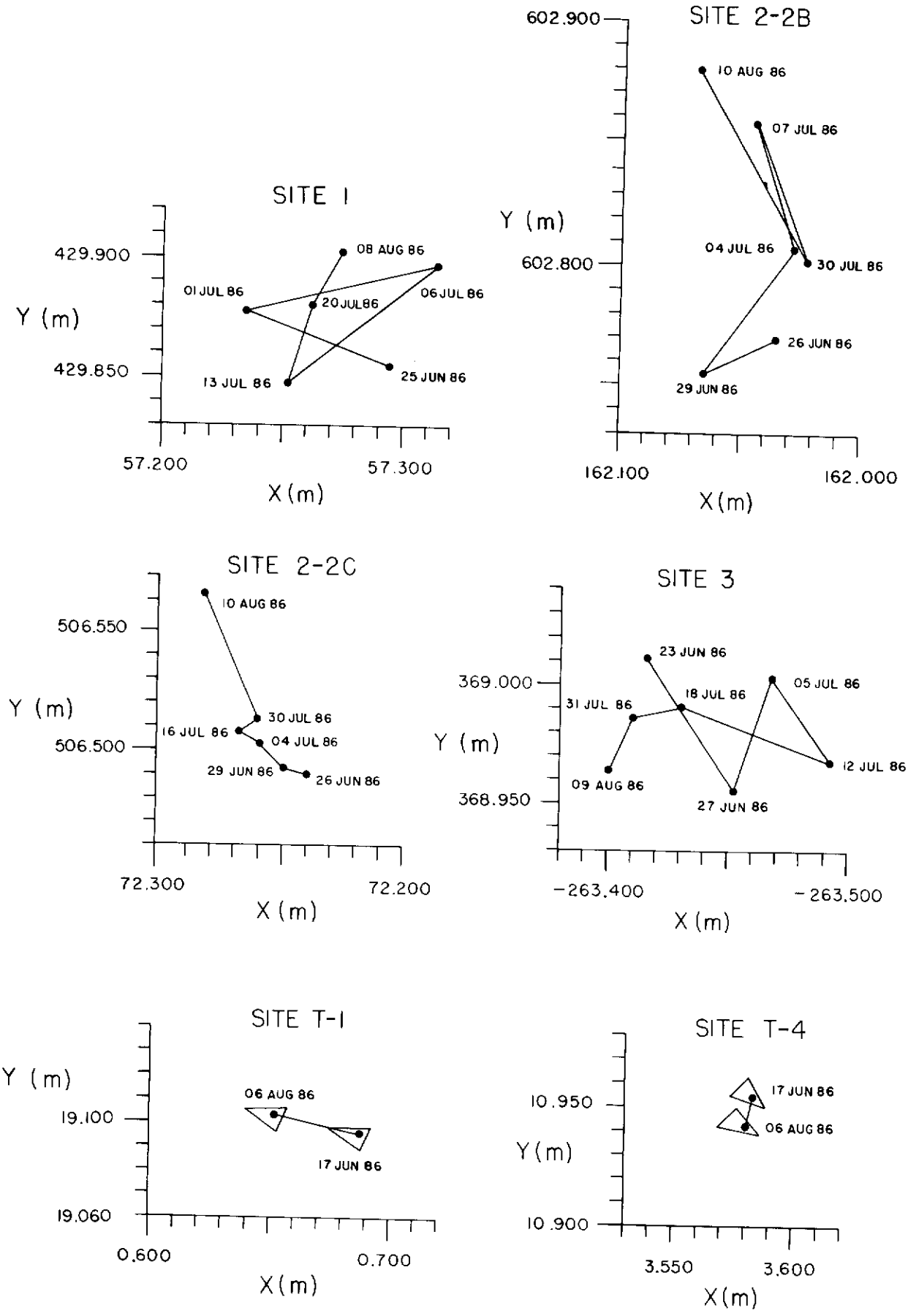

Figure 8. Absolute and relative displacement of survey points on the main slide mass. Date of measurement and position of the points relative to fixed origins are recorded.

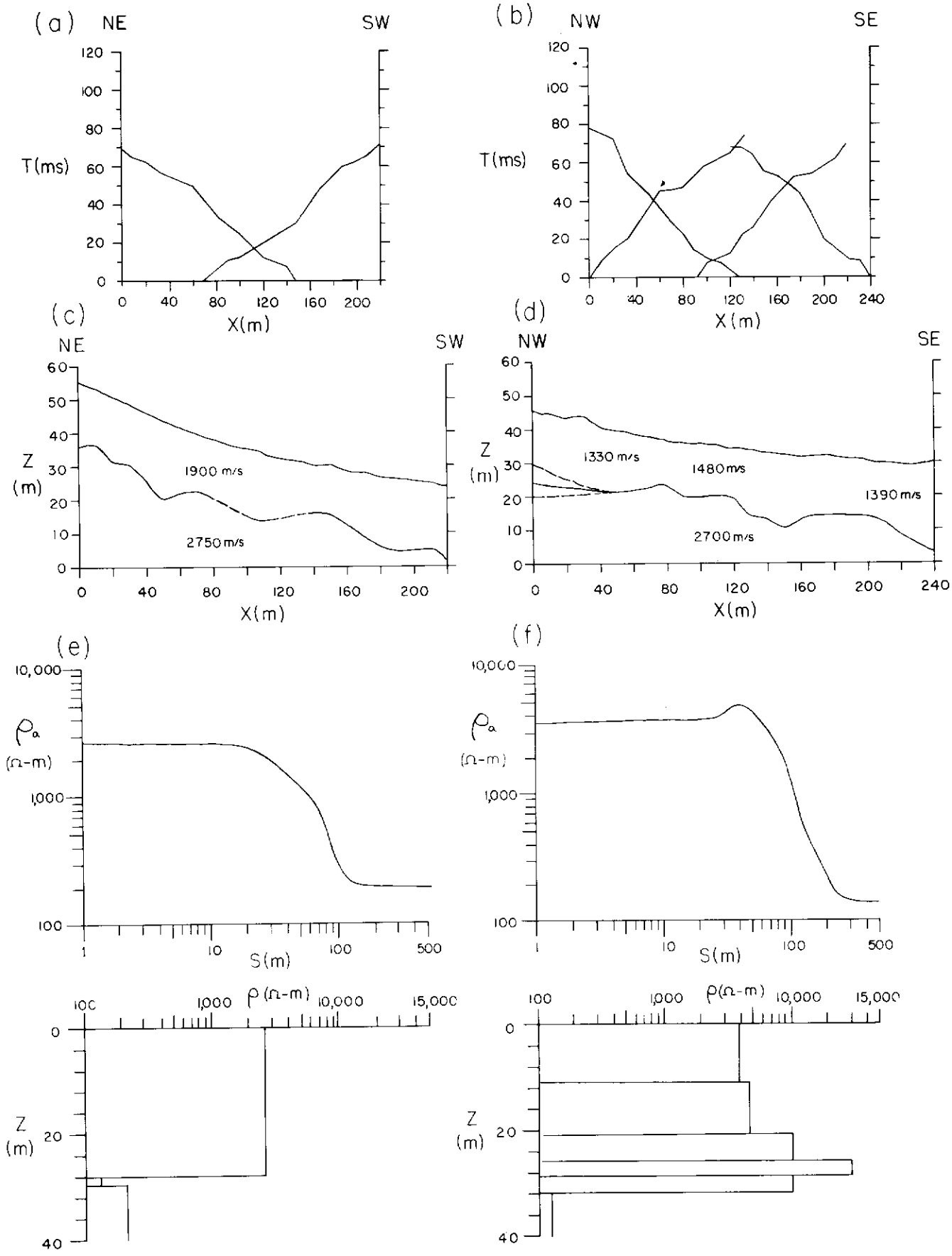

Figure 9. Results of geophysical surveys conducted on main slide. (a) - (b) Travel-time curves for seismic refraction surveys. (c) - (d) Profiles of ground surface and seismic refractors along each line. (e) - (f) Apparent resistivity curves at sites A and B respectively. Best-fit models are shown beneath with the resistivity and depth of each layer indicated.

develops there, and groundwater can be perched at this level. The juxtaposition of fractured low velocity material over intact high velocity material presents a situation where the interface between them can be mapped using the seismic refraction technique. Electrical resistivity soundings can detect perched groundwater as a conductive layer. For an ideal single rupture surface, electrical resistivity and seismic surveys should complement each other, with a conductive layer being detected immediately above a seismic refractor. At Cement Creek, geophysical surveys failed to detect the rupture surface at depth because of instrumental limitations and interference of permafrost.

Seismic refraction surveys were conducted using a Bison 1570B single channel seismograph and a maximum shot-geophone spacing of 150 m. A 4.5 kg sledgehammer and plate set and explosives were used as energy sources. Poor transmission properties of the surficial cover rendered the hammer useless at spacings greater than 60 m and necessitated the use of up to 3 sticks of 60% Forcite at end of line shots. A shot spacing of 10 m was used on each of the three lines shown in Figure 7. A test section was run at survey station 1 to determine the electrical cap delay time and to determine velocities in the Wrangell Lavas. Two section lines were on the landslide, oblique to the inferred dip of the rupture surface. Travel time curves for these lines are shown in Figure 9a-b.

The data was inverted using the method of Wyrobek (1956) which was selected because only a single refractor, subparallel with the surface, was detected. Cross sections along seismic lines shot on the slide, showing both ground surface and refractor topographies are displayed in Figure 9c-d. Depths to the refractor are considered accurate to within 10%. Significant changes in the velocity of the upper layer were apparent in the NW-SE section while that of the NE-SW line was constant. The velocity of the lower layer remained essentially constant along both lines.

The average depth to the refractor, between 15 and 20 m, was too deep to explain it as being the base of frozen surficial deposits since shots frequently exposed bedrock at 0.5 m depths. The refractor seems to represent the base of a combined layer of weathered rock and surficial cover. The anisotropic velocity profile of the upper layer along the NW-SE line most likely relects the presence of ground cracks; this line is transverse to them, while the NE-SW line parallels ground failure and does not intersect any major cracks. The absence of velocity anisotropy in the layer below suggests that ground failure is confined to a layer of weathered rock and till. The seismic profiles did not cross any of the deep cracks which subdivide the slide into major blocks. The ground failure along the seismic profiles may therefore have resulted from strong ground motion during the 1983 landslide. This mechanism may also explain the ground failure immediately west of the landslide.

Electrical reistivity soundings were conducted at two sites using an expanding Schlumberger array and apparatus built at the University of Alberta. Current electrode spacing was expanded in increments of 20 m with potential electrode spacing being widened when the measured voltage dropped below 4.0 mV. Apparent resitivity profiles for the two sites are shown in Figure 9e-f.

The results were inverted using a resistivity transform technique suggested by Koefoed (1979) since more than two layers were apparent in the profile at site B and master curves for such cases are not readily available. The method involved comparison of actual and model values of the resistivity transform function at selected values of the current electrode spacing (s). The data was sampled at s-intervals of six per decade and converted into values of the resistivity transform by the application of a digital filter developed by O'Neill (1975). Model parameters were then specified and values of the resistivity transform for corresponding spacings were calculated using the Pekeris Recurrence Relations (Pekeris, 1940). The model was adjusted until the transform values of the data and the model agreed within 2%. Best fit models for sites A and B are displayed immediately below their corresponding apparent resistivity profiles.

The resistivity profiles seem to delineate the lower limit of permafrost in the slide mass. The abrupt change in resistivity at around 30 m does not correspond with either the base of the weathered rock layer or with any reasonable projection of the rupture surface at depth. The most likely interpretation of the models is that they delineate an upper layer of frozen, high resistivity rock and till underlain by thawed rock whose resistivity has been lowered by jointing and clay alteration. The difference in upper layer resistivity between sites A and B is probably due to greater hydrothermal alteration of rock at site A; hydrothermal alteration of rock exposed in the headwall scarp decreases from east to west. The effect of clay alteration on rock conductivities has been summarized by McNeill (1980). Bound water in clay minerals allows relatively high rock conductivities to persist below the freezing point because electrolytes inhibit bound water from freezing and allow current paths to remain open.

The resistivity soundings indicate that groundwater near the rupture surface is unlikely to freeze at any time. Groundwater seepage was observed from portions of the landslide toe during the summer of 1986. Saturated conditions could develop near the base of the landslide once freeze-up has occurred and might persist for a considerable period. By lowering the effective shear strength of the rock, trapped groundwater may play an important role in preparation of the landslide for failure.

CONCLUSIONS

Landsliding at Cement Creek is confined to lower Wrangell Lavas in the core of a synclinal pericline. Hydrothermal alteration of flow-top breccias has lowered the mechanical stength of these beds and shear failure is largely localized along them. Jointing controlled the location of major ground cracks and a portion of the headwall scarp. Non-cylindrical folding of bedding imparted a rotational component of motion to the slide mass and this is reflected in current displacement vectors and in the pattern of cracks in the slide mass. The 1983 landslide was a single low-velocity block slide with maximum displacement of approximately 40 m. Debris in the toe appears to have arrested the slide although blocks near the head are creeping towards the toe at about 5 $\pm$ 3 cm per month, perhaps on a seasonal basis. The area involved in the 1983 slide has undergone minor mass movement prior to 1943 and probably has been stable for the past century.

Trapped groundwater may have prepared the slide mass for failure with such instability developing after freeze-up when permeablility in the toe of the slide was minimal. Local seismicity may have provided a trigger; the landslide is 300 m south of a major fault in a seismically active area. A single low magnitude event or a series of them could have initiated creep which accelerated into catastrophic failure. If shallow ground failure on and immediately adjacent to the landslide is ascribed to strong ground motion, the slide must have occurred in a matter of seconds.

ACKNOWLEDGEMENTS

This work was supported by D.I.A.N.D. contract Y6-MG02 and by funds from a Natural Sciences and Engineering Research Grant to D.I. Gough. The author wishes to thank D.I. Gough and P. Erdmer for help received in the planning and conduct of field work. P. Von Gaza rendered capable assistance in the field. X-Ray diffraction work was performed by G. Speirs. The author benefited from discussions with A. Peterson, T Skulski and D. Cruden. E. Nyland provided help throughout this work and reviewed this paper.

REFERENCES

CAMPBELL, R.B. and DODDS, C.J., 1979. Operation St. Elias, British Columbia; in Current Research Part A. Geological Survey of Canada, Paper 79-1A, p. 17-20.

CAMPBELL, R.B. and DODDS, C.J., 1978. Operation St. Elias, Yukon Territory; in Current Research Part A, Geological Survey of Canada, Paper 78-1A, p. 35-41.

CLAGUE, J.J., 1979. The Denali Fault System in southwest Yukon Territory - A geologic hazard?; in Current Research Part A, Geological Survey of Canada, Paper 79-1A, p. 50-56.

DODDS, C.J., 1979. Geology of the southwest Kluane Lake map area; Geological Survey of Canada, Open File 829 (Map).

DRYSDALE, J.A., HORNER, R.B. and WETMILLER, R.J., 1983. Canadian Earthquakes - National Summary January - March, 1983; Seismological Services of Canada, Earth Physics Branch.

EISBACHER, G.J., 1975. Operation St. Elias, Yukon Territory: Dezadeash Group and Amphitheatre Formation; in Current Research Part A, Geological Survey of Canada, Paper 75-1A, p. 60-61.

HORNER, R.B., 1983. Seimicity in the St. Elias Region of Northwestern Canada Bulletin of the Seismological Society of America, Vol. 73, No. 4, pp. 1117-1137.

KOEFOED, O., 1980. Geosounding Principles, 1 (Resistivity Sounding Measurements); New York, Elsevier.

LAHR, J. and PLAFKER, G., 1980. Holocene Pacific - North American Plate interaction in Southern Alaska: implications for the Yakataga Seismic, Gap; Geology, Vol. 8, p. 483-486.

MCNEILL, J.D., 1980. Electrical Conductivity of Soils and Rocks; Technical Note TN-5, Geonics Ltd.

MULLER, J.E., 1967. Kluane Lake Map Area, Yukon Territory; Geological Survey of Canada, Memoir 340.

MULLER, K., 1977. Geophysical methods in the investigation of slope failures; International Association of Engineering Geology Bulletin, Vol. 16, p. 227-229.

NATIONAL EARTHQUAKE FORMATION SERVICE (NEIS), 1983. Preliminary determination of epicenters - March, 1983.

O'NEILL, D.J., 1975. Improved linear filter coefficients for application in apparent resistivity computations; Bulletin of Australian Society of Exploration Geophysicists, Vol. 6., p. 104-109.

PERKERIS, C.L., 1940. Direct method of interpretation in resistivity prospecting; Geophysics, Vol. 5, p. 31-46.

READ, P.B. and MONGER, J.W.H., 1975. Operation St. Elias, Yukon Territory: The Mush Lake Group and Permo-Triassic rocks in the Kluane Ranges; in Current Research Part A, Geological Survey of Canada Paper 75-1A, p. 55-59.

SKULSKI, T. and FRANCIS, D., 1986. On the Geology of the Tertiary Wrangell lavas in the St. Clare Province, St. Elias Mountains, Yukon; in Yukon Geology Vol. 1; Exploration and Geological Services Division, Yukon, Indian and Northern Affairs Canada, p. 161-170.

SOUTHER, J.G. and STANCIU, C., 1975. Operation St. Elias, Yukon Territory: Tertiary Volcanic Rocks; in Current Research Part A, Geological Survey of Canada Paper 75-1A, p. 63-70.

STEPHENS, C.D., FOGLEMAN, K.A., PAGE, R.A. and LAHR, J., 1985. Seismicity in southern Alaska, October, 1982 - September, 1983; in Bartsch-Winkler S. and Reed, K.M. (eds), The United States Geological Survey in Alaska - Accomplishments during 1983, United States Geological Survey, Circular 945, p. 83-86.

TER STEPANIAN, G., 1980. Measuring displacements of wooded landslides with trilateral signs; Proceedings of the International Symposium on Landslides, Vol. 1, New Delhi: Sarita Prakashan.

WYROBEK, S.M., 1956. Application of delay and intercept times in the interpretation of multilayer refraction time distance curves; Geophysical Prospecting, Vol. 4, p. 112-130.

MICROEARTHQUAKE SEISMICITY ON THE DUKE RIVER, DENALI FAULT SYSTEM

M.A. Power
Department of Physics,
University of Alberta
Edmonton, Alberta
T6G 2E1

POWER, M.A., 1988. Microearthquake seismicity on the Duke River Fault, Denali Fault System: in Yukon Geology, Vol. 2; Exploration and Geological Services Division, Yukon, Indian and Northern Affairs Canada p. 61 - 68.

ABSTRACT

A seven station seismograph array operated at two sites on the western segment of the Duke River Fault between May 22, 1987 and August 13, 1987 detected 146 earthquakes of which 44 were located. Distribution of microearthquake epicentres, S-P times and moderate earthquake epicentres delineate three zones of seismicity. Most microseismicity is confined to a 15 km wide central zone, parallel to the Duke River Fault and centered approximately 5 km north of it, where shallow and midcrustal microearthquake focii are centered beneath structures deforming the Tertiary cover. Faulting here is well constrained to oblique thrusting on a slip plane striking parallel to the Cement Creek fault. A northern zone of shallow focus micro seismicity is centered on the Wolverine Plateau and the valley of the White River. A southern zone of microearthquake focii centred on the Icefield Ranges delineates an unmapped fault, 40 km long and striking west from known faults south of the Duke River Fault. The distribution of epicentres and a composite focal plane solution suggest that reverse faulting with southward vergence is occurring in this zone. The results of this study and the historical record of epicentres suggest that the Totschunda and Duke River Fault segments of the Denali Fault System are structurally linked and that no connection between the Denali Fault System and the Pacific margin is in this area.

RÉSUMÉ

En utilisant un réseau sismographique de sept stations dans deux sites du segment ouest de la faille de Duke River, entre le 22 mai 1987 et le 13 août 1987, on a pu déceler 146 séismes, et localiser 44 d'entre eux. La distribution des épicentres microsismiques, les temps de propagation des ondes S-P et la distribution d'épicentres de séismes d'intensité moyenne nous ont permis de délimiter trois zones de sismicité. La microsismicité est principalement limitée à une zone centrale de 15 km de large, parallèle à la faille de Duke River, centrée à environ 5 km au nord de celle-ci, et où des foyers microsismiques peu profonds et localisés dans la partie moyenne de la croûte sont centrés au-dessous de structures qui déforment la couverture tertiaire. A cet endroit, le faillage est bien limité à un charriage oblique qui s'est produit au-dessus d'un plan de glissement d'orientation parallèle à la faille de Cement Creek. Une zone microsismique septentrionale, avec foyer peu profond, est centrée sur le plateau Wolverine et dans la vallée de la rivière White. Une zone microsismique régionale, dont les foyers sont centrés sur les monts Icefield, délimite une faille non cartographiée de 40 km de long, de direction ouest à partir de failles connues situées au sud de la faille de Duke River. La distribution des épicentres et la résolution d'un plan focal composite suggèrent que dans cette zone, apparaissent des failles inverses caractérisées par une vergence sud. Les résultats de cette étude, et les enregistrements chronologiques des épicentres, suggèrent que les segments faillés de Totshunda et de Duke River qui appartiennent au réseau de failles de Denali sont liés du point de vue de leur structure, et qu'il n'existe aucun lien entre le réseau de failles de Denali et la marge pacifique dans cette région.

INTRODUCTION

Seismicity in the southwest Yukon Territory is generally restricted to two zones; one along the Pacific/North American plate boundary and the other straddling the Denali Fault System (Fig. 1) (Horner 1983). Earthquakes up to magnitude 8.6 have occurred at the plate boundary, where the Yakutat Block is actively accreting to the North American Plate along the Fairweather, Chugach-St. Elias and Border Ranges faults. The Dalton, Shakwak and Duke River segments of the Denali Fault System display a lower level of seismicity with recent earthquakes up to magnitude 6.5. Historically, the greatest number of small to moderate earthquakes has occurred on the Duke River Fault between the Duke River Depression and the Yukon/Alaska boundary. Displacement on the Denali Fault System is dominantly right-lateral (Campbell and Dodds 1978) but the western portion of the Duke River Fault has been mapped as transpressional bend across which crustal shortening is occurring (Plafker et. al., 1978). This report describes a survey of earthquake activity along this portion of the Duke River Fault during May - August 1987. Previous surveys of microseismicity along the Denali Fault System in the Yukon Territory were conducted by Boucher and Fitch (1969) and Horner (1983); neither were conducted in the area described in this paper.

FIELD PROCEDURE

An array of seven seismographs was installed and operated for 5-6 weeks at two locations shown in Figure 3. Sites A-G were located near Big Boundary Creek and operated from May 22, 1987 to July 2, 1987 and sites H-N were centered south of the confluence of St. Clare and Bull Creeks and operated from July 5, 1987 to August 13, 1987. The array consisted of 2 Sprengnether DR-100 and 2 Teledyne MCR digital event recorders and 3 Sprengnether MEQ-800 smoked paper drum seismographs; one MCR was configured with a vertical and pair of horizonatal seismometers, whereas the rest were equipped solely with vertical component seismometers. Digital event recorders are triggered by ground motion exceeding backround noise by a preset amplitude and record the 1.5 seconds of signal preceeding the trigger together with subsequent high amplitude ground motion whereas the drum seismographs provide a continuous record of ground motion. The array bandwidth was 29.75 Hz with a low cut at 0.25 Hz; individual instruments had wider response characteristics. Instrument gain varied between 66078 dB depending upon site conditions and the level of microseisms. Seismograph sites were serviced every 1-4 days and this schedule together with terrain conditions limited the size of the networks. To ensure accurate timing, 2 Benest Portable Precision Clocks were synchronized daily with WWV and

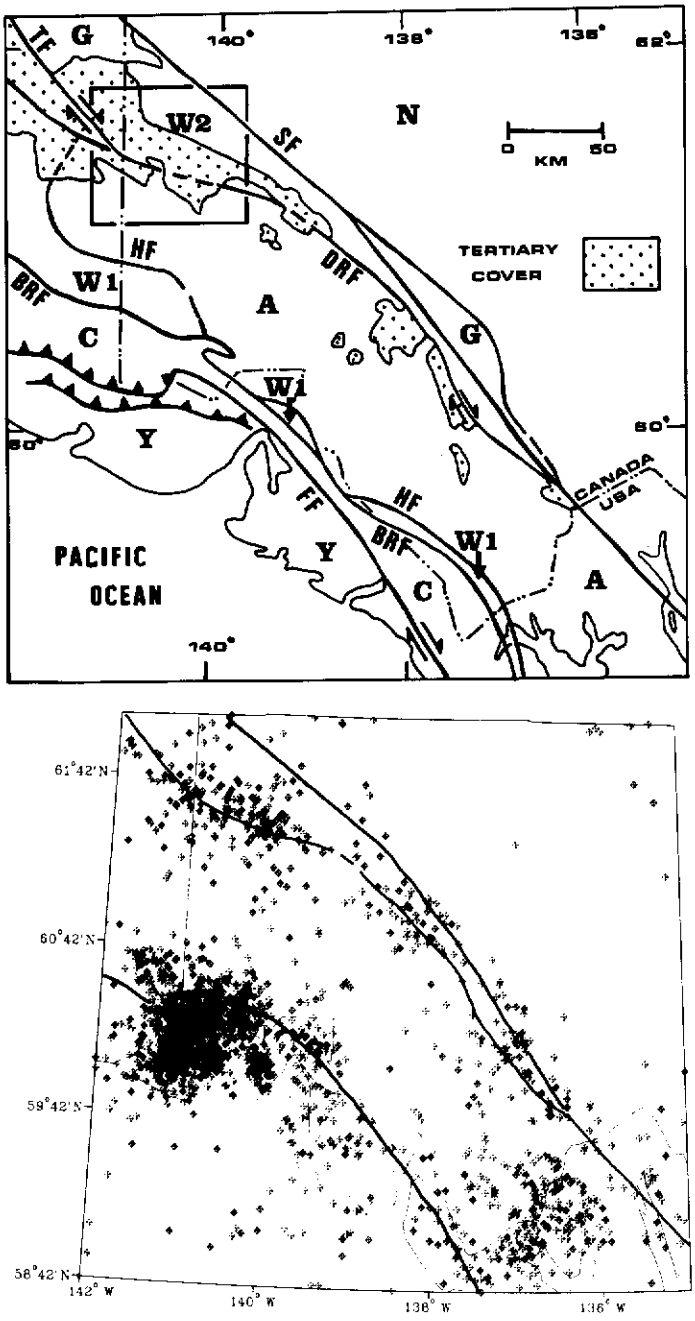

Figure 1. Tectonic elements and seismicity in the southwest Yukon Territory and southeastern Alaska (a) Principal faults and terrane distributions after Campbell and Dodds (1987). The study area is the rectangular region enclosed in the top left corner of the map. Symbols for elements of the Wrangell Terrane; W1 and W2, Alexander Terrane; A, Chugach Terrane; C, Yakutat Block, Y, in-board elements of the North American plate; N, Border Ranges Fault; BRF, Hubbard Fault, HF, Fairweather Fault; FF, Totschunda Fault; TF, Duke River Fault; DRF, Shakwak Fault; SF (b) Distribution of epicentres in the area of (a) from the Canadian Earthquake Catalogue superimposed on the traces of the Fairweather-Chugach- St. Elias Faults and the Denali Fault System.

in turn used to drift-correct seismograph clocks.

The smoked paper seismographs provided continuous coverage and produced the most useful records for the purpose of this study. Cool wet weather had a deleterious effect upon the performance of the digital event recorders by causing rapid battery deterioration and often large clock drifts. Limited tape and pre-event buffer capacity also restrict the usefulness of such instruments in reconnaissance studies: site noise or teleseismic earthquakes can fill tapes rapidly and emergent P-wave onsets from local earthquakes are often not recorded if the S-P separation exceeds the buffer capacity. Earthquakes located in this study were usually detected by three of the smoked paper instruments and by up to two of the digital event recorders.

DATA ANALYSIS

A total of 146 earthquakes were detected at one or more sites. Impulsive, high amplitude P- and S-wave arrivals were timed to within ± 0.05 s and ± 0.2 s respectively; arrivals of lesser quality had larger errors and were weighted accordingly. All arrivals were corrected for clock drift using double interpolation to correct for portable clock drift with respect to WWV and seismograph clock drift with respect to the portable clock. DR-100 and MEQ-800 seismograph clock drifts rarely exceeded 20 ms per day but MCR clock drift occasionally exceeded 100 ms per day and appeared to be disconcertingly non-linear. Arrivals detected at MCR sites were only used in solutions when their drift corrected arrival times were judged to be consistent with those recorded at surrounding stations.

Most earthquakes occurred outside of the detecting arrays and this created difficulty in determining focal coordinates. Least-squares methods are usually applied to the earthquake location problem and often fail to converge to an acceptable solution when an event is outside of an array or when no site is closer to the epicentre than the focal depth (Lee and Stewart 1981). A method was devised to eliminate origin time as an explicit variable and thus permit a more stable geometric search for a solution. It is fully described in Power (1988) and is summarized here.

Consider an array of n stations at which P and S arrivals t_{Pk} and t_{Sk} [k= 0, 1, 2...n] are recorded. For a trial focus and origin time, theoretical arrival times t^*_{Pk} and t^*_{Sk} may be calculated. The difference in trial and recorded arrival times between stations i and j denoted as $t_{ij}=t_i-t_j$, the difference in theoretical recorded S-P separations for any station i (t_{SPi} and t^*_{SPi}) and weighting factors for each recorded arrival (w_{pi}, w_{si}) may be used to define a time-difference residual.

$$\tau=\sqrt{\frac{1}{2}\sum_{i=1}^{n}\sum_{j=1}^{n}\left\{w_{p_i}w_{p_j}\left(t_{p_{ij}}-t^*_{p_{ij}}\right)^2+w_{s_i}w_{s_j}\left(t_{s_{ij}}-t^*_{s_{ij}}\right)^2\right\}+\sum_{i=1}^{n}w_{p_i}w_{s_i}\left(t_{SP_i}-t^*_{SP_i}\right)^2} \qquad (1)$$

This form of residual depends only on the geometry of the incoming body wave with terms in the summation affected to various degrees by the azimuth, radial distance and depth of focus. S-P separations were incorporated into the residual to restrain the search to the region surrounding the global minimum; tests with real data showed that in cases where the distribution of arrival times differs from that expeced in simple layered velocity models, the location algorithm tends to search for a best-fit plane wave solution (ie. a solution at infinity).

Since these residuals are solely a function of spatial coordinates, geometric search techniques may be applied to the earthquake location problem. We found that the combination of a geometric search to locate the general area of the global minimum and a modified conjugate gradient search to pinpoint it works satisfactorily. The geometric search consists of evaluating the time-difference residual at the corners and centre of a rectangular volume, selecting the minimum and reconstructing a reduced search volume about this point. The initial volume has dimensions of 100 x 100 x 30 km and the process is repeated until the search volume has contracted to a cube of 0.001 km^3. This generally locates a search point near the global minimum. From this point, a parallel tangents search is initiated to determine a solution. A suitable search cutoff value can be determined by substituting the sum of absolute timing errors for the arrival time differences in equation (1). Origin times are back calculated using the average of the recorded P-wave arrival times less the travel times from focus to the array stations.

This location algorithm was tested using synthetic data (Fig. 2). Two sets of 36 earthquakes at epicentral distances of 20 and 40 km and focal depths of 0-30 km were located by a 10 km wide tripartite array with a constrast in station elevation of 1.0 km. The earthquakes were distributed at 10°intervals on the circles shown in Figure

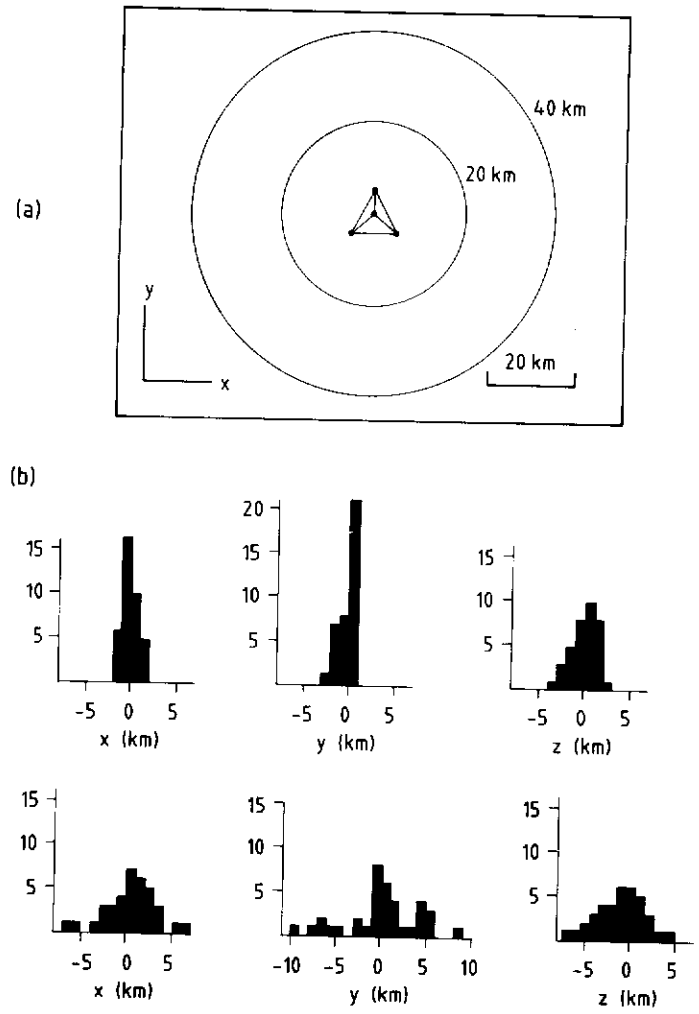

Figure 2. Test of the time-difference residual method using earthquakes in a half-space velocity model and a 10 km wide tripartite array. (a) Array configuration showing coordinate axes (positive z is down). Test earthquakes with epicentres 20 km and 40 km from the centre of the array are located at 10° intervals on the circles. (b) Histograms of error in focal coordinates. Error in focal coordinates for the set of earthquakes 20 km from the centre of the array are shown on the top row and for the set 40 km from the centre of the array on the bottom row.

2(a) and their P and S wave arrival times, rounded to ± 0.01 s, were calculated using a half-space velocity model (V_p=6.0 km/s, V_s= 3.5 km/s). The location algorithm was then tested by locating the earthquakes using the arrival times and velocity model as input. Histograms of error in the determination of focal coordinates are shown in Figure 2(b). This test was performed without the addition of S-P separations into the residual calculation. Such a modification improves convergence behavior when dealing with real arrival times and will probably further reduce the location error; additional tests are being conducted. A plane of symmetry parallel to the yz-plane through the centre of the array accounts for the rapid deterioration in the determination of the y-coordinate with increasing epicentral distance; no such plane of symmetry exists in the field arrays.

The earthquakes detected in this study were located using the velocity model determined by Stephens et al. (1984). This minimized residuals in a limited test data set and is probably the best regional velocity model available. Focal coordinates of earthquakes more than 2 array widths from the centre of the detecting array are considered accurate to ± 5 km while focal coordinates of events nearer the arrays are probably accurate to ± 3 km. A number of events had focal depths restrained to 5.0 km but this did not significantly alter their epicentral coordinates.

RESULTS

Focal coordinates and time-difference residuals of earthquakes detected in this study are tabulated in Table 1 and displayed together with geological structures in Figure 3. Most events are located near the Duke River Fault and structures associated with it. Very little activity was detected near the Totschunda Fault but this may be a consequence of the distance of the arrays from this feature. The Duke River Fault, in the cental portion of the map area, juxtaposes the Mesozoic and older Wrangellia Terrane against the Alexander Terrane and is overlain by deformed calc-alkalic volcanic rocks (Neogene Wrangell Lavas). The Tertiary rocks are most intensely deformed

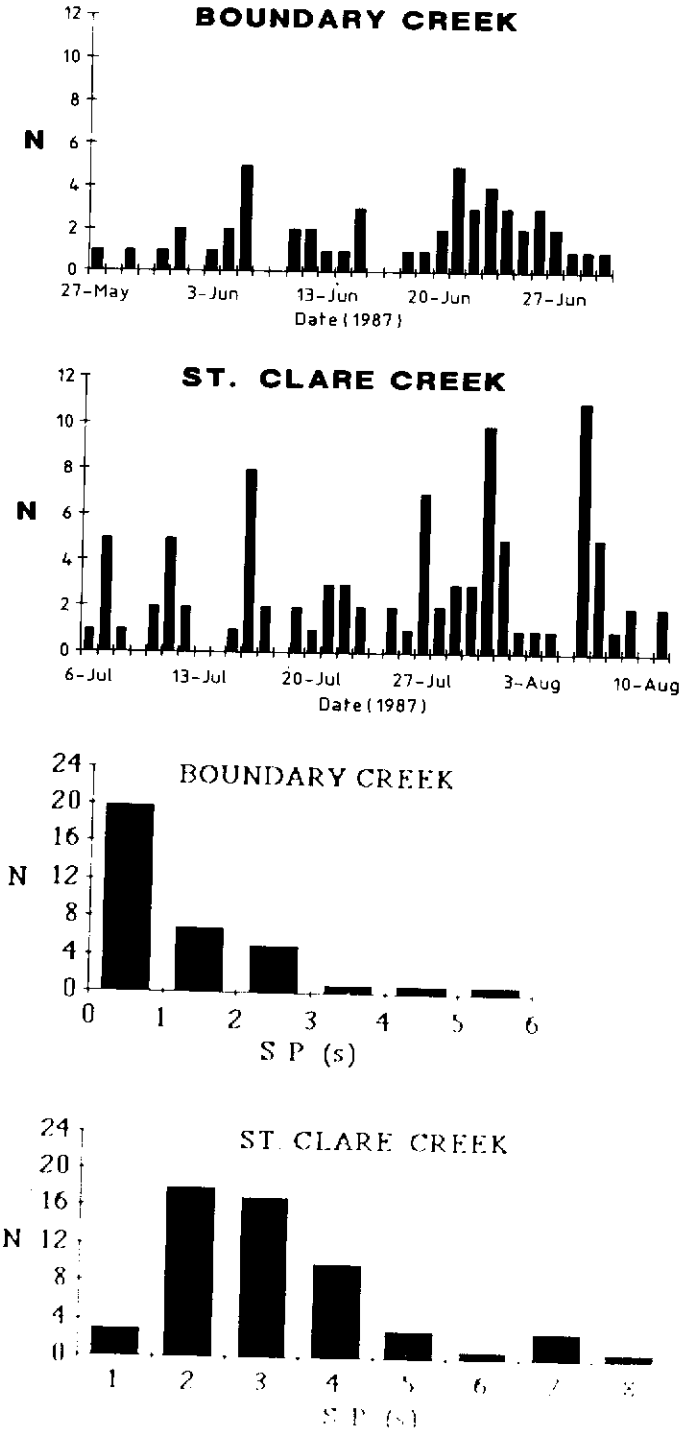

Figure 4. Histograms of S-P separation and daily earthquake frequency. (a) Histograms of S-P separations for unlocated earthquakes are both arrays. N is the number of events. (b) Daily frequency of earthquakes at both arrays. All events are included.

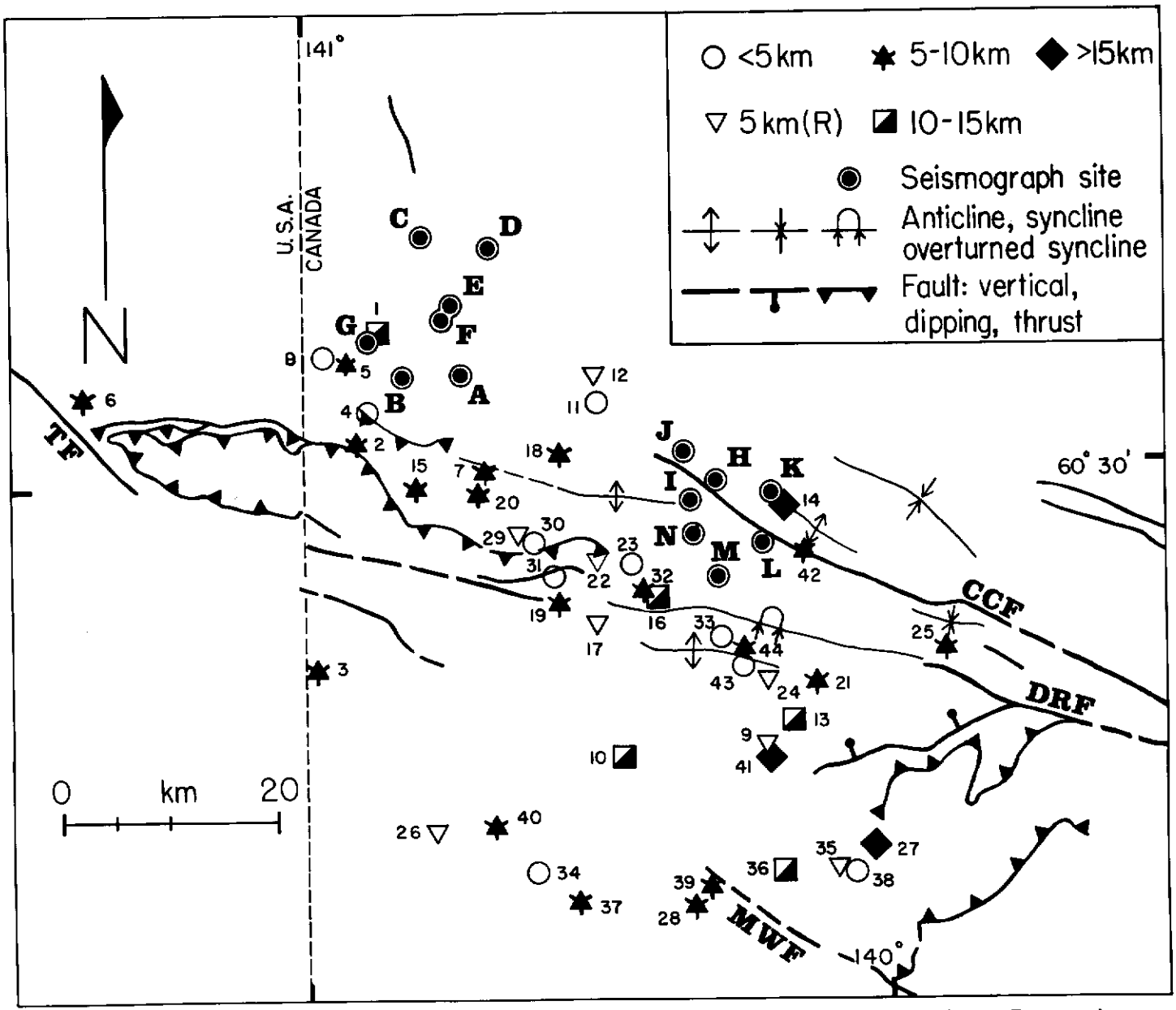

Figure 3. Seismograph sites, microearthquake epicentres coded for focal depth and geological structure in the study area. Event numbers correspond to those in Table 1. Symbols include: TF- Totschunda Fault, DRF- Duke River Fault, CCF- Cement Creek Fault, MWF- Mount Wood Fault. Geology after Campbell and Dodds (1982) and MacKevett (1978).

in a wide zone astride the exposed and buried trace of the Duke River Fault and most of the detected seismicity occurs there.

A number of events are located in the Icefield Ranges, a rugged region south of the Duke River Fault where extensive glaciers limit geological mapping. Ten events on July 31 and August 6, 1987 define a slightly curved band of seismicity which originates near mapped faults south of the Duke River Fault and extends to the west for 40 km, cutting across the inferred trace of the Mt. Wood Fault (Campbell and Dodds 1987). North of the Duke River Fault and its associated structures, a small number of earthquakes were located beneath the Wolverine Plateau and the valley of the White River, a low lying region covered by undisturbed Quaternary surficial deposits.

All but three of the located earthquakes had focal depths less than 15 km. Event 41 was an isolated earthquake detected nearly simultaneously at sites H, J, K and N which yielded a focal depth of 36 km. No deep focus events have been detected in this area by the regional network (R. Horner 1987, personal communication) but earthquakes at this depth have been detected beneath Quaternary volcanoes 100 km west of this site (Stephens et al., 1984).

The paucity of earthquakes north of the Duke River Fault is partially the result of instrument problems encountered during the operation of the Boundary Creek array. Figure 4(a) is a histogram of S-P separations for unlocated events detected at both arrays. The large number of events with S-P separations of 0-1 s recorded at Boundary Creek indicate that significant shallow earthquake activity occurs beneath the valley of the White River. The pattern of S-P separation recorded at the St. Clare Creek array is consistent with the distribution of earthquakes recorded there; most are 10-30 km from the array along the length of the Duke River Fault.

The temporal pattern of earthquakes is characterized by bursts of seismicity (Fig. 4(b)). The sequences recorded on July 31 and August 6, 1987 define the 40 km long trend of seismicity beneath the Icefield Ranges and occurred between 09:11 and 09:16 hrs (UTC) on July 31 and between 14:14 and 14:29 hrs on August 6, 1987. During July and August episodes of increased activity recurred every 4-6 days.

The epicentral distributions and geological structure suggest that the study area can be subdivided into 3 domains (Fig. 5): (1) the northern domain, centered on the Wolverine Plateau and the valley of the White River and characterized by relatively shallow seismicity, (2) the central domain straddling the Duke River Fault and its

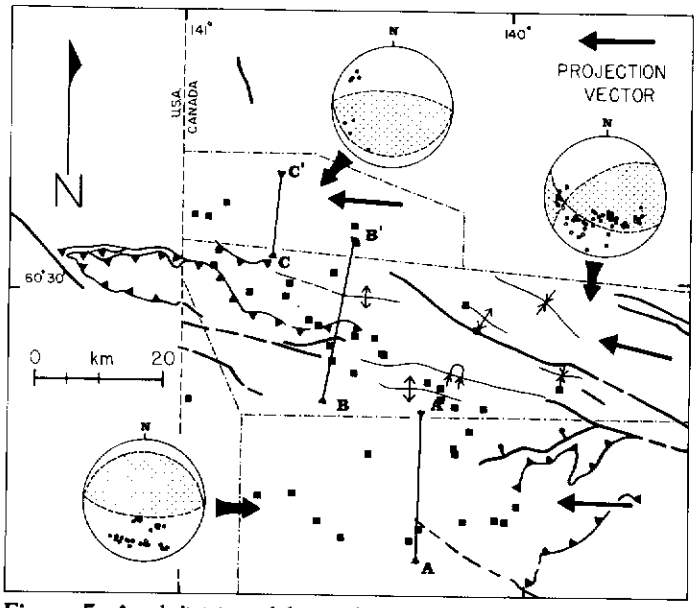

Figure 5. A subdivision of the study area based on microseismicity and geological structure. A-A', B-B' and C-C' are the traces of vertical projection planes in the south, central and north microseismicity zones. Focii are projected into the projection planes along the horizontal vectors shown in each domain. Equal area projections of first motions prepared using events with focal depths less than 15 km show compressions as filled circles and compressional quadrants with stippling.

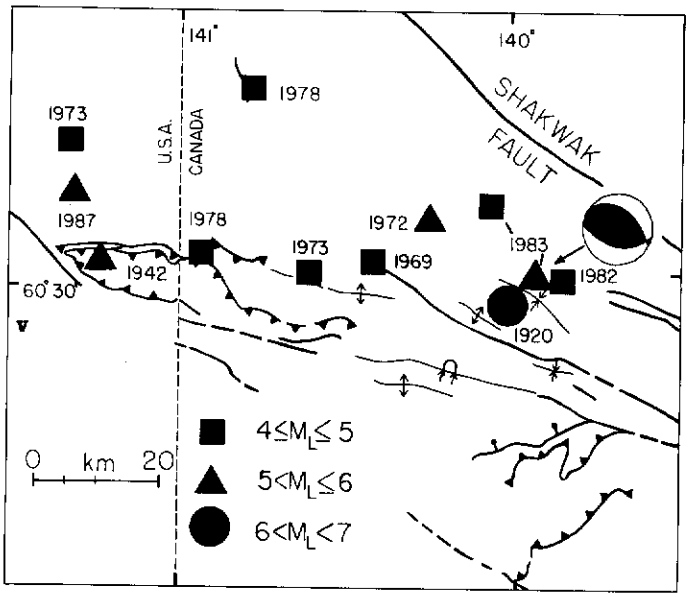

Figure 7. Epicentres of earthquake with local magnitudes greater than 4.0 from the Canadian Earthquake Catalogue.

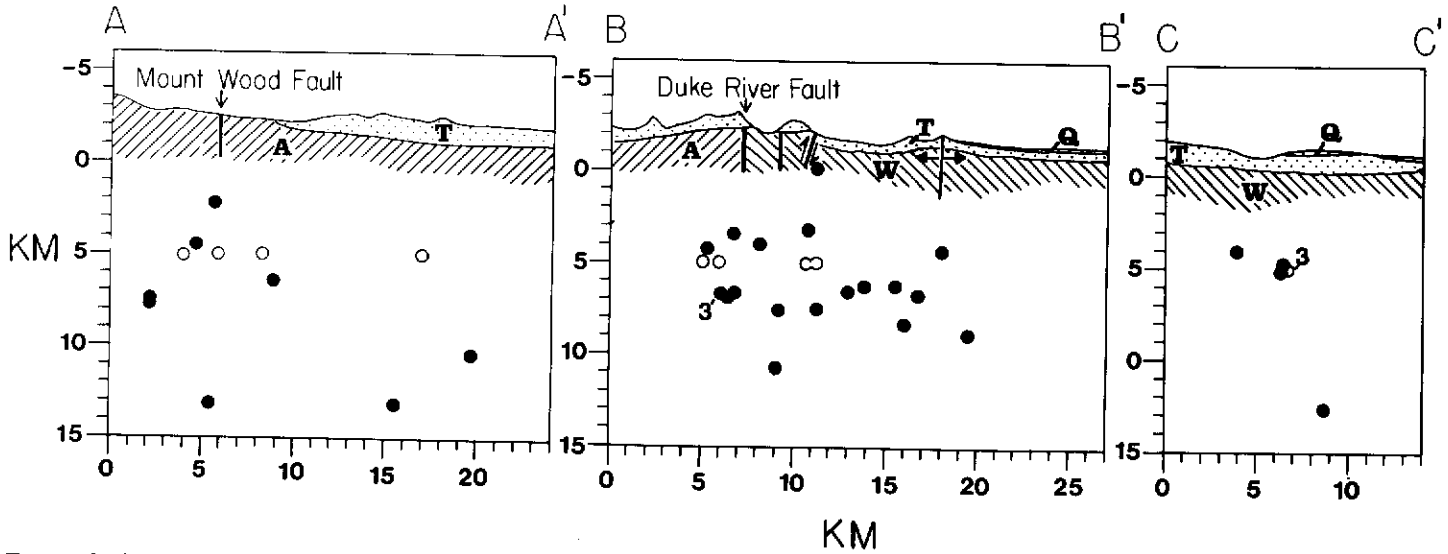

Figure 6. Cross-sections showing projections of earthquake focii into the planes of section together with the structural geology along the line of section. Lines of section correspond to those in Figure 5 and open circles designate earthquakes restricted to focal depths of 5.0 km. A- Alexander Terrane W- Wrangellia Terrane, T- Tertiary cover rocks (Wrangell Lavas), Q- Quarternary surficial deposits.

associated structures and (3) the southern domain, centered on the Icefield Ranges.

Axial traces of major faults and folds are essentially parallel in the central domain, suggesting that the relationship between earthquake focii and geological structures may be clarified by projecting hypocentres up or down a vector parallel to the structural trend. This procedure was performed using TRIPOD (Charlesworth et al., 1987) for focii in all 3 domains, horizontal projection vectors parallel to the mountain front separating the north and central domains in the north domain, the mean structural trend in the central domain, and the mean trend of the July 31/August 6, 1987 earthquake sequence in the south domain. Lines of section and projection vectors are indicated in Figure 5 and the sections are shown in Figure 6. The trend of the projection vector in the central domain could arguably be varied by ± 5° but the distribution of focii would not be seriously altered since most are near the projection plane.

No conclusive results can be inferred from projections in the north and south domains; the association between earthquake focii and the Mt. Wood Fault is coincidental. In the central domain, seismicity is concentrated beneath the Duke River Fault and structures north of it in a zone approximately 15 km wide. Earthquakes in this domain are well located and the distribution of focii suggests a complex zone of disruption rather than a single fault or set of discrete faults in the subsurface.

Equal-area projections of the first motions and preferred composite focal plane solutions for the three domains are shown in Figure 5. Solutions involving pure strike or dip slip may be constructed for data in the north domain; the arbitrary solution shown was con-

structed by restraining the strike of nodal planes to the trend of the mountain front separating the north and central domains. First motions from 21 earthquakes in the central domain constrain a unique solution with oblique thrusting along either 147° 30° (hanging wall up) or 25° 40° (hanging wall up). Eight of the 50 first motions are inconsistent with this solution but 6 of these are very close to the focal planes and are thus probably subject to reading errors. The southwest-dipping nodal plane conains the first of the two displacement vectors, strikes parallel to the trace of Cement Creek Fault (Skulski and Francis 1986) and the axial traces of a number of minor folds associated with it, and seems to be the most probable slip plane. Antithetic faulting are common in the map area although a splay from the Duke River Fault 10 km west of site M seems appropriately oriented. Thus slip on the other nodal plane cannot be ruled out. In the south domain, the first motion pattern is more complex with 7 compressions evenly distributed amongst 23 dilatations. The dominant first motion is dilatational and the preferred solution was constructed by setting the strike of the nodal planes parallel to the trend of the July 31, 1987 and August 6, 1987 earthquake sequences. This solution is non-unique but other solutions involving substantial components of strike slip will produce nodal planes which are oblique to the traces of mapped faults and to the trend of the earthquake sequences. This suggests that oblique thrusting or reverse faulting probably is occurring here. Campbell and Dodds (1982) have mapped a fault with unspecified displacement dipping steeply to the north and a thrust fault cutting a small pocket of Wrangell Lavas in the northeast corner of this domain. The orientation and vergence of these two faults suggests that any current displacement will be to the south.

THE HISTORICAL RECORD

Figure 7 shows the distribution of earthquakes, with local (Richter) magnitudes greater than 4.0 in the Canadian Earthquake Catalogue, superimposed on the geological structure in the study area. Horner (1983) stated that earthquakes occurring prior to 1965 are probably located to ± 50 km whereas more recent events are considered accurate to ± 25 km. Complete coverage down to magnitude 5.0 and 4.0 dates from the 1950's and 1971. Despite limitations in the historical record, the prevalence of moderate earthquakes north of the Duke River Fault and the absence of seismicity on the Shakwak Fault north of its divergence from the Duke River Fault are apparent. Even if the 1920 earthquake occurred on the Shakwak Fault, the complete record indicates relative quiescence on this feature (see Fig. 1(b)). The pattern of moderate earthquake seismicity on the Duke River Fault resembles the pattern of microseismicity; most activity is confined to the area immediately north of the Duke River Fault with some earthquakes of moderate magnitude occurring beneath the Wolverine Plateau and the valley of the White River. A catalogue of focal plane solutions for these earthquakes would be useful. A solution prepared by Alaskan Geophysical Institute for the 1983 M_L = 5.0 earthquake beneath the Wolverine Plateau indicated thrust faulting along a southwest dipping nodal plane (Alaska Geophysical Institute 1984). Given the absence of any vertical faults in the north domain, the prevalence of compressional features in the central zone and the transpressional nature of the regional tectonic setting, oblique thrusting is probably the most prevalent failure mechanism.

POSSIBLE EVIDENCE FOR HOLOCENE TECTONISM

No geomorphological evidence of Holocene displacement on the Duke River Fault or any of its subsidiary faults is evident in airphotographs (Clague 1979), while up to 146 m of dominantly right-lateral displacment has occurred on the Totschunda Fault (Plafker et al., 1977). Till and alluvial deposits adjacent to the Cement Creek (near site H - Fig. 3) dated as "Pliocene and (?) Pleistocene" by Campbell and Dodds (1982) show evidence of tectonic disturbance (C. Dodds 1987, personal communications, Souther and Stanciu 1976). Where exposed at Bull Creek, the succession is uniformly tilted 20° to the southwest (Figure 8). These deposits appear to be Late Wisconsin (S. Morison 1987), personal communication) and thus are essentially part of a blanket of Quaternary surficial deposits covering most of the low lying area north of the Duke River Fault. Tilting does not seem to have resulted from glacial tectonism; the section at Bull Creek shows no evidence of internal disruption in a 400 m section extending from the valley floor to the top of the adjacent ridge.

CONCLUSIONS

Microearthquake activity near the Duke River Fault defines 3

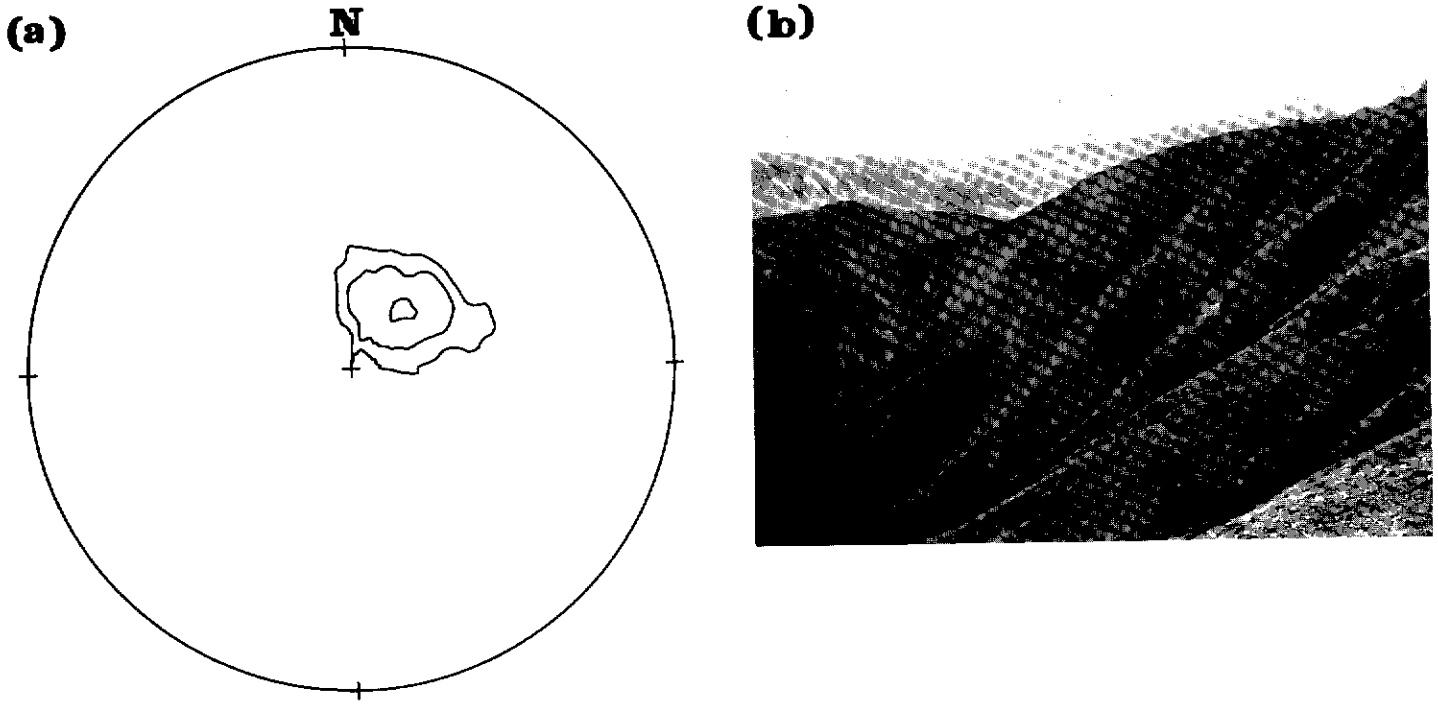

Figure 8. Tectonically disturbed tills and fluvial deposits at Bull Creek. (a) Equal area projection of poles to bedding measured from the base to the top of the exposed section. Contours denote 5% 20% and 50% of 28 poles in a 1% counting circle. The mean pole to bedding (first eigenvalue of the distribution of orientations) is 38.7° 70.1°. (b) Photograph of the uppermost part of the till unit 200 m north of site H.

zones of seismicity which are related to known structures and the pattern of moderate earthquake epicentres. Most seismicity occurs in a central zone straddling the Duke River Fault and structures north of it. The complex pattern of focii observed in projections parallel to the trend of the local structure suggests that a wide zone of faulting exists beneath structures in the deformed Tertiary cover. Shallow seismicity occurs beneath low lying areas north of the Duke River and Cement Creek faults and a number of moderate earthquakes have been reliably located in this zone. A southern zone, centered on the Icefield Ranges, is characterized by a low level of microseismicity, by crustal shortening along high angle reverse faults or thrust faults and by an absence of moderate earthquake activity. The July 31 and August 6, 1987 earthquake sequences appear to have resulted from failure along a single discrete structure; the two bursts of seismicity (3 events in 5 minutes on July 31 and 7 events in 15 minutes on August 6, 1987) define a simple curved trend originating near the traces of known faults. First motions and the trend of the structure in relation to the local stress field strongly suggest that it is either a thrust fault or high angle reverse fault. Both possibilities are consistent with faults observed on the eastern end of the trend.

Microearthquake activity in the central zone constrains a focal plane solution consistent with local structure and the regional tectonic setting. Displacement on the Totschunda Fault is dominantly horizontal and its mean trend (-140°) differs by approximately 7° from that of the displacement vector in the central zone (147°). The trend of the central zone displacement vector and the mean trend of the Duke River Fault (-285°) differ by approximately 42° suggesting that nearly equal components of dextral displacement and crustal shortening characterize the local tectonic regime. The overall pattern of earthquake activity suggests that the deformation front has migrated north from the Duke River Fault. Tilted surfical deposits at Bull Creek may provide evidence of Holocene tectonism but this hinges on definitive dating. Holocene compression and the concomitant folding or thrust faulting of strata north of the Duke River Fault are consistent with the observed pattern of microseismicity and moderate earthquake activity in this area.

Recent models for Holocene tectonics in the Gulf of Alaska involve a connecting transform fault between the Totschunda and Fairweather faults through the St. Elias Mountains (eg. Lahr and Plafker 1980, Richter and Matson 1971). The data summarized in this report suggest that no such connection exists; faulting in the southern zone cuts across the inferred trend of this transform at a high angle, no microearthquake activity was observed at the southern end of the Totschunda Fault and no firm evidence of such a connecting fault exists in the regional record of epicentres (Figure 1(b)). The discrepancy between displacements on the Duke River and Totschunda segments of the Denali Fault System may be resolved if large, predominantly dextral strike-slip displacements on the Totschunda Fault and small oblique displacements along faults in a wide zone parallel to the Duke River Fault are equivalent.

ACKNOWLEDGMENTS

This work was supported by grants from the Boreal Institute for Northern Studies, by logistical support from the Exploration and Geological Services Division of Indian and Northern Affairs Canada in Whitehorse, Y.T. and by funds from the Natural Sciences and Engineering Research Council. Drs. R. Ellis (University of British Columbia) and D. Bingham (Alberta Environment) are thanked for generously loaning seismographs and ancillary equipment to the field party. The author profited from discussions with R. Horner, C. Dodds, P. Erdmer and L. Tober. E. Nyland advised the author throughout this work and reviewed this paper. The author extends special thanks to Wilf Kruggel for his capable and cheerful assistance in the field.

REFERENCES

BOUCHER, G. and FITCH, T.J., 1969. Microearthquake seismicity of the Denali Fault; Journal of Geophysical Research, Vol. 74, p. 638-6648.

CAMPBELL, R.B. and DODDS, C.J., 1978. Operation Saint Elias, Yukon Territory; Geological Survey of Canada, Paper 78-1A, p. 35-41.

CAMPBELL, R.B. and DODDS, C.J., 1982. S.W. Kluane Lake Map Area (115 G and F (E 1/2); Geological Survey of Canada; Open File 829.

CAMPBELL, R.B. and DODDS, C.J., 1987. Structural elements, terrane distributions and cover rock sequences, Saint Elias Mountains (unpublished).

CLAGUE, J.J., 1979. The Denali Fault System southwest Yukon Territory - A geologic hazard; in Geological Survey of Canada, Paper 79-1A, p. 169-178.

CHARLESWORTH, H.A.K., GOLD, C., WYNNE, D. and GUIDOS, J., 1987. TRIPOD 2.1, A microcomputer-based system for collecting, storing, retrieving and processing structural, stratigraphic and positional data from outcrops and drillholes; University of Alberta, Edmonton: Department of Geology, 70 p.

GEOPHYSICAL INSTITUTE OF ALASKA - FAIRBANKS, 1984. Biennial report 1983-84.

HORNER, R., 1983. Seismicity in the St. Elias region of northwestern Canada and southeastern Alaska; Bulletin of the Seismological Society of America, Vol. 73, No. 4, p. 1117-1137.

LAHR, J.C. and PLAFKER, G., 1980. Holocene Pacific-North American plate interactions in southern Alaska: implications for the Yakataga Seismic Gap; Geology Vol. 8, p. 483-486.

LEE, W.K.H. and STEWART, S.W., 1981. Principles and applications of microearthquake networks; Advances in Geophysics, Supplement 2, Academic Press.

MACKEVETT, E.M.Jr., 1978. Geologic map of the McCarthy quadrangle; United States Geological Survey, Miscellaneous Inventory Series, Map I-1032.

PLAFKER, G., HUDSON, T. and RICHTER, D.H., 1977. Preliminary observations on late Cenozoic displacements along the Totschunda and Denali Fault Systems; United States Geological Survey, Circular 733, p. 67-69.

PLAFKER, G., HUDSON, T. and BRUNS, T., 1978. Late Quaternary offsets along the Fairweather Fault and crustal plate interactions in southern Alaska; Canadian Journal of Earth Sciences, Vol. 15, p. 805-816.

POWER, M.A., 1988. Seismicity and neotectonics of the Duke River Fault, Yukon Territory; Unpublished M.Sc. Thesis, University of Alberta, (in prep.).

RICHTER, D.H. and MATSON, N.A.Jr., 1971. Quaternary faulting in the Eastern Alaska Range; Geological Society of America Bulletin, Vol. 82, p. 1529-1540.

SKULSKI, T. and FRANCIS, D., 1986. On the geology of the Tertiary Wrangell Lavas in the St. Clare Province, St. Elias Mountains, Yukon Territory; Yukon Geology 1984, Vol. I, p. 161-170.

STEPHENS, C.D., FOGLEMAN, K.A., LAHR, J.C. and PAGE, R.A., 1984. Wrangell Benioff zone, southern Alaska, Geology Vol. 12, No. 6, p. 373-376.

Table 1. Microearthquake coordinates and residuals.

Event	Date	Time (UTC)	UTM	X (km)	Y (km)	Z (km)	Residual	n-m
1	June 7, 1987	10:19:56.7	EU	6.86	31.56	12.69	0.00	0
2	June 12, 1987	13:04:27.9	EU	4.95	21.62	6.21	1.56	2
3	June 12, 1987	18:04:58.9	EU	1.16	0.60	7.91	1.18	1
4	June 25, 1987	00:38:40.5	EU	5.70	24.00	4.33	0.55	1
5	June 25, 1987	16:35:08.7	EU	4.09	29.4	5.24	1.10	1
6	June 29, 1987	09:08:37.9	DU 79.61	25.85	8.06	0.63	0	
7	June 30, 1987	09:01:26.3	EU	16.86	18.93	8.32	0.04	0
8	June 31, 1987	18:11:39.7	EU	1.98	29.69	4.81	0.59	3
9	July 17, 1987	01:58:52.6	ET	42.87	93.25	5.00(R)	1.62	2
10	July 21, 1987	05:06:45.0	ET	29.53	92.25	13.15	1.82	2
11	July 22, 1987	12:00:08.8	EU	27.35	25.36	4.10	0.75	2
12	July 22, 1987	12:01:49.5	EU	27.06	28.10	5.00(R)	0.74	2
13	July 27, 1987	08:06:44.7	ET	45.40	95.84	10.43	0.82	2
14	July 27, 1987	08:11:15.8	EU	44.62	15.76	20.72	0.57	1
15	July 27, 1987	10:22:06.5	EU	10.59	17.47	6.55	1.44	1
16	July 27, 1987	23:31:36.8	EU	31.95	7.71	10.73	0.50	1
17	July 28, 1987	14:48:10.2	EU	27.17	4.89	5.00(R)	0.59	1
18	July 29, 1987	12:04:02.0	EU	23.82	20.63	8.89	0.74	1
19	July 29, 1987	17:40:45.6	EU	23.72	6.80	6.69	0.25	2
20	July 29, 1987	23:19:35.8	EU	16.25	16.88	6.25	0.30	0
21	July 30, 1987	18:14:49.3	ET	47.58	99.45	6.58	1.89	3
22	July 30, 1987	18:15:25.2	EU	27.28	10.65	5.00(R)	0.86	1
23	July 30, 1987	23:38:29.4	EU	30.41	10.37	-0.31	1.10	1
24	July 31, 1987	08:34:57.0	ET	43.01	99.71	500(R)	0.38	1
25	July 31, 1987	09:10:33.8	EU	59.58	2.60	7.50	3.20	3
26	July 31, 1987	09:11:35.7	ET	12.20	85.6	5.00(R)	1.10	1
27	July 31, 1987	09:12:21.9	ET	52.88	84.09	17.31	0.51	1
28	July 31, 1987	09:16:09.9	ET	36.06	78.62	7.75	1.15	2
29	July 31, 1987	13:09:50.5	EU	19.92	13.17	5.00(R)	1.11	2
30	August 1, 1987	15:53:57.7	EU	21.44	12.29	3.21	0.67	1
31	August 1, 1987	15:24:39.8	EU	23.38	9.08	4.00	1.14	1
32	August 1, 1987	18:58:39.5	EU	31.56	7.94	7.56	0.24	0
33	August 2, 1987	03:13:08.2	EU	38.72	3.50	3.45	0.59	1
34	August 6, 1987	14:14:39.4	ET	21.51	81.64	4.47	0.59	2
35	August 6, 1987	14:15:01.5	ET	49.49	81.90	5.00(R)	0.24	1
36	August 6, 1987	14:15:40.7	ET	44.44	81.64	13.14	1.30	1
37	August 6, 1987	14:16:05.8	ET	25.34	79.02	7.42	0.85	2
38	August 6, 1987	14:16:34.9	ET	51.09	81.64	2.23	0.88	1
39	August 6, 1987	14:17:58.7	ET	37.51	80.4	5.07	0.96	2
40	August 6, 1987	14:29:41.1	ET	17.59	85.99	6.40	2.80	2
41	August 7, 1987	09:39:20.3	ET	43.17	92.34	36.64	0.96	2
42	August 7, 1987	21:07:16.8	EU	46.49	11.77	6.73	1.51	2
43	August 11, 1987	05:23:36.1	EU	40.73	0.81	4.26	0.86	1
44	August 12, 1987	05:47:12.2	EU	40.8	2.61	6.89	0.51	1

BIMODAL VOLCANISM ALONG THE TINTINA TRENCH, NEAR FARO AND ROSS RIVER

Monica J. Pride

PRIDE, M.J., 1988. Bimodal volcanism along the Tintina Trench near Faro and Ross River: in Yukon Geology, Vol. 2; Exploration and Geological Services Division, Yukon, Indian and Northern Affairs Canada, p. 69 - 80

ABSTRACT

Bimodal Tertiary volcanic rocks are exposed along the Tintina Trench in central Yukon in the Glenlyon, Grew Creek, and Ketza areas. Basalt and rhyolite are interbedded with coarse sedimentary rocks and preserved in grabens. The basalt forms both subaqueous and subaerial flows, hydrovolcaniclastic, pyroclastic, and autoclastic deposits. Rhyolite forms intrusions, lava flows, and volcaniclastic deposits. The volcanic and sedimentary rocks probably formed in a series of extensional basins whose original size and shape is yet to be determined. At Grew Creek, gold-bearing chalcedony veinlets and associated argillic alteration are near rhyolite dykes. In the Glenlyon Area, quartz, chalcedony, and fluorite veins and associated silicification are in and near rhyolite dykes.

RÉSUMÉ

Des roches volcaniques tertiaires de caractère bimodal affleurent le long de la fosse de Tintina dans la partie centrale du Yukon, dans les régions de Glenlyon, de Grew Creek et de Ketza. Les basaltes et rhyolites sont interstratifiés avec des roches sédimentaires grossières et conservés dans des grabens. Le basalte forme à la fois des coulées subaquatiques et subaériennes, des dépôts volcanoclastiques sous-marins, et des dépôts pyroclastiques et autoclastiques. Les rhyolites forment des intrusions, des coulées de laves et des dépôts volcanoclastiques. Les roches volcaniques sédimentaires se sont probablement formées dans une série de bassins en expansion, dont la dimension et la configuration originelles restent encore à déterminer. A l'emplacement de Grew Creek, on observe à proximité de dykes rhyolitiques des veinules aurifères de calcédoine, et une altération argilique associée à ces veinules. Dans la région de Glenlyon, il existe à l'intérieur et près de dykes rhyolitiques des filons de quartz, de calcédoine et de fluorine, et l'on observe une silicification associée à ceux-ci.

INTRODUCTION

This report examines the volcanofacies of the Tertiary volcanic rocks in Tintina Trench and their relationship to epithermal precious metal mineralization. Interest in these rocks was spurred by the discovery of the Grew Creek epithermal gold silver prospect, 1 km west of the Robert Campbell Highway halfway between the communities of Ross River and Faro, in south-central Yukon. The Grew Creek property is the first reported Tertiary volcanic-hosted epithermal gold-silver showing in Tintina Trench.

The Tintina volcanics comprise basalt and rhyolite that are interbedded with coarse clastic sedimentary rocks, and preserved in grabens along the Tintina Trench. This report describes three areas of volcanic rocks: Glenlyon, Grew Creek and Ketza River (Fig. 1). The trench is characterized by a dense cover of forest, brush and bog and a thick blanket of glacial and fluvial deposits. Rock distribution is complicated by strike-slip and dip-slip faults along the Tintina Fault Zone that moved during and subsequent to volcanic activity. The poor outcrop exposure and complex tectonic setting obscure stratigraphic relations within the volcanic piles.

Field work was undertaken during a two month period in the summer of 1986 with local geological mapping at a scale of 1:30 000. Eighty samples were chosen for petrographic study; 40 of those were selected for geochemical analysis. Geochemical analyses using x-ray fluorescence were done by X-ray Assay Laboratories, Don Mills, Ontario. Fifteen samples of vein material were analysed for 26 trace elements (including gold and silver) by Bondar Clegg, Whitehorse, Yukon.

ACKNOWLEDGEMENTS

This project was funded by Exploration and Geological Services Division of the Northern Affairs Program in Whitehorse, Yukon Territory, under the supervision of Chief Geologist J.A. Morin. The writer extends special thanks to Robert Stroshein of Hudson Bay Exploration and Development Company Ltd for a tour of the Grew Creek property, as well as allowing access to Hudson Bay's geological maps of the Grew Creek area. I would also like to thank Craig Hart of Noranda for information and maps on the Glenlyon area. Lastly I thank very much Teresa Potter and Bill LeBarge for their excellent field support.

PREVIOUS WORK

Volcanic rocks along Tintina Trench were first recognized by J.R. Johnson (1936), who assigned a tentative Tertiary age to them. He described them as comprising rhyolite, dacite, trachyte, andesite and basalt with associated conglomerate. The area covers parts of three 1:250 000 scale map sheets and reconnaissance geological mapping was done at various times: Wheeler et al (1960) mapped Quiet Lake map area (105 F), Roddick and Green (1961) mapped Tay River map area (105 K) and Campbell (1967) mapped Glenlyon

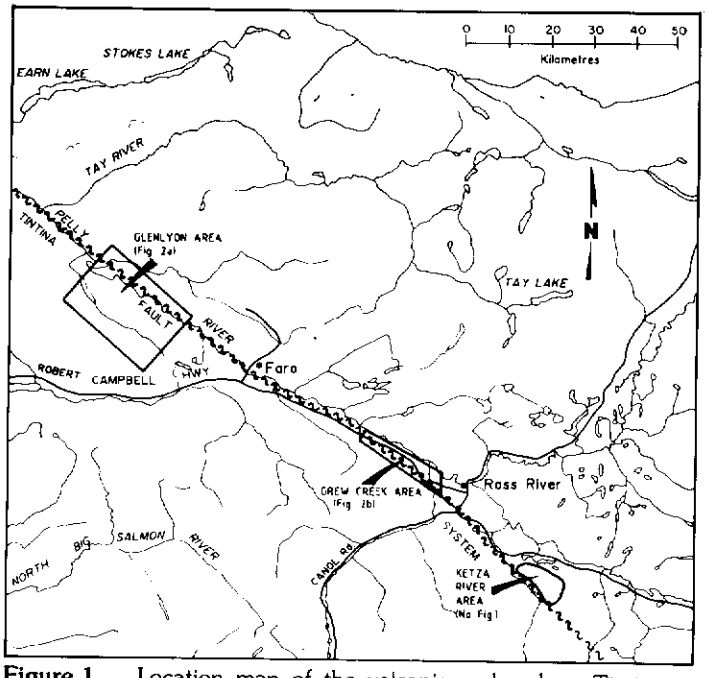

Figure 1. Location map of the volcanic rocks along Tintina Trench.

map area (105 L). Tempelman-Kluit (1972) mapped part of the Tay River map area at a scale of 1:125 000, and in 1977, published an open file report on the Quiet Lake map area. S. Gordey (1988) updated Tay River map area.

In 1983, Mr Al Carlos of Whitehorse discovered the Grew Creek gold deposit. Hudson Bay Exploration and Development Company Ltd optioned the property and in 1984, 1985 and 1986, explored with trenching, diamond drilling, geochemical sampling and geophysics. The discovery led to increased interest in the volcanic rocks along the trench and the staking of claims in the Glenlyon area. Duke and Godwin (1986) undertook a detailed study of the geology and alteration of the Grew Creek deposit and obtained an Eocene radiometric age for the volcanic rocks.

TECTONIC SETTING

The tectonic setting for the Tintina volcanics is complex. Presumably they relate to strike slip movement along the Tintina Fault Zone. Late Cretaceous or Early Tertiary right lateral movement along Tintina Fault amounted to at least 450 km (Roddick, 1967, Tempelman-Kluit, 1979, and Gabrielse, 1985) and juxtaposed Cambrian and Ordovician slates and phyllites of the Pelly Cassiar Platform on the southwest against rocks of the Anvil allochthon on the northeast (Gordey, 1983). The Tintina Trench follows the Tintina Fault Zone and is a physiographic feature that formed by normal faulting in Pliocene time (Tempelman-Kluit, 1980).

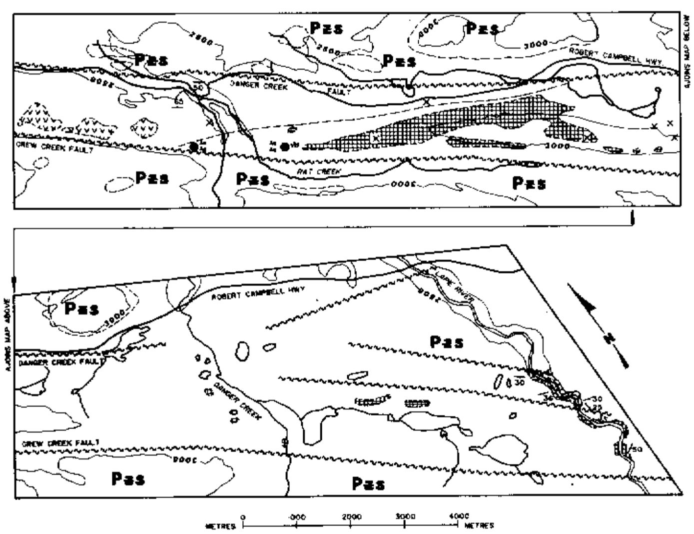

Figure 2a. Geological map of the Grew Creek area.

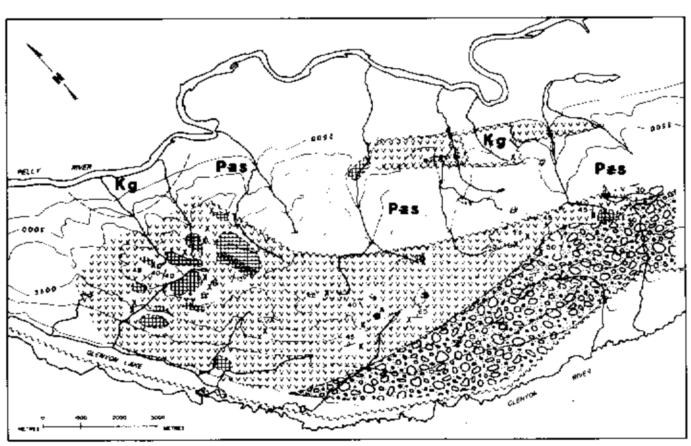

Figure 2b. Geological map of the Glenlyon area.

GEOLOGY

Volcanic rocks in the Tintina Trench include basalt, rhyolite and rare andesite interbedded with coarse clastic sedimentary rocks. The rocks are preserved in elongate, internally faulted grabens (Fig. 2a, b). Extensive faulting and lack of continuous outcrop preclude stratigraphic correlations, but the isolated outcrops still provide information on the type of volcanism. The morphology and petrography of basalt, rhyolite and clastic sediments, are described here. Table 1 summarizes the different characteristics observed in the three areas studied.

BASALT

The basalts comprise subaqueous to subaerial lava flows, intrusions and volcaniclastic rocks. Most exposures are poorly preserved, massive to partly brecciated, altered, fractured and faulted, and contain few or diagnostic morphological features. Basaltic lava flows are the most abundant lithology and locally fill U-shaped valleys (Fig. 3) or are stacked and in places interbedded with clastic sediments and basaltic volcaniclastic rocks (Fig. 4). The flows vary in thickness and are either subaqueous and pillowed (Fig. 5a, b) or subaerial. The latter are massive, columnar jointed, blocky with brecciated and vesicular tops, rarer hyaloclastic basal contacts, and occassional pipe vesicles (Fig. 6).

The textures indicate hydrovolcaniclastic, pyroclastic and autoclastic depositional processes. Two distinct types of hydrovolcaniclastic deposits were observed. The first, found along Grew Creek, is a relatively thick sequence of plane parallel beds and laminae that are commonly subtly cross bedded or lenticular over short distances (Fig. 7a, b). Beds are graded, moderately to poorly sorted, have erosional to gradational contacts and are locally disrupted by soft sediment deformation. They contain approximately

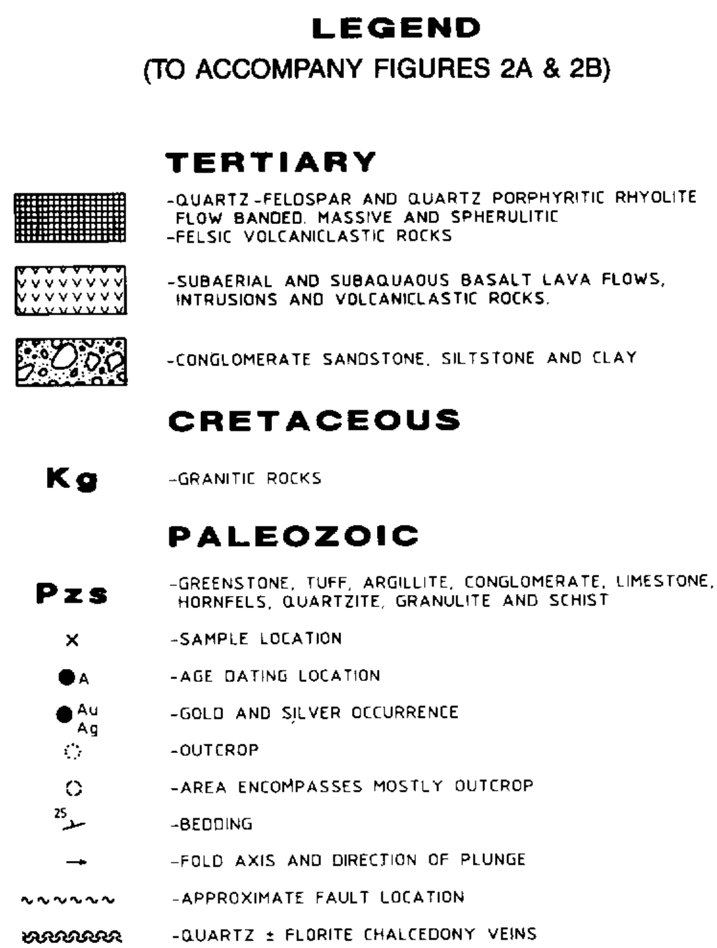

Figure 3. Ketza River area: a columnar jointed basaltic lava flow filling a broad channel.

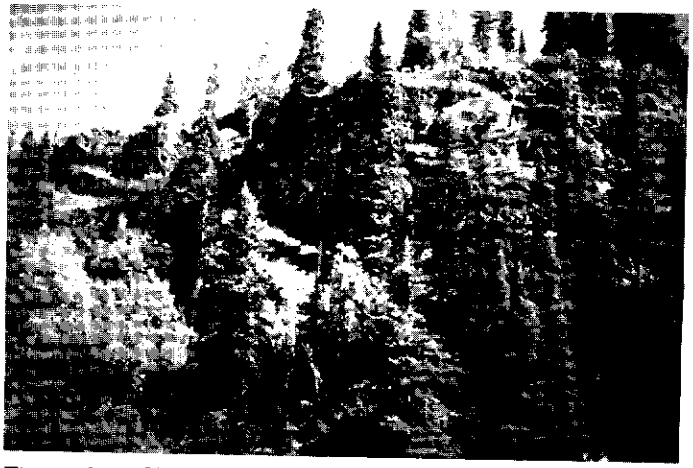

Figure 4. Glenlyon area: a series of stacked subhorizontal basaltic lava flows.

Figure 5a. Ketza River area: photograph of subhorizontal basaltic lava flows interbedded with bedded to laminated basaltic tuff.

Figure 5b. The base of the lava flow above yellow-weathering tuff. The lava presumably flowed into a small lake, forming pillows.(Fig. 5b).

five percent subangular, mostly nonvesicular blocks that are associated with bedding sags in places. Beds comprise mostly basaltic nonvesicular to vesicular, tuff and lapilli size fragments, quartz and feldspar crystals with subordinate accidental fragments, carbonized plant fragments and occasional beds rich in accretionary lapilli. Void spaces are filled with calcite. Although outcrop is limited, this sequence of finely bedded rocks resembles descriptions of base surge deposits in maar volcanoes.

The second type of hydrovolcaniclastic deposit outcrops in the Ketza River area and comprises a relatively thick sequence of one to three meter thick, poorly sorted beds (Fig. 8a). Beds contain variable amounts of subangular, nonvesicular to vesicular blocks and rounded bombs; the bombs are cut by radial cooling joints (Fig. 8b). Blocks and bombs are set in a groundmass of equant, lapilli size, angular, vesicle-free sideromelane shards that are cut by a mosaic of cracks. Void spaces within the breccia are filled with secondary zeolites and minor calcite and quartz. This description resembles the deposits of a littoral cone (Fisher and Schminke, 1984).

Isolated pillow breccias are exposed in one outcrop in the central part of the Glenlyon area. Poorly sorted lapilli size breccia with no observable bedding locally contains about ten percent isolated pillows in a finer equant, angular nonvesicular lapilli-size matrix (Fig. 9). Pillows are slightly vesicular, rounded and have chilled margins. The exact origin of the breccia is unknown. They may have formed by autoclastic processes or secondary processes such as slumping.

Plane parallel beds and laminae of lapilli tuff and tuff are interbedded with pillowed lava flows in the Ketza River area (Fig. 5). Beds and laminae are slightly wavy, lenticular, graded and moderately

Figure 6. Glenlyon area: well developed pipe vesicles in a basaltic lava flow.

to poorly sorted. Some beds comprise well preserved rod-shaped to triangular slightly concave shards, and are interpreted as pyroclastic. These beds probably represent slightly reworked waterlain, airfall and surge deposits.

Poorly sorted heterolithic breccia containing variable amounts of accidental fragments are common in Glenlyon and Grew Creek areas (Fig. 10). These outcrops contain anomalously large boulders

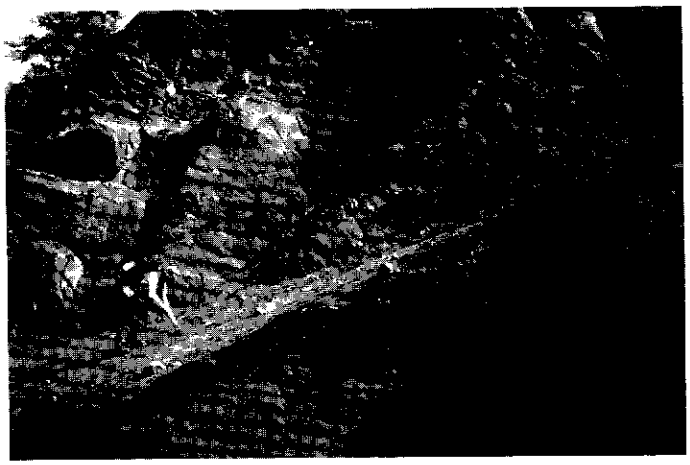

Figure 7a. Grew Creek area: photograph of the bedded and laminated hydro- volcaniclastic deposit. Bedding is near vertical and runs approximately right to left across the photograph. Note the large fragments scattered throughout the outcrop.

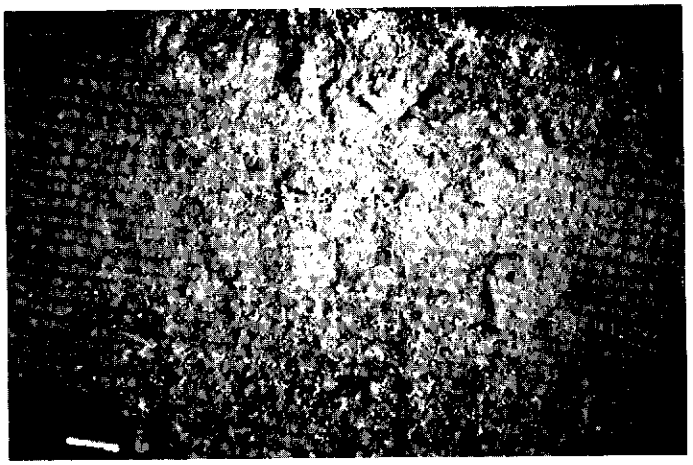

Figure 7b. Grew Creek area: photograph of the bedding in Figure 7a. Note the beds are subtly cross bedded on the upper right hand side of the photograph.

Figure 8a. Ketza River area: photograph of a hyaloclastic bed. The bed is poorly sorted, contains approximately 20% blocks and bombs that are mostly nonvesicular. Matrix comprises lapilli size, equant altered basaltic glass shards that are cut by a mosaic of cracks.

Figure 8b. Ketza River area: photograph of a bomb in a hyaloclastite bed. Note the chilled margin and the radial cooling joints.

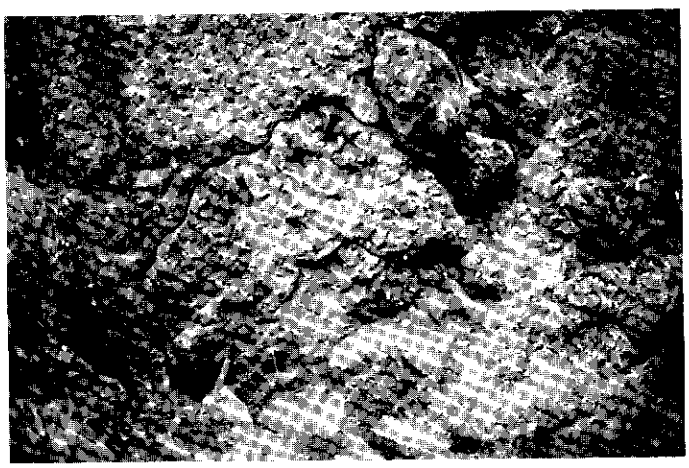

Figure 9. Glenlyon area: a photograph of a hyaloclastite deposit that contains variable amounts of isolated pillows in a groundmass of equant basaltic altered glass shards.

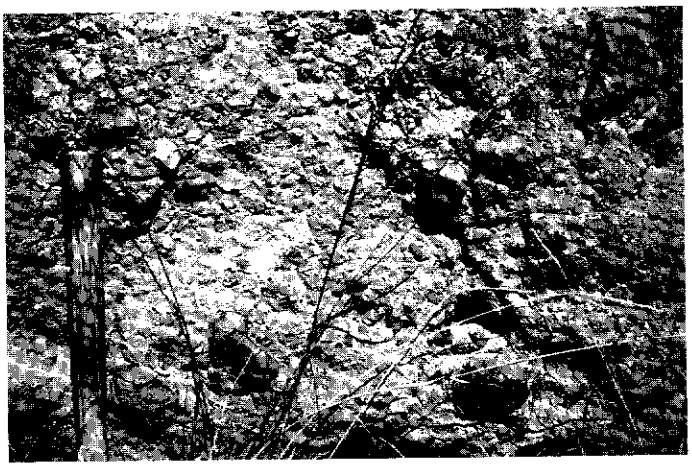

Figure 10. Grew Creek area: photograph of a poorly sorted, matrix supported and heterolithic debris flow.

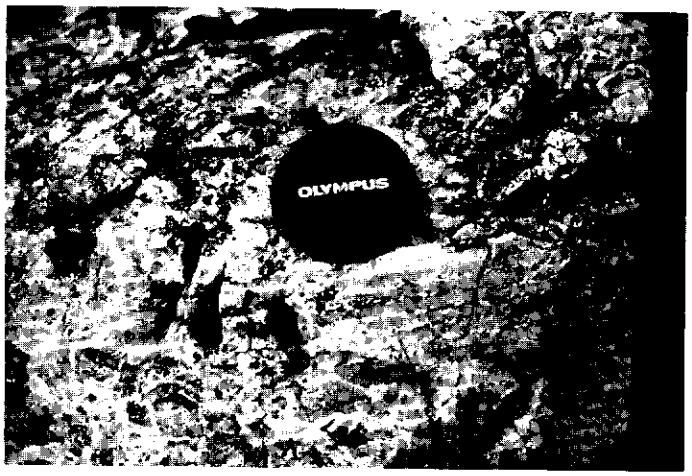

Figure 11. Glenlyon area: photograph of intense quartz veining that forms about 50% of the total rock in a rhyolite intrusion.

Figure 12. Grew Creek area: intensely folded, terrestrial, thinly bedded and laminated fissile, micaceous, carbonaceous and silty shales and sandstone beds.

set in a poorly sorted matrix and represent a series of debris flows. Other epiclastic deposits appear to grade into some of the primary volcanic deposits already described. They may be bedded, contain more rounded clasts, and are commonly more heterolithic.

PETROGRAPHY

The basalts are porphyritic, glomeroporphyritic or aphyric and contain in order of abundance, 0-25% phenocrysts of feldspar, olivine, clinopyroxene and rare quartz. Feldspar phenocrysts are up to 1 cm in length and are mostly labradorite in composition. They are euhedral to subhedral, show textures such as internal melting, resorption, reaction rims, oscillatory zoning and may be fractured and broken. Olivine phenocrysts commonly occur in clusters of small rounded grains that are partly or totally replaced by iddingsite or more commonly completely altered to pseudomorphs of calcite and chlorite. Clinopyroxene phenocrysts are typically poikilitic and enclose feldspar laths. They are commonly more resistant to alteration than olivine and altered to calcite, chlorite, and biotite. One sample contains a few rounded quartz phenocrysts surrounded by reaction rims. Magma mixing or incorporation of foreign fragments are possible explanations for the presence of quartz. Single crystals and sheaf-like aggregates of plagioclase predominate in the groundmass with mafic minerals or glass surrounding them. Opaques, magnetite and ilmenite occur as bladed crystals in the matrix.

RHYOLITE

Rhyolite occurs as intrusions, lava flows and volcaniclastic rocks. Most common are massive or flow-banded plug-like intrusions with near vertical intrusive or fault contacts. Most intrusions are poorly exposed except along creek sections and some cliff outcrops that locally exhibit columnar jointing. Dykes are massive to flow-banded, locally intensely folded and faulted, and rarely continuous for any great distance. Most intrusions are moderately to highly argillized and silicified, making the outcrops easily recognizable from a distance by their pale pastel color.

In the Glenlyon area, subhorizontal lava flows exhibit partly folded flow banding and surface ropey textures, and are associated with breccia. The flows surround a massive quartz-veined rhyolite intrusion of similar composition. The association resembles that of a dissected dome, and suggests that other less well exposed intrusions may also be domes.

Felsic volcaniclastic rocks comprise a small percentage of the rhyolitic rocks along the trench, their original extent being unknown. The volcaniclastic rocks are poorly sorted, nonwelded and contain variable amounts of lithic fragments and broken crystals set in a fine grained tuffaceous and glass shard matrix. Lithic fragments comprise rhyolite, metamorphic rocks and rare basalt. Nonwelded crystal lithic tuff is well exposed in a section along Grew Creek, though alteration has obliterated much of the structure and complicated interpretation of its origin. Presence of relatively unbroken and unworn glass shards suggests a primary volcanic deposition for most of the rocks. Clast size and sorting varies along the Grew Creek section, suggesting more than one type of volcanic deposit or deposition of volcanic ash flows along a relatively hilly topography. Large blocks in some sections suggest a proximal source.

Quartz, minor banded and brecciated chalcedony and late fluorite veins are intimately associated with the altered intrusions. In the central part of the Glenlyon area, rhyolite contains a zone of quartz veins 1.5 km long. Quartz comprises up to 50% of the rock (Fig. 11). Fluorite veins up to 1 m wide cut the quartz veins.

The main Grew Creek gold deposit is in a westward-pointing wedge of altered felsic volcaniclastic rocks bounded to the south by the Grew Creek Fault and to the north by steeply dipping sedimentary rocks that are intercalated with basalts. Gold occurs in banded and brecciated quartz-chalcedony veinlets and stringers that cut crystal lithic tuff (Duke and Godwin, 1986). The mineralization at surface is surrounded by zones of acid sulphate and argillic alteration and includes montmorillonite, kaolinite, jarosite, alunite and iron oxides. About 2 km east of the main deposit, gold-bearing quartz and fluorite veins occur in a large sericite alteration zone (Duke and Godwin, 1986).

PETROGRAPHY

The rhyolites are porphyritic to glomeroporphyritic and contain up to 25% phenocrysts of feldspar (mainly sanidine) and embayed quartz. Feldspar phenocrysts are euhedral to subhedral and altered, commonly cloudy, moth eaten or partly leached. Some rhyolites contain small amounts of primary biotite, but most contain about 5% altered mafic or oxide minerals. The matrix is graphic in texture, and in places spherulitic or partly spherulitic. Typically the rhyolite has undergone a combination of argillic, sericitic and silicic alteration.

CLASTIC SEDIMENTARY ROCKS

Clastic sedimentary rocks along the Tintina Trench are described by Hughes and Long (1979). They are moderately to steeply dipping, are locally tightly folded (Fig. 12) and occur in isolated fault blocks. Only rarely are they interbedded with volcanic rocks. Well to poorly sorted, spheroidal-weathered sandstone beds containing variable amounts of plant debris are interbedded and locally form load structures in finer thinly bedded and laminated, fissile, micaceous, carbonaceous and silty shales. Minor coal seams also form thin lenticular beds through the sequence. Some conglomerate forms normally graded lenticular beds and channels in the dominant fine-grained sequence. One relatively thick exposure of pebble conglomerate forms an erosional contact with the fine beds. The conglomerate is well sorted, normally to reversely graded, plane to planar cross-bedded and fills channels. These coarse conglomerates are in-

terbedded with finer bedded and laminated sandstones that are crossbedded, graded, and in places severely slumped. The conglomerate primarily contains rounded to subrounded clasts of relatively resistant chert, quartzite, vein quartz, metamorphic rock, granite and rare volcanic rock. Hughes and Long (1980) interpreted the sediments to have formed as lake deposits, alluvial fans, fan deltas and minor river deposits.

CHEMISTRY

Table 2 contains whole rock analyses for 38 samples of basaltic and rhyolitic rocks from the Tintina Trench. Samples were collected in geographically isolated areas from rocks with uncertain stratigraphic relations and varying degrees of alteration; therefore the geochemical analyses only provide limited information on petrogenetic evolution.

Binary and ternary plots illustrate the strongly bimodal nature of the Tintina volcanics; SiO_2 contents between 52 to 72% are rare. Solid and blank symbols on the elemental plots distinguish the relatively unaltered samples from the altered samples respectively. Major, minor and trace element contents plotted against silica content show no consistent variation between altered and unaltered samples, although points from unaltered samples tend to cluster more closely than points from altered samples. Generally basalts are high in $A1_20_3$, TiO_2 and FeO and low in K_20 and MnO. Basalts have no iron enrichment trends (Fig. 13) and have high FeO/MgO ratios (Fig. 14). The plot of Na_20+K_20 versus SiO_2 (Fig. 15) shows the apparent subalkaline nature of the basalt, whereas a plot using the less mobile elements (Zr, TiO_2, Nb & Y) shows the basalt to lie in the alkali field (Fig. 16). A Pearce and Cann plot confirms the intraplate affinity of the basalts (Fig. 17). The rhyolites are moderately altered, with high SiO_2 and K_20 (Fig. 18).

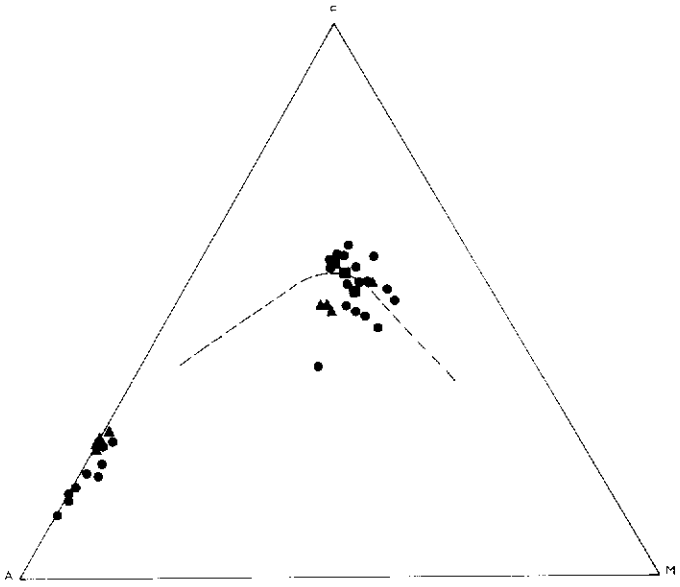

Figure 13. AFM plot (Irving and Barager, 1971) for rhyolite and basalt from Tintina Trench A= K20+Na20, F= Fe203, M= MgO. The dotted line separates the tholeiitic field (above) from the calc-alkaline field (below). The volcanic rocks along the Tintina Trench straddle the dotted line and show no iron enrichment trends. Open symbols = altered samples; closed symbols = relatively unaltered samples.

SYNTHESIS

Bimodal volcanism (basalt and high silica rhyolite) resulting from extension of continental crust is well documented in the western United States (Christiansen and Lipman, 1972 and Snyder et al, 1976). The Tintina Trench bimodal volcanics presumably developed in response to crustal attenuation caused by strike slip movement along Tintina Fault. Basalt and rhyolite intrusions outside the trench

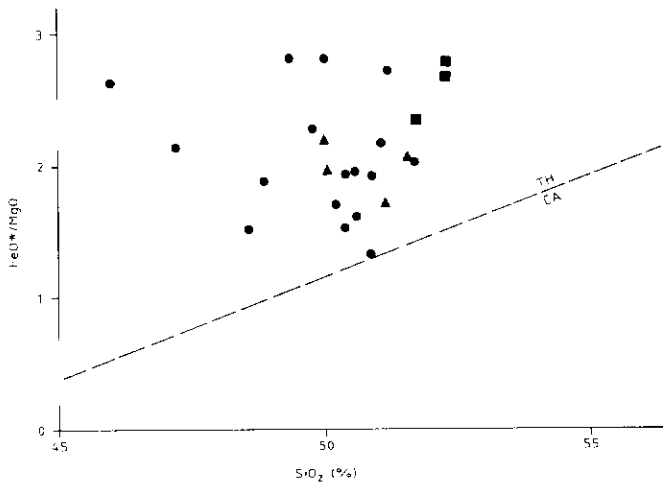

Figure 14 FeO/MgO versus %SiO2 diagram (FeO= total Fe as FeO) (Miyashiro, 1974) for basalt from Tintina Trench. The boundary line separates the tholeiitic (TH) and calc-alkaline (CA) fields.

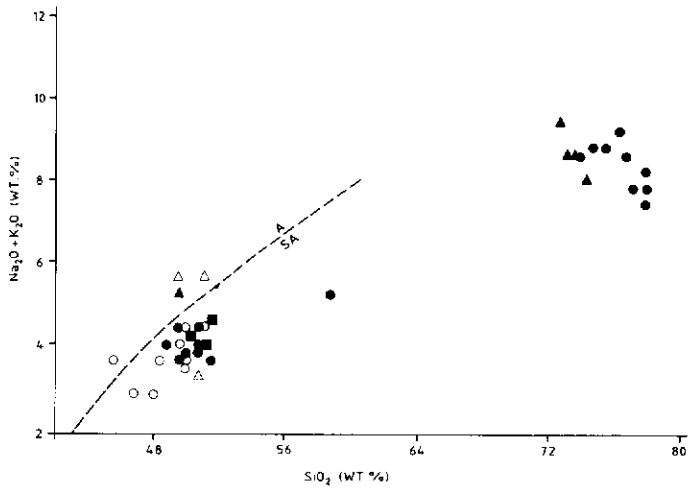

Figure 15. Alkali versus silica diagram (Irvine and Baragar, 1971) for volcanic rocks from the Tintina Trench. Boundary line separates the alkaline (A) and subalkaline (SA) fields, the volcanic rocks plotting dominantly within the subalkaline field.

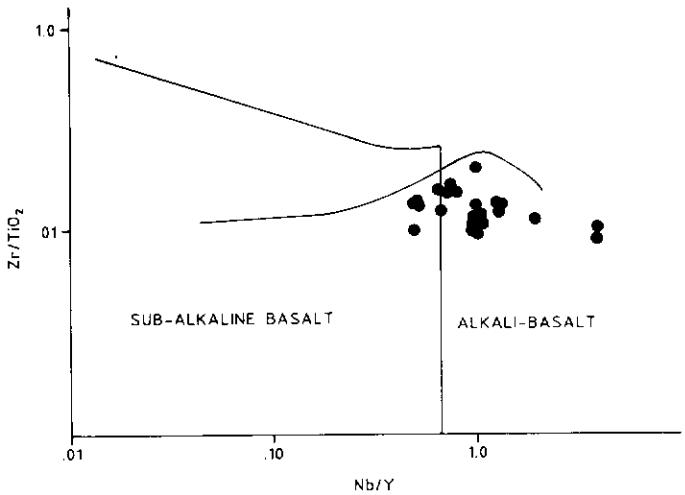

Figure 16. Discrimination diagram (Winchester and Floyes, 1977) for basalts from the Tintina Trench. The discrimination diagram uses immobile elements to separate the alkali verses subalkali fields. The volcanic rocks plot mostly in the alkali field.

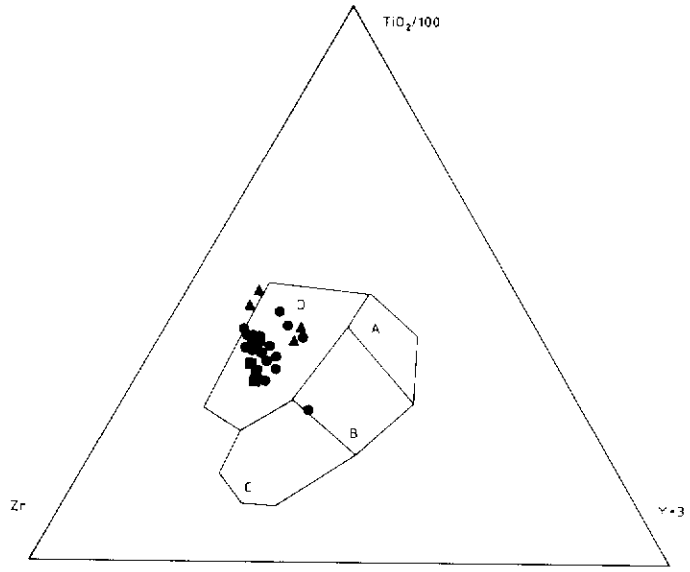

Figure 17. Pearce, Cann plot (1973) for basalts from the Tintina Trench. A+B= K tholeiites; B= Ocean floor basalts; B+C= Calc alkali basalts; D= Within plate basalts.

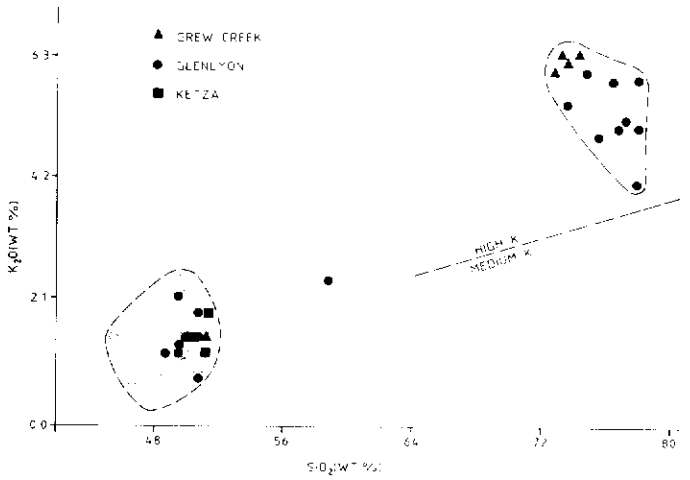

Figure 18. K_2O versus SiO_2 plot for Tintina Trench volcanic rocks. The heavy line separating the high K field from the medium K field suite of rocks is from Gill, (1981). The diagram shows the bimodal nature of the volcanic rocks and places the rhyolite in the high K rhyolite field.

and immediately north of the study area (Jackson et al, 1986) indicates that extension was not restricted to the Tintina Trench. Ultimately, examination of other bimodal volcanic suites in Yukon will help improve our understanding of the tectonic environment that prevailed during Tertiary time.

The terrestrial clastic sedimentary rocks along the Tintina Trench are products of fluvial and lacustrine deposition in isolated basins or a series of interconnected basins which formed in grabens along Tintina Trench (Hughes and Long, 1980). Basalts erupted in the source basins. No basaltic vents are yet known in the trench, but the presence of bombs and large blocks in some of the hydrovolcaniclastic deposits suggests a proximal environment, and indicates that at least some of the volcanics erupted in the trench. Rhyolite intrusions in the trench were probably emplaced along faults and fault intersections.

The volcanic rocks exhibit several differences from one area to another (Table 1). Some differences may be explained by poor exposure and different levels of exposure, but others probably reflect variatious in type, composition and environment of volcanism. The speculation that rhyolitic volcanism may be structurally controlled is suggested by the association with structurally complex areas, (Table 1).

Whether the volcanic rocks were deposited prior to, or subsequent to volcanism is uncertain. Lack of volcanic fragments in most sedimentary rocks suggests that they were deposited after volcanism. Alternatively the sediment source was outside the trench, whereas volcanism was in the trench.

Alteration and mineralization in rhyolite at Grew Creek and the Glenlyon area are different. Argillic alteration is better developed in the Grew Creek area whereas silicification is more pronounced in the Glenlyon area. Quartz and chalcedony, and later fluorite veining are intimately associated with the rhyolite intrusions in the Glenlyon area, whereas at Grew Creek, veins are associated with argillic, acid-leached, and silicified pyroclastic rocks. Mineralization in the Grew Creek area is epithermal (Duke and Godwin, 1986) and was presumably driven by a heat source at depth (rhyolite intrusion). Other deposits similar to Grew Creek probably formed elsewhere along the Tintina Trench. Pyroclastic rocks may not be the only host; clastic sedimentary rocks in particular are exploration targets. The Glenlyon area, although associated with at least three zones of extensive quartz veining and subordinate chalcedony and fluorite veining in rhyolite intrusions, contains no known precious metals. However, the intrusions resemble silicified caps of domes that are associated with precious metal deposits in other areas and their potential should not be ignored.

The chemical data confirms the bimodality of the volcanic suite. However, altered samples are difficult to separate from relatively unaltered samples.

TABLE 1 GEOLOGICAL FEATURES OF VOLCANIC ROCKS ALONG TINTINA TRENCH

STUDY SITE	GLENLYON	GREW CREEK	KETZA RIVER
Lithology	Basalt† basalt† sediments	Rhyolite†	Basalt
sediments† rhyolite			
Stratigraphy	Rhyolite intrudes basalt; clastic sediments interbedded with basalt	Basalt intrudes rhyolite; basalt clasts in rhyolitic volaniclastic rocks	
Relative abundance of subaerial vs subaqueous deposits	subaerial	subaerial = subaqueous	subaerial = subaqueous
Relative abundance of lava flows (intrusions) vs volcaniclastic rocks	Basalt: lava flows Rhyolite: intrusions	Basalt: volcaniclastic Rhyolite: intrusions, volcaniclastic rocks	Basalt: lava flows = volcaniclastic rocks
Structure	Highly to moderately deformed	Highly deformed (strike 120 with steep dips)	Slightly deformed (minor dip slip faults)
Alteration and mineralization	Basalt: highly altered; calcite and chlorite rhyolite: altered; silicification and argillic	Basalt: highly altered, calcite and chlorite Rhyolite: altered; argillic, silification and acid leaching	Relatively unaltered
	Barren quartz, chalcedony veins and later fluorite veins in rhyolite.	Au and Ag mineral-ization	No mineralization

TABLE 2

	86-GR-76	86-GL-8	86-GL-9	86-GL-9A	86-GL-37	86-GL-38	86-GL-41	86-GL-42
SiO_2	47.30	46.40	46.70	46.20	48.30	47.70	45.10	47.10
Al_2O_3	16.00	15.20	16.60	14.60	15.80	16.0	17.10	16.40
Fe_2O_3	10.50	11.70	12.30	10.50	10.80	10.9	10.80	11.10
MgO	4.82	3.75	3.94	5.87	4.42	5.13	5.17	5.18
CaO	8.13	8.94	8.96	8.63	9.03	8.5	9.11	7.55
Na_2O	3.26	2.09	2.96	2.41	2.66	2.45	2.88	2.59
K_2O	2.0	2.01	1.03	.90	1.27	1.37	.71	1.11
TiO_2	2.32	2.34	2.10	2.19	2.11	2.25	1.85	2.0
P_2O_5	.58	.91	.68	.56	.73	.87	.45	.71
MnO	.17	.24	.22	.19	.14	.14	.18	.17
LOI	4.23	6.23	4.16	6.93	4.16	3.85	5.16	5.70
SUM (includes trace elements)	**99.6**	**100.0**	**99.9**	**99.2**	**99.4**	**99.4**	**99.8**	**99.8**
NORMS IN WEIGHT PERCENT								
Q	-	4.49	1.11	3.99	4.71	4.41	-	3.82
C	-	-	-	-	-	-	-	-
OR	12.54	12.82	6.44	5.83	7.97	8.57	4.54	7.05
AB	29.23	19.07	26.49	22.33	23.86	21.92	26.33	23.54
AN	24.49	28.20	30.63	28.86	29.07	30.26	34.18	32.06
DI	8.73	6.80	5.56	8.72	7.65	4.96	6.40	1.79
HE	2.69	3.97	4.04	2.50	3.15	1.73	2.90	.79
EN	4.99	6.91	7.8	11.96	8.13	11.21	8.15	13.03
FS	1.76	4.62	6.5	3.94	3.84	4.49	4.23	6.60
FO	2.58	-	-	-	-	-	1.96	-
FA	1.00	-	-	-	-	-	1.72	-
MT	5.87	6.00	5.52	5.86	5.55	5.75	5.25	5.45
IL	4.67	4.79	4.22	4.55	4.25	4.52	3.80	4.08
CR	.03	.03	.03	.04	.03	.03	.02	.03
HM	1.43	2.28	1.67	1.42	1.80	2.14	1.13	1.77
AP	-	-	-	-	-	-	-	-
RU	-	-	-	-	-	-	-	-
WO	-	-	-	-	-	-	-	-
TRACE ELEMENTS IN PPM								
Ba	1090	870	660	580	660	790	1740	750
Cr	150	130	120	170	140	140	80	140
Zr	230	300	250	270	280	290	180	260
Sr	680	500	630	370	530	580	660	550
Rb	30	80	40	30	20	20	30	40
V	20	40	30	30	40	30	30	30
Nb	80	20	20	40	20	40	30	30
Ni	44	49	56	65	31	39	54	49
Co	28	34	35	31	26	28	40	35
Cu	29	15	18	23	14	17	18	16

	86-GL-43	86-GL-51	86-GL-52	86-GL-54	86-GL-55	86-GL-60	86-GL-63	86-GL-65
SiO_2	49.40	46.20	48.20	46.90	48.90	56.20	42.80	41.20
Al_2O_3	15.90	15.20	16.90	15.10	16.00	15.80	16.60	16.30
Fe_2O_3	12.80	10.10	10.30	11.60	11.90	6.45	12.30	11.60
MgO	4.18	5.38	6.11	4.62	3.96	4.25	5.17	3.99
CaO	6.53	8.38	8.48	9.52	8.04	6.49	8.75	10.10
Na_2O	1.77	2.94	3.26	2.44	2.57	2.90	2.40	2.41
K_2O	1.78	1.40	1.11	1.20	1.82	2.30	.46	1.23
TiO_2	2.12	2.04	1.94	2.43	2.29	1.05	2.21	2.41
P_2O_5	.71	.83	.61	.90	.68	.18	.74	.93
MnO	.19	.17	.16	.19	.17	.1	.15	.18
LOI	4.16	6.54	2.85	4.39	3.31	3.77	7.82	9.0
SUM (Includes trace elements)	**99.8**	**99.4**	**100.1**	**99.5**	**99.8**	**99.7**	**99.4**	**99.6**
NORMS IN WEIGHT PERCENT								
Q	10.63	.59	-	4.22	4.84	11.77	.47	-
C	.84	-	-	-	-	-	-	-
OR	11.15	9.01	6.82	7.55	11.28	14.27	3.00	8.13
AB	15.86	27.05	28.63	21.94	22.78	25.74	22.40	22.77
AN	29.40	26.26	29.28	28.38	28.02	24.44	36.58	33.54
DI	-	8.01	6.27	8.83	4.69	5.28	3.2	8.48
HE	-	2.46	1.96	3.76	2.75	1.18	1.65	4.23
EN	11.03	10.86	10.38	8.14	8.16	8.66	12.72	1.82
FS	9.38	3.83	3.73	3.98	5.50	2.22	7.5	1.04
FO	-	-	1.78	-	-	-	-	3.75
FA	-	-	.70	-	-	-	-	2.36
MT	5.56	5.56	5.18	6.06	5.76	3.88	5.93	6.33
IL	4.27	4.21	3.83	4.91	4.56	2.09	4.83	5.11
CR	.03	.04	.02	.03	.03	.04	.03	.03
HM	-	-	-	-	-	-	-	-
AP	1.75	2.09	1.47	2.22	1.65	.44	1.89	2.41
RU	-	-	-	-	-	-	-	-
WO	-	-	-	-	-	-	-	-
TRACE ELEMENTS IN PPM								
Ba	820	920	680	700	670	710	520	750
Cr	140	180	80	110	110	160	130	140
Zr	310	260	220	280	260	170	270	300
Sr	430	650	620	550	470	360	540	680
Rb	80	40	30	20	90	100	30	40
V	40	40	20	40	30	40	30	30
Nb	30	20	40	40	30	30	30	30
NI	43	44	40	40	30	46	55	57
Co	38	24	32	28	32	21	37	38
Cu	12	15	20	18	11	19	18	20

TABLE 2 Continued

	86-KZ-1	86-KZ-2	86-KZ-6	86-GR-52	86-GR-72	86-GR-75
SiO_2	49.7	50.4	49.7	45.9	46.9	46.6
Al_2O_3	15.3	12.9	14.9	14.1	14.3	15.8
Fe_2O_3	12.0	12.9	11.6	10.4	11.5	10.6
MgO	5.66	4.34	4.45	5.13	5.07	4.37
CaO	8.41	8.06	8.9	8.84	5.57	7.83
Na_2O	2.76	2.79	2.95	2.45	4.37	3.35
K_2O	1.4	1.74	1.06	.75	1.3	2.17
TiO_2	2.31	2.98	2.41	1.98	2.13	2.36
P_2O_5	.78	1.01	.89	.53	.42	.65
MnO	.20	.19	.18	.19	.2	.17
LOI	1.31	1.93	2.39	8.85	8.08	5.93
SUM (includes trace elements)	100.0	98.5	99.4	99.3	100.1	100.1
NORMS IN WEIGHT PERCENT						
Q	8.48	7.83	5.68	5.11	-	-
C	-	-	-	-	-	-
OR	8.48	10.68	6.53	4.95	8.46	13.77
AB	23.91	24.49	25.99	23.12	40.67	30.42
AN	25.83	18.19	25.29	26.18	17.12	23.25
DI	6.85	9.23	8.95	9.46	5.68	8.33
HE	2.79	4.08	4.00	3.56	2.63	2.83
EN	11.35	8.93	7.39	9.86	3.81	2.87
FS	5.45	3.51	3.79	4.26	2.02	1.12
FO	-	-	-	-	5.22	3.47
FA	-	-	-	-	3.06	1.49
MT	5.66	6.74	5.90	5.63	5.79	6.00
IL	4.49	5.87	4.77	4.20	4.45	4.81
CR	.04	.03	.03	.04	.03	.03
HM	-	-	-	-	-	-
AP	1.85	2.43	1.67	1.63	1.07	1.62
RU	-	-	-	-	-	-
WO	-	-	-	-	-	-
TRACE ELEMENTS IN PPM						
Ba	700	870	750	460	880	1220
Cr	200	150	140	150	120	140
Zr	340	460	330	250	210	210
Sr	380	290	430	420	560	880
Rb	40	50	60	60	80	50
V	50	60	40	30	40	20
Nb	40	40	50	30	20	80
Ni	27	5	40	68	57	44
Co	26	13	26	36	35	28
Cu	17	21	19	26	22	33

TABLE 2 Continued

	86-GL-3	86-GL-6C	86-GL-16A	86-GL-24	86-GL-50	86-GL-62	86-GL-76	86-GL-84
SiO_2	76.00	75.60	71.90	73.50	75.70	75.80	76.20	75.40
Al_2O_3	11.10	12.00	13.20	13.60	11.10	11.00	11.10	12.30
Fe_2O_3	.09	.06	.35	.10	.30	.30	.12	.07
MgO	.72	.29	1.10	.43	.07	.09	.34	.27
CaO	3.24	3.62	3.42	2.77	2.89	2.09	3.42	3.49
Na_2O	4.93	4.96	5.28	5.98	5.05	5.72	3.98	5.75
K_2O	.13	.14	.30	.22	.18	.16	.17	.12
TiO_2	.02	.02	.06	.04	.02	.02	.02	.02
P_2O_5	.03	.04	.06	.01	.05	.03	.06	.01
MnO	1.54	.77	2.16	1.54	1.06	1.47	1.39	.77
LOI	-	-	-	-	-	-	-	-
SUM (includes trace elements)	**99.3**	**99.2**	**100.0**	**100.0**	**99.5**	**99.2**	**99.6**	**99.5**
NORMS IN WEIGHT PERCENT								
Q	38.04	35.51	29.76	34.07	40.04	42.29	41.11	32.97
C	-	.20	-	1.91	.90	1.28	.61	-
OR	29.87	29.86	31.97	35.96	30.49	34.77	24.07	34.49
AB	28.08	31.17	29.62	23.82	24.53	18.17	29.58	29.94
AN	1.2	1.33	5.18	1.90	.22	.32	1.59	.91
DI	.49	-	.01	-	-	-	-	.24
HE	-	-	-	-	-	-	-	-
EN	-	.15	.89	.25	.78	.77	.31	.06
FS	-	-	-	-	.17	-	-	-
FO	-	-	-	-	-	-	-	-
FA	-	-	-	-	-	-	-	-
MT	-	-	.04	-	2.48	1.03	2.07	-
IL	.06	.08	.58	.02	.35	.31	.38	.02
CR	.01	.01	.01	.01	.01	.01	.01	.01
HM	1.38	1.55	1.82	1.75	-	.99	.28	1.20
AP	.05	.05	.14	.09	.05	.05	.05	.05
RU	.10	.10	-	.21	-	-	-	.11
WO	.71	-	-	-	-	-	-	-
TRACE ELEMENTS IN PPM								
Ba	540	290	660	700	750	1310	460	250
Cr	30	30	30	30	30	30	30	30
Zr	220	230	360	390	1120	840	1090	150
Sr	170	40	70	50	10	10	10	40
Rb	310	310	260	340	440	460	300	430
V	130	120	70	90	190	160	210	110
Nb	80	80	50	40	130	120	140	50
Ni	2	2	5	2	1	1	1	3
Co	1	1	3	1	1	1	1	1
Cu	2	.5	2	.5	2	.5	1.5	15

	86-GL-78	86-GL-80	86-GL-81	86-GL-83	86-GL-84	86-GL-85	86-GL-89	86-GL-2
SiO_2	48.00	48.70	42.80	71.40	70.80	71.00	72.50	74.80
Al_2O_3	15.30	16.70	15.90	13.00	12.90	12.90	13.20	12.50
Fe_2O_3	10.10	9.08	9.89	3.06	2.83	2.88	3.04	2.13
MgO	4.95	6.32	5.90	.08	.09	.07	.12	.15
CaO	8.18	9.49	9.41	.67	.86	1.05	.30	.40
Na_2O	3.09	3.10	2.65	3.54	2.51	2.59	1.90	3.88
K_2O	1.34	.73	.24	5.84	6.12	6.02	6.14	4.87
TiO_2	1.83	1.57	1.44	.32	.31	.30	.31	.22
P_2O_5	.58	.44	.43	.05	.05	.01	.06	.04
MnO	.15	.11	.16	.08	.07	.07	.08	.06
LOI	5.77	5.20	10.5	1.7	2.16	2.47	2.00	.93
SUM (includes trace elements)	**99.5**	**99.5**	**99.5**	**100.0**	**99.0**	**98.6**	**99.9**	**100.0**
NORMS IN WEIGHT PERCENT								
Q	2.02	.33	-	27.68	32.03	31.26	38.13	32.80
C	-	-	-	-	.72	.32	3.07	.21
OR	8.54	4.52	1.61	35.28	37.50	36.90	37.25	29.15
AB	28.17	27.43	25.45	30.59	22.00	22.71	16.49	33.22
AN	25.78	30.85	34.94	2.37	4.08	5.13	1.91	1.74
DI	8.09	9.68	8.54	.35	-	-	-	-
HE	3.16	2.62	3.46	.22	-	-	-	-
EN	9.56	11.97	8.34	.04	.23	.18	.31	.38
FS	4.31	3.71	3.88	.03	-	1.06	.15	-
FO	-	-	3.07	-	-	-	-	-
FA	-	-	1.57	-	-	-	-	-
MT	5.20	4.66	4.84	2.70	2.83	2.30	2.69	.74
IL	3.75	3.12	3.10	.62	.61	.06	.60	.42
CR	.03	.05	.07	.01	.01	.01	-	.01
HM	-	-	-	-	.06	-	-	1.23
AP	1.45	1.07	1.13	.12	.12	.10	.12	.09
RU	-	-	-	-	-	-	-	-
WO	-	-	-	-	-	-	-	-
TRACE ELEMENTS IN PPM								
Ba	870	520	450	690	740	730	750	420
Cr	140	240	270	30	30	30	20	30
Zr	250	150	140	640	850	610	640	450
Sr	610	460	550	30	40	20	20	110
Rb	50	30	10	300	300	290	310	250
V	40	30	20	80	80	100	90	100
Nb	20	30	30	50	70	50	60	60
Ni	38	73	100	3	2	2	2	2
Co	27	27	39	2	2	2	2	2
Cu	17	29	27	3	2	5	3	1

REFERENCES

CAMPBELL, R.B., 1967. Geology of the Glenlyon map area; Geological Survey of Canada, Memoir 352 (includes Map 1221-A and 1222-A).

CHRISTIANSEN, R.L. and LIPMAN, P.W., 1972. Cenozoic volcanism and platetectonic evolution of the western U.S. II Late Cenozoic. Royal Society of London Philosophical Transactions Ser. A, Vol. 271, p. 249-284.

DUKE, J.L. and GODWIN, C.I., 1986. The geology and alteration of an epithermal gold and silver prospect at Grew Creek, south central Yukon; in Yukon Geology, Vol. 1. Exploration and Geological Services Division, Yukon, Indian and Northern Affairs Canada p. 72-82.

FISHER, R.V. and SCHMINCKE, 1984. Pyroclastic Rocks; Springer-Verlag, New York, 472 p.

GABRIESLE, H., 1985. Major dextral transcurrent displacements along the Northern Rocky Mountain Trench and related lineaments in north-central British Columbia. Geological Society of America Bulletin, Vol. 96, p. 1-14.

GILL, J.B., 1981. Orogenic Andesites and Plate Tectonics; Springer-Verlag, New York, 390 p.

GORDEY, S.P., 1983. Thrust faults in the Anvil Range group and a new look at the Anvil Range group, south-central Yukon Territory; in Current Research, Part A, Geological Survey of Canada Paper 83-1A, p. 225-227.

HUGHES, J.D. and LONG, D.G.F., 1979. Geology and coal resource potential of early Tertiary strata along Tintina Trench, Yukon Territory; Geological Survey of Canada Paper 79-32, 21 p.

IRVINE, T.N. and BARAGAR, W.R., 1971. A guide to the chemical classification of the common volcanic rocks; Canadian Journal of Earth Sciences, Vol. 8, p. 523-548.

JACKSON, L.E., GORDEY, S.P., ARMSTRONG, R.L., and HARAKAL, J.E., 1986. Bimodal Paleogene volcanics near Tintina Fault, east-central Yukon Territory, and their possible relationship to placer gold; in Yukon Geology, Vol.1; Exploration and Geological Services Division, Yukon, Indian and Northern Affairs Canada, p. 139-147.

JOHNSON, J.R., 1936. A reconnaissance of Pelly River between Macmillan River and Hoole Canyon, Yukon; Geological Survey of Canada, Memoir 200 (includes Map 394A).

MIYASHIRO, A., 1974. Volcanic rock series in island arcs and active continental margins; American Journal of Science, Vol. 274, p. 321-355.

NOBLE, D.C., 1972. Some observations on the Cenozoic volcano-tectonic evolution of the Great Basin, Western United States; Earth and Planetary Science Letters, Vol. 17, p. 142-150.

PEARCE, J.A. and CANN, J.R., 1973. Tectonic setting of basic volcanic rocks determined using trace element analysis; Earth and Planetary Science Letters, Vol. 19, p. 290-300.

RODDICK, J.A. and GREEN, L.H., 1961. Geology, Tay River, Yukon Territory; Geological Survey of Canada, Map 13-1961.

RODDICK, J.A., 1967. Tintina Trench; Journal of Geology, Vol. 75, p. 23-33.

SNYDER, W.S., DICKINSON, W.R. and SIBERMAN, M.L., 1976. Tectonic implications of space-time patterns of Cenozoic magmatism in the western United States; Earth and Planetary Science Letters, Vol. 32, p.359-362.

TEMPELMAN-KLUIT, D.J., 1972. Geology and origin of Faro, Vangorda and Swim concordant zinc-lead deposits, central Yukon Territory; Geological Survey of Canada Bulletin 208, 73 p.

TEMPELMAN-KLUIT, D.J., 1977. Geology of Quiet Lake (105 F) and Finlayson Lake (105 G) map areas; Geological Survey of Canada Open File Report 486.

TEMPELMAN-KLUIT, D.J., 1979. Transported cataclastic, ophiolite and granodiorite in Yukon: evidence of arc-continent collision; Geological Survey of Canada Paper 79-14, 26 p.

TEMPELMAN-KLUIT, D.J., 1980. Evolution of physiography and drainage in southern Yukon; Canadian Journal of Earth Sciences, Vol. 17, No. 9, p. 1189-1203.

WHEELER, J.O., GREEN, L.H., and RODDICK, J.A., 1960. Geology, Quiet Lake, Yukon Territory; Geological Survey of Canada Map 7-1960.

WINCHESTER, J.A., and FLOYDE, P.A., 1977. Geochemical discrimination of different magma series and their differentiation products using immobile elements; Chemical Geology, Vol. 20, p. 325-343.

CAMBRO-ORDOVICIAN VOLCANIC ROCKS IN EASTERN DAWSON MAP-AREA OGILVIE MOUNTAINS, YUKON

C.F. Roots
Carleton University and
Ottawa Carleton Centre for
Geoscience Studies,
Ottawa, Ontario, KIS 5B6

ROOTS, C.F., 1988. Cambro-Ordovician volcanic rocks in eastern Dawson map-area, Ogilvie Mountains, Yukon; in Yukon Geology, Vol. 2; Exploration and Geological Services Division, Yukon, Indian and Northern Affairs Canada, p. 81 - 87

ABSTRACT

Basalt and minor rhyolite flows and breccias in the northwestern extension of Selwyn Basin are stratigraphically above maroon argillite (Lower Cambrian Hyland Group) and beneath black chert (Middle Ordovician Road River Group). All are intensely folded and repeated by shallow thrust faults.

The lower part of the volcanic succession is dominated by subaqueous flows, and the upper part includes shallow and subaerial breccias and limestone pods. The volcanic unit is interpreted as many small overlapping seamounts fed by gabbroic dykes.

The basaltic rocks are alkalic and contain high concentrations of TiO_2 (1.7 - 3.6%), P_2O_5 (0.5 - 1.2%) and Zr (140 ppm). They resemble the volcanic Marmot Formation in the northeastern part of Selwyn Basin, and are consistent with extension and thinning of continental crust.

The volcanic rocks lack significant sulphide mineralization, except where hornfelsed near Cretaceous intrusions. Local high barium concentrations suggest that volcanism may have contributed to stratabound barite in overlying Devonian shales.

RÉSUMÉ

Dans le prolongement nord-ouest du bassin de Selwyn, des coulées et brèches basaltiques et quelques coulées et brèches rhyolitiques se situent stratigraphiquement au-dessus d'argilites marron (groupe de Hyland, du Cambrien inférieur) et au-dessous d'un chert noir (formation de Road River, de l'Ordovicien moyen). Toutes ces coulées et brèches sont intensément plissées et redoublées par des failles chevauchantes peu profondes.

La partie inférieure de la succession volcanique est dominée par des coulées subaquatiques, et la partie supérieure comprend des brèches peu profondes et subaériennes et des lentilles calcaires. On a interprété l'unité volcanique comme étant composée de nombreux petits guyots empiétant les uns sur les autres, et alimentés par des dykes de gabbro.

Les roches basaltiques sont alcalines, et contiennent des concentrations élevées de TiO_2 (1,7 - 3,6 %), de P_2O_5 (0,5 - 1,2 %) et de Zr (140 ppm). Elles ressemblent à la formation volcanique de Marmot dans la partie nord-est du bassin de Selwyn, et leur formation s'expliquerait bien par une expansion et un amincissement de la croûte continentale.

Les roches volcaniques ne contiennent pas de minéralisation sulfurée notable, excepté là où elles ont été transformées en cornéennes près des intrusions crétacées. Des concentrations localement élevées en baryum suggèrent que le volcanisme a peut-être contribué au dépôt stratiforme de barytine dans les argiles litées dévoniennes sus-jacentes.

INTRODUCTION

Among the generally subdued and thickly vegetated ranges south of the high Ogilvie Mountains are strips of volcanic rock that form castellated spines and grey towers. The enclosing dark shale, grit, and chert comprise Selwyn Basin, in which large, stratabound zinc-lead deposits of the Anvil and Howards Pass type are hosted by Lower and Middle Paleozoic phyllite. Dawson map-area contains similar strata and abundant volcanic rocks. Reconnaissance stream sediment geochemical surveys have located anomalous Cu, Zn, Ba, Mo and Ni concentrations draining from the volcanics and black shale (i.e. STYX claims; INAC 1981, p. 285).

Volcanism might have been accompanied by metalliferous fluids or circulating hydrothermal systems and thus caused massive sulphide deposition.

The volcanic rocks also have tectonic implications for for the region. In the Ogilvie Mountains, clastic and igneous rocks record three distinct extension events at about 1200, 750 and 530-450 Ma (Thompson et al, in press). The ca. 750 Mount Harper Complex, in a carbonate shelf environment, contains similar mafic rock types to those of the early Paleozoic Selwyn Basin volcanic unit described here.

This report addresses the economic potential of the volcanics, their stratigraphic position and presents first analyses of their composition. Field work in 1986 consisted of 1:50 000 scale mapping in specific areas as part of the regional program of stratigraphic correlation and structural assessment by the G.S.C. (see Thompson and Roots, 1981). The structural model expressed here was derived from field study since 1980 by Thompson and co-workers, and is based on the excellent reconnaissance map of Green (1972). Previous work has outlined the distribution of the volcanics, but not their stratigraphic position or internal structure. Figure 1 indicates localities described here; further map detail is available in G.S.C. Open File reports.

REGIONAL SETTING AND STRUCTURE

Sedimentary rocks north of the Tintina Fault are part of the Cordilleran fold and thrust belt, and in Dawson map-area comprise two major successions of shelf and basin affinity (Thompson and Roots, 1981). Both were displaced northward during the late Jurassic, and the basin succession has been considerably shortened by thrusts and folds. Stratigraphic packages of different ages comprise three structural sheets (see Anderson, 1987). Volcanic rocks are confined to numerous linear outcrops in the northernmost sheet (Fig. 1), which also includes two other principal rock units; the Hyland Group and the Road River Formation.

The oldest exposed basinal strata are grit, limestone and maroon

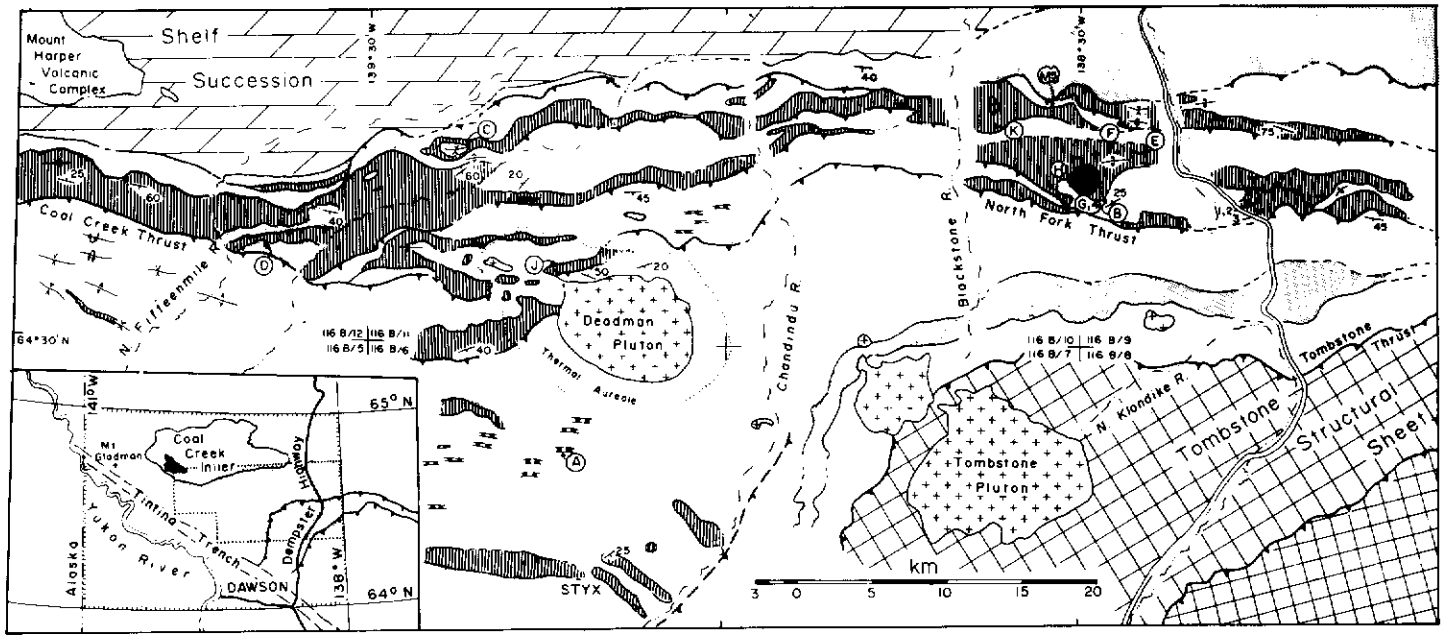

Figure 1. Generalized distribution of Cambro-Ordovician rocks (vertical stripes), Road River Formation (fine dots), and Hyland Group (no pattern) in the basin succession of the southern Ogilvie Mountains. The study area is the lowest of three structural sheets: overlapping sheets (gridded) are described in Anderson (1987). Limestone pods are short, thick lines within the volcanic belts (Dempster Highway area). Gabbro dykes (checkered) are more numerous than shown, particularly north and south of Deadman Pluton. Circled letters are localities mentioned in the text; numbers are sample locations (Table 1). Quadrants labelled with 116 B- suffix correspond to 1:50 000 map sheets available on Open File. Geology from Green (1972), Thompson and Roots (1982) and recent mapping.

argillite provisionally correlated with the latest Proterozoic and Lower Cambrian Hyland Group of Nahanni map-area (S.P. Gordey, in prep.). The Road River Group includes black argillite, siltstone and chert. In places where volcanics do not occur between them, the contact between the Hyland and Road River Groups is unclear. On both sides of the Dempster Highway, clean quartzite and wispy laminated, olive-coloured argillite and siltstone are in or overlying typical Hyland Group strata. In other places, rusty phyllitic siltstone, silvery weathering black mudstone and bioturbated green and yellow chert lie at or below the base of typical Road River Group strata. The Backbone Ranges, Kechika and Rabbitkettle formation are Cambrian units from the eastern edge of the Selwyn Basin that are missing in Dawson Map area, but which may be represented by these unassigned units (R. Thompson and G. Abbott, pers. comm., 1986).

AGE OF THE VOLCANICS

Previous studies have not made clear whether the volcanics were local accumulations, possibly of various ages, or were remnants of a single extensive sheet and stratigraphic contacts are exposed in only a few places and many contacts are now recognized as thrusts, based upon older over younger stratigraphic relationships. Broad areas of volcanic rocks shown on the map (Fig. 1) result from tight folding (Fig. 2).

Observed stratigraphic relationships and evidence for age are summarized below:

At Localities A and B (Fig. 1) pillows and lapillistone tuff layers conformably overlie maroon argillite of the Hyland Group which contain **Oldhamia** and worm burrows (resemble **Rusophycus**) that indicate a Lower or Middle(?) Cambrian age (see Hoffman and Cecile, 1981; Nowlan et al, 1985).

At Locality C, volcanic debris flows and a subaqueous pyroclastic succession is directly overlain by graptolitic chert of the Road River Group of Middle Ordovician age (Green, 1972; R. Thompson, unpubl. data).

The volcanic succession includes discontinuous pods of white- or grey-weathering limestone that have yielded mollusc and brachiopod fragments (M. Orchard, pers. comm. 1982) at Locality D and **an Early Ordovician conodont** (M. Cecile, pers. comm. 1987) at Locality E (Fig. 3).

Figure 2. Tight upright folds of basaltic pillows and breccia, cut by a thrust and overlain by flat-lying flows of the same volcanic unit. The triangular scree slope below the thrust is black shale, possibly Road River Formation. Looking westward at locality K.

The upper contact of the volcanics is less clearly defined. At Locality F, hematized flows and conglomerate are interbedded with grey mudstone and calcareous siltstone. The overlying section is poorly exposed, but is lithologically similar to the unassigned units seen elsewhere between the Road River Formation and Hyland groups.

Volcanic rocks of lower to middle Paleozoic age occur along the margin of Selwyn Basin and in northeastern B.C. (occurrences reported in Cecile, 1982). Most consist of submarine flows and volcaniclastic deposits that form thin or lenticular bodies; some are in dominantly sedimentary units. The Marmot Formation of Misty Creek Embayment (**Bonnet Plume** map-area, 500 km to the east), which resembles the early Paleozoic volcanics of Dawson map-area in composition and setting, is Middle Ordovician to Lower Devonian (Cecile, 1982).

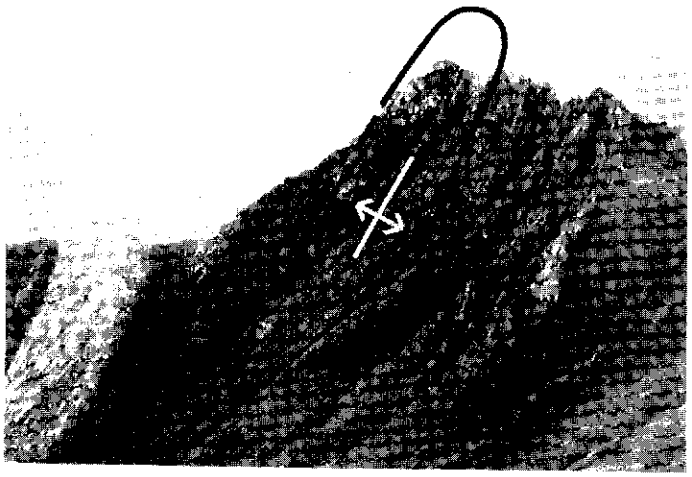

Figure 3. Isoclinal anticline of steeply dipping vesicular basalt, deduced from outward facing directions of flows and interbedded tuff. White area is a limestone pod - one in a discontinuous, 10 km long limestone layer near the top of the volcanic unit. Looking east at locality E, with East Blackstone valley and the Dempster Highway in background.

Figure 4. Inversely graded basaltic block and ash breccia interbedded with pillowed flows at locality L. The poor sorting and clast- supported texture of the angular fragments suggest proximal pyroclastic deposition. Such textural preservation is common in thicker volcanic accumulations.

STRATIGRAPHY

The principal volcanic rock types, described in Roots (1981) and Roots and Moore (1982), are subaqueous pyroclastic breccias (Fig. 4), debris flows and submarine lapillistone-tuff. Their areal extent implies multiple vents that probably constructed overlapping volcanoes. Continuity of pyroclastic layers and thick pillow flow units over 5 km long indicate their size. In general, pillows and massive flows dominate near the base of the volcanic units, and lapillistone tuff, heterolithic breccias and hematized volcanics dominate near the top. These features suggest a progression from a deep water to a shallow water environment.

Volcanic outcrops near the Dempster Highway (km 87-93) are capped by hematitic vesicular flows and breccia that are likely subaerial. They are interbedded with maroon conglomerate containing well-rounded basaltic pebbles and cobbles in a volcanic mudstone matrix. Pods of crudely bedded limestone with textures indicative of shallow water deposition are common stratigraphically beneath the oxidized flows and breccias. The association of subaerially erupted and shallow water deposits imply the former presence of volcanic islands.

HYPABYSSAL MAFIC AND FELSIC INTRUSIONS

Large areas south of the Deadman Pluton where maroon argillite predominates are cut by west-trending dykes spaced 50-250 m apart. The dykes are compositionally similar to the volcanics and were observed in two places to directly feed pillow flows. At locality A, texturally distinctive breccia is interfingered along the contact of the dyke, stratigraphically overlies maroon argillite and is intercalated with overlying pillows. It consists of ragged, 1-3 cm lenticles of vesicular basalt in a fine grained, indurated matrix (Fig. 5). The breccia is clearly related to the breaching intrusion, and may be useful as a guide in the recognition of vents. Northeast of the Cretaceous Deadman Pluton, medium to coarse-grained augite gabbro intrusions up to 1 km^2, in the Hyland Group may have been shallow magma chambers feeding early Paleozoic volcanism.

A light brown-weathering felsic intrusion outcrops in a subcircular area 5 km west of the Dempster Highway (Locality G). In the centre, leucocratic felsite contains up to 15% rounded, 1-2 mm quartz phenocrysts and ghost rectangular shapes (probably feldspar) with size gradations suggestive of rhythmic layering. Near the southern edge, a breccia composed of angular 1-20 cm fragments of basalt, meta-siltstone and quartzite appears to be derived from host rocks because it grades into intact volcanic flows; all rocks in the vicinity are silicified and probably constitute a hornfels around this felsic intrusion. Siliceous apophyses and felsite dykes radiate southeast.

Felsic flows are exposed in a 12 km long area east of Mount Gladman (west Dawson map-area). Greenish feldspar-phyric rhyolite flows and lithic-crystal ignimbrite are directly overlain by Road River chert.

COMPOSITION

The basalts contain chlorite, sericite, quartz, illite and local prehnite, indicating lower greenschist metamorphic grade. Hyalopilitic textures are well preserved and the most densely crystallized flows contain skeletal plagioclase with swallow-tail shapes and irregular interstitial opaques.

Many flows near the base of the volcanic unit contain augite megacrysts (up to 1 cm across) with clean rhombic and hexagonal shapes (Fig. 6). In many thin sections, augite is partly or totally replaced by zoisite. The groundmass of these flows is extremely fine-grained, with poorly crystallized plagioclase microlites and skeletal opaques (probably titanomagnetite). These flows were probably extruded rapidly from shallow magma chambers crystallizing augite. In contrast, medium-grained dykes contain abundant skeletal augite crystals (Fig. 7) that probably formed rapidly during intrusion. Unlike the Marmot Formation, phlogopite phenocrysts (Goodfellow et al, 1980) were not encountered in the Ogilvie Mountains volcanics.

Whole rock analyses of three mafic flows, a gabbroic dyke and a felsite sample (Table 10) show that the basalts are compositionally similar to intrusions of the Marmot Formation. Like these rocks, the felsite is high in Ba, Zr, and has an equivalent Nb/Y ratio. The mafic rocks have alkali-silica ratios near the alkalic-subalkalic boundary (Fig. 8a) and, if subalkalic, are a tholeiitic suite (Fig. 8b). Two of the samples are alkalic according to the criteria (1% K_2O, 35 ppm Rb and 300 ppm Ba) of Mahoney et al (1985). During alteration, major elements normally used to determine the alkalinity may be mobile such that the original nature of these rocks is obscured. Alternatively, immobile minor and trace element ratios may also be used to determine whether the volcanics were alkalic (Fig. 8c).

Volcanic rocks may indicate something of the character of underlying crust and the regional tectonic setting at the time of eruption. Specifically, was Cambro-Ordovician volcanism related to continental extension or to separation and production of volcanic crust? Relative to mid-oceanic ridge basalt (MORB), these samples are low in silica, have low MgO/Mgo and FeO^{tot} (.35 - .45), and have relatively high TiO_2, P_2O_5 and Zr. On discriminant diagrams that are used

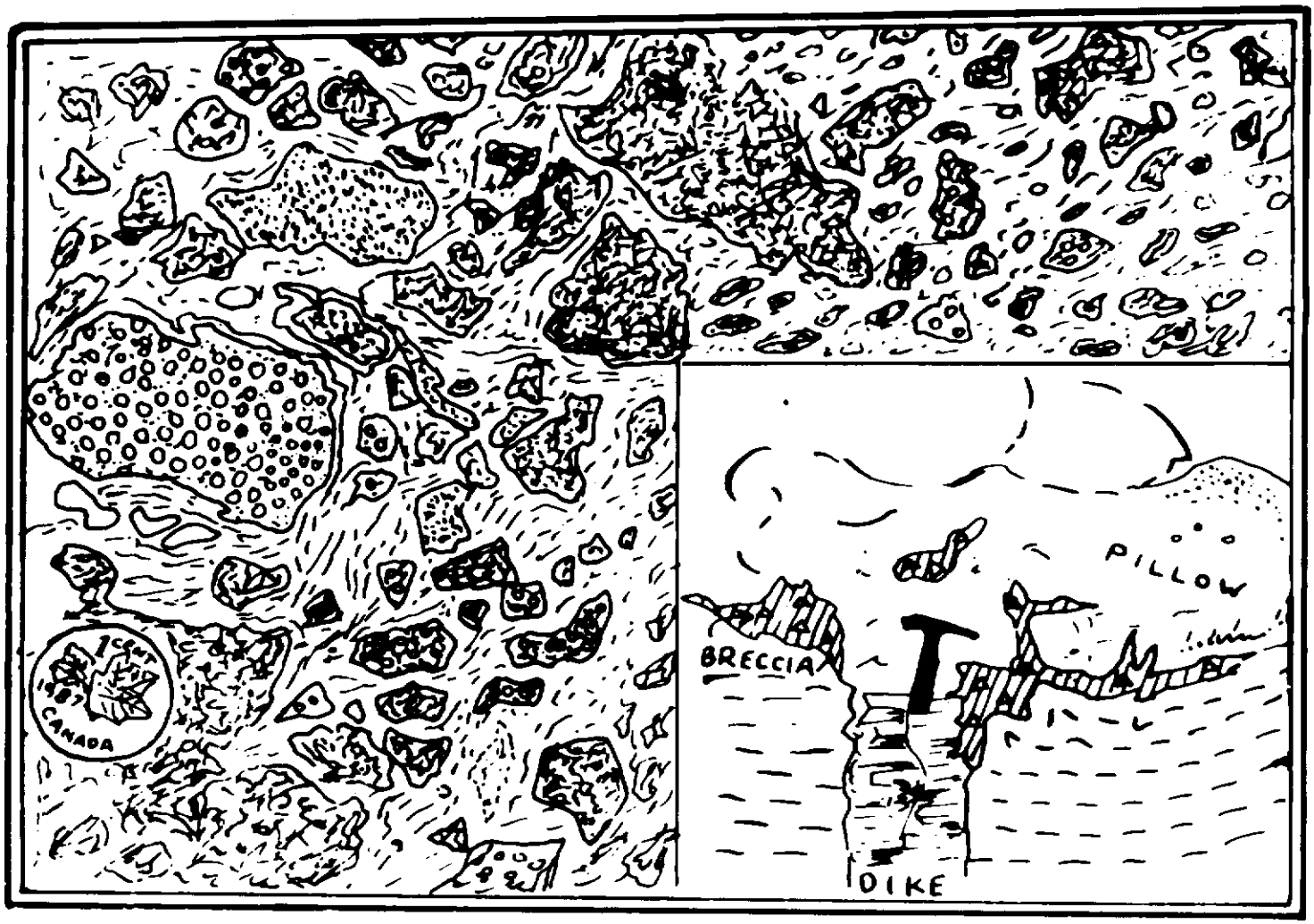

Figure 5. Texture and setting of breccia related to breaching dykes. Fragments are vesicular and non-stratified, but show foliation suggesting flowage. Sketch from photographs, at locality A.

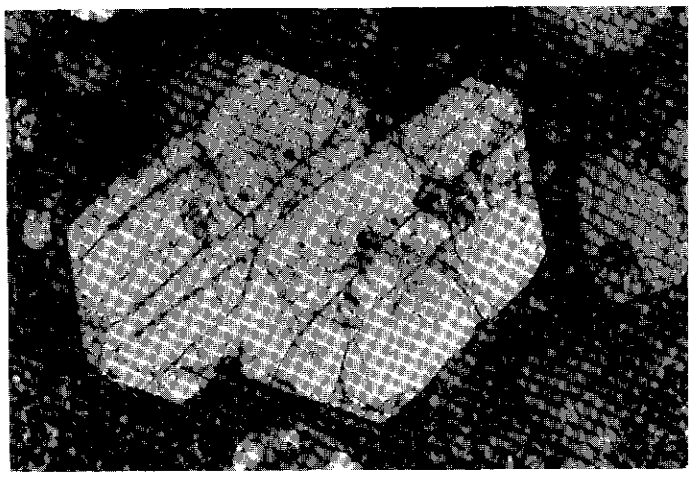

Figure 6. Basal basalt flow contains large, well formed augite phenocrysts (this one 2 mm long), smaller zoned phenocrysts (possibly orthopyroxene, replaced by calcite) in a groundmass of plagioclase microlites, interstitial opaques with sphene overgrowths. Plane- polarized light. From locality M.

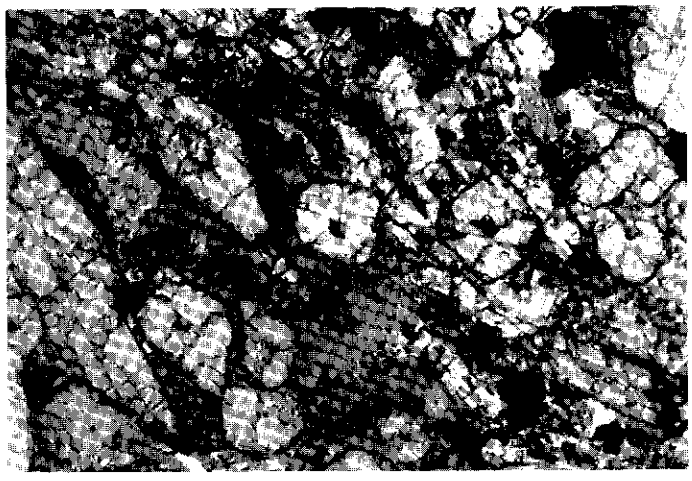

Figure 7. Gabbroic dyke containing hollow, spindle-shaped and skeletal titaniferous augite crystals, with decayed plagioclase (whitish), interstitial chlorite (grey) and opaques. Largest crystal at left edge is 1.2 mm long. Plane polarized light. From east of Dempster Highway (km 82), at location of sample #3.

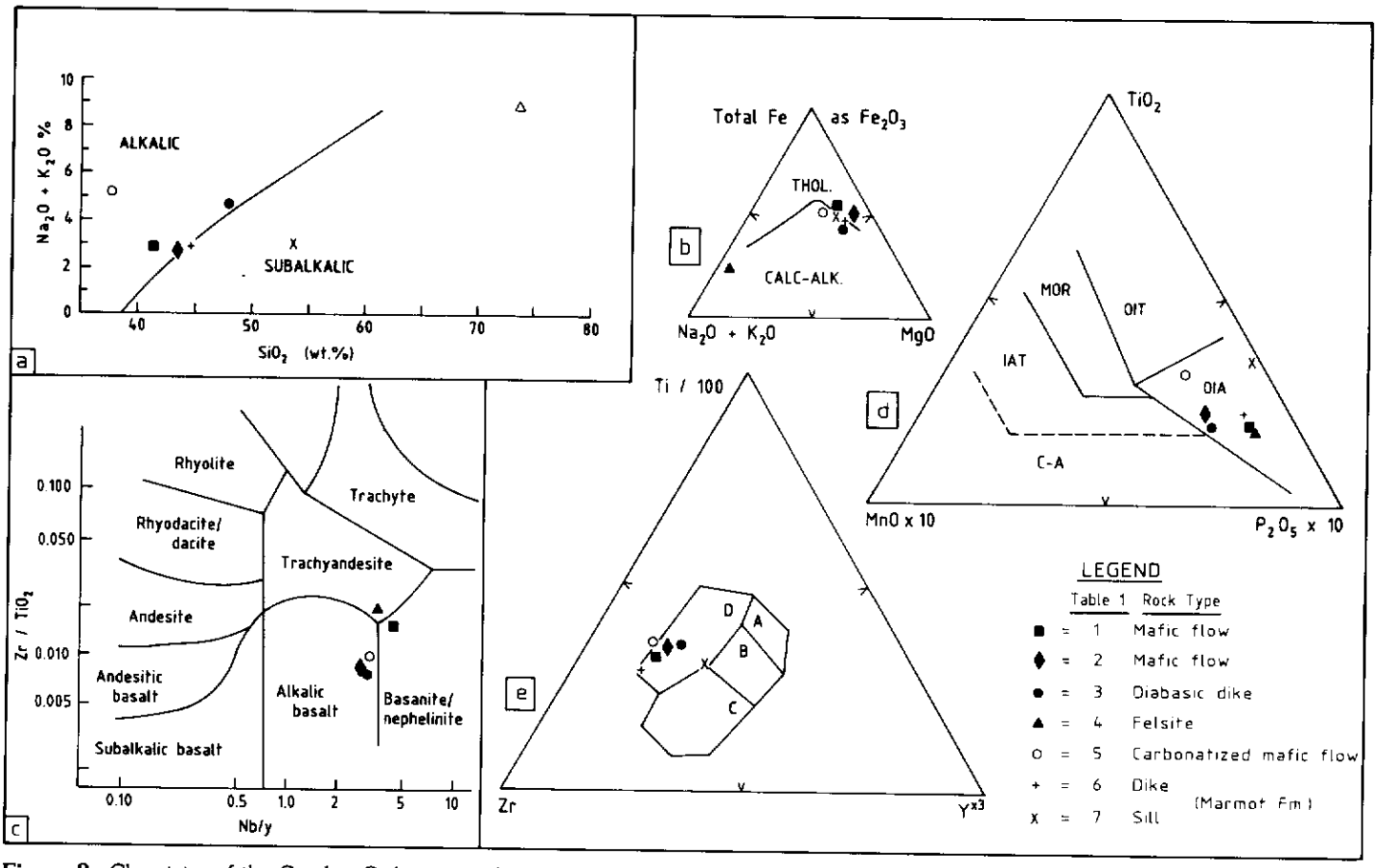

Figure 8. Chemistry of the Cambro-Ordovician volcanics: a) Total alkali- silica diagram, with dividing line from Irvine and Baragar, 1971; b) A-F-M diagram for subalkalic rocks: boundary between tholeiitic and calc-alkalic from Irvine and Baragar (1971); c) Fractionation ($Zr-TiO_2$) and differentiation (Nb/Y) ratio diagram devised by Winchester and Floyd (1977); d) Mn-Ti-P discriminant diagram (Mullen, 1983): OIA = oceanic island alkalic; OIT = Oceanic island tholeiitic; MORB = mid-oceanic ridge basalt; IAT = Island arc tholeiite; C-A = calc-alkalic basalt; e) Zr-Ti-Y diagram for basalts (Pearce and Cann, 1975); A+B = low K tholeiite; B = Ocean floor basalts; C+B = calc-alkalic basalts, and D = within plate basalts.

to indicate paleo-tectonic setting, these rocks plot in the "oceanic island alkalic" and "intraplate" fields (Figs. 8d and 8e), which reflect their high P_2O_5 and low Y concentrations, relative to other types of basaltic. Intrusions from the Marmot Formation also plot in similar fields.

It is not possible to conclude whether the crust was thinned to the point of developing oceanic characteristics, but the high Nb and P_2O_5 relative to oceanic islands, such as Hawaii (Table 1), imply a crustal contribution (see Dupuy and Dostal, 1983). They are, however, significantly different from average MORB composition, and it is unlikely that oceanic crust was produced in the Selwyn Basin.

MINERALIZATION

The volcanics show little economic mineral potential. Sulphide showings are sparse, few quartz veins were located, and there is no evidence of large hydrothermal systems (such as zoned alteration or epidote-encrusted fissures) that might indicate that sulphides precipitated on the ancient sea floor.

The most likely areas are limonitized and thermally metamorphosed basalt near the Cretaceous and other intrusions. Siderite rosettes, azurite and malachite in comb quartz and 1 cm pockets of chalcopyrite and galena occur about 500 m west of the felsite intrusion (locality H). Possible freibergite occurs in the vicinity (G. Carlson, pers. comm., 1979).

At locality J, about 700 m from the northwest edge of Deadman Pluton, hornfelsed volcanics contain marcasite and ferroactinolite (?) and pyrrhotite in fractures. The mineral assemblage and setting resembles mineralization at THOR Occurrence on Antimony Mountain (INAC 1981, p. 289). The thermal aureoles developed in Hyland Group grit and argillite are comparatively barren, but could contain mineralization where they intersect carbonate-rich volcanics. West of Deadman Pluton the fused volcanics are non-vesicular and contain little calcite; however, any included limestone pod may be highly mineralized.

The high barium content, particularly of the felsite (Table 1) suggests that the volcanics may have contributed to stratabound barite in the overlying Devonian black shales (e.g. REIN; INAC, 1981) several kilometres north in the East Blackstone River drainage.

DISCUSSION

The Cambro-Ordovician volcanics, fed by the spaced, subparallel gabbroic dykes, reflect minor extension. Centres of volcanic activity are numerous, small and therefore were probably short-lived. Some developed into volcanic islands, and the preservation of subaerial and submarine facies demonstrates rapid subsidence and tectonic instability. All these features suggest that Selwyn Basin volcanism was not related to a "hot spot", but was the result of magma seepage through fractures in crust under extension.

The volcanic centres may have extruded close to the northwest axis of the Selwyn Basin, a setting similar to the Marmot Formation, but were displaced toward the north side by thrust faults.

The older Mount Harper Volcanic Complex occupies a smaller extensional basin in the shelf succession (Fig. 1). It consists mostly of subalkalic pillows and breccias, with lesser subaerially erupted tholeiitic basalt and rhyolite (Roots, 1986). In outcrop, however, these rocks indicate similar depositional environments to the Cambro-Ordovician suite. Mount Harper Complex reflects a brief extension event on thick continental crust; in contrast, the alkalic Cambro-Ordovician volcanics developed on thinned crust. These two occurrences illustrate the variety of igneous response to periodic extension along the continental margin of ancient North America.

ACKNOWLEDGEMENTS

This project was initiated by Bob Thompson, promoted by Grant Abbott and jointly supported by the Geology Section (Indian and Northern Affairs Canada) and the Geological Survey of Canada. I am grateful to Bob Thompson for his input on most of the ideas presented here, and his model of episodic extension. Errors remain my responsibility. Robin Roots provided cheerful assistance and superior logistic ability in the field.

Table 1

		Ogilvie Mtns.	basalt		Marmot.	Fm.	OIB	Felsite
	1	2	3	5	6	7	8	4
SiO_2	41.20	42.80	46.60	30.70	50.00	41.80	49.36	73.18
Al_2O_3	13.60	11.90	13.50	9.20	15.00	11.60	13.94	12.70
TiO_2	3.47	2.18	1.74	3.58	2.00	3.40	2.50	0.38
Fe_2O_3	12.00	13.00	11.70	11.40	9.30	9.30	11.40	2.40
MgO	7.49	10.70	7.37	6.34	8.00	7.30	8.49	0.41
MnO	0.19	0.18	0.18	0.20	0.10	0.03	0.16	0.02
CaO	14.60	11.40	9.24	13.20	1.00	7.50	10.30	0.25
Na_2O	1.07	1.13	4.22	4.33	0.0	0.0	2.13	0.82
K_2O	1.92	1.69	0.15	0.15	3.00	3.00	3.80	7.65
P_2O_5	1.26	0.57	0.56	0.53	0.60	0.76	0.26	0.14
Cr_2O_3	0.01	0.05	0.02	0.01	0.03	0.05	n.r.	0.01
H_2O	3.10	3.20	3.00	0.60	5.90	5.20	n.r.	0.60
CO_2	0.10	0.68	0.92	20.00	0.60	5.00	n.r.	0.0
Total	**99.40**	**99.60**	**99.20**	**98.10**	**95.80**	**96.85**	**99.03**	**99.70**
Ba	260	570	140	110	†4000	17400	135	2330
Nb	140	60	50	110	n.r.	n.r.	19	30
Rb	90	40	20	30	56	97	14	310
Sr	680	210	290	1250	398	804	375	
Y	30	20	20	20	45	70	27	80
Zr	370	190	140	340	277	351	180	320

Note: samples 1, 2, 5 are mafic flows, *3 is medium-grained dyke and *4 is felsite. Their locations are shown on Figure 1.
Samples 6 and 7 are a dyke and sill from Marmot Formation of Misty Creek Embayment (Goodfellow et al (1980).
Sample *8 represents oceanic island alkalic rocks: major elements are the average of 181 shield-forming tholeiitic flows from Hawaii (Macdonald and Katsura, 1964), minor elements from BHVO-1 standard (Abbey, 1983).
Samples from Ogilvie Mountains were analyzed by XRF; H_2O and CO_2 by wet chemical (X-Ray Assay Laboratories, Toronto). Precision quoted by laboratory is: ± 0.10% major oxides; ± 10 ppm trace elements; n.r. = not reported.

REFERENCES

ABBY, S., 1983. Studies in "Standard samples" of silicate rocks and minerals, 1969-1982; Geological Survey of Canada, Paper 83-15.

ANDERSON, R.G., 1987. Plutonic rocks in the Dawson map-area, Yukon Territory; Geol. Surv. Can. Paper 87-1a, p. 689-697.

CECILE, M.P., 1982. The Lower Paleozoic Misty Creek Embayment, Selwyn Basin, Yukon and Northwest Territories; Geological Survey Of Canada Bull., 335, 78 p.

DUPUY, C. and DOSTAL, J., 1983. Trace element geochemistry of some continental tholeiites; Earth and Planetary Science Letters, Vol. 67, p. 61-69.

GOODFELLOW, W.D., JONASSON, I.R. and CECILE, M.P., 1980. Nahanni Integrated Multidisciplinary Pilot Project. Geochemical studies part 1: Geochemistry and mineralogy of shales, cherts carbonates and volcanic rocks from the Road River Formation, Misty Creek Embayment, Northwest Territories; in Current Research, Geological Survey Of Canada, Paper 80-1B, p. 149-161.

GREEN, L.H., 1972. Geology of Nash Creek, Larson Creek and Dawson map-areas, Yukon Territory; Geological Survey of Canada, Memoir 364, 157 p.

HOFMANN, H.J. and CECILE, M.P., 1981. Occurrence of Oldhamia and other trace fossils in Lower Cambrian argillites, Niddery Lake map-area, Selwyn Mountains, Yukon Territory; Geological Survey of Canada Paper 81-1a, p. 281-290.

I.N.A.C., 1981. Summaries of assessment work, description of mineral properties and mineral claims staked in 1980; in Yukon Geology and Exploration 1979-80, Exploration and Geological Services Division, Yukon, Indian and Northern Affairs Canada, 364 p.

IRVINE, T.N. and BARAGAR, W.R.A., 1971. A guide to the chemical classification of common volcanic rocks; Canadian Journal Of Earth Science, Vol. 8, p. 523-548.

MACDONALD, G.A. and KATSURA, T. 1964. Chemical composition of Hawaiian lavas; Journal of Petrology, 5, p. 82-133.

MAHONEY, J.J., MACDOUGALL, J.D., LUGMAIR, J.W., GOPALAN, K., and KRISHNAMURTHY, P., 1985. Origin of contemporaneous tholeiitic and K-rich alkalic lavas: a case study from the northern Deccan Plateau, India; Earth and Planetary Science Letters, Vol. 72, p. 39-53.

MULLEN, E.D., 1983. MnO/TiO2/P2O5: a minor element discriminant for basaltic rocks of oceanic environments and its implications for petrogenesis; Earth Planetary Science Letters, Vol. 62, p. 53-62.

NOWLAN, G.S., NARBONNE, G.M. and FRITZ, W.H., 1985. Small shelly fossils and trace fossils near the Precambrian-Cambrian boundary in the Yukon Territory, Canada; Lethia, Vol. 18.

PEARCE, J.A. and CANN, J.R., 1973. Tectonic setting of basic volcanic rocks determined using trace element analyses; Earth and Planetary Science Letters, Vol 19, p. 290-300.

ROOTS, C.F., 1982. Ogilvie Mountains project, Yukon; Part B: Volcanic rocks in north-central Dawson map-area; Geological Survey of Canada, Paper 82-1A, p. 411-414.

ROOTS, C.F., 1986. Petrogenetic evolution of the Late Proterozoic Mount Harper Volcanic Complex, west central Yukon; Geological Association of Canada, Program with abstracts, Vol. 11, p. 121.

ROOTS, C.F. and MOORE, J.M., Jr., 1982. Proterozoic and early Paleozoic volcanism in the Ogilvie Mountains: an example from Mount Harper, west-central Yukon; in Yukon Exploration and Geology 1982, Indian and Northern Affairs Canada, Whitehorse, Yukon, p. 55-62.

TEMPELMAN-KLUIT, D.J., 1981. Geology and mineral deposits southern Yukon: in Yukon Geology and Exploration 1979-80, Exploration and Geological Services Division, Yukon, Indian and Northern Affairs Canada, p. 7-31.

THOMPSON, R.I., MERCIER, E. and ROOTS, C.F., in press. Extension and its influence on Canadian Cordilleran passive margin evolution; in M.P. Coward, J.F. Dewey and P.L. Hancock, (eds.), Continental extension tectonics, Geological Society of London, Special Publication.

THOMPSON, R.I. and ROOTS, C.F., 1982. Ogilvie Mountains project, Yukon: Part A: a new regional mapping program; Geological Survey of Canada, Paper 82-1A, p. 405- 411.

WINCHESTER, J.A. and FLOYD, P.A., 1977. Geochemical discrimination of different magma series and their differentiation products using immobile elements; Chemical Geology, Vol. 20, p. 325-343.

THE ORIGIN AND SETTING OF ANOMALOUS ARC MAGMATISM IN THE WRANGELL VOLCANIC BELT, SOUTHWEST YUKON

Thomas Skulski
Department of Geological Sciences,
McGill University
3450 University Street,
Montreal Quebec
H3A 2A7

SKULSKI, T., 1988. The origin and setting of anomalous arc magmatism in the Wrangell volcanic belt, southwest Yukon; in Yukon Geology, Vol. 2; Exploration and Geological Services Division, Yukon, Indian and Northern Affairs, Canada, p. 88 - 89

ABSTRACT

In the Wrangell Volcanic Belt (WVB) a northwesterly increase in volume of calc-alkaline versus transitional (sodic alkaline/calc-alkaline) magmatism is accompanied by a migration in the locus of magmatic activity. The space-time-composition relationships reflect oblique convergence between the North American and Pacific plates over the last 17.3 million years. Compositional- temporal trends are particularly well preserved in the four stages of volcanic stratigraphy in the St. Clare Creek field (17.3 - 6.5 Ma). Initially, alkaline olivine basalts, hawaiites and mugearites were erupted from small, isolated shield volcanoes in the axis of a continental molasse basin. The alkaline lavas were followed by an early stratovolcano stage of transitional trachybasalts and high-Fe basaltic trachyandesites, succeeded by basaltic trachyandesites, trachyandesites, trachytes, rhyolites and rare basaltic andesites. Widespread basaltic fissure eruptions dominated the third volcanic stage. The late stratovolcano stage consisted of renewed eruption of intermediate and felsic transitional lavas.

A systematic temporal-chemical relationship between early alkaline and younger transitional and calc-alkaline lavas in the St. Clare Group is illustrated by a decrease in FeO/MgO, Na+K/Si, Nb/Zr and Zr/Y, and an increase in Rb/Zr with increasing stratigraphic levels. Primitive basalts are non-primary and show variable degrees of fractionation between large ion lithophile (LILE) and high field strength element abundances.

A model is proposed in which the alkaline shield volcano and early stratovolcano stage magmas formed by progressive melting of a rising mantle diapir in response to local extension along the Duke River fault. Early Fe-rich magmas may have undergone clinopyroxene fractionation at high pressures, but most magmas appear to have differentiated in the near surface environment via fractional crystallization and local magma mixing. With the onset of Yakutat subduction, progressively larger amounts of slab-derived, LILE-enriched fluids metasomatised overlying peridotite, which in turn melted to form primitive, late-stratovolcano stage magmas.

RÉSUMÉ

Dans la zone volcanique de Wrangell (WVB), une augmentation, dans le sens nord-ouest, du volume de roches magmatiques calco-alcalines comparativement aux roches magmatiques transitionnelles (alcalines sodiques/calco-alcalines) a été accompagnée d'une migration du foyer d'activité magmatique. Les relations espace-temps-composition reflètent une convergence oblique des plaques nord-américaine et pacifique au cours des derniers 17,3 millions d'années. Les tendances du couple composition-temps sont particulièrement bien conservées dans les quatre étages stratigraphiques volcaniques du champ de St. Clare Creek (17,3-6,5 Ma). Initialement, des basaltes alcalins à olivine, des hawaiites et des mugéarites ont été émis au cours d'éruptions par de petits volcans isolés en bouclier dans l'axe d'un bassin molassique continental. Le dépôt des laves alcalines a été suivi d'une phase initiale d'émission par des stratovolcans, de trachybasaltes transitionnels et de trachyandésites basaltiques riches en Fe, auxquels ont succédé des trachyandésites basaltiques, des trachyandésites, des trachytes, des rhyolites et rarement, des andésites basaltiques. Des éruptions fissurales basaltiques étendues ont dominé la troisième phase volcanique. La phase stratovolcanique tardive s'est traduite par de nouvelles éruptions de laves transitionnelles, de caractère intermédiaire et felsique.

Dans le groupe de St. Clare, la relation systématique temps-composition chimique, qui existe entre les laves alcalines initiales et les laves plus récentes de caractère transitionnel et calco-alcalin, s'est traduite par une diminution des rapports FeO/MgO, Na + K/Si, Nb/Zr et Zr/Y et par une augmentation du rapport Rb/Zr à mesure que l'on remonte les niveaux stratigraphiques. Les basaltes primitifs sont non primaires, et montrent divers degrés de fractionnement entre les abondances des éléments lithophiles à ions de grande taille (LILE) et celles des éléments sidérophiles.

On propose un modèle dans lequel les magmas alcalins de volcans en bouclier et les magmas initiaux de l'étape stratovolcanique, se sont formés par fusion progressive d'un diapir ascendant du manteau, en réponse à une expansion locale de la croûte, le long de la faille de Duke River. Dans les magmas initiaux riches en Fe, a peut-être eu lieu une cristallisation fractionnée des clinopyroxènes sous des pressions élevées, mais il semble que la plupart des magmas se soient différenciés à proximité de la surface, par cristallisation fractionnée et mélange localisé des magmas. Avec le démarrage des processus de subduction de Yakutat, des quantités progressivement plus importantes de fluides dérivés de tranches de terrain et enrichis en éléments lithophiles, ont métasomatisé la péridotite sus-jacente, qui à son tour a fondu et formé des magmas primitifs d'étape strato-volcanique tardive.

INTRODUCTION

Magmas with sodic-alkaline affinity are a minor component of arc volcanism and are usually associated with specific Neogene tectonic settings. Examples of these settings include: lateral terminations of subduction zones undergoing hinge-faulting (e.g. Grenada, Lesser Antilles, DeLong et al., 1975); areas of subduction of fracture zones or other major linear features (e.g. Kanaga, Aleutians, DeLong et al., 1975) and intra-arc rifts (e.g. Penguin Island, South Shetlands, Weaver et al., 1979). Transitional magmas in these tectonic environments have been interpreted as mixtures of calc-alkaline (subduction- related) and sodic-alkaline (intra-plate) components (Pearce, 1982). However, such interpretation can be problematic since arc-terminating transform faults can be the sites of calc-alkaline, shoshonitic, boninitic or sodic-alkaline volcanism (Gill, 1982). Transitional magmatism may also postdate subduction by incorporating partial melts of peridotite metasomatised during a previous event (e.g., northern Azerbaijan, northwestern Iran, Riou et al., 1981).

The late Cenozoic Wrangell Volcanic Belt (WVB) in the northwestern Canadian Cordillera is an ideal study area for anomalous arc magmatism. The WVB occupies an area where late Cenozoic oblique convergence between the northeastern Pacific and North American plates has been accommodated both by transform fault movement and subduction of the Pacific plate beneath the North American continent. This study documents the occurrence and petrogenesis of sodic-alkaline, transitional and calc-alkaline volcanic rocks in the St. Clare Creek area of the WVB. A formal stratigraphy is proposed, and field, petrographic and chemical relationships are used to elucidate the volcanic and tectono-magmatic history of the lavas.

TECTONIC SETTING AND THE NATURE OF MAGMATISM WITHIN THE WVB

The 440 km long Wrangell Volcanic Belt includes a diverse group of volcanic rocks up to 2500 m thick, that range in age from 17.3 Ma to present. The Wrangell Volcanic Belt outcrops through parts of the Kluane and Icefield Ranges of the St. Elias Mountains in northwestern British Columbia and south-western Yukon, and Wrangell Mountains in southeastern Alaska (Fig. 1). In Alaska the WVB comprises mid-Tertiary to Recent Wrangell Lavas. These include mainly shield volcanoes covering older Tertiary lavas (Mendenhall, 1905; MacKevett, 1970; Deininger, 1972, MacKevett, 1978; Richter et al., 1976; Richter et al., 1979) and Nye, 1983). Recent studies in the St. Elias Mountains (Souther and Stanciu, 1975; Skulski and Francis, 1986) extend the usage of the term "Wrangell Lava" (Mendenhall, 1905) to include all volcanic rocks in the WVB. The term "St. Clare Group" (Miller, 1967) is used in, and redefined by the present study. The St. Clare Group is mid to late Tertiary and comprises outliers along the Duke River Fault (DRF, Fig. 1).

The volcanic rocks in the St. Clare Group are chemically classified in this study on the basis of total alkali/silica ratios using the TAS diagram of Le Bas et al (1986). The rocks are grouped by petrographic and chemical characteristics into four magma types. The calc-alkaline type plots in the subalkaline field and has nearly constant Fe/Mg ratios and modal orthophyroxene. Transitional magmas (sodic alkaline/calc-alkaline) lie within the alkaline field, are hypersthene- and rarely nepheline-normative, show moderate Fe-enrichment, and contain modal olivine over a wide range in silica content. Alkaline magmas lie within the alkaline field contain normative nepheline and shows significant Fe-enrichment. The high-Fe transitional magma type is hypersthene- and rarely nepheline-normative and is characterized by high Ti, Fe, Na, K, P and incompatible trace elements abundances over a narrow range of silica contents.

On the basis of stratigraphy, structure (Souther and Stanciu, 1975), chemical composition and petrography, the St. Clare Group includes four distinctive volcanic fields; from southeast to northwest, the Stanley Creek, Lava Creek, Nines and St. Clare Creek fields (Fig. 1). The Nines and Stanley Creek fields are composed of transitional volcanic rocks. The St. Clare Creek field contains dominantly transitional volcanic rocks with minor calc-alkaline and sodic-alkaline

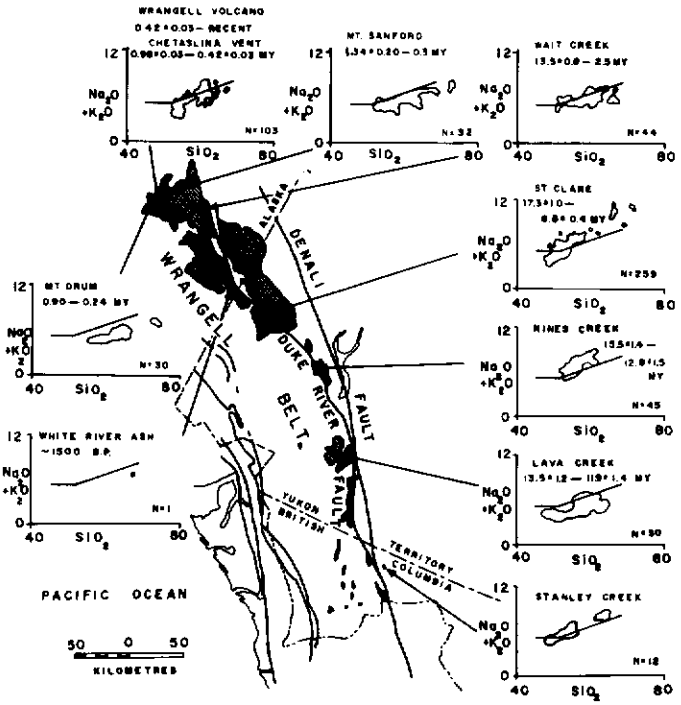

Figure 1. Outline of the Wrangell Volcanic Belt showing total alkali versus silica (TAS, wt%) variations for the various volcanic fields. Individual volcanoes are denoted by filled circles, the ruled pattern presents lavas and the black pattern sedimentary rocks. Chemical and K-Ar age data are from the following sources: Stanley, Lava, Nines and St Clare areas, this study, Francis and Ludden unpublished, and Souther and Armstrong, writ. comm. (1987); Wait Creek area, Deiniger (1972); Mt. Sanford area, Richter and Smith (1976); Wrangell area, Nye (1983); Mt. Drum area, Richter et al. (1979); White River Ash, Lerbekmo (1969). The dividing line on the TAS diagram separates alkaline from subalkaline compositions (LeBas et al., 1986). Chemical analyses in this study were obtained by X-ray fluorescence spectrometry of whole rock samples. For further details on methodology, accuracy and precision see Eiche et al. (1987).

lavas. The Lava Creek field is composed of calc-alkaline volcanic rocks with lesser transitional and sodic-alkaline lavas. Post-volcanic deformation in the Stanley, Lava and Nines Creek fields is restricted to minor faulting and tilting. In the St. Clare Creek field, folding and faulting are intense in the central part of the field, which overlies the DRF (Souther and Stanciu, 1975 and Skulski and Francis, 1986). The volume and thickness of the St. Clare Group increases from the Stanley Creek field in the southeast to the St. Clare Creek field in the northwest. The ages of the youngest St. Clare Group rocks decrease from the Lava Creek field (11.9 +/- 1.4 Ma), through the Nines (12.8 +/- 1.5 Ma) and St. Clare Creek fields (6.5 +/- 0.4 Ma, minimum age) to the Recent Wrangell Lavas in Alaska (Souther and Armstrong writ. comm., 1987).

Prior to the onset of St. Clare Group volcanism (17.3 Ma in the St. Clare Creek field, Souther and Armstrong, writ. comm., 1987), continental molasse sediments of the Amphitheatre Formation were deposited in northwest- trending, fault-controlled, fluvial basins such as those along the DRF (Eisbacher and Hopkins, 1977). This dextral strike-slip fault juxtaposed Paleozoic rocks of the Alexander terrane in the south, against Permo-Triassic rocks of the Wrangellia terrane in the north during Late Mesozoic time (Campbell and Dodds, 1978). Displacement along the DRF continued into the early phases of St. Clare Group volcanism (Souther and Stanciu, 1975). The Cenozoic tectonic stress orientation in the southwest Yukon is dominated by north-trending principal, and east-trending minor stress axes (Eisbacher and Hopkins, 1977). This stress regime is consistent with the northerly strikes and steep dips (75°) of mafic dykes,

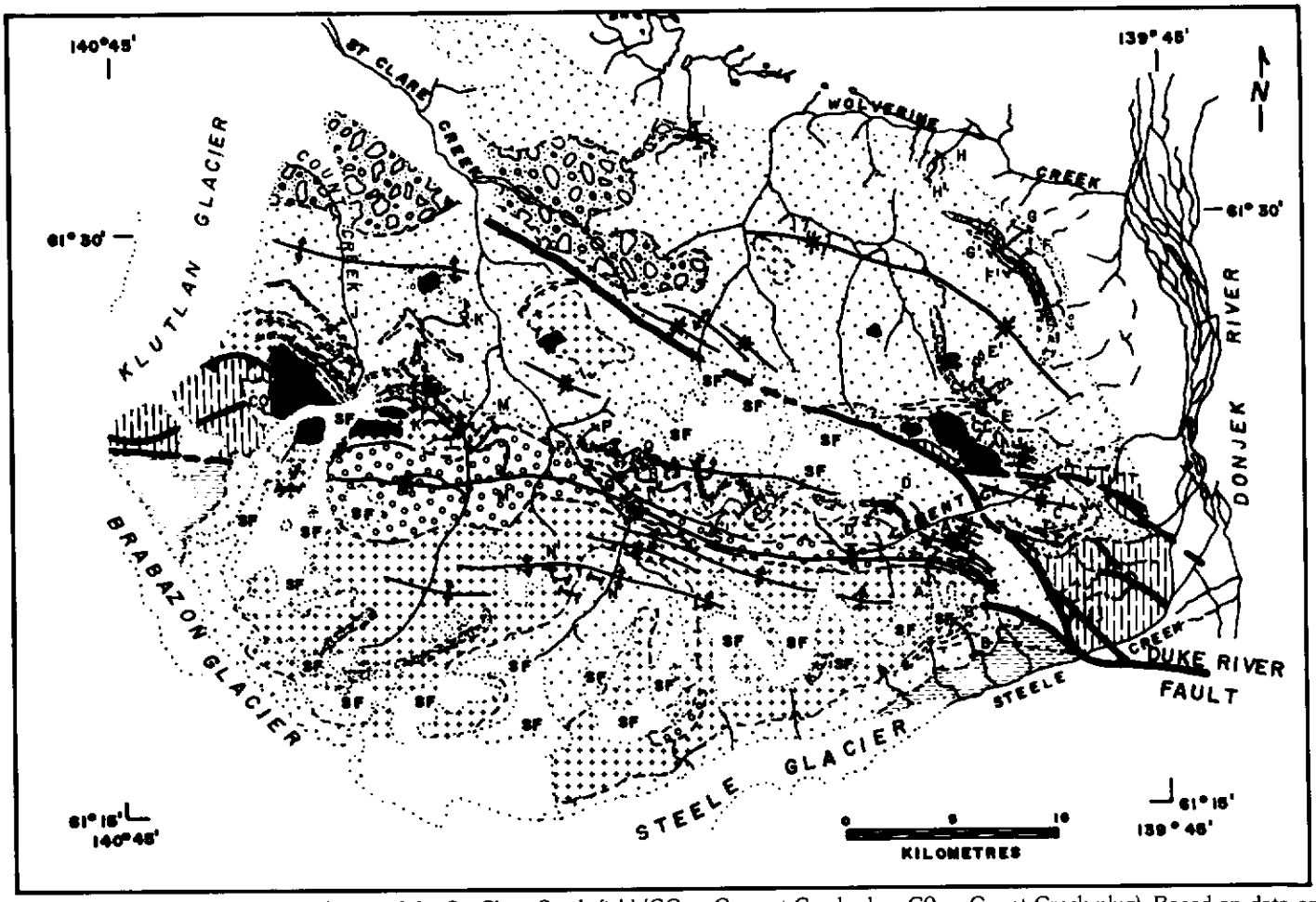

Figure 2. Generalized geological map of the St. Clare Creek field (CC = Cement Creek plug, C0 = Count Creek plug). Based on data collected during this study and by Souther and Stanciu (1975).

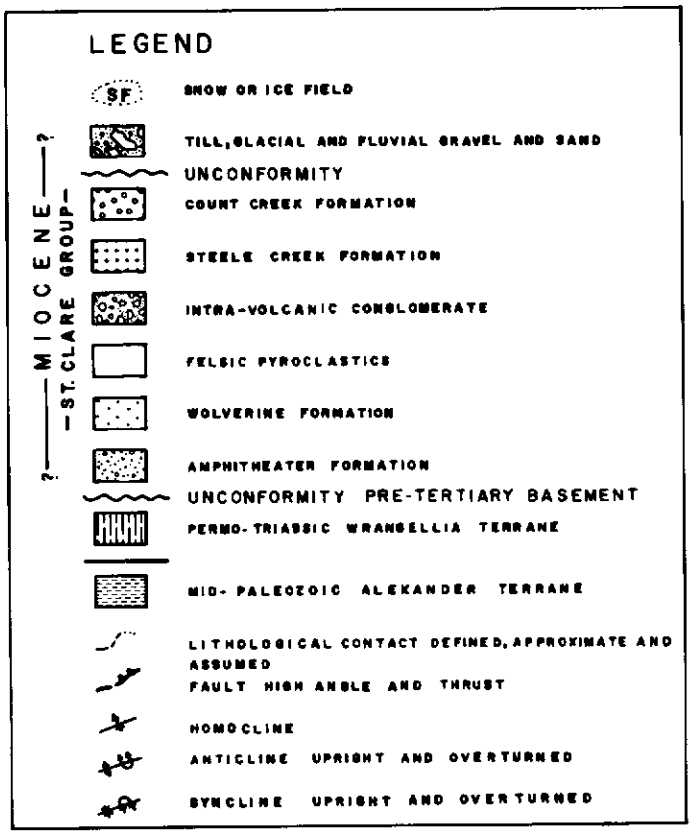

and east-trending fold hinges in the St. Clare Creek field (Fig. 2). TThe youngest deformed lavas in the WVB are 1.6 Ma (White River valley, Denton and Armstrong, 1969).

Calc-alkaline volcanism in the WVB began about 13.5 Ma, over a 300 km strike length from Wait Creek (southeast Alaska) to the Lava Creek field (southwest Yukon). This volcanic activity appears to have been short-lived in the southeastern parts of the WVB (1.6 million years in the Lava Creek field) but has extended to the Recent in Alaska (Mendenhall, 1905). Calc- alkaline magmatism in the WVB is related to the north-dipping subduction of Pacific oceanic lithosphere at the leading-edge of the composite oceanic- continental Yakutat terrane (Lahr et al., 1983; Bruns, 1983; and Nye, 1983). Stephens et al. (1984) have described NNE-dipping Benioff Zone beneath southeastern Alaska.

FIELD RELATIONSHIPS IN THE ST. CLARE CREEK FIELD

Extrusive and Volcanoclastic Rocks

The extreme stratigraphic relief (up to 2650 m), large surface area (1400 km²), and spectrum of magma types of the St. Clare Creek field are well suited for an investigation of temporal magmatic variations. Previous geological descriptions of the area include Muller (1967), Souther and Stanciu (1975) and Skulski and Francis (1986). This paper subdivides the St. Clare Group, in the St. Clare Creek field, into the Wolverine, Steele Creek and Count Creek formations.

The Wolverine Formation includes a basal sequence of extrabasinal sediments, alkaline lavas, and plagioclase-phyric (15%, up to 1 cm) Fe-rich transitional lavas; and an upper sequence of transitional lavas and interbedded epiclastic and felsic pyroclastic rocks

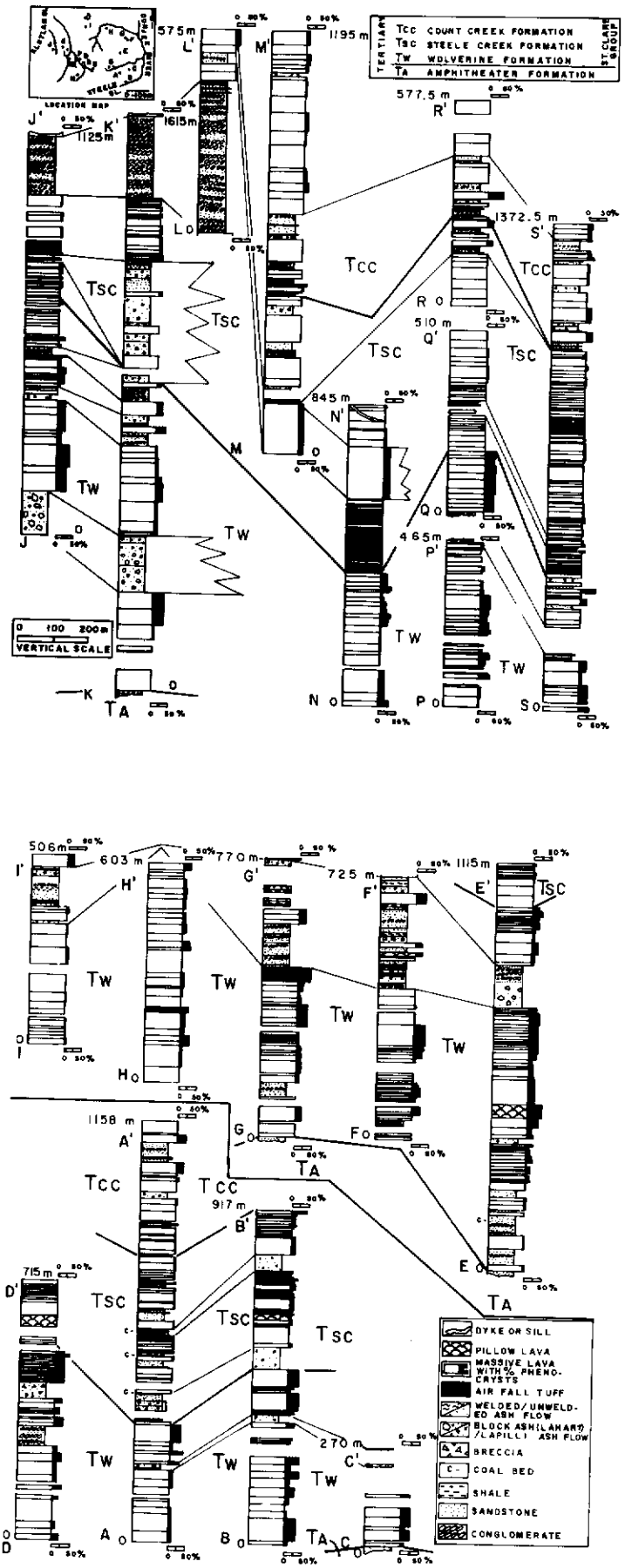

Figure 3. Stratigraphic sections of the St. Clare Creek field showing lithological types, phenocryst abundances, and stratigraphic markers and boundaries.

(locally welded trachytes, rhyolites and comendites). Calc-alkaline lavas occur near the top of the formation. The Wolverine Formation rests unconformably on Paleozoic rocks in the south, where it is relatively thin, and conformably on the Amphitheatre Formation in the central and northern parts of the field, where it attains maximum thickness (Figs. 3 and 4). The type section is 968 m thick (section E-E', Figs. 2. 3 and 4) and overlies the Amphitheatre Formation. The lower part consists of thin, massive, flint-like lava flows of aphyric hawaiite, mugearite, and alkaline olivine basalt, interbedded with feldspathic sandstones, siltstones, conglomerates and thin lignite seams. The early lavas are overlain by closely-stacked, thin aa flows of basaltic trachyandesite, altered felsic pyroclastic rocks, and thin units of flow-banded rhyolite. Overlying porphyritic, Fe-rich basaltic trachyandesite lava flows are thick and pillowed near the base, and closely-stacked and thin near the top where they include trachyandesite flows. The top of the section consists of thin flows of basaltic andesite, basaltic trachyandesite and trachyandesite, and a thick, coarse-grained volcaniclastic deposit.

The Steele Creek Formation is characterized by a large proportion (90%) of basaltic lava flows either interbedded with basaltic trachyandesites, dacites and volcaniclastic rocks, or comprise thick successions of thin, individual lava flows (Figs. 3 and 4). The type section is 468 m thick (section A-A', Figs. 2, 3 and 4). Basal units consist of amygdaloidal (calcite) transitional basalts which have rusty-brown weathered surfaces and typically occur as thin, closely-stacked, pahoehoe flows. Stacks of 5-10 lava flows are interbedded with epiclastic sandstones, siltstones, conglomerates, thin lignite beds, and felsic pyroclastic flow- and fall-deposits.

The Count Creek Formation contains the youngest lavas in the St. Clare Group and is distinguished by thick flows of intermediate and evolved transitional lavas with low abundances (0-20%) of small (1 cm plagioclase) phenocrysts. The type section is 752 m thick (Section M-M', Figs. 2, 3 and 4). The lower part consists of cyclic epiclastic sandstones and conglomerates, with felsic tuffs (flow and fall) interbedded with basaltic trachyandesite and trachyandesite lava flows. The upper units consist of thick, basaltic trachyandesite, trachyandesite and trachyte lava flows, and a thin ash-flow bed near the top.

The relative volumes of rock types found in the St. Clare Creek field have been estimated assuming flat-lying stratigraphy and data from sections E-E' (Wolverine Fm.), M-M' (Count Creek Fm.), and Q-Q' and R-R' (Steele Creek Fm.). The volcanic pile consists of approximately 80% lavas and 20% volcaniclastic rocks. About 85% of the lavas are transitional, and 15% consist of equal proportions of alkaline and Fe-rich transitional types with less than 1% calc-alkaline lava. The transitional type consists of 30% basalts, 50% basaltic trachyandesites, 10% trachyandesites and 10% trachyte/rhyolite (excluding felsic pyroclastic and intrusive rocks).

Intrusive Rocks

The most prominent intrusive rocks in the St Clare Creek field are large felsic plugs which outcrop in the east-central and west-central parts of the area (Fig. 2). The eastern intrusions comprise the polyphase, trachytic and rhyolitic Cement Creek plug (13.6 +/- 1.2 Ma, Souther and Armstrong writ. comm., 1987) and two smaller trachyte plugs. In the west, the Count Creek plug is an aplite of 6.5 +/- 0.4 Ma (minimum age, Souther and Armstrong, writ. comm., 1987). The roof of the Count Creek plug consists of brecciated and bleached volcanic rocks and aplite which are cut by east- and north-trending mafic dykes (up to 3 m wide). The oldest dykes are oxidized and carbonatized, whereas younger dykes have thick (30 cm) vitrophyric chilled margins. A small dyke-like intrusion immediately north of this roof zone is composed of porphyritic trachyte and contains numerous, partly resorbed xenoliths of volcanic rock. A small plug just east of St Clare Creek is a porphyritic andesite. Basaltic sills and north-trending dykes are common in the ridges underlain by the Steele Creek Formation between the southeast and southwest forks of St Clare Creek (Fig. 2). The sills are up to 6 m in width, have vitrophyric chilled margins, and contain vesicles and small calcite amygdules. A 3.7 km long, 150 m thick, composite gabbro, pyroxenite sill is exposed in the Cement Creek valley.

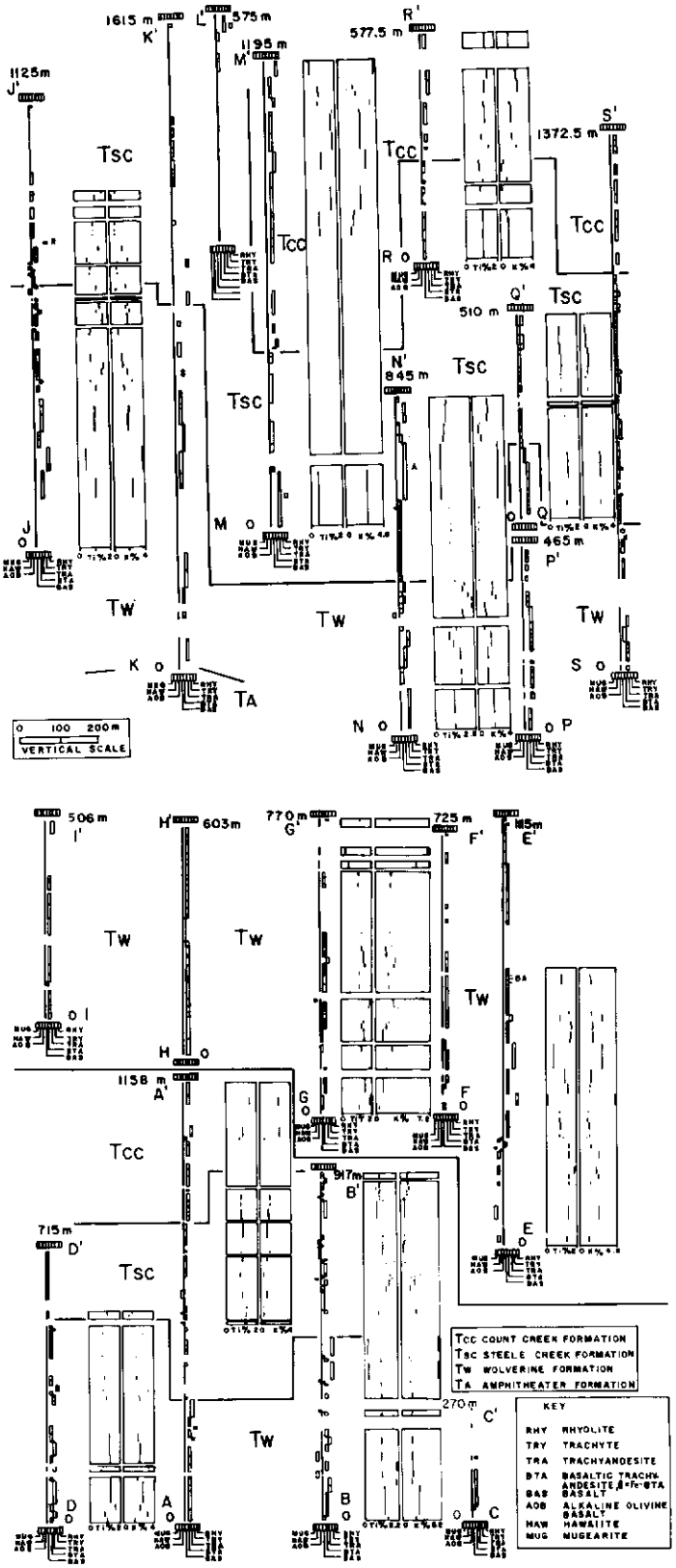

Figure 4. Chemical-stratigraphic sections showing rock types and Ti and K abundances in cation units. Calc-alkaline rocks are labelled as follows: BA = basaltic andesite, A = andesite, D = dacite; and R = rhyolite.

PETROGRAPHY OF THE LAVAS

Alteration of lava flows is minor and is characterized by subzeolite assemblages. Glass in basaltic rocks is replaced by clinopyroxene spherulites and/or carbonate. The alteration products of olivine include aggregates of carbonate, goethite, hematite, celadonite or iddingsite. Incipient oxidation of titanomagnetite results in ilmenite exsolution lamellae and in extreme cases causes replacement by hematite or goethite. Biotite and hornblende are commonly replaced by hematite. Plagioclase is rarely altered, but may be replaced by patchy carbonate or clay minerals. Clinopyroxene is unaltered in these rocks.

The alkaline magma type includes alkaline olivine basalts, hawaiites and mugearites. The alkaline olivine basalts are porphyritic to seriate rocks with phenocrysts of olivine (Fo 82-88), zoned plagioclase and titanomagnetite in a trachytic groundmass of plagioclase, olivine, an opaque phase and clinopyroxene (Figs. 3 and 4 for phenocryst abundance). Seriate varieties have a fine-grained ophitic texture with euhedral olivine and plagioclase chadacrysts in anhedral clinopyroxene oikocrysts. The hawaiites are porphyritic to seriate rocks with phenocrysts (trace - 15%) of olivine Fo 71-79), plagioclase (An-30 up to 1.5 cm), titanomagnetite and ilmenite, and clinopyroxene (with hourglass twinning) in a trachytic groundmass of plagioclase, clinopyroxene, olivine and an opaque phase. Mugearites are typically aphyric, with microphenocrysts of olivine (Fo 53-55), plagioclase, titanomagnetite and ilmenite and minor amounts of hornblende and biotite, in a trachytic groundmass of plagioclase and an opaque phase. One sample of mugearite contains black melt schlieren with abundant fine-grained opaque minerals in the groundmass. The rock also contains resorbed orthoclase xenocrysts mantled by fine-grained reaction products.

The Fe-rich transitional magma type includes trachybasalts and Fe-rich basaltic trachyandesites. The trachybasalts are porphyritic (trace - 20%) with phenocrysts of olivine, plagioclase (up to 8 mm), titanomagnetite and clinopyroxene, in a trachytic groundmass of similar mineralogy. Clinopyroxene phenocrysts commonly exhibit corroded rims and occasional hourglass twinning. The Fe-rich basaltic trachyandesites contain phenocrysts (trace - 30%) of olivine, plagioclase (up to 1 cm), titanomagnetite and clinopyroxene, in a trachytic groundmass of similar composition. One sample of Fe-rich basaltic trachyandesite near the top of section E-E1 contains embayed clinopyroxene phenocrysts with resorbed cores of orthopyroxene.

The transitional magma type comprises basalts, basaltic trachyandesites, trachytes, rhyolites and comendites. Basalts are either porphyritic, seriate or equigranular. Porphyritic varieties contain phenocrysts of olivine (Fo 85-86), plagioclase (An 67-72) and occasionally titanomagnetite, in an intergranular to intersertal groundmass of olivine (Fo 62-75), plagioclase (An-55), clinopyroxene, an opaque phase and glass. A group of basalts at the base of section G-G^1 contain resorbed and zoned clinopyroxene phenocrysts rimmed by fine-grained reaction products (rarely olivine). Equigranular basalts contain euhedral olivine within subophitic plagioclase, clinop- pyroxene and magnetite. Basaltic trachyandesites contain phenocrysts (0-40%, generally high) of olivine (Fo 81-84), zoned plagioclase (An 58-73), titano- magnetite, and subrounded clinopyroxene (first appearance of clinopyroxene, Wo:En:Fs 38:52:9) in a trachytic groundmass of plagioclase (An 49-56), clinopyroxene (Wo:En:Fs 35:56:9), opaque phase, and occasional olivine (Fo 64) and glass.

Trachyandesites contain phenocrysts (trace - 40%) of olivine, plagioclase (An 32-51), titanomagnetite, clinopyroxene (Wo:En:Fs -35:49:16), and rarely olivine, ilmenite, hornblende and apatite. The phenocrysts are contained in a fine-grained trachytic groundmass of feldspar, an opaque phase and local clinopyroxene. Clinopyroxene phenocrysts are commonly subrounded to embayed and sometimes exhibit cores of resorbed othopyroxene (Wo:En:Fs -2:72:30). Resorbed and sieve-textured plagioclase phenocrysts also occur in the orthopyroxene-bearing rocks. In the more evolved lavas, clinopyroxene is occasionally present as resorbed cores in hornblende. Trachytes, rhyolites and comendites usually occur as intrusions and pyroclastic deposits (comendites only outcrop in the latter form). These evolved rocks have highly variable mineralogy, and contain phenocrysts of olivine (rare in the most primitive trachytes), plagioclase (An 46 in trachytre, An:Ab:Or -11:81:8 in comendite), and occasional magnetite, clinopyroxene (in evolved trachyte, Wo:En:Fs -43:12:45), hornblende, biotite, anorthoclase (An:Ab:Or -4:82:13), apatite and zircon. Anorthoclase appears to be restricted

to sills and plugs, where it forms either phenocrysts or rims around plagioclase. The groundmass of more evolved rocks is trachytic and consists of feldspar microlites, fine-grained opaques, and quartz.

The calc-alkaline magma type includes basaltic andesites, andesites, dacites and rhyolites. The basaltic andesites contain phenocrysts of subrounded orthopyroxene, plagioclase and occasional olivine (rounded), magnetite and clinopyroxene, in a very fine-grained groundmass of clinopyroxene, an opaque phase and plagioclase. Andesites and dacites contain phenocrysts of orthopyroxene, plagioclase, titanomagnetite, hornblende and biotite in a fine trachytic groundmass of feldspar and an opaque mineral. Calc-alkaline rhyolites (including aplite) contain microphenocrysts of plagioclase and quartz in a very fine trachytic groundmass of feldspar microlites.

CHEMISTRY

The St Clare Creek field lavas comprise a chemical continuum between magmas of alkaline and calc-alkaline affinities, and exhibit systematic compositional variation with stratigraphic level. A concomitant decrease in slope in SiO_2 versus FeO/MgO (Fig. 5 in Skulski and Francis, 1986) and SiO_2 versus Na_2O+K_2O compositional space (Figs. 1 and 5) progresses from early erupted alkaline lavas through high-Fe transitional, transitional and calc- alkaline type lavas. Petrographically similar transitional lavas in the Wolverine and Count Creek formations have overlapping chemical abundances in terms of Si-Mg-Fe-Na-K, although the former contain some Fe-, Na- and K- rich differentiates. Variations between the two formations of high field strength (HFSE) and large ion lithophile element (LILE) abundances are more pronounced. The St Clare Group is enriched in LILE relative to HFSE (Figs. 6 and 7), and Rb and Y increase and Nb decreases with stratigraphic height. These features are illustrated by average respective values of the ratios of Rb/Ba, Rb/Nb, Nb/Zr, Nb/Y and Zr/Y in the Wolverine Formation: alkaline 0.034, 0.79, 0.097, 0.75 and 7.74; high-Fe transitional 0.043, 0.98, 0.087, 0.59 and 6.86; transitional 0.052, 1.48, 0.076, 0.55 and 7.16; the Steele Creek Formation: 0.041, 0.91, 0.072, 0.41 and 5.67; and the Count Creek Formation: 0.70, 2.52, 0.062, 0.39 and 6.40, respectively.

Primitive Magmatic Compositions

The chemical differences between basaltic lava types are far less apparent than difference between more evolved lava types (Fig. 5). However, some of the least evolved rocks display chemical characteristics of significance to the derivation of the various magma compositions. The most primitive alkaline lava, from the base of section E-E' (Fig. 4, TS-15-85) is an olivine (Fo 82-88) phyric, plagioclase and titano magnetite microphyric alkaline olivine basalt. Magma of this composition is probably non-primary since the Mg# ($Mg/Mg+Fe^{2+}$ =0.60-0.64 for XFe^{3+} =0-0.15) and Ni abundances (98 ppm) are too low to be in equilibrium with upper mantle peridotite (cf. Frey et al., 1978). The presence of normally-zoned, olivine phenocrysts with core compositions as magnesian as Fo 88 indicates that a TS-15-85 magma may have been derived by olivine (+/- plagioclase and titanomagnetite) fractionation from potential primary magma with an Mg# of 0.68 (assuming XFe^{3+} =0, cf. Roeder and Emslie, 1970).

The only other basalts with comparable and higher Mg# in the St Clare Creek field belong to the transitional series, of which the olivine (Fo 85-86) + plagioclase (An 67-72) phyric basalt (TS-101-85) is the best preserved and most magnesian example. However, a magma of TS-101-85 composition is probably also non-primary as suggested by a low Ni abundance (42 ppm). Trachybasalts are almost certainly non-primary and are likely to be released to more primitive magmas by olivine+plagioclase+magnetite+clinopyroxene fractionation. Least evolved calc-alkaline lavas are orthopyroxene, plagioclase and clinopyroxene phyric basaltic andesites (e.g. TS-192-85) with high Ni abundances (up to 492 ppm).

Evolved Compositions

The alkaline lavas at the base of section E-E' comprise a chemically distinctive magma group which spans the alkaline olivine

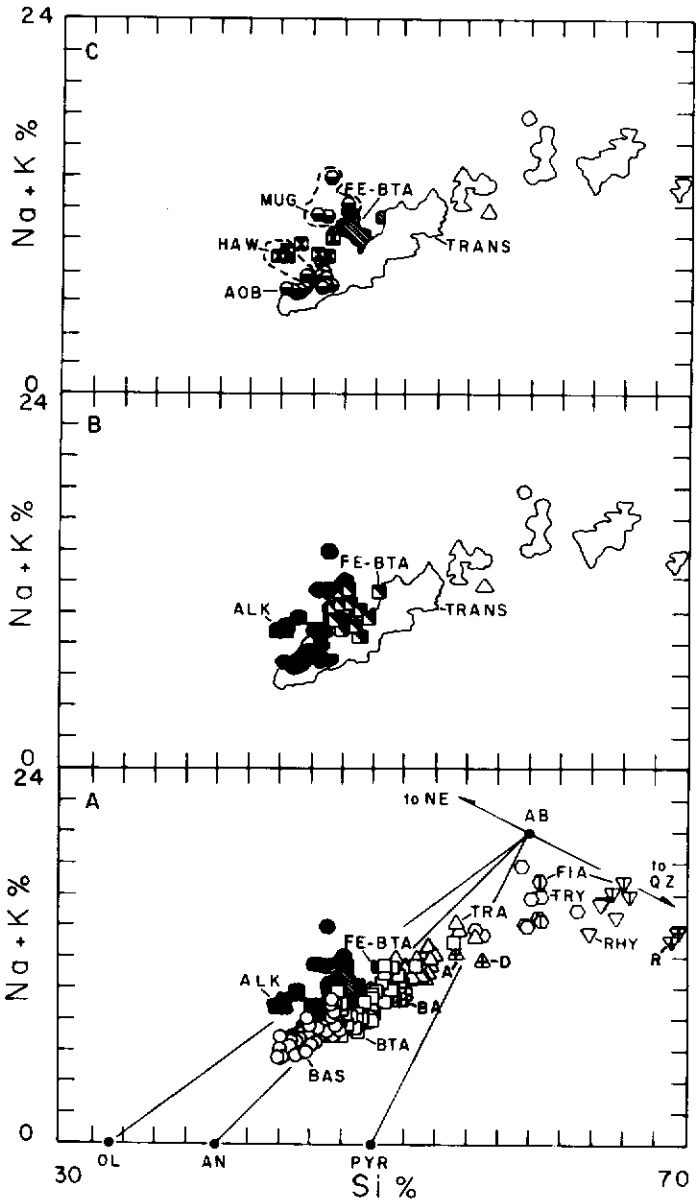

Figure 5. Total alkali versus silica diagram (cation units) showing the ideal positions of minerals: OL = olivine; AN = anorthite; PYR = pyroxene; AB = albite; QZ = quartz and NE = nepheline. Figure 5A illustrates the transitional (TRANS) and calc-alkaline magma types where: BAS = basalt; BTA = basaltic trachyandesite; TRA = trachyandesite; TRY = trachyte; THY = rhyolite; FIA = fiamme; BA, A, D and R as in Figure 4; ALK = alkaline type; FE-BTA = Fe-rich transitional type. Figure 5B shows Fe-rich basaltic trachyandesites and trachybasalts. Figure 5C Alkaline magma type where: AOB = alkaline olivine basalt; HAW = hawaiite; MUG = mugearite. Dashed field encloses alkaline lavas from the base of section E-E' (Fig. 3 and 4).

basalt-hawaiite- mugearite compositions. These lavas are characterized by high Ti, Fe, Na, K, P and incompatible trace elements, and low Si abundances relative to other lavas (Figs. 4, 5, 7 and 8). Elsewhere in the St. Clare Creek field, (e.g., section J-J1) petrographically indistinguishable alkaline olivine basalt and transitional basalt lava flows have similar trace element abundances, and can only be discriminated by higher Ca contents in the former. The fractionation history of the alkaline lavas in section E-E' can be divided into alkaline olivine basalt-hawaiite and hawaiite-mugearite stages. The first stage is characterized by decreasing abundances of Si, Mg, Cr and Ni, near-constant Ca, V and Rb, and enrichment in all other elements as hawaiite is approached. The transition from hawaiite

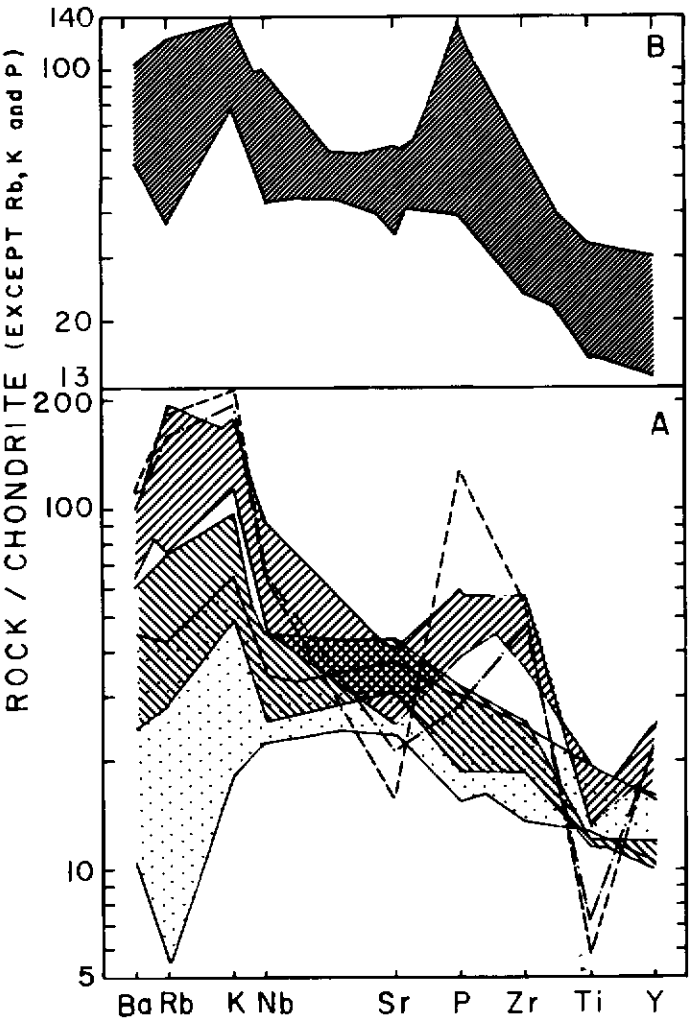

Figure 6. Chondrite-normalized trace element abundances of lavas. Normalization factors from Thompson (1983). Figure 6A illustrates transitional lavas and figure 6B the Fe-rich transitional lavas. In Figure 6A the dotted pattern = basalts (lower part of field is defined by TS-101-85, see text), NW-SE ruling = basaltic trachyandesites, NE-SW ruling = trachyandesites; dash-dot pattern = trachyte and dashed pattern = rhyolite.

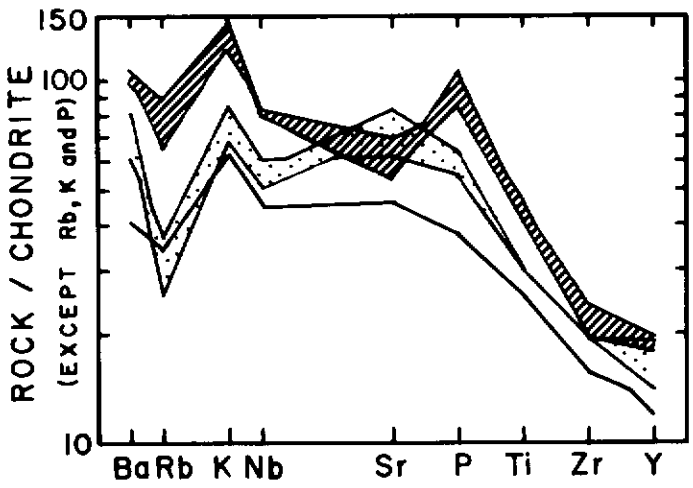

Figure 7. Chondrite-normalized trace element abundances for the alkaline lavas from the base of section E-E1. The single line is an alkaline olivine basalt (TS-15-85), the dotted pattern = hawaiites and the ruled pattern = mugearites.

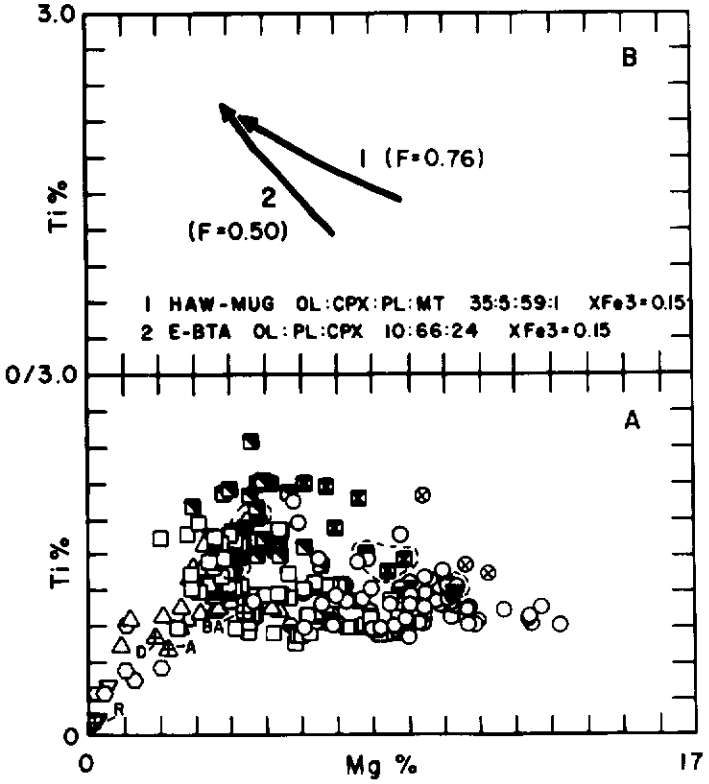

Figure 8. Ti versus Mg in cation units. Figure 8A utilizes the symbols as in Figure 5 with the addition of circles with an X which are clinopyroxene-phyric basalts from the base of section G-G'. Figure 8B shows the model fractional crystallization paths for (1) hawaiite to mugearite 76% fractionation, and (2) Fe-rich basaltic trachyandesites 50% fractionation. Proportions of phenocrysts removed are shown for olivine (OL), plagioclase (PL) and clinopyroxene (CPX). The algorithm calculates equilibrium compositions for olivine and plagioclase (at a fixed clinopyroxene composition) which are then removed in 0.1% fractionation steps from a starting liquid composition.

to mugearite is characterized by increasing Si, Na, K, P, Rb, Zr, Nb and Y and a decrease in Ca, Al and Sr. An initial rise in Ti and Fe contents is followed by a drop in these elements with further differentiation (Fig. 8a).

The high-Fe transitional magma type represents a hypersthene-normative intermediary between the transitional and alkaline magma types. These lavas have HFSE and LILE abundances that are similar to those in the alkaline rocks (Figs. 6 and 7). The lavas are characterized by a restricted range of Si variation (47.1 - 50.9%) over which there is ~50% enrichment in incompatible trace element abundances with increasing differentiation. The aphyric lavas (◄10% phenocrysts) contain increasing Fe, Ti, Na, K, P, and Si, and decreasing Al, Ca, Cr, Ni and Sr with progressive differentiation. Many high-Fe transitional lavas contain abundant (~10%) plagioclase phenocrysts, which is reflected by high Al, Ca and Sr and low Fe and Ti contents.

The transitional magma type encompasses a continuous range of evolved compositions that extend from basalt to rhyolite. In the St. Clare Creek field a magma composition of approximately 57-59% Si (Fig. 5) coincides with an abrupt change in eruptive style from flows to pyroclastic eruptives, and an increase in the relative volume of intrusive rocks. The nature and proportion of liquidus phases in the evolved lavas has strongly influenced the course of transitional magmatic evolution. The liquidus effects are superimposed on primary chemical differences between the various basaltic progenitors. The order of appearance of phenocryst phases and the corresponding Mg cation abundance of the lavas is olivine (►13.2% Mg), plagioclase (~13.2%), titanomagnetite (~9.5%), clinopyroxene (~7.7%), apatite (~3.0%), hornblende (~2.8%), biotite (~1.3%) and anorthoclase

(-0.5%). The basalt flows with resorbed clinopyroxene phenocrysts at the base of section G-G¹ (Fig. 4) contain 11.2 - 9.4% Mg and the highest Fe and Ti abundances (Fig. 8a) of all Mg-rich transitional basalts (►9% Mg). The appearance of titanomagnetite at high Mg abundances (-10.7%) also reflects the character of these basalts. Since titanomagnetite has a significant effect on Si abundances, variations in the initial appearance and separation of this phase may explain the overlap of Mg abundance (between 5 and 9%) of basalts and basaltic trachyandesites.

The early crystallization of olivine, plagioclase and titanomagnetite relative to clinopyroxene in the transitional lavas results in a decrease in the abundance of Mg, Fe, Ti, Cr and Ni, the buffering of Ca (and to a lesser extent A) and an increase in the abundances of most other elements. The appearance of clinopyroxene on the liquidus causes an abrupt decrease in Ca, and an increase in Fe and Ti abundances (Fig. 8a). The increase in Fe and Ti abundances with the onset of clinopyroxene saturation in titanomagetite-phyric basaltic trachyandesites suggests a physical control on the separation of titanomagnetite. The inflection at -3.5% Mg in Ti-Mg space (Fig. 8a) corresponds to an abrupt increase in Si, and the formation of Ti and Fe-poor trachyandesitic differentiates. Assuming Stokes Law behaviour, titano-magnetite crystals must attain a critical diameter at this inflection point, permitting physical separation. Intermediate compositions which do not have high Ti abundances at 3.5% Mg are invariably plagioclase-rich (►15%) and lie on a crystal-liquid mixing line.

DISCUSSION

Volcanic History of the St. Clare Creek Field

Four physical stages of volcanism in the St. Clare Creek field are; (1) alkaline shield volcano, (2) early-stratovolcano, (3) basaltic fissure, and (4) late-stratovolcano. These stages comprise the Wolverine (1 & 2) Steele (3) and Count Creek Formations, (4) respectively.

The alkaline shield stage initiated St. Clare volcanism (►17.3 Ma) with the formation of small volume (◄1 km³, e.g., vicinity of section E-E¹), shield volcanoes composed of alkaline lavas in the lower part of the Wolverine Formations.

The early-stratovolcano stage or upper part of the Wolverine Formation marked the initiation of the main basin-filling phase by the formation of two major, central volcanoes. Vents were apparently centred over the Cement and Count Creek plugs as indicated by: the presence of large volume hypabyssal felsic intrusions, abundant dykes, local hydrothermal alteration (bleaching and weak argillic alteration), thickness of the Wolverine Formation, proximity of coarse pyroclastic rocks (sections E-E¹), central location relative to welded ashflow tuffs (section C-C¹, F-F¹ and G-G¹); and similarity in chemical composition of trachyte fiamme in sections F-F¹ and G-G¹ and the Cement Creek plug (Fig. 5). The early stratovolcano stage commenced by erupting high-Fe transitional lavas, followed by intermediate and evolved transitional lavas and local calc-alkaline basaltic andesites. Periodic erosion of the volcanic edifices and eruption of felsic pyroclastic rocks due to probable caldera collapse post-dated the high-Fe transitional lavas. Crosscutting relationships indicate that the Count Creek centre was the locus of volcanism from Wolverine time to possibly as late as 6.5 +/- 0.4 Ma (Souther and Armstrong, writ. comm., 1987). The age of the Cement Creek center, and the relative age of associated pyroclastic rocks bracket the age of early-stratovolcano activity between 17.3 +/- 1.0 and at least 13.6 +/- 1.2 Ma (Souther and Armstrong, writ. comm., 1987).

The Steele Formation represents eruption of a large volume of basaltic magma from north-trending fissures on the southern flanks of the Cement and Count Creek centers. The morphology of the flows suggest rapid eruption. This stage is estimated to have occurred between 13.6 +/- 1.3 and 9.9 +/- 0.4 Ma (data from Souther and Armstrong, writ. comm., 1987).

The late stratovolcano represented by the Count Creek Formation was largely centered around the Count Creek plug. The Count Creek Formation in the southeast part of the map area (Figs. 2 and 3; e.g., section A-A¹) is interbedded with distal epiclastic deposits, whereas more proximal deposits are found towards the west (e.g., sections M-M¹ and R-R¹). Distinctive pyroclastic-epiclastic cycles in the Count Creek Formation suggest that periods of erosion alternated with explosive volcanism. The late stratovolcano stage was characterized by the eruption of intermediate and evolved transitional lavas (post 9.9 +/- 0.4 Ma, data from Souther and Armstrong, writ. comm., 1987).

Magmatism in the St. Clare Creek Volcanic Field

Most volcanic samples from the St. Clare Creek field are of differentiated lavas. The continuous spectrum of magma compositions and the variability of compatible/incompatible element ratios suggest that the most important differentiation process was fractional crystallization. The majority of lavas appear to have fractionated in a near surface environment; the phenocryst assemblages are dominated by olivine, plagioclase, titanomagnetite and clinopyroxene. Resorbed clinopyroxene phenocrysts in some early-erupted, Fe-rich lavas may attest to a period of high pressure fractionation. Magma mixing may have been a locally important differentiation process as evidenced by orthopyroxene phenocrysts mantled by clinopyroxene with coexisting resorbed plagioclase and/or melt schlieren. The restricted stratigraphic occurrence of basalts suggest that their ability to erupt was a sensitive function of their buoyancy.

The applicability of fractional crystallization models in explaining the chemical compositions of differentiated alkaline and high-Fe transitional lavas in the St. Clare Creek field was assessed. The transition alkaline olivine basalt-hawaiite is characterized by decreasing silica contents that probably reflect pyroxene fractionation (Fig. 5c), however quantitative assessment of this process awaits additional mineralogical data. The hawaiite-mugearite stage requires (-26%) fractionation of olivine, clinopyroxene, plagioclase and titanomagnetite in the proportions 35:5:59:1 (Fig. 8b, assuming $XFe^{3}+^{5}$ 0.15). The enrichment of the incompatible elements K, P, Rb, Ba, Y, Zr and Nb over this transition is 32, 36, 43, 26, 27 and 28%, respectively. These higher degrees of fractionation for the LILE are somewhat problematic. It is unlikely that fractional crystallization alone can account for the chemical variation between hawaiites and mugearites. Local crustal contamination, as evidenced by orthoclase xenocrysts in mugearite, could explain the discrepancy between trace and major element fractionation models in the transition from hawaiite to mugearite.

The chemical compositions of high-Fe basaltic trachyandesites can be modelled by 50% fractional crystallization of olivine, plagioclase and clinopyroxene in the proportions 10:66:24 when $XFe^{3}+^{5}$ 0.15 (Fig. 8b). The indicated rise in Ti and constant Si abundances require that these melts did not fractionate titanomagnetite. The principal difference between the high-Fe transitional and transitional magma types is the enhanced role of clinopyroxene fractionation in the former.

It is possible to directly compare the whole rock compositions of least evolved alkaline and transitional basalts by correcting for the effects of fractional crystallization. The analysis is recalculated by adding olivine and plagioclase (in a ratio of 40:60, cf. Presnall et al., 1978) in small (0.2%) fractionation steps until the Mg abundance (14%) in the least evolved basalt in attained (cf. Eichl et al., 1987). Although magmas of 14% Mg may not be primary, a minimum correction is required to attain this concentration. In addition, the effects of further olivine "back fractionation" do not change the relative imcompatible element abundances. Fractionation-corrected alkaline magma is distinguished from transitional basalts by higher Ti, K, P, Sr, Zr, and Nb abundances. In the transitional lavas, key element ratios such as Na+K/Si (0.12 - 0.15), Na+K/Al (0.29 - 0.43), K/Na (0.06 - 0.16), Ti/P (4.76 - 7.75) and Zr/Y (4.43 - 6.35) overlap, or are close to, values for the alkaline magma (TS-15-85; 0.15, 0.41, 0.17, 3.93 and 6.74 respectively). These data are internally consistent since basalts with "alkaline-like" Na+K/Al ratios have similar elemental ratios. Thus there is a clear spectrum of basaltic magma compositions in the St Clare Creek field.

The wide range of magmatic compositions may be related to one or more primary magmas. A single primary magma would need to account for both critically undersaturated basalts with high LILE/HFSE ratios (e.g., TS-15-85) and silica-saturated basalts with

low LILE/HFSE ratios (e.g., TS-101-85). Alkaline olivine basalt can be derived from a silica-saturated primary magma at high pressures (Presnall et al., 1978). However, both alkaline and lower pressure transitional differentiates would need to variably assimilate a LILE-enriched component to produce the observed trace element abundances. Typical mass and energy balance calculations require that the assimilant outweigh the contaminant (cf. Grove and Kinzler, 1986). However, large-scale crustal assimilation is unlikely to have been important in the St. Clare Creek field. The volume of LILE-enriched lavas outweighs the relatively LILE-depleted counterparts, and crustal xenoliths are rare. Sr^{87}/Sr^{86} data from a zoned pluton in the Nines Creek area also have typical mantle values (Downey et al., 1980). Therefore it is suggested that a spectrum of primary magma compositions were generated beneath the WVB.

Adiabatic melting of a rising mantle diapir could account for the chemical-temporal relationships between primitive lavas of the alkaline sheild volcano, early stratovolcano and basaltic fissure stages. Both high pressure and CO_2/H_2O ratios favor the generation of alkaline magmas from upper mantle peridotite (Yoder and Tilley, 1962, Kushiro, 1972; Eggler, 1974). Since volatile activities appear to have been relatively low during the alkaline shield volcano stage, pressure is probably the more important variable. The lack of pyroclastic activity, and the restricted occurrence of volatile bearing minerals in evolved compositions (mugearite) support this conclusion. Alkaline olivine basalt magma could be produced by approximately 10% melting a LILE-enriched spinel lherzolite at pressures of 12 kb (i.e. a result of Cretaceous subduction?; c.f. Frey et al., 1978). Progressive ascent and melting of a diapir could generate the required silica-saturated trachybasaltic and transitional basaltic magmas. Segregation of these magmas would progressively deplete the source region to the extent that low LILE/HFSE ratios could be produced in later basaltic derivatives.

Subduction-related metasomatism of the overlying, depleted mantle wedge by LILE-enriched fluids could produce a source region appropriate for the generation of calc-alkaline magmas. Lavas erupted during the late stratovolcano stage may be the precursors of "true" arc magmas. The suggested model predicts that alkaline shield volcano, earlystratovolcano and basaltic fissure magmas should be in isotopic equilibrium, and reflect minimal crustal contamination. Similarly, latestratovolcano stage magmatism should have a decoupled alkaline and light rare earth element signature and have a distinctive isotopic signature.

A Tectonic Model of the Wrangell Volcanic Belt

The petrogenetic model proposed for the St. Clare Group implies that the alkaline shield volcano, earlystratovolcano and basaltic fissure stages reflect extension along the Duke River Fault, whereas the latestratovolcano stage reflects subduction and convergent tectonism. This suggestion is consistent with the 17.3 - 6.5 Ma of the St Clare Creek field (Souther and Armstrong, writ. comm., 1987) and the onset of calc-alkaline magmatism in the WVB at - 13 Ma (Deininger, 1970). The Ti-Zr-Sr, Ti-Zir-Y and Ti/Y - Nb/Y abundances of St Clare Creek basalts that precede the late stratovolcano stage overlap the compositional fields of arc and ocean floor basalts (cf. Pearce and Cann, 1973; Pearce, 1982). However, the St Clare basalts have Nb/Ba ratios which approach the maximum values (Perfit et al., 1980) found in oceanic arcs and the Ti/V ratios are similar to those of ocean floor and within-plate basalts (Shervais, 1980). Thus those of the occurrence of alkaline and calc-alkaline magmatism in the WVB may reflect two contrasting styles of tectonic activity along the convergent plate margin; transcurrent fault motion and subduction.

ACKNOWLEDGEMENTS

Funding for this project was arranged through a contract with the Exploraiton and Geological Services Division, Northern Affairs Program, Yukon. Further funding was made available through NSERC grants to D. Francis and J. Ludden, and DNSR Summer Field Fellowships (McGill University). I thank J. Souther and R. Armstrong for generously providing unpublished K-Ar age determinations, and C. Nye for data from his thesis. However, I claim full responsibility for the interpretation of this data. I am grateful to A. Sasso and M. Diner for assistance in the field and T. Ahmedali and M. MacKinnon for consultation in laboratory work. This paper has benefited from a thoughful, brutal yet brilliant review by J. Clark, and discussions with D. Francis, J. Ludden and my colleagues at McGill.

REFERENCES

BRUNS, T.R., 1983. Model for the origin of the Yakutat block, an accreting terrane in the northern Gulf of Alaska; Geology, Vol. 11, p. 718-721.

CAMPBELL, R.B. and DODDS, C.J., 1978. Operation St. Elias, Yukon Territory; Geological Survey of Canada; Paper 78-1A, p. 35-41.

DEININGER, J.W., 1972. Petrology of the Wrangell Volcanics near Nabesna, Alaska; unpublished M.Sc. thesis, University of Alaska, 65 p.

DELONG, S.E., HODGERS, F.N. and ARCULUS, R.J., 1975. Ultramafic and mafic inclusions, Kanaga Island, Alaska, and the occurrence of alkaline rocks in island arcs; Journal of Geology, Vol. 83, p. 721-737.

DENTON, G.H. and ARMSTRONG, R.L., 1969. Miocene-Pliocene glaciations in southern Alaska; American Journal of Science, Vol. 267, p. 1121-1142.

DOWNEY, M.E., ARMSTRONG, R.L. and PARRISH, R.R., 1980. K-Ar, Rb-Sr, and fission track geochronometry of the Bock's Brook Stock, Kluane Ranges, southwestern Yukon Territory; Current Research, Part B, Geological Survey of Canada, Paper 80-1B, p. 189-193.

EGGLER, D.H., 1974. Effect of CO_2 on the melting of peridotite; Carnegie Institution of Washington Yearbook, Vol. 72, p. 457-467.

EICH'E, G.E., FRANCIS, D.M. and LUDDEN, J.N., 1987. Primary alkaline magmas associated with the Quaternary Alligator Lake volcanic complex, Yukon Territory, Canada; Contributions to Mineralogy and Petrology, Vol. 95, p. 191-201.

EISBACHER, G.H. and HOPKINS, S.L., 1977. Mid-Cenozoic paleogeomorphology and tectonic setting of the St. Elias Mountains, Yukon Territory; Geological Survey of Canada, Paper 77-1B, p. 319-335.

FREY, F.A., GREEN, D.H. and ROY, S.D., 1978. Integrated models of basalt petrogenesis: A study of quartz tholeiites to olivine melilitites from southeastern Australia utilizing geochemical and experimental petrological data; Journal of Petrology, Vol. 19, p. 463-513.

GILL, J.B., 1982. Mountain building and volcanism; in Mountain Building Processes, Academic Press, p. 13-17, (Hsu, K.J. ed.).

GROVE, T.L. and KINZLER, R.J., 1986. Petrogenesis of andesites; Annual Reviews of Earth and Planetary Sciences, Vol. 14, p. 417-454.

HART, S.R. and DAVIS, K.E., 1978. Nickel partitioning between olivine and silicate melt; Earth and Planetary Science Letters, Vol. 40, p. 203-219.

KUSHIRO, I., 1972. Effect of water on the compositions of magmas formed at high pressures; Journal of Petrology, Vol. 13, p. 311-334.

LAHR, J.C. and PLAFKER, G., 1980. Holocene Pacific-North American plate interaction in southern Alaska: implications for the Yakataga seismic gap; Geology, Vol. 8, p. 483-486.

LE BAS, M.J., LE MAITRE, R.W., STRECKEISEN, A. and ZANETTIN, B., 1986. A chemical classification of volcanic rocks based on the total alkali- silica diagram; Journal of Petrology, Vol. 27, p. 745-750.

LERBEKMO, J.F. and CAMPBELL, F.A., 1969. Distribution, composition, and source of the White River ash, Yukon Territory; Canadian Journal of Earth Sciences, Vol. 6, p. 109-116.

MACKEVETT, JR., E.M., 1970. Geology of the McCarthy B-4 quadrangle, Alaska; United States Geological Survey, Bulletin 1333, 31 p.

MACKEVETT, JR., E.M., 1978. Geologic map of the McCarthy quadrangle, Alaska; United States Geological Survey, Misc. Inv. map I-1032, scale 1:250,000.

MENDENHALL, W.C., 1905. Geology of the Copper River region, Alaska; United States Geological Survey, Profesional Paper 41, p. 54-62.

MULLER, J.E., 1967. Kluane Lake map-area, Yukon Territory (115 G, 115 F east half); Geological Survey of Canada, Memoir 340, 137 p.

NYE, C.J., 1983. Petrology and geochemistry of Okmok and Wrangell volcanoes, Alaska; unpublished Ph.D. thesis, University of California Santa Cruz, 115 p.

PEARCE, J.A. and CANN, J.R., 1973. Tectonic setting of basic volcanic rocks determined using trace element analyses; Earth and Planetary Science Letters, Vol. 19, p. 290-300.

PEARCE, J.A., 1982. Trace element characteristics of lavas from destruction plate boundaries; in: Andesites, John Wiley and Sons, p. 525-548, (Thorpe, R.S., ed.).

PERFIT, M.R, GUST, D.A., BENCE, A.E., ARCULUS, R.J. and TAYLOR, S.R., 1980. Chemical characteristics of island-arc basalts: implications for mantle sources; Chemical Geology, Vol. 30, p. 227-256.

PRESNALL, D.C., DIXON, S.A., DIXON, J.R., O'DONNELL, T.H., BRENNER, N.L., SCHROCK, R.L. and DYEUS, D.W., 1978. Liquidus phase relations on the join diopside-forsterite-anorthite from 1 atm to 20 kbar: their bearing on the generation and crystallization of basaltic magma; Contribution to Mineralogy and Petrology, Vol. 66, p. 203-220.

RICHTER, D.H. and SMITH, R.L., 1976. Geologic map of the Nabesna A-5 quadrangle, Alaska; United States Geological Survey, Map GQ-1292, scale 1:63,360.

RICHTER, D.H., SMITH, R.L., YEHLE, L.A. and MILLER, T.P., 1979. Geologic map of the Gulkana A-2 quadrangle, Alaska; United States Geological Survey, Map GQ-1520, scale 1:63,360.

RIOU, R., DUPUY, C. and DOSTAL, J., 1981. Geochemistry of coexisting alkaline and calc-alkaline volcanic rocks from northern Azerbaijan (N.W.) Iran; Journal of Volcanology and Geothermal Research, Vol. 11, p. 253-275.

ROEDER, P.L. and EMSLIE, R.F., 1970. Olivine-liquid equilibrium; Contributions to Mineralogy and Petrology, Vol. 29, p. 275-289.

SHERVAIS, J.W., 1982. Ti-V plots and the petrogenesis of modern and ophiolitic lavas; Earth and Planetary Science Letters, Vol. 59, p. 101-118.

SKULSKI, T. and FRANCIS, D., 1986. On the geology of the Tertiary Wrangell Lavas in the St. Clare Province, St. Elias Mountains, Yukon; in Yukon Geology, Vol. 1, Exploration and Geological Services Division, Yukon, Indian and Northern Affairs Canada, p. 161-170.

SOUTHER, J.G. and STANCIU, C., 1975. Operation Saint Elias, Yukon Territory: Tertiary volcanic rocks; Geological Survey of Canada, Paper 75-1A, p. 63-70.

STEPHENS, C.D., FOGLEMAN, K.A., LAHR, J.C. and PAGE, R.A., 1984. Wrangell Benioff zone, southern Alaska; Geology, Vol. 12, p. 373-376.

STOUT, J.H. and CHASE, C.G., 1980. Plate kinematics of the Denali fault system; Canadian Journal of Earth Sciences, Vol. 17, p. 1527-1537.

THOMPSON, R.N., 1983. Continental flood basalts...Arachnids rule OK?; in Continental Basalts and Mantle Xenoliths, Shiva Geology Series, p. 158-185, (Hawkesworth, C.J. and Norry, M.J., eds.).

WEAVER, S.D., SAUNDERS, A.D., PANKHURST, R.J. and TARNEY, J., 1979. A geochemical study of magmatism associated with the initial stages of back-arc spreading; Contributions to Mineralogy and Petrology, Vol. 68, p. 151-169.

YODER, H.S. Jr. and TILLEY, C.E., 1962. Origin of basaltic magmas: an experimental study of natural and synthetic rock systems; Journal of Petrology, Vol. 3, p. 342-532.

ENHANCED LANDSAT THEMATIC MAPPER IMAGERY FOR EXPLORATION GEOLOGY IN THE WHEATON RIVER DISTRICT, SOUTHERN YUKON

Peter von Gaza and J. Ronald Eyton
Department of Geography
University of Alberta
Edmonton, Alberta
T6G 2H4

VON GAZA, P. and EYTON, J.R., 1988. Enhanced Landsat Thematic Mapper imagery for exploration geology in the Wheaton River District, southern Yukon; in Yukon Geology, Vol. 2; Exploration and Geological Services Division, Yukon, Indian and Northen Affairs Canada, p. 99 - 107

ABSTRACT

Digitally enhanced Landsat Thematic Mapper (TM) imagery was evaluated as a mapping aid for the exploration geology in the Wheaton River District of the southern Yukon. Landsat TM data acquired on September 1986 was digitally processed to enhance lineaments and alteration zones. Geological mapping was conducted at a reconnaissance scale of 1:250 000 for a 45 km by 45 km area centered the Wheaton District and at a detailed scale of 1:50 000 for the Mt. Skukum Volcanic Complex. Reconnaissance investigations showed that the TM imagery was valuable for detecting and mapping small scale geological lineaments and for recognizing limonitic rocks. The imagery, however, was not useful for identifying or differentiating lithologic units. A further limitation of the imagery was the loss of information in the shadows created by the extreme topography of the region and the low sun angle present at the time of image acquisition. Detailed field investigations conducted on the Mt. Skukum Volcanic Complex showed that edge enhanced Landsat images were capable of detecting most of the previously mapped faults and fractures, and some dikes. Three unmapped and potentially significant lineaments were mapped using the TM imagery. These new lineaments (Vesuvius-Chieftian Hill, Sulphide Creek, and Rhyolite Creek) are probably deep-seated fractures. Alteration zones, primarily iron oxide rich rocks, were also mapped successfully. Attempts at identifying hydrothermally altered rocks failed. Overall, Landsat TM imagery was found to be a valuable tool for mapping geological lineaments and iron oxide alteration zones at scales between 1:250 000 and 1:50 000.

RÉSUMÉ

On a évalué l'imagerie cartographique thématique Landsat accentuée numériquement, dans le but de faciliter la cartographie en rapport avec l'exploration géologique du district de Wheaton River dans le sud du Yukon. On a traité numériquement les données cartographiques thématiques Landsat (TM) obtenues en septembre 1986, pour accentuer les linéaments et les zones d'altération. On a réalisé la cartographie géologique à une échelle de reconnaissance de 1/250 000, dans une région de 45 kilomètres par 45 kilomètres centrée dans le district de Wheaton, et à une échelle de 1/50 000 pour le complexe volcanique de Mt. Skukum. Les travaux de reconnaissance ont montré que l'imagerie TM était précieuse, lorsqu'il s'agissait de déceler et de cartographier des linéaments géologiques de petite envergure, et d'identifier les roches limonitiques. Toutefois, l'imagerie n'a pu servir à identifier ou à différencier les unités lithologiques. Une autre limitation de l'imagerie était la perte d'information causée par les ombres résultant de la topographie extrêmement prononcée de la région, et du faible angle de la lumière solaire incidente par rapport au sol, au moment de l'acquisition des images. L'exploration détaillée effectuée sur le terrain à l'emplacement du complexe volcanique de Mt. Skukum a montré que les images Landsat à contours accentués permettaient de repérer la plupart des failles et des fractures déjà cartographiées, et quelques dykes. On a cartographié, en employant l'imagerie TM, trois linéaments encore non cartographiés et potentiellement importants. Ces nouveaux linéaments (Vesuvius-Chieftian Hill, Sulphide Creek et Rhyolite Creek) sont probalement des fractures installées en profondeur. On a aussi cartographié avec succès les zones d'altération, surtout composées de roches riches en oxydes de fer. Par contre, on n'a pu identifier les roches qui ont subi une altération hydrothermale. Dans l'ensemble, on a constaté que l'imagerie TM Landsat était un outil précieux pour cartographier les linéaments géologiques et les zones d'altération avec oxydes de fer, à des échelles comprises entre 1/250 000 et 1/50 000.

INTRODUCTION

Landsat Thematic Mapper (TM) imagery was evaluated as an aid for mineral exploration in the Wheaton River District of the southern Yukon during the field season of 1987. This paper briefly describes some commonly used digital image enhancement techniques, and discusses the application of these techniques to the geology of the Wheaton River District. This part of the Yukon was selected as the study area because the overall geology of the region is reasonably well understood, the landscape is not densely vegetated, and the area is currently the focus of intense exploration for potential epithermal gold-silver deposits.

Remote Sensing for Exploration Geology

Satellite remote sensing technology has played an increasingly larger role in the search for mineral resources over the past two decades. Landsat TM images can provide geologists with a synoptic view of the earth's surface in seven spectral bands at a 30 metre resolution. Satellite images have not yet replaced (nor are they likely to in the future) the necessity for field geology, nor have they diminished the role of conventional aerial photographic interpretation in geological mapping and exploration. Landsat imagery combined with all other available exploration methods provides a more effective means for addressing and solving geological problems (Siegal and Gilliespie, 1980).

Research has shown that of the many potential uses of remote sensing imagery for exploration geology, two specific applications are valuable: 1. the mapping of regional and local lineaments, and 2. the detection of hydrothermally altered rocks (Henderson and Rock, 1983; Rowan and Lathram, 1980; Sabins, 1987). Many mining districts and individual ore deposits occur along or near linear

trends. These faults and fractures may represent conduits through which hydrothermal fluids migrated, and therefore controlled the distribution of ore deposits. More recently, Sibson (1987) has discussed the importance of the structural control of epithermal mineralization in dilational fault jogs, at macroscopic through regional scales. Modern day exploration geologists spend a considerable amount of time and funds actively seeking and developing techniques for identifying lineaments. The view of extensive areas provided by Landsat is a valuable tool for mapping potential fracture and/or fault patterns, especially in areas where very little is known about the geological environment.

The multispectral characteristics of the Landsat sensing systems provided a means of detecting and mapping altered rocks (primarily limonitic rocks), and the addition of the TM sensor system to the Landsat platform in 1982 considerably improved the potential for detecting hydrothermally altered rocks (Henderson and Rock, 1983). The inclusion of TM band 7 centered at 2.2 um in the electromagnetic spectrum (a region where hydrous minerals have a distinct absorption feature in their spectral curve) theoretically provides the capability for identifying clay minerals associated with hydrothermal alteration (Podwysocki, et al., 1980). This characteristic of band 7 has been used successfully to detect iron oxide free alterations, such as advanced argillic and silicic rocks that are highly leached (Abrams, 1982). The identification of altered rocks, especially hydrothermally altered rocks commonly associated with ore deposits, indicates likely areas for field exploration.

Data

The digital image data used for this study was captured by the TM multispectral scanner onboard the Landsat 4 satellite on September 6, 1986 at approximately 9:30 A.M.. The image was obtained with a sun azimuth of 153 degrees and a sun elevation of 34 degrees. A quarter of a full Landsat scene (a quadrant), with a footprint of approximately 85 km, was obtained from the Canada Centre for Remote Sensing (CCRS) satellite receiving station located at Prince Albert, Saskatchewan. The TM sensing system has a spatial resolution of 30 metres and records seven spectral bands consisting of three visible bands, three near-infrared bands (reflected solar radiation), and one thermal infrared band (emitted terrestrial radiation).

PHYSICAL SETTING

The study area (Fig. 1) lies mostly in the Wheaton River District, on the eastern edge of the Coast Mountains, just north of the British Columbia boundary. The district is approximately 50 km south-southwest of Whitehorse. While the general study area covers a 45 km by 45 km square, the primary focus of this paper is on a 15 km by 15 km subset of the Mt. Skukum area. The topography is moderately rugged, and is described by Cairnes (1912) as an uplifted and deeply dissected peneplain in which the valleys have been greatly modified by Pleistocene glaciation. The major valleys are over 1 km wide and valley slopes rise in excess of 1000 metres to the plateau surfaces. These extensive upland plateaus are undissected and gently rolling.

The vegetation cover is distributed primarily as a function of topography. Spruce, fir, poplar, and pine forests are found in the valleys and on hillsides to an elevation of 1300 metres. Willows are abundant along flood plains, while dwarf birch is plentiful in the higher valleys. Upland plateaus, generally occurring at elevations above the tree line, are characterized by alpine vegetation, including ericaceous shrubs, prostrate willows, and a ground cover of mosses and lichen.

The basic geology described here is confined to the Mt. Skukum Volcanic Complex as it is the focus of the study. The Skukum Volcanic Complex, the northern most extension of the Sloko Volcanic Province found in western British Columbia, is a series of Paleocene-Eocene andesitic and felsic volcanic rocks that have been deposited unconformably on Cretaceous granitic rocks and older metasedimentary rocks of the Yukon Group (Pride, 1986; Smith, 1983; Wheeler, 1961). The complex is highly fractured, is intruded locally by felsic stocks and dikes, and is fault bounded. Iron staining and gossans are prominent; locally, rocks are highly leached and hydrothermally altered. The discovery of the Mt. Skukum gold-silver deposit in 1980 has resulted in considerable exploration activity, focused primarily on locating epithermal gold deposits. The Mt. Skukum deposit is in andesites of the Skukum Complex and consists of low sulphide, high level, gold-silver bearing quartz-calcite veins (McDonald, 1986). Omni Resources Inc. and Skukum Gold Inc. are currently exploring deposits located along Skukum Creek. These deposits are mesothermal, are hosted in granitic basement rocks, and consist of gold-silver bearing rhyolite and andesite dikes, and brecciated quartz veins that have a high sulphide content (Elliot, 1988, pers. comm.). The Skukum Volcanic Complex may be analogous to the setting of epithermal deposits of Silverton, Colorado and is thought to have the potential to yield multiple small tonnage and possibly a few large tonnage, high grade ore deposits (Doherty, 1988, pers. comm.).

DIGITAL IMAGE PROCESSING

Remote sensing strategies for mineral exploration have been steadily moving away from the direct photogeologic interpretation of conventional, unenhanced photography to the analysis of computer manipulated digital imagery (Goetz, 1980). A digital TM image consists of a regularly gridded set of picture elements, or pixels, that represent 30 metre square ground areas. Each pixel contains a numerical record (called Digital Numbers or DNs) of the amount of electromagnetic radiation reflected or emitted from the earth's surface in a particular band. This section of the paper provides a brief

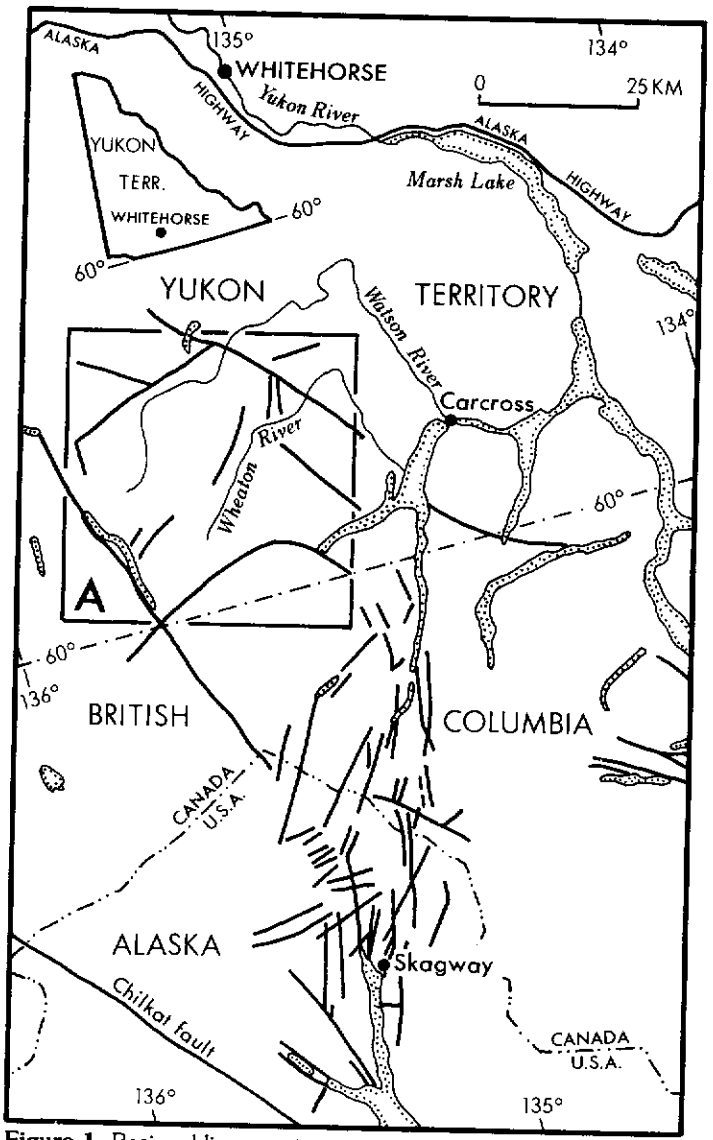

Figure 1. Regional lineament map interpreted from a 1:1 000000 TM Landsat scene and showing the location of the general study area (box A).

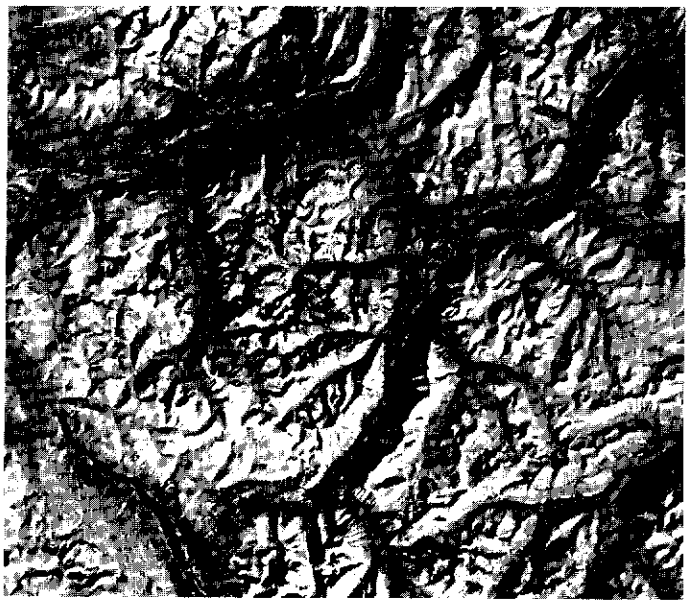

Figure 2. Edge enhanced Landsat TM band 5 image of the general study area.

description of the computer processing techniques used in this study to enhance the TM digital images. A detailed discussion of basic image processing can be found in Schowengerdt (1982), Drury (1987), and Sabins (1987).

The image enhancement techniques used in this study consisted of contrast stretching, spatial frequency filtering, principal components analysis, and band ratioing. Although this paper is restricted to the printing of only black and white photographs, color compositioning techniques are discussed because they are often the end product of the enhancement process. The work was done on a Decision Images image processing system at the University of Alberta, and on a Dipix Aries system operated by the Government of Alberta. Hardcopies of the images were recorded on either a 35 mm Dunn Camera or an 8 x 10 Optronics image writer.

Contrast stretching is a procedure for improving the overall contrast of an image. The raw image will normally have poor contrast when displayed; this is because the image data rarely encompass the full brightness range of the TM sensors. In general a contrast stretch transforms the data to make use of the full range of the output device, resulting in an image that is easier to interpret.

A colour composite is an image produced by simultaneously displaying three bands, with each band assigned one of three additive primary colours (red, green, and blue). This technique for combining bands is valuable because the composite usually displays more information about surface materials than can be found in a single band image. A normal colour composite simulates a natural colour image; it is produced by displaying the visible TM bands 1, 2 and 3 as blue, green, and red respectively. A false colour composite is produced when one or more infrared (IR) bands are combined with one or more visible bands. False colour composites produce colours that are not natural but in many instances provide increased differentiation between surface features because of the addition of the infrared information that is not visible to the human eye.

High-pass spatial frequency filtering is a technique for enhancing tonal boundaries or edges in an image. These edges are important to the geologist as they may represent faults or fractures, or boundaries between geologically significant materials. Tonal boundaries are produced by the juxtaposition of different surface materials, and by the differences in illumination between areas of differing topography. Edge enhanced images are most commonly created by high-pass convolution filtering (Drury, 1985, 1986).

Principal components analysis (PCA) is a statistical method of trans-forming the raw image data to produce new data sets that are uncorrelated. Certain TM image band pairs are often highly correlated and therefore composite images may contain redundant information. PCA produces transformed data, or principal component images, in which all inter-band correlation has been removed. PCA is often used to produce images that are often more interpretable than the original data (see Jensen, 1986, for a thorough discussion of this technique).

Ratio images are generated by dividing the DN of one band by the DN of another band. Certain ratios can be used to enhance the subtle tonal differences between specific cover types while suppressing the effects of illumination (Sabins, 1987). This technique has been extensively used by geologists for enhancing the detectability of altered rocks (Rowen et al., 1974).

REGIONAL ANALYSIS

The Landsat satellite program has proven to be an ideal, cost effective tool for investigating small scale regional structural patterns and for reconnaissance analysis of iron oxide occurrences (Abrams, et al., 1982). Two scales of imagery were used for this part of the study: 1:1 000 000 and 1:250 000. A 1:1 000 000 false colour composite, produced by CCRS, was interpreted for very small scale lineaments. This scale of imagery is generally not useful for reconnaissance studies, but is included in this paper because it helps to place the study area in a regional perspective (Fig. 1). A prominent set of lineaments trending north were visible between the Skagway area in Alaska and Lake Bennett in the Yukon. These lineaments have very strong topographic expression, and likely control the orientation of major lakes, valleys, and ridges. They may represent conjugate fractures related to a compressional environment, bounded on the south by the Chilkat fault and on the north by the Whitehorse Trough.

Digitally enhanced images were produced at a scale of 1:250 000 for the 45 km by 45 km general study area and interpreted as part of a detailed reconnaissance study. A false colour composite (TM bands 5, 4 and 3 assigned red, green, and blue respectively) and a spatially filtered band 5 black and white image (Fig. 2) were used to examine regional lineament patterns and to detect gross areas of iron oxide occurrences. Ground truthing indicated that the images were very useful for detecting limonitic rocks and for mapping regional and local fracture patterns. However, it was not possible to identify rock types or discriminate between different lithologic units. The ubiquitous cover of lichens on virtually all exposed and unaltered rock outcrops, irrespective of rock type, controlled the spectral response in all bands. The extreme topography in the region, and the low sun angle at the time of image acquisition, also complicated interpretation because of the resulting shadows on many northwest facing slopes. In some instances there is a complete loss of image information in the shadows.

Most areas of iron staining and extreme surface alterations were easily detected on the IR false colour composite. This is principally due to the fact that most of these altered areas were devoid of a lichen cover and were spectrally distinct. The majority of the bright areas in Fig. 2 represent limonitic rocks. Areas characterizing by intensely leached rocks had strong spectral responses in all bands, and were easily recognized on the imagery as the brightest reflectors. Field inspection revealed that these leached areas are sometimes characterized by hydrothermal alterations. Alterations in the Mt. Skukum area, on Mt. Vesuvius, and the south face of Mt. Reid are prominent. Generally, limonitic rocks appeared turqoise or pinkish in color and leached rocks appeared bright white on the false colour composite.

The potential fracture map (Fig. 3) represents a conservative interpretation of the regional lineament pattern. Major linear features were easily seen in Fig. 2. The northwest trending fault mapped by Cairnes (1912), along the north side of the Watson River, exhibited a strong topographic expression. A series of linears trending north-northwest were seen in the upper right portion of the image. These features were mapped and named the Tally-Ho Shear Zone by Doherty and Hart (1987, pers. comm.) who used the false colour Landsat image for projecting the trend of the shear zone during field mapping. This feature is a 1-4 km wide, 35 km long zone of sheared greenstones and mylonites (Hart, 1988, pers. comm.). In the bottom right of the image, part of the ring-dike fracture zone around the Bennett Lake Caldron complex is visible. Overall, the image shows that the region is dominated by north to northeast trending

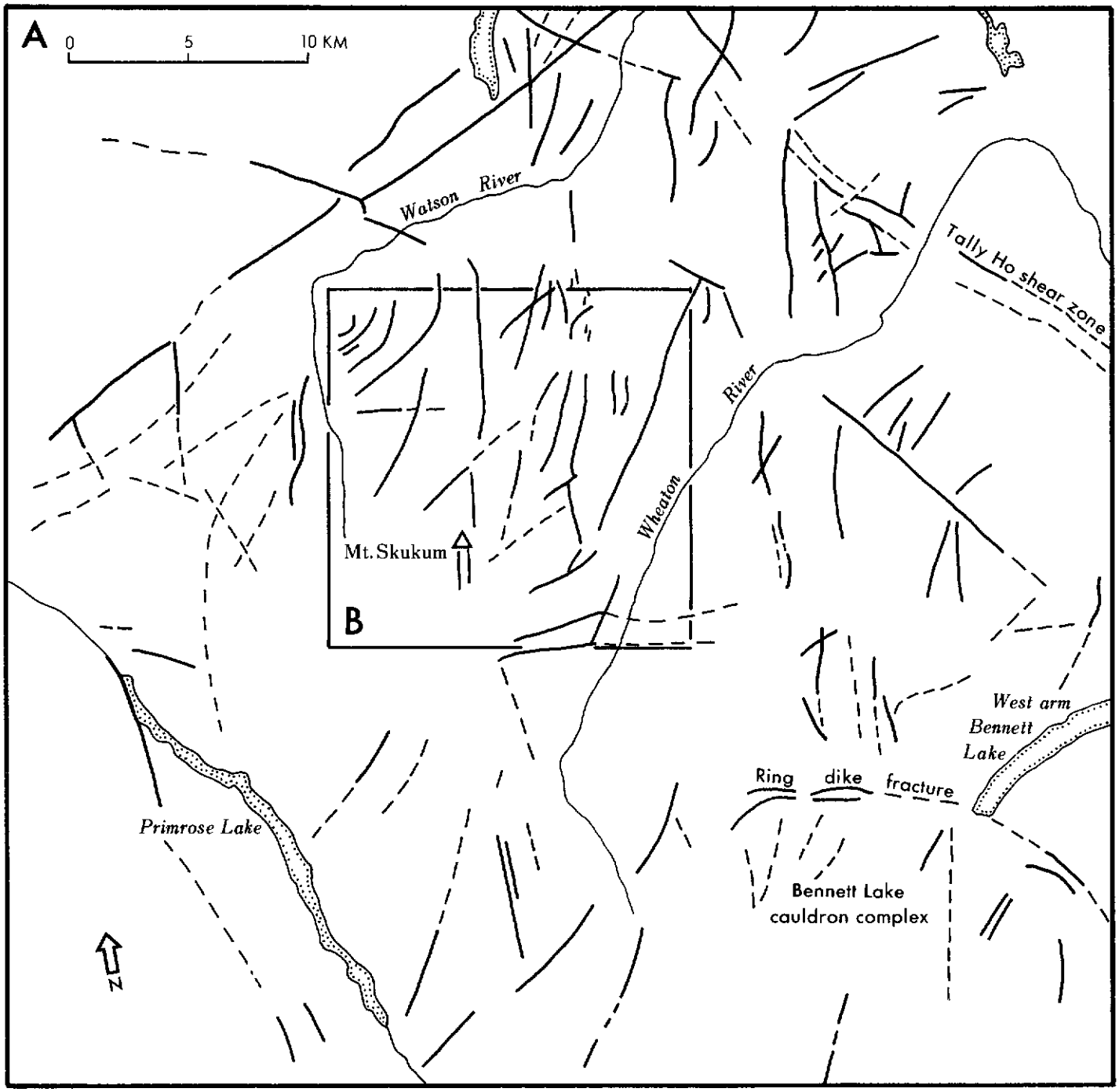

Figure 3. Interpretation of lineaments on 1:250 000 TM imagery centered over the general study area and showing the Mt. Skukum study area (box B) in Fig. 8. Solid lines are distinct lineaments and dashed lines are possible lineaments.

lineaments. These fractures which are often associated with zones of strong surface alteration, may represent areas of possible mineralization, and therefore should be considered for more detailed field investigation.

LOCAL INTERPRETATION

A 15 km by 15 km subset centred over the Mt. Skukum Volcanic Complex was used for mapping altered rocks and fractures at a scale of 1:50 000. The objective of this part of the study was to determine to what degree TM imagery was useful for local, detailed mapping. Image enhancement techniques included black and white contrast stretching (Fig. 4), spatial filtering, normal and IR false colour compositing, band ratioing, and principal components analysis.

Alterations

A series of ratio principal component images and their composites were examined for evidence of spectral response to iron oxide minerals and possible differentiation of hydrothermally altered rocks. The 3/1 ratio image (Fig. 5) proved valuable for isolating and enhancing areas rich in iron oxide minerals. Band 3 detects light in the red portion of the electromagnetic spectrum and is useful for detecting limonitic rock that exhibit a red colouration. The 3/1 ratio removed the confusion that existed in the band 3 image between altered areas and snow (compare Fig. 4c and Fig. 5). Attempts at detecting clays using the 5/7 ratio image as either a single band image or in conjunction with other ratio images to form a colour composite, were not successful. Areas of known argillic alteration in areas dominated by limonitic rocks were used as training samples; intensely altered areas in Sulphide and Rhyolite Creeks were chosen as the specific test sites. Most of the clay alteration was associated with highly leached areas which had very strong spectral responses on

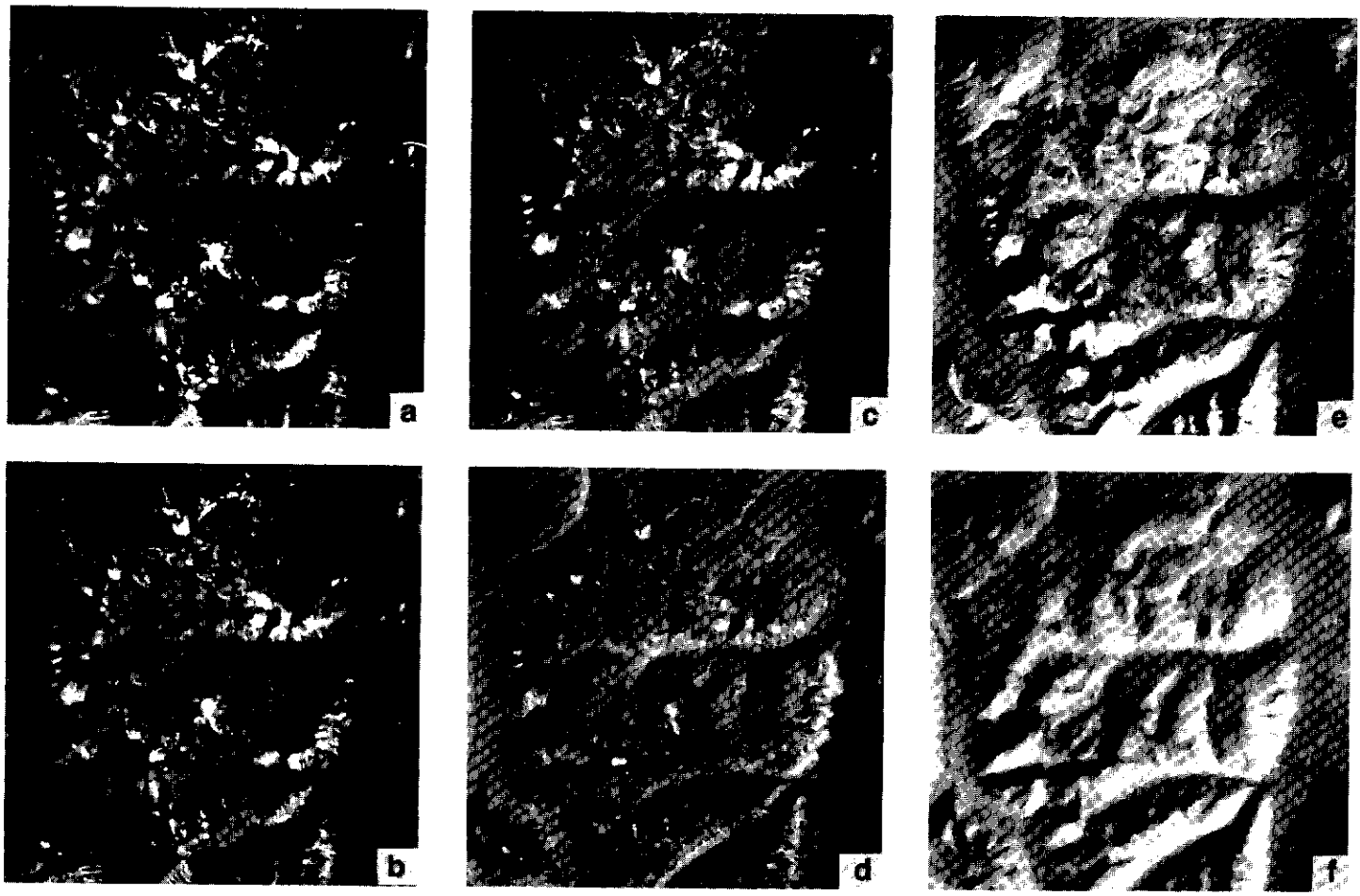

Figure 4. Contrast stretched images of all seven Landsat TM bands. (a) TM1: reflected blue-green light, .45 - .52 um, (b) TM2: reflected green light, .52 .60 um, (c) TM3: reflected red light, .63 - .69 um, (d) TM4: reflected infrared radiation, .76 - .90 um, (e) TM5: reflected infrared radiation, 1.55 - 1.75 um, (f) TM6: emitted thermal infrared radiation, 10.40 - 12.50 um, (g) TM7: reflected infrared radiation, 2.08 2.35 um.

the imagery because of their high albedo. The ability to spectrally detect clays would have aided in the differentiation of hydrothermally altered rocks from weathered bedrock and surface materials containing iron oxide minerals. It is important to realize that these techniques were developed for detecting altered rocks found in desert environments and characterized by sparse vegetation, little weathering, and well defined outcrops typical of the geological environment found in Goldfield, Nevada (Goetz and Ashley, 1979). The application of these techniques to wet, vegetated, and highly weathered environments such as the Yukon, is conjectural.

Inverted principal components analysis (Williams, 1983) was investigated as a possible method for detecting altered rocks. The analysis was undertaken on image data covering areas of known alteration. The resulting seven principal component images are shown in Fig. 6; PC images 1, 3 and 4 were used to created a color composite. These three components were chosen to construct the composite because they exhibited a strong contrast between altered areas and the rest of the image, and the effects of snow were suppressed. The resulting colour composite was dramatic and proved to be extremely useful. All vegetation generally appeared purple, except for lichen covered rocks which were green. Areas of alteration were bright yellow to orange and were very distinct in the image.

The use of a normal colour composite (bands 3, 2, 1) and a false colour composite (bands 5, 4, 3) were found to be generally effective for detecting most of the areas of alteration. In the normal colour composite, areas of iron staining appeared yellow to red, while in the false colour composite they exhibited a turquoise to pink hue. Highly leached areas appeared white in both images. A disadvantage of these images, over the ratio and principal component images, is that much closer examination of the images was required to detect the altered areas; the chance of missing an altered area was greater because these areas did not stand out from the rest of the image.

Lineaments

Local lineaments were identified by examining a spatially filtered band 5 image (Fig. 7) and the false colour composite. Lineaments mapped from both images (Fig. 8) were compared to existing geological maps (1:25 000) compiled by Pride (1985) and checked in the field by one of the authors (von Gaza). Analysis of lineaments

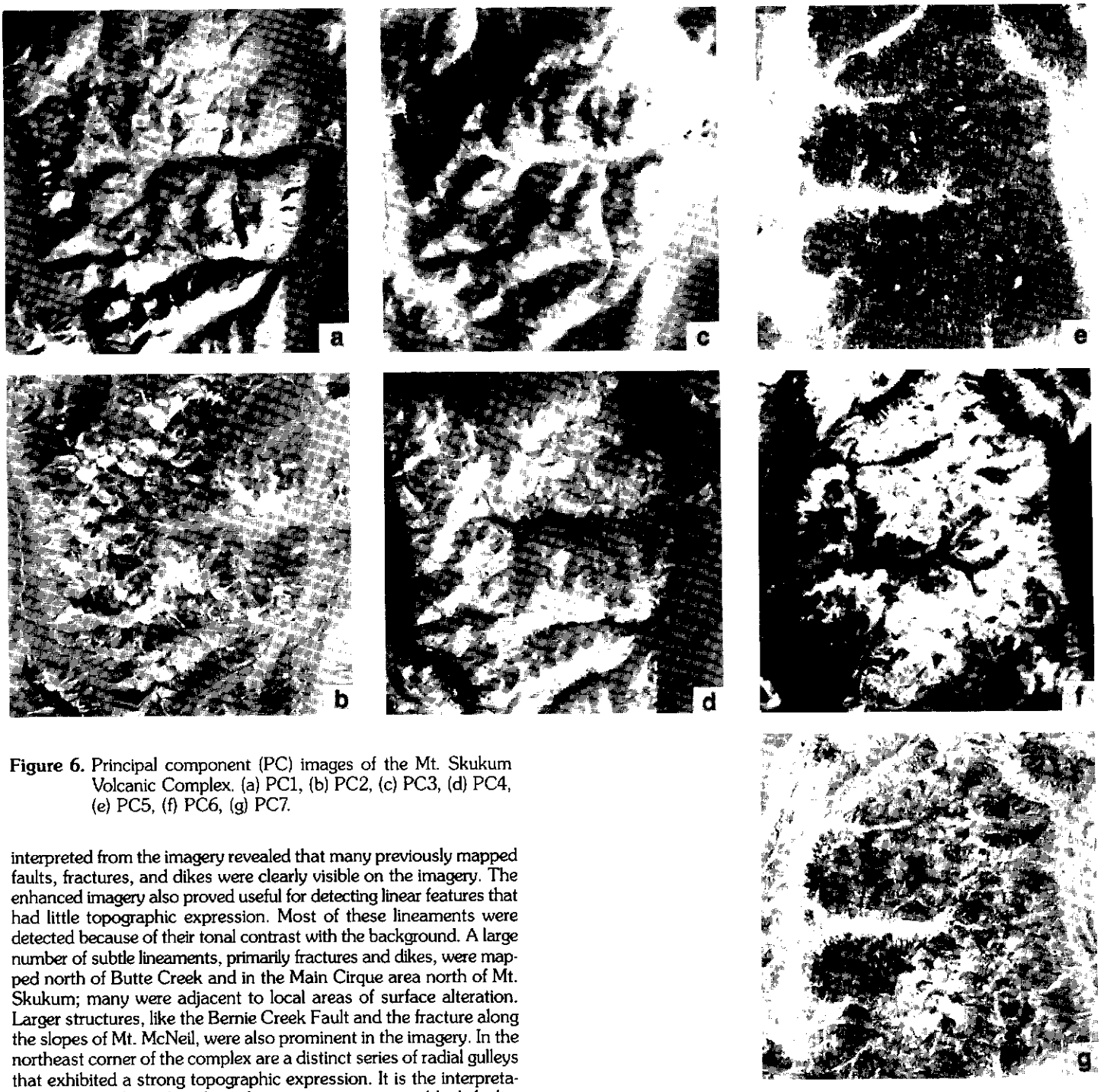

Figure 6. Principal component (PC) images of the Mt. Skukum Volcanic Complex. (a) PC1, (b) PC2, (c) PC3, (d) PC4, (e) PC5, (f) PC6, (g) PC7.

interpreted from the imagery revealed that many previously mapped faults, fractures, and dikes were clearly visible on the imagery. The enhanced imagery also proved useful for detecting linear features that had little topographic expression. Most of these lineaments were detected because of their tonal contrast with the background. A large number of subtle lineaments, primarily fractures and dikes, were mapped north of Butte Creek and in the Main Cirque area north of Mt. Skukum; many were adjacent to local areas of surface alteration. Larger structures, like the Bernie Creek Fault and the fracture along the slopes of Mt. McNeil, were also prominent in the imagery. In the northeast corner of the complex are a distinct series of radial gulleys that exhibited a strong topographic expression. It is the interpretation of the authors that these features may represent block-faults, or slump features, that formed during the collapse of the volcanic complex. Previously unmapped lineaments, some quite significant, were detected on the imagery. These include a series of three north-northwest trending lineaments, all loosely parallel and approximately 15 km in length; these were given the preliminary names of the Vesuvius-Chieftain Hill, the Sulphide Creek and the Rhyolite Creek Lineaments.

The Vesuvius-Chieftain Hill Lineament extends from north of Mt. Vesuvius, across Summit Creek, across Chieftain Hill and joins the Bernie Creek Fault. This lineament was identified primarily because of the vegetation contrast exhibited in the IR bands. The Sulfide Creek lineament also intersects the Bernie Creek Fault and forms a shallow angle to the Vesuvius-Chieftian Hill Lineament. This lineament is expressed in the form of a V-shaped valley along the western margin of Chieftain Hill before becoming part of Sulphide Creek; to the north, the same lineament becomes an incomspicuous depression over Mt. Kopjie and then branches into a series of discontinuous shallow fractures. The Rhyolite Creek Lineament originates at Pyroclastic Cirque, extends through Rhyolite Creek, and then runs parallel to the Sulphide Creek Lineament. The Sulfide and Rhyolite Creek Lineaments are topographic features that were identified because of their conspicuous small scale appearance on the TM imagery. This demonstrates the value of the synoptic view afforded by Landsat; these features would have been difficult to identify from the ground or from large scale aerial photographs. No evidence for faulting was found along any of the three lineaments. Gravity and magnetic aerial surveys conducted for the Mt. Skukum Gold Mining Corporation over these lineaments indicate that they may represent deep-seated fractures (Gossan, 1987, pers. comm.). The association of these fractures with zones of intense alteration indicate areas that are potential exploration targets.

Figure 5. Band ratio (3/1) image of the Mt. Skukum Volcanic Complex. Altered rocks, primarily limonite, have been enhanced and appear bright white.

MISCONCEPTIONS OF REMOTE SENSING

The experience of one author (von Gaza) during the 1987 field season in the Yukon indicated that some individuals have either overestimated the potential value of remote sensing technology or have avoided it because of reports of bad experiences by a few individuals. Remote sensing technology to aid exploration geology in the Yukon has only recently been introduced and therefore is not well understood. There are relatively few users of this technology in the Yukon, and even fewer that have the training and the background for properly applying or making judgments of potential uses.

The approach that some researchers have taken to Landsat image interpretation has resulted in skepticism and disquiet among many scientists to the entire field or remote sensing. This cynicism is primarily related to the interpretation of the images by investigators with little or no photogeological skills. Some critics perceive remote sensing specialists as little more than computer analysts, with inadequate training in the earth sciences. This view grew out of the plethora of lineament studies that inundated scientific journals from the mid- to late seventies (Drury, 1987). During this period almost every conceivable lineament study was attempted and maps saturated with lines, both real and imaginary, were produced in profusion. Donald Wise (1982) wrote of this period, "There have been few fields of geology so marked by uneven quality of collection, digestion and interpretation of the basic data". To many, the term "lineament", when used in the same sentence with "remote sensing", became a dreaded word associated with bad science.

Remote sensing has also been perceived by some as a magic tool that can identify ore deposits or worse still, actual drill sites. This is primarily an educational problem and can be traced to the early days when the justification of the Landsat satellite data products resulted in extravagant and unrealisitic claims of its incredible potential. Orbital satellite imaging systems, it was claimed, were capable of finding ore deposits, oil fields, groundwater, and renewable resources--and all by computer! The ability to directly detect and identify certain surface materials, especially those associated with ore deposits, has always intrigued a large proportion of the geological remote sensing community. To the disappointment of many, two decades of remote sensing has clearly shown that spectral remote sensing, though extremely valuable, has not lived up to its original expectations.

Much of current remote sensing research for exploration geology is entrenched in what is referred to as "spectral-target" remote sensing. Concern and consternation has arisen among some scientists

Figure 7. Edge and contrast enhanced Landsat band 5 image of the Mt. Skukum Volcanic Complex.

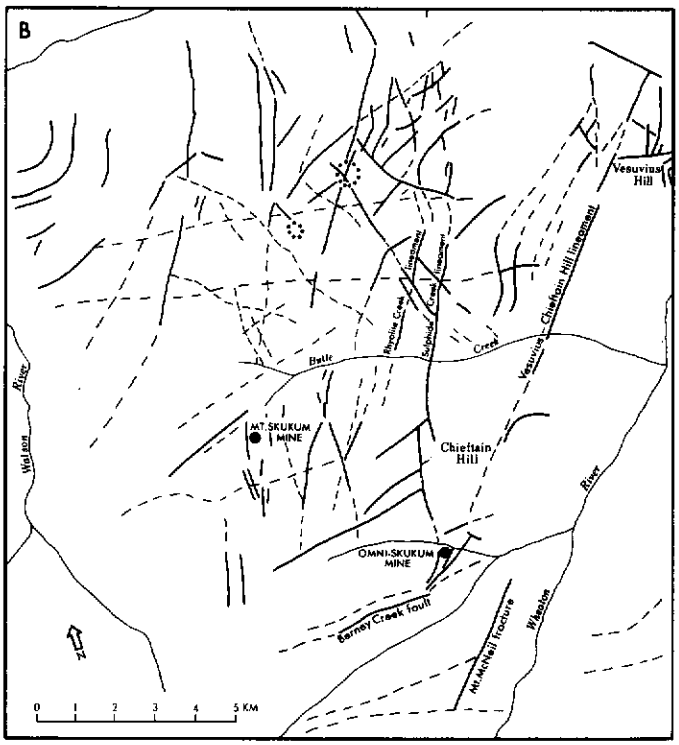

Figure 8. Interpretation of 1:50 000 Landsat TM imagery centered over the Mt. Skukum Volcanic Complex. Solid lines are distinct lineaments, dashed lines are possible lineaments, and dotted circles are anomalous circular features.

because this approach has focused on low-flying aircraft with imaging systems recording several hundred channels of spectral information and is being developed at the expense of what many feel is the most important benefit of the Landsat system--the synoptic view. These efforts have been labeled by Wilson (1986) as, "geodermatology", because it is a two-dimensional approach that takes into account only the surface or "skin" of the earth. The danger of this approach is that the image interpreter becomes singularly interested in determing only the "colour" of a specific spectral response, while taking no interest in understanding the underlying geological environment.

The exploration geologist involved in reconnaissance studies should be interested in images or maps displaying potential fractures and faults, and areas of alteration. No geologist, however, should

be gullible enough to think that Landsat imagery can provide specific exploration targets; the intersection of lineaments associated with an area of anomalous spectral responses should not be interpreted as a specific drill site. Sadly enough, some individuals, from university educated geologists to self-taught prospectors, have been led to believe that remote sensing is the panacea they have always desired, that "high-tech" can solve all of their problems. Nothing could be further from the truth.

CONCLUSIONS

Digitally enhanced remote sensing imagery is a valuable tool for exploration geology when interpreted properly and appropriately used. Educated and experienced users of Landsat data realize that the images are invaluable in reconnaissance studies and provide a viable basis for detailed mapping. When interpreted by a geologist knowledgeable about a specific region, the imagery may help in the decision making processes involved in selecting areas for more detailed examination. Combined with the traditional methods of mineral exploration, satellite imagery provides a more cost- effective means for conducting reconnaissance studies.

Specific conclusions and limitations of this study include the following:

1. TM imagery proved useful for mapping at a variety of scales ranging from a regional overview scale (1:1 000 000), for reconnaissance studies (1:250,000), to detailed mapping (1:50,000).

2. The synoptic and multispectral characteristics of Landsat TM imagery were valuable for mapping regional and local structural patterns.

3. The multispectral characteristics of the imagery were useful for detecting areas of strong surface alteration, primarily limonitic and intensely leached areas. This study, however, was not successful in detecting clay minerals associated with hydrothermally altered rocks.

4. The identification and differentiation of lithologic units was not possible because of the presence of lichen on virtually all exposed rock surfaces.

5. The extreme topography of the region and the low sun angle present during image acquisition resulted in dark shadows on northwest slopes that masked ground features.

ACKNOWLEDGEMENTS

This project was supported by the Exploration and Geological Services Division, Department of Indian and Northern Affairs Canada in Whitehorse, Yukon and by a grant from the Boreal Institute of North America at the University of Alberta. Many thanks to S. Morison and G. Abbott for suggesting the study and for their constructive comments. Thanks to Omni Resources Inc. and the Mt. Skukum Gold Mining Corporation for their cooperation and hospitality during field studies. Discussions with A. Doherty, T. Elliot, G. Gossan, L. Dobbins and C. Hart were very helpful. The assistance of J. Hooper in the field investigations was greatly appreciated.

REFERENCES

ABRAMS, M.J., BROWN, D., LEPLEY, L., SADOWSKI, R., 1983. Remote sensing of porphyry copper deposits in southern Arizona; Economic Geology, Vol. 78, p. 591-604.

CAIRNES, D.D., 1912. Wheaton District, Yukon Territory; Geological Survey of Canada, Memoir 31, 153 p.

DRURY, S.A., 1986. Remote sensing of geological structure in temperate agricultural terrains, Geology Magazine, Vol. 123, No. 2, p. 113-121.

DRURY, S.A., 1987. Image interpretation in Geology; Allen and Unwin Ltd., 243 p.

GOETZ, A.F.H., ROCK, B.N., and ROWAN, L.C., 1983. Remote sensing for exploration: an overview; Economic Geology, Vol. 78, p. 573-590.

GOETZ, A.F.N., 1980. Geological remote sensing in the 1980's: in Remote Sensing in Geology (Siegal, B.A., and Gillespie, A.R., editors), John Wiley and Sons, New York, p. 679-685.

HENDERSON, F.B., and ROCK, B.N., 1983. Frontiers for geological remote sensing from space: report of the Fourth Geosat Workshop, Flagstaff, Arizona, June 12-17, 1983.

JENSEN, J.R., 1986. Introductory Digital Image Processing; Prentice Hall, 379 p.

MCDONALD, B.W.R., STEWART, E.B., and GODWIN, C.I., 1986. Exploration geology of the Mt. Skukum epithermal gold deposits, southwestern Yukon; in Yukon Geology, Vol. 1; Exploration and Geological Services Division, Yukon, Indian and Northern Affairs Canada, p. 11-18.

PODWYSOCKI, M.H., SEGAL, D.B., and ABRAMS, J.M., 1983. Use of multispectral scanner images for assessment of hydrothermal alteration in the Marysvale, Utah, mining area; Economic Geology, Vol. 78, p. 675-687.

PRIDE, M.J., 1985. Preliminary geological map of the Mount Skukum Volcanic Complex, 105 D 2, 3, 4, 5; Exploration and Geological Services Division, Yukon, Indian and Northern Affairs Canada, Open File, 1:25 000 scale map.

PRIDE, M.J., 1986. Description of the Mount Skukum Volcanic Complex southern Yukon; in Yukon Geology, Vol. 1; Exploration and Geological Services Division, Yukon, Indian and Northern Affairs Canada, p. 148-160.

ROWAN, L.C., and LATHRAM, E.H., 1980. Mineral exploration; in Remote Sensing in Geology (Siegal, B.S., and Gillispie, A.R., editors), John Wiley and Sons, New York, p. 553-605.

ROWAN, L.C., WETLAUFER, P.H., GOETZ, A.F.H., BILLINGSLEY, F.C., and STEWART, J.H., 1974. Discrimination of rock types and detection of hydrothermally altered areas in south-central Nevada by the use of computer-enhanced ERTS images: U.S. Geological Survey Professional Paper 883, 35 p.

SABINS, F.F., Jr., 1987. Remote Sensing Principles and Techniques, 2nd ed.; Remote Sensing Enterprises, Inc., 449 p.

SCHOWENGERDT, R.A., 1983. Techniques for image processing and classification in remote sensing; Academic Press, Inc., 249 p.

SIBSON, R.H., 1987. Earthquake rupturing as mineralizing agent in hydrothermal systems; Geology, Vol. 15, p. 701-704.

SIEGAL, B.S., and GILLIESPIE, A.R., editors, 1980. Introduction; in Remote Sensing in Geology, John Wiley and Sons, New York, p. 1-2.

SMITH, M.J., 1983. The Skukum Volcanic Complex, 105 D SW: Geology and comparison to the Bennett Lake cauldron complex; in Yukon Exploration and Geology 1982, Exploration and Geological Services Division, Yukon, Indian and Northern Affairs Canada, p. 68-73.

WHEELER, J.O., 1961. Whitehorse map-area, Yukon Territory, 105 D, Geological Survey of Canada, Memoir 312, 156 p.

WILLIAMS, R.S., Jr., et al., 1983. Geological applications; in The Manual of Remote Sensing (Estes, J.E., and Thorley, G.A., editors), American Society of Photography, The Sheridan Press, p. 1667-1951.

WILSON, J.G., 1985. Remote sensing for exploration geology; geodermatology, geomorphology, or both?: Fourth Thematic Conference, "Remote Sensing for Exploration Geology", San Francisco, California, April 1-4, 1985.

WISE, D.U., 1982. Linesmanship and the practice of linear go-art; Bulletin of the Geological Society of America, Vol. 93, p. 886-888.